THE WRITING, READING AND CHROMATIN SIGNATURES OF HISTONE H3K23 ON MAMMALIAN CHROMATIN

By
David A. Vinson

A dissertation submitted to Johns Hopkins University
in conformity with the requirements for the degree of
Doctor of Philosophy

Baltimore, Maryland
October 2022

Abstract

The DNA of eukaryotes is wrapped around histone proteins to form the nucleosome, the fundamental repeating unit of chromatin. Post-translational modifications (PTMs) on histone proteins can act to regulate chromatin compaction by shifting towards a permissive/open state in which DNA is accessible to the environment (euchromatin) or towards a transcriptionally repressive/closed state that restricts access of the DNA to the environment (heterochromatin). Lysine methylation is a prominent histone PTM that has been implicated in the formation of both repressive and permissive chromatin states. Methylation of histone H3K23, a novel yet poorly understood class of histone methylation, has proven critical for preserving genomic integrity in *T. thermophila*, maintaining RNAi pathways in *C. elegans*, and transposon silencing in *A. thaliana*, but very little information is known about the function of H3K23 methylation on mammalian chromatin.

Here, we performed *in vitro* histone methyltransferase assays to screen canonical H3K9 writers, and identified EHMT1/GLP and EHMT2/G9a as writers of H3K23 methylation. To follow up, we used a combination of *in vitro* and *in vivo* tools to perturb both enzymes at the protein and DNA level, and we identified differential activity between the two enzymes on H3K23. While both enzymes can mediate mono- and di-methylation of histone H3K23, only EHMT1/GLP can catalyze tri-methylation of H3K23. Interestingly, our studies also identified H3K18 as a target for mono-, di- and tri-methylation, *de novo*, by both EHMT1/GLP and EHMT2/G9a *in vitro* and *in vivo*.

Additionally, we performed nChIP-Seq on H3K23me3 and found it to be a promoter mark that is often heavily bivalent with H3K4me3 at promoters. Our data also

shows that monovalent H3K23me3 occupies transcription start sites (TSSs) while bivalent H3K23me3 (with H3K4me3) occupies gene promoters. Additionally, we have evidence that H3K23me3 dampens gene expression relative to H3K4me3, suggesting that H3K23me3 might serve to silence gene expression on mammalian chromatin. Lastly, we found that perturbations in H3K4me3 effect H3K23me3, but not vice versa. This suggests unique one directional cross-talk between H3K4me3 and H3K23me3 and future studies should aim to elucidate the functional interplay of these bivalent chromatin modifications.

Primary reader and graduate co-advisor: Sean D. Taverna, Ph.D., Associate Professor, Department of Pharmacology and Molecular Sciences, JHU SOM

Primary reader and graduate co-advisor: Srinivasan Yegnasubramanian, M.D., Ph.D., Professor, Department of Oncology, JHU SOM

Secondary reader and thesis committee chair: Xin Chen, Ph.D., Professor, Department of Biology, Johns Hopkins University

Acknowledgements

I would like to extend a sincere and heartfelt 'Thank You!' to my friends, family and mentors who have helped bring me to this point. To my high school science teachers: Ms. Katrina Ellis, Mrs. Holly Crowson, Mrs. Molly Penrod, Ms. Liz Golowenski and Ms. Melinda Wesley. To my college professors: Profs. Bruce Armitage, Karen Stump, Catalina Achim, Brooke McCartney and Gizelle Sherwood. Your dedication and guidance, in the classroom and in the lab, have played an instrumental role in my intellectual and scientific maturation.

I am also grateful to my two co-mentors Drs. Vasan Yegnasubramanian and Sean D. Taverna. Merging Dr. Yegnasubramanian's cancer epigenetics background with Dr. Taverna's expertise in histone PTM biochemistry proved to be invaluable in exploring complex histone biology. Their unwavering patience and enthusiasm throughout this journey was much appreciated. I would also like to thank my thesis committee members Drs. Xin Chen and Alan Tackett. Dr. Chen served on the first H3K23me3 project and was invaluable in connecting the tetrahymena and mammalian work. Dr. Alan Tackett, a long-time proteomics collaborator, proved paramount in our proteomics analyses. I would also like to thank Dr. Bob Cole and Bob O'Meally of the JHU Mass Spectrometry and Proteomics facility for proving essential in the validation of our *in vitro* work and for their discovery of H3K18 as a target of EHMT1/GLP and EHMT2/G9a. I would also like to thank Dr. Kim Stephens, for being a source of both scientific and emotional support in the early years of my Ph.D. I would also like to thank my parents, Shirley and David Vinson, and my twin sister, Leah Vinson, for their continued love and support throughout this journey. I would also like to thank the

Taverna and Yegnasubrmanian labs for their support and generosity in sharing reagents, knowledge and camaraderie. I would also like to thank the Department of Pharmacology administrative staff Mimi Guercio, Amy Paronto, Brenda Figueroa and Debbie Saylor for their administrative thoroughness, diligence and patience. The completion of my Ph.D. would not be possible without all of you!

Table of Contents

List of Tables

List of Figures

Chapter 1: General Introduction

i. Chromatin and Epigenetic Regulation

All eukaryotic cells possess a genome that is necessary to sustain normal cellular function [1]. The complete eukaryotic genome is composed of the information-storing, double-stranded deoxyribonucleic acid (DNA) molecules contained within the nucleus of each cell [2]. The average nucleus contains approximately two meters of DNA packaged into an approximate 10 μM space, which poses an enormous topological challenge as to how the cell packages such a large amount of material into such a small space. The cell partially overcomes this topological challenge through the association of DNA with histone proteins [3]. Histone proteins are small, highly positively-charged nuclear proteins that oligomerize to form a hetero-octamer composed of two copies of the four-core histone proteins: H2A, H2B, H3 and H4 [3]. Approximately 147 base-pairs of DNA wraps around one histone octamer to form the nucleosome, the single fundamental repeating unit of the genome, and the association of DNA and histones is collectively referred to as chromatin [1]. Chromatin can have varying degrees of compaction, from the naked, accessible DNA in between nucleosomes to intact chromosomes [1] (Figure 1, adapted from *Creative Diagnostics*).

Regulation of chromatin compaction is critical for cellular processes that require access to DNA such as gene transcription, DNA replication, DNA repair, and maintaining chromosome fidelity during mitosis [4]-[8]. Regulation of these various levels of compaction is facilitated, in part, through modifications to DNA or histone proteins [3], [9]. These modifications can serve to alter the biochemical interaction between the DNA

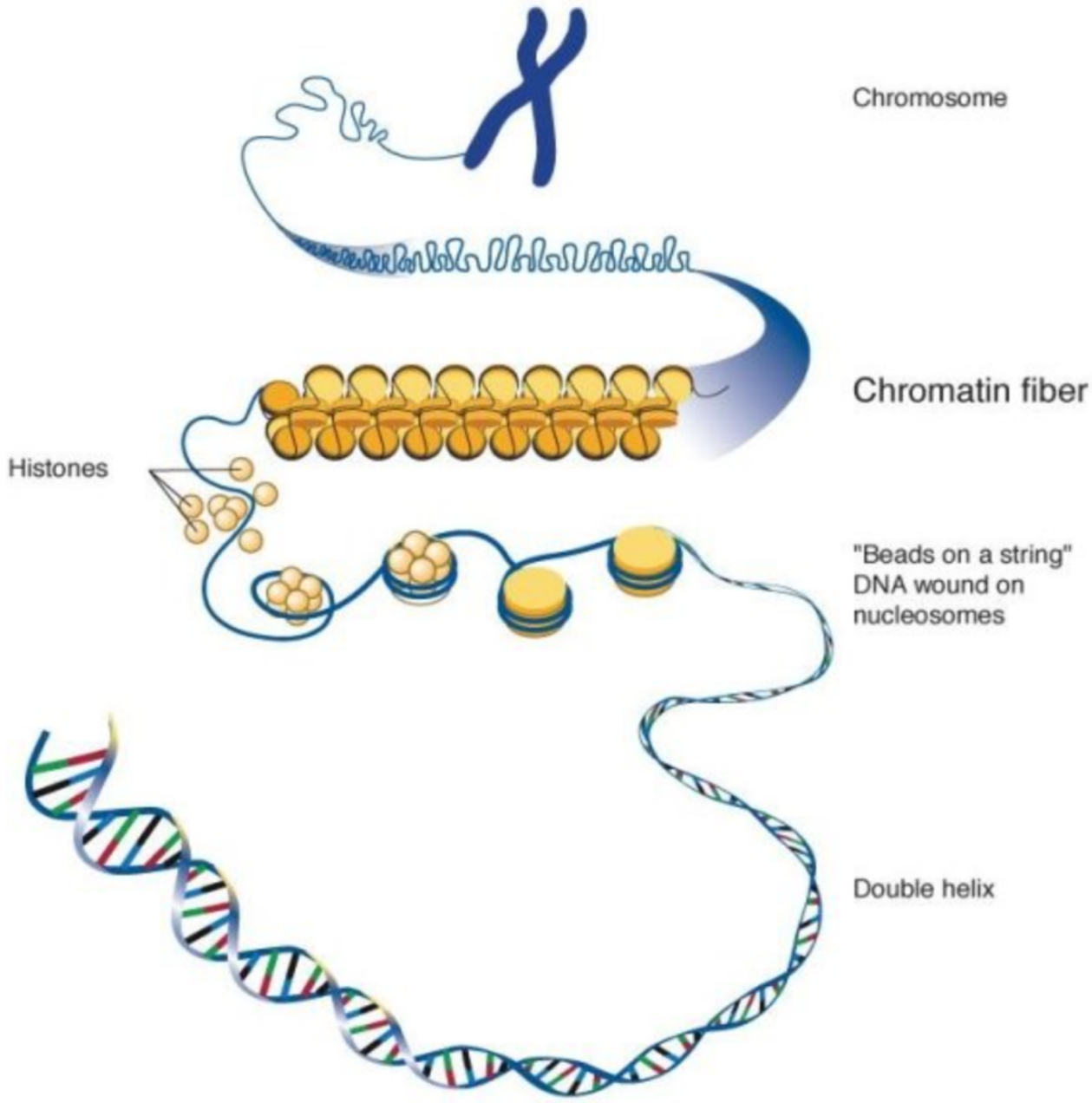

Adapted from Creative Diagnostics; The structure and function of chromatin

Figure 1. Eukaryotic genomes are packaged with histone proteins. DNA wraps around histone proteins to form chromatin. The single fundamental repeating unit of chromatin, the nucleosome, can condense to form higher order chromatin structures including intact chromosomes.

and histones, making the DNA more or less accessible to environmental factors [9], [10]. Collectively, modulation of the accessibility of DNA to the environment by elements that are independent of the DNA sequence itself are collectively referred to as *epigenetic* regulation [11]. This type of regulation is critical for proper embryonic development, cellular homeostasis, repair pathways and, when perturbed, has been linked to a number of pathologies including neurodegeneration and cancer [6], [12], [13].

ii. Histone proteins, histone variants and histone posttranslational modifications

Histone proteins are some of the most abundant nuclear proteins and are highly conserved throughout many higher eukaryotes. While there are multiple histone proteins, there are four core histone proteins that comprise the core particle of the nucleosome: histones H2A, H2B, H3 and H4. Structurally, each histone contains three alpha-helices, which are responsible for mediating hetero-dimerization with other histone proteins [14]. Upon assembly of the nucleosome core particle, histones H2A and H2B dimerize through the second alpha helix. This occurs twice to form two, H2A-H2B dimers. In contrast, histones H3 and H4 form a tetramer, composed of two H3-H4 dimers, also interacting through their second alpha fold. Following independent assembly of the H2A-H2B and H3-H4 tetramers, both tetramers combine to form the histone octamer (Figure 2A, adapted from PMID: 28377609). There are also histone proteins that do not comprise the core octamer, called ‘linker’ histones, which sit on the exposed DNA in between adjacent nucleosomes [15]. One such example is histone H1. Of the canonical histones, histone H1 is the most divergent class with up to 12 naturally occurring subtypes found in mammals [15], [16].

A.

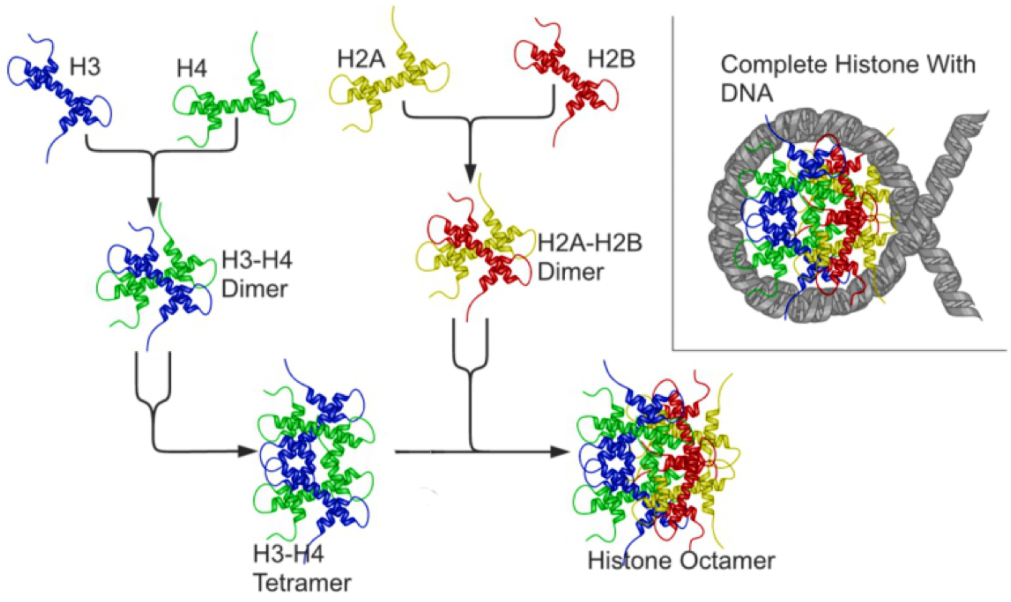

Adapted from Richard Wheeler (Zephyris)

B.

H1	1	MSETAPAAPA	APAPAEKTPV	KKKARKSAGA	AKRKASGPPV	SELITKAVAA
	51	SKERSGVSLA	ALKKALAAAG	YDVEKNNSRI	KLGLKSLVSK	GTLVQTKGTG
	101	ASGSFKLNKK	AASGEAKPKA	KKAGAAKAKK	PAGAAKKPKK	ATGAATPKKS
	151	AKKTPKKAKK	PAAAAGAKKA	KSPKKAKAAK	PKKAPKSPAK	AKAVKPKAAK
	201	PKTAKPKAAK	PKKAAAKKK			
H2A	1	MSGRGKQGGK	ARAKAKTRSS	RAGLQFPVGR	VHRLLRKGNY	AERVGAGAPV
	51	YLAAVLEYLT	AEILELAGNA	ARDNKKTRII	PRHLQLAIRN	DEELNKLLGK
	101	VTIAQGGVLP	NIQAVLLPKK	TESHHKAKGK		
H2B	1	MPEPAKSAPA	PKKGSKKAVT	KAQKKDGKKR	KRSRKESYSV	YVYKVLKQVH
	51	PDTGISSKAM	GIMNSFVNDI	FERIAGEASR	LAHYNKRSTI	TSREIQTAVR
	101	LLLPGELAKH	AVSEGTKAVT	KYTSSK		
H3	1	MARTKQTARK	STGGKAPRKQ	LATKAARKSA	PATGGVKKPH	RYRPGTVALR
	51	EIRRYQKSTE	LLIRKLPFQR	LVREIAQDFK	TDLRFQSSAV	MALQEACEAY
	101	LVGLFEDTNL	CAIHAKRVTI	MPKDIQLARR	IRGERA	
H4	1	MSGRGKGGKG	LGKGGAKRHR	KVLRDNIQGI	TKPAIRRLAR	RGGVKRISGL
	51	IYEETRGVLK	VFLENVIRDA	VTYTEHAKRK	TVTAMDVVYA	LKRQGRTLYG
	101	FGG				

Adapted from PMID: 28377609

Figure 2 Histone proteins are small, highly basic and oligomerize (A) crystal structure of the assembly of the histone octamer **(B)** the primary sequence of the five main histones. Surface exposed residues are in blue. lysines are in yellow. Cysteines are in red.

Analysis of the primary sequence shows that histone proteins contain many basic lysine and arginine residues (Figure 2B, adapted from PMID: 28377609). At physiologic pH, ~7.4, these residues are positively charged, which creates an attraction to the negatively charged backbone of DNA. This creates an inherently stable confirmation in which the negatively charged phosphate backbone of DNA is electrostatically complemented by the positively charged, unmodified lysine and arginine residues [10], [17]-[19].

Nature has evolved several versions of each of the histone proteins, dubbed histone variants. Histone variants, although overwhelmingly similar to their canonical counterparts, contain single amino acid changes at select residues [20]. These differences can often help regulate distinct biological differences separate from canonical histones (Figure 3, adapted from PMID: 15688000). Two examples are histone H2A.X and H2A.Z. H2A.X is heavily phosphorylated in response to double-stranded DNA breaks, with γH2A.X (H2A.Xser129ph) having been identified as a marker for DNA damage [21] . On the other hand, H2A.Z has been implicated in thermosensory regulation in *A. thaliana* [22] and in transcriptional activation by destabilizing nucleosome contacts with DNA and allowing for downstream gene activation [23], [24]. Other examples include variants H3.1, H3.2 and H3.3. Histones H3.1 and H3.2 are coupled to DNA-replication to package the newly synthesized DNA; however, histone H3.3 is replication independent, accumulates in post-mitotic cells and has been implicated in life-span extending signaling pathways independent of S-phase [25].

.

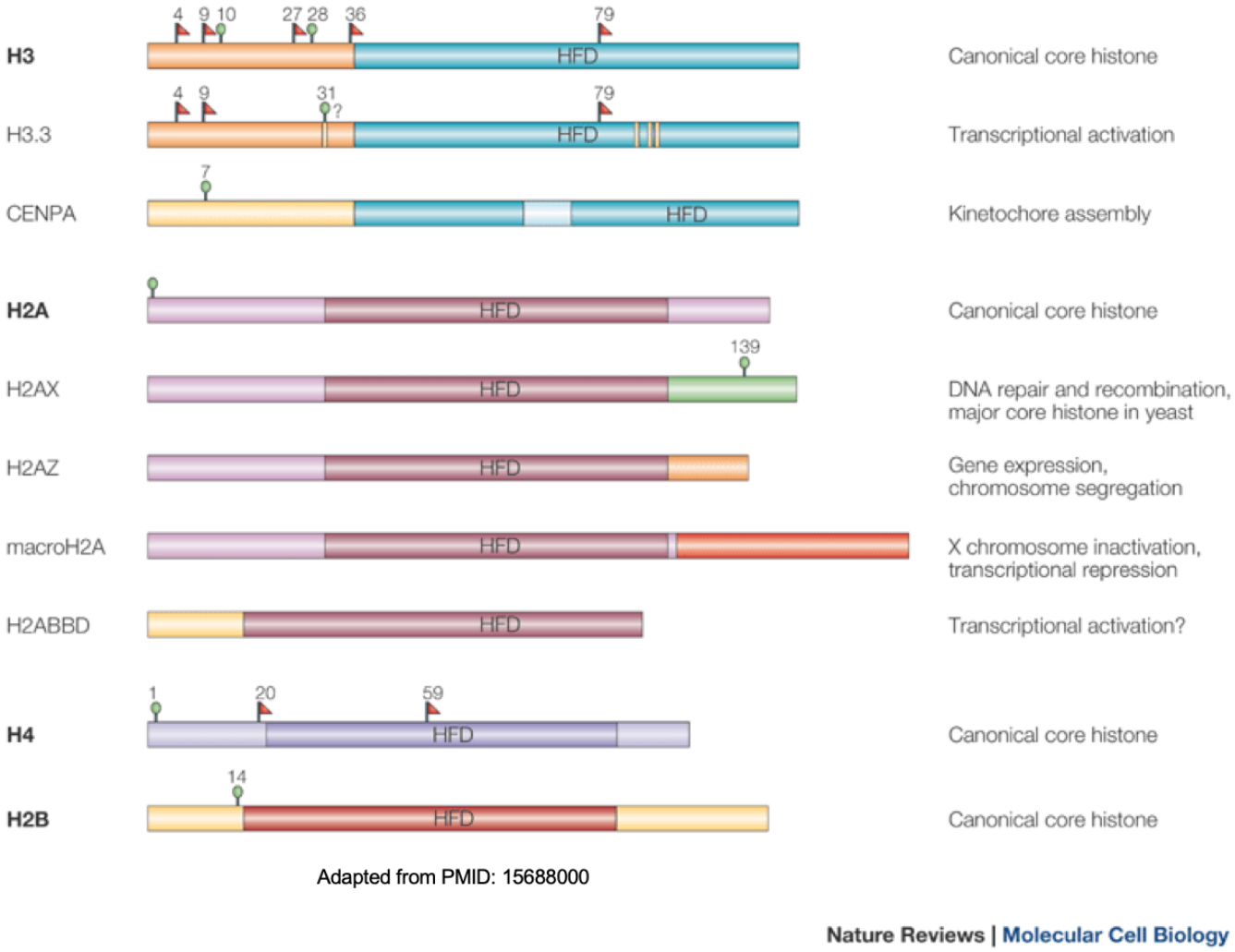

Figure 3 1D schematic of protein domains within common histone variants and their associated biological function.

Histone proteins, like all proteins, can be posttranslationally modified (PTM). Due to their unique relationship with DNA, posttranslational modifications on histone proteins carry implications as it relates to template dependent processes. Some of the more well-characterized PTMs include acetylation, phosphorylation and methylation (Figure 4, adapted from *CUSABIO*), but the full ensemble of histone PTMs has expanded over the years to include ubiquitylation, farnesylation, proponiylation, dopaminalytion and seritonylation, and many others. Despite the abundance of modifications, not every amino acid can carry every modification. In particular, lysine and arginine are some of the more heavily and diversely decorated amino acids within histones.

iii. Histone methylation: writing, reading and erasing

One of the most abundant and well-characterized PTMs is methylation. Methylation can assume multiple methylation states, unlike other PTMs which have either an unmodified or modified state. Lysine and arginine are primary targets of methylation within histones. Both lysine and arginine can accommodate multiple methyl groups. The modified heteroatom that is the substrate for the methylation reaction are the terminal nitrogens within the R group of the respective amino acids. The addition of one methyl group is referred to as mono-methyl, whereas the addition to two and three methyl groups is called di- and tri-methyl, respectively. In the R-group of arginine, there are two terminal amines that have the potential to be modified. With its two terminal amines, arginine can be either mono- or di-methylated; however, the addition of a second methyl group can occur on the already modified nitrogen or on the remaining unmodified terminal nitrogen. This creates confirmations where arginine can be either

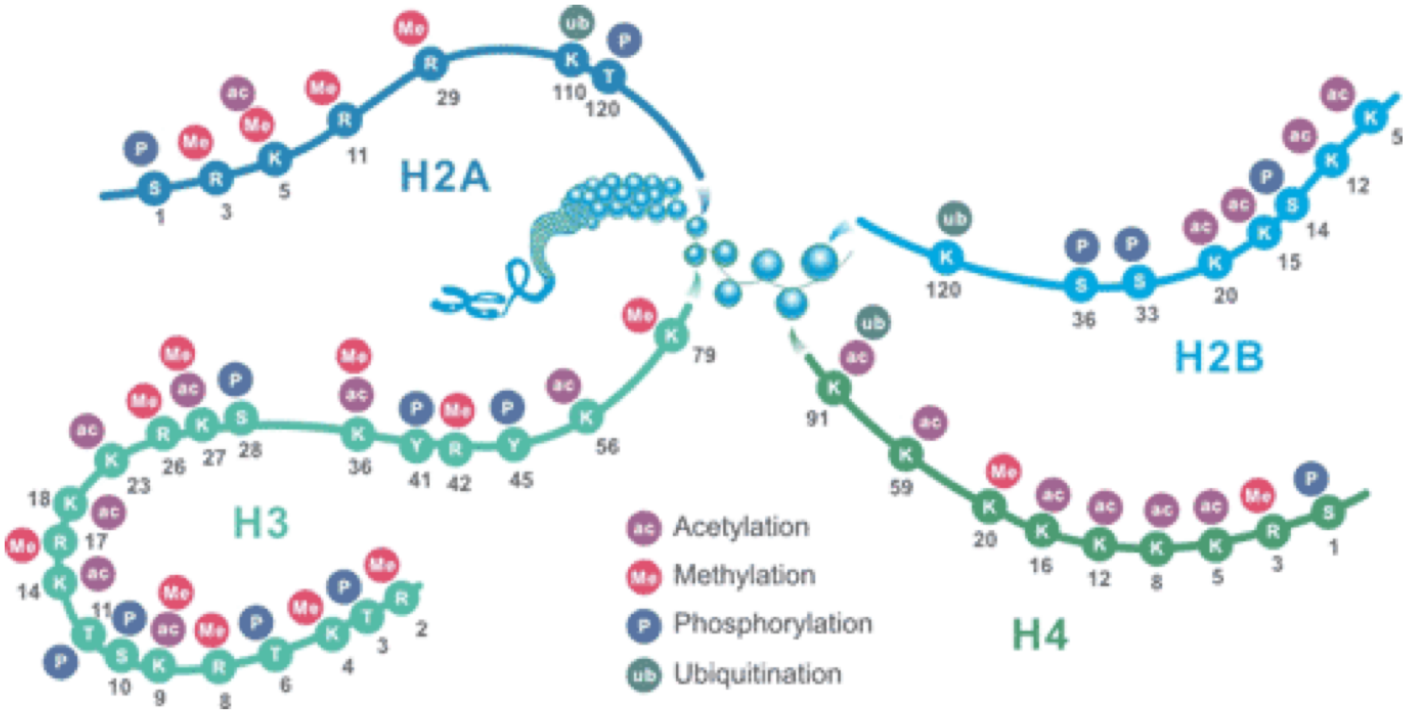

Adapted from CUSABIO

Figure 4 Graphical display of the diversity of posttranslational modifications on histone proteins.

symmetrically or asymmetrically methylated. The singularly terminal amine in lysine can accommodate up to three methyl groups. Mono- and di-methylation of arginine and mono-, di- and tri-methylation of lysine are some of the most abundant histone PTMs on mammalian chromatin.

The addition of methyl groups to histone proteins are facilitated by enzymes called histone methyltransferases (HMTs). There are many families of protein methyltransferases that transfer methyl groups onto specific amino acids within unique proteins. Lysine and arginine specific methyltransferases are responsible for transferring methyl groups to each respective residue. The precise mechanism for how each residue is mono-, di- or tri-methylated (lysine only) is shown in Figure 5 (adapted from PMID: 11562345).

In each case, S-adenosyl methionine (SAM) is the methyl-donor. The lone electron pairs from the terminal nitrogen of arginine or lysine, attacks the methyl carbon of SAM, which moves the electrons from the target carbon onto the positively charged sulfur atom within SAM, alleviating its unstable positive charge. The resulting S-adenosyl homocysteine (SAH) is recycled, and the mono-methylated residue is generated. This process can be repeated to add additional methyl groups until the methylated nitrogen runs out of donor electrons.

The enzymes or *writers* that facilitate the transfer of methyl groups to lysine and arginine contain specialized, catalytically active domains that accommodate the SAM cofactor and histone peptide substrate to coordinate transfer of the methyl group from one species to the other. Protein arginine methyltransferases (PRMTs) are classified into two main types: type I and type II [26]. While both types can catalyze mono-

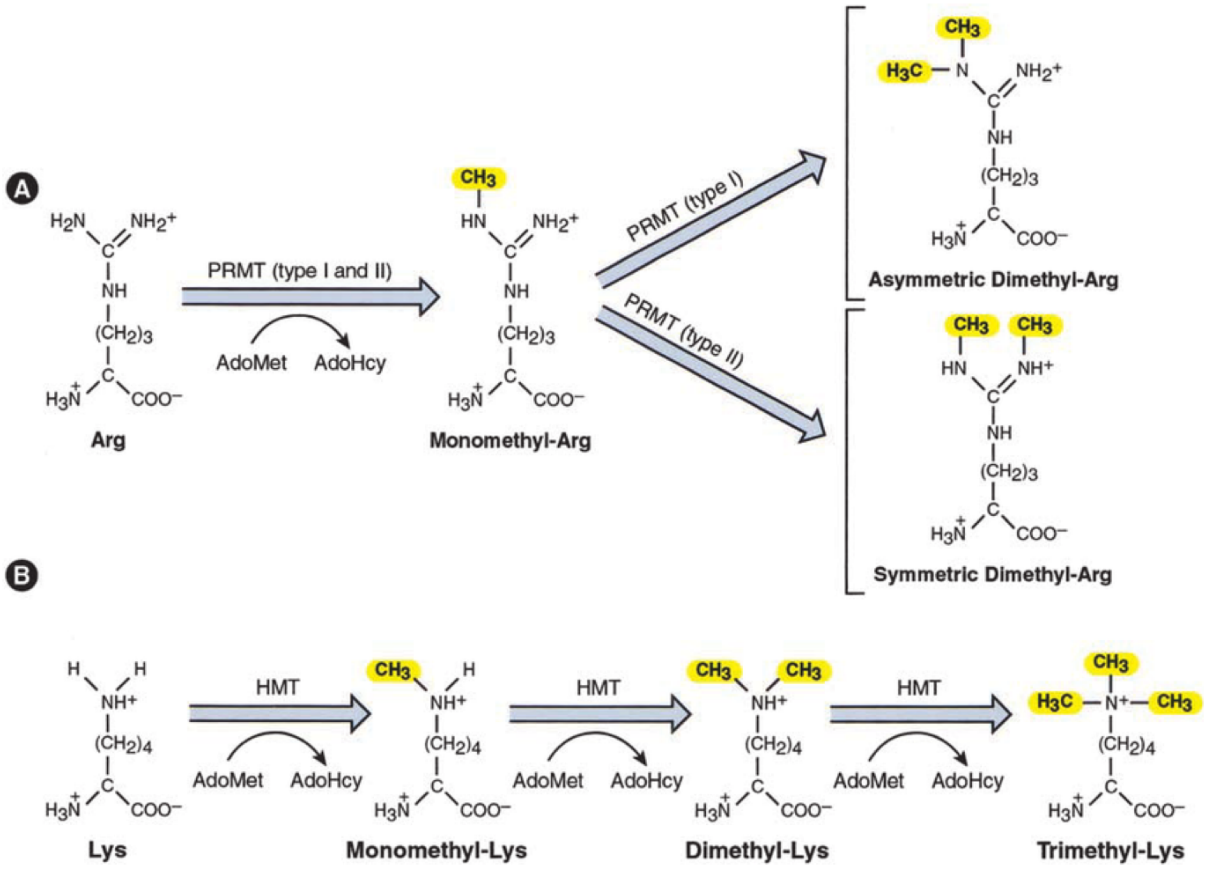

Adapted from PMID: 11562345

Figure 5 Mechanism of lysine and arginine methylation.

methylated arginine, they differ in their generation of symmetric or asymmetric di-methylation. Type I PRMTs, including PRMT 3, 4, 6 and 8, are responsible for generating asymmetric di-methylation, while type II PRMTs, including PRMT 5, 7, and 9, are responsible for generating symmetric di-methylation [27]. To date, there are nine known PRMTs expressed in humans[27], [28].

Distinct from PRMTs are lysine methyltransferases. Most lysine methyltransferases are structurally similar as they contain pre-SET, SET and post-SET domains that must fold together to form a catalytically functional methyltransferase domain [17], [29], [30]. There are over twenty different lysine methyltransferase genes expressed in humans and much of that diversity comes with a wide range of specific targets for these enzymes [31]. Well-characterized targets of methylation within histone H3 include lysines 4, 9, 27, 36, 79, and H4 lysine 20, many of whom are methylated by their own specific HMT. A few examples of common histone methyltransferase enzymes include MML1- 4 (a writer of H3K4 methylation), EZH2 (a writer of H3K27 methylation), EHMT1-2 (a writer H3K9 methylation) and SetD2 (a writer of H3K36 methylation) [32].

In addition to *writer* proteins, *reader* proteins also play a substantial role in interpreting epigenetic signatures, such as lysine methylation, on chromatin. While these proteins don't play a direct role in either adding or removing chromatin modifications, they interact with or *read* chromatin signatures and subsequently initiate downstream chromatin remodeling events including deposition or removal of other epigenetic marks, compaction or expansion of chromatin fibers, rearrangement of nucleosomes, and histone exchange [33], [34]. This is facilitated through interactions with protein complexes whose members possess various functions that help influence

the chromatin structure and subsequent epigenetic state [34]. Examples of prominent epigenetic complexes relevant to lysine methylation include the BAF complex, an essential ATP-dependent chromatin remodeling complex implicated in binding H3K36me2 [34], [35] and PRC1 and 2 complexes, which have been implicated in deposition of H3K27 methylation and subsequent heterochromatin formation [36]. As previously mentioned, methylation of lysine and arginine can assume multiple methylation states. Reader proteins interact with certain residues and *read* specific methylation states (e.g. mono, di or tri-methyl, etc.). For example, Shanle and colleagues [37] show how various members of the HP1 heterochromatin protein family interact with specific methylation states of H3K9 and H3K23. HP1 proteins function by dimerizing after their subsequent interaction with its target methyl-lysine. The subsequent oligomerization of the heterochromatin proteins causes clumping of nucleosomes and condensation of chromatin (Figure 6, adapted from PMID: 24618358) [38].

Epigenetic marks, although stable and covalent, are irreversible. This phenomenon is facilitated by *eraser* proteins, which are proteins that remove covalent modifications by enzymatically cleaving them from their native substrates [32]. As it relates to methylated-lysine, there are two main classes of enzymes that remove methylation from lysine: Fe^{2+}-oxoglutarate dependent and FAD-dependent demethylases [39]. While both can remove methylation from lysines, Fe^{2+}-oxoglutarate dependent demethylases, often containing specialized domains called Jumonji (Jmj) domains, mechanistically incorporate the extracted methyl group into the byproduct to form formaldehyde [40]. A few examples of Fe^{2+}-oxoglutarate dependent lysine

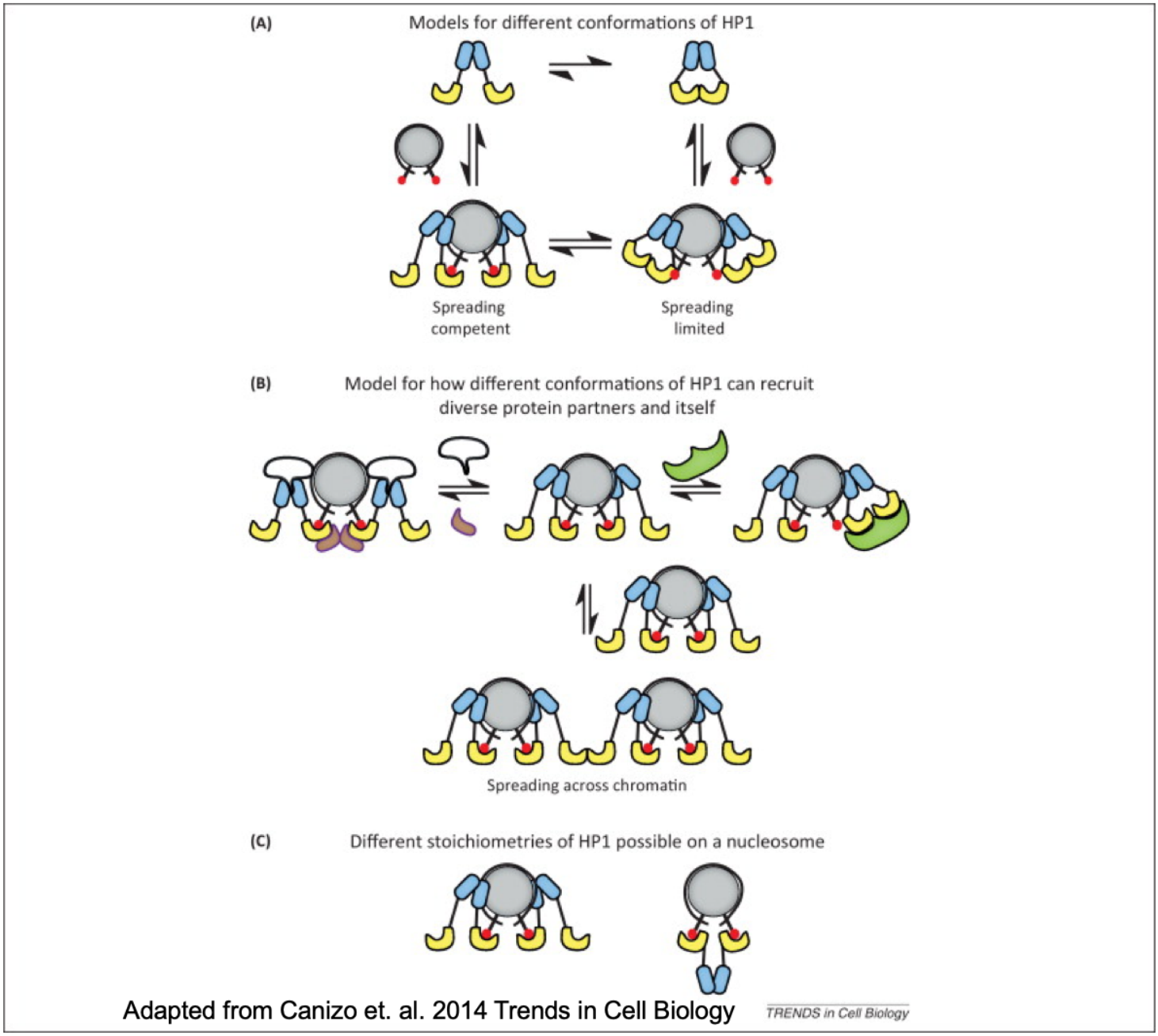

Figure 6 Reader proteins interact with epigenetic marks and affect nucleosome and chromatin structure (A) proposed confirmations of HP1 binding H3K9me3 on nucleosomes **(B)** model for how HP1 further recruits additional proteins **(C)** proposed stoichiometries for HP1 oligomerization.

demethylases include the KDM4 family of lysine demethylases, of which there are 5 isoforms responsible for targeting H3K9 and H3K36 for demethylation [41]. Conversely, FAD-dependent demethylases are Flavin-dependent and contain specialized amine-oxidase and SWIRM domains that help facilitate catalysis [42]. Mechanistically, FAD-dependent demethylases use the FAD molecule as an electron sink to facilitate the removal of methyl groups. A few examples of FAD-dependent demethylases include LSD1 and LSD2, which has been shown to specifically demethylate histone H3K4. Many eraser proteins associate in complexes and work, in concert with other protein complex members, to edit the surrounding chromatin environment and regulate which modifications decorate the epigenetic landscape [32], [42].

iv. Combinatorial and bivalent modification states

The histone code hypothesis postulates that, rather than existing alone, histone modifications appear in specific combinations and differentially decorate chromatin to exert locus-specific chromatin remodeling events [10], [18], [43]. It has been reported that repressive marks such as H3K9me and H3K27me, and various activation marks such as H3K4me and H3K36me, group together to reinforce either an open or closed state by differentially recruiting various factors that propagate pathways that reinforce either a closed or open state [44]-[47]. One example is H3K9me2 and H3K23me1 in Arabidopsis to silence transposons [48]. Trejo-Arellano and colleagues showed that in *A. thaliana*, H3K9me2 and H3K23me1 were encoded by the same HMT, called kryptonite, and both co-located at transposons to reinforce silencing of these regions. Another example includes from Taverna et. al. 2007 PNAS [49]. Taverna and

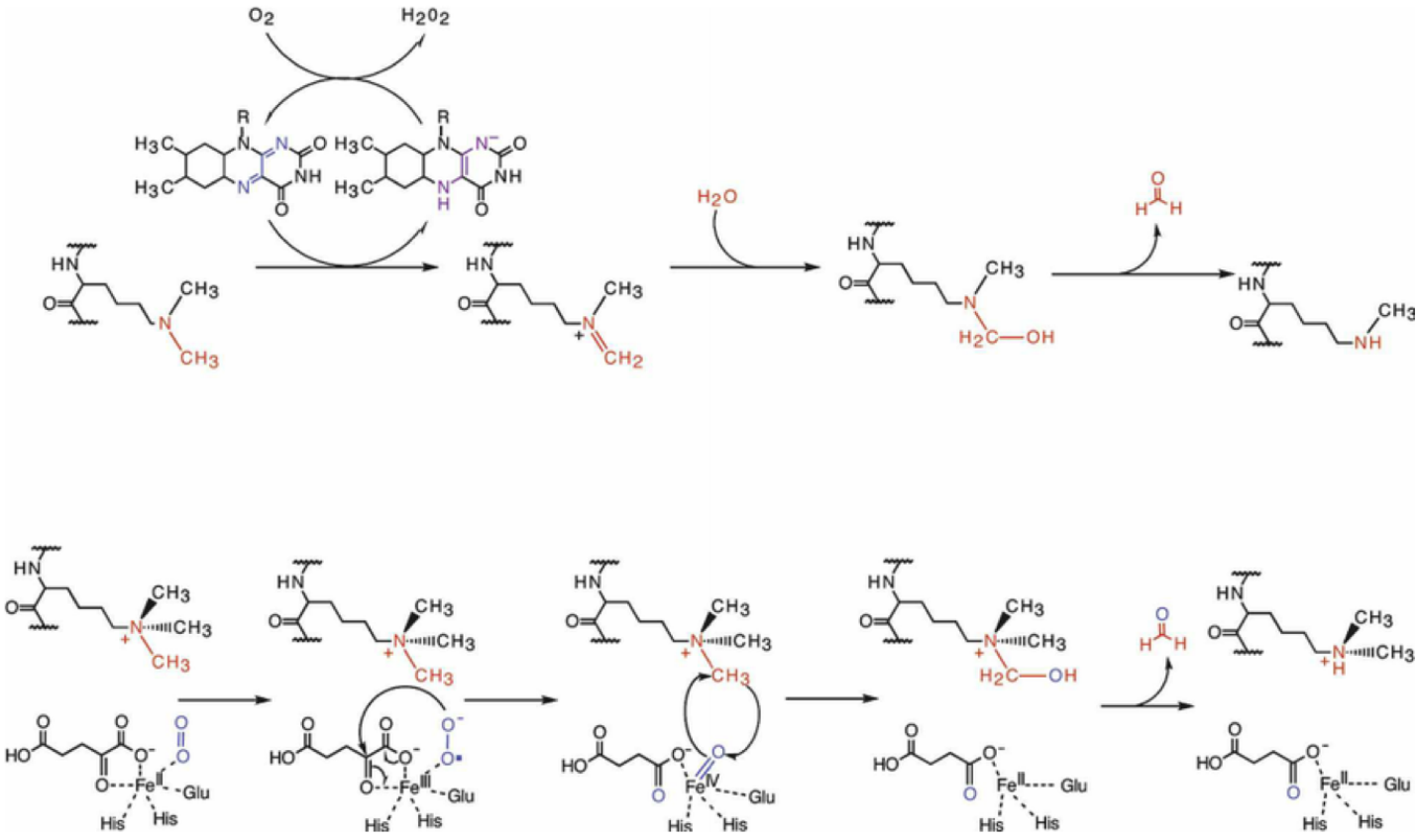

Figure 7 Mechanisms of demethylation of lysine. Mechanism of Fe^{2+}-oxoglutarate dependent (**top**) vs FAD-dependent (**bottom**) lysine demethylation.

colleagues show that, in yeast, H3K4me3 interacts with the NuA3 histone acetylation transferase (HAT) complex and stimulates acetylation of histone H3 lysine 14. This creates an H3K4me3-K14Ac combinatorial state that promotes transcriptional activation in a subset of genes that contain this signature. Although there are many examples of epigenetic marks that functionally reinforce each other to drive a particular open or closed state, there are examples of epigenetic marks with opposing functions collocating within the genome.

In 2007, Bernstein et. al. reported the existence of chromosomal regions with co-occurring repressive H3K27me3 and active H3K4me3 marks [12]. These were dubbed *bivalent*. At the time, it was thought that bivalent domains were used in differentiating cell types to *poise* gene expression, keeping expression low until the cell received a differentiation cue upon which the bivalent domain would *resolve* into either a monovalent H3K4me3 or H3K27me3; however, it is gaining appreciation that bivalent chromatin domains are (a) not restricted to differentiating cells, and (b) do not necessarily resolve upon differentiation and, instead, might be a more general transcriptional regulatory phenomenon [50]. While it remains unclear the exact mechanism of how bivalent domains are established and the exact confirmation of the histone PTMs on the nucleosome, it has been reported that some bivalent histone PTM domains have readers capable of independently reading both repressive and active histone PTMs [41], [50], [51] . For example, members of the KDM4 family have been found to *read* both repressive H4K20 methylation and active H3K4 methylation marks independently, KDM4A being one example [41]. This protein contains a double-Tudor

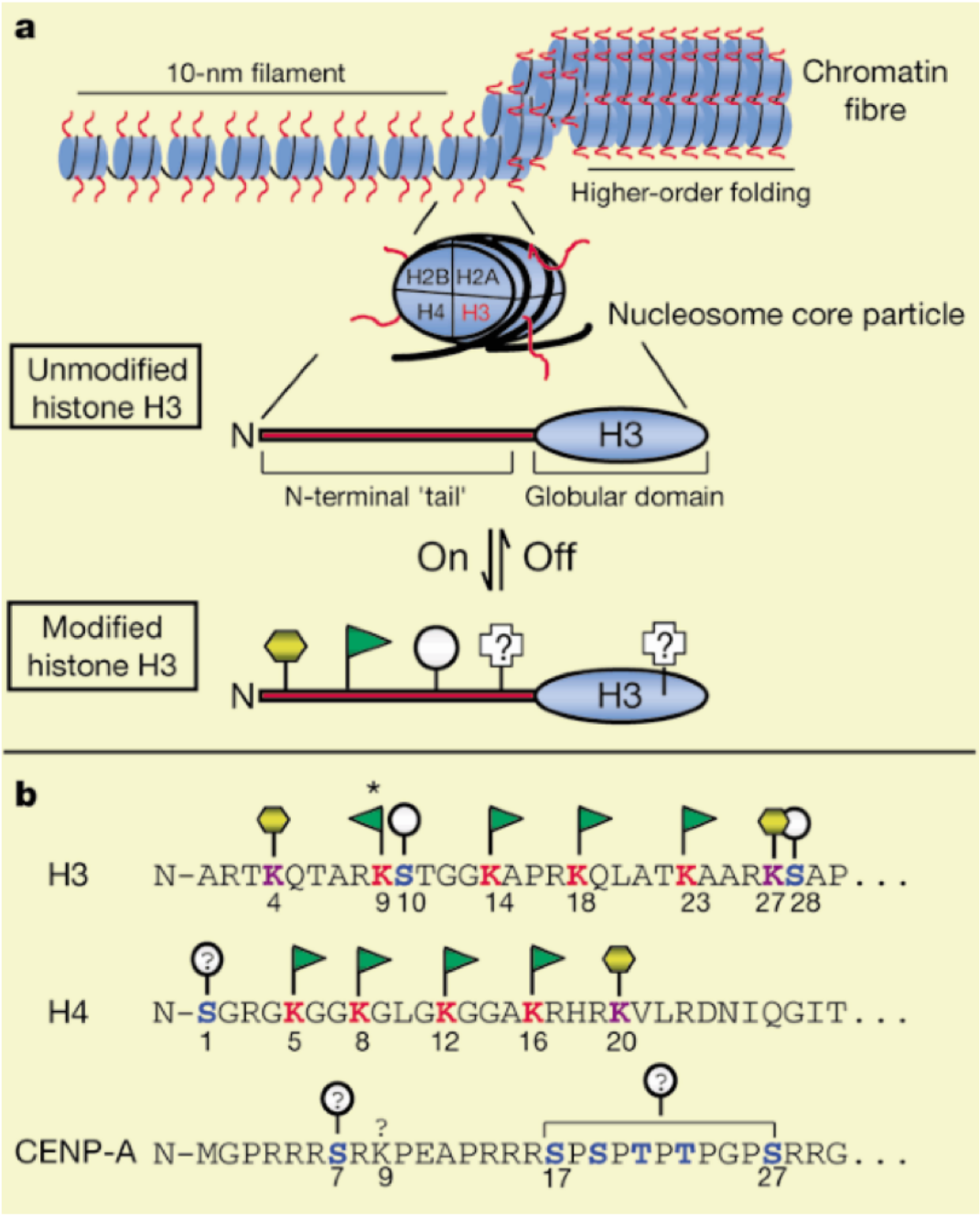

Adapted from Strahl et. al. 2000 Nature

Figure 8 Combinatorial posttranslational modification states differentially decorate chromatin (A) Schematic display how histone tails are differentially decorated with PTMs **(B)** examples of combinatorial modification states on histone tails.

domain which is a class of reader proteins that have an affinity for methyl-lysines. While it is unclear how these proteins function in a bivalent context, it is thought that these proteins can assist in the *resolution* of bivalent domains by reading either the repressive or active mark and subsequently propagating either an open or closed chromatin state by removing/erasing epigenetic marks that antagonize the desired chromatin states [12], [50]. This interesting, yet mechanistically ambiguous phenomenon highlights the need to understand the histone code and elucidate how combinatorial modifications states are established, propagated and influence chromatin structure.

v. Relevance of histone PTMs to health and disease

Epigenetic modifications have large implications for maintaining genome integrity. Perturbations in epigenetic modifications or their mediators can differentially effect gene expression and cause inappropriate gene activation/repression, which has been linked to a plethora of human diseases [52]-[54].

One relevant example are onco-histones. These are mutations in genes encoding histone proteins that, when expressed, have been linked to cancer phenotypes. One example is H3K27M, in which histone H3 lysine 27 has been mutated to a methionine. This specific mutation has been found in pediatric glioblastoma [52]-[55]. Another example H3K36M, where histone H3 lysine 36 has been mutated to a methionine. This has been linked to chondroblastoma [56]. The K-to-M mutations exert their effect by knocking down methylation at wild-type residues complementary to those on the mutant histone harboring the K-to-M mutation (e.g. H3K9 methylation on wild-type histones is perturbed in H3K9M expressing cells, H3K27 methylation perturbed in

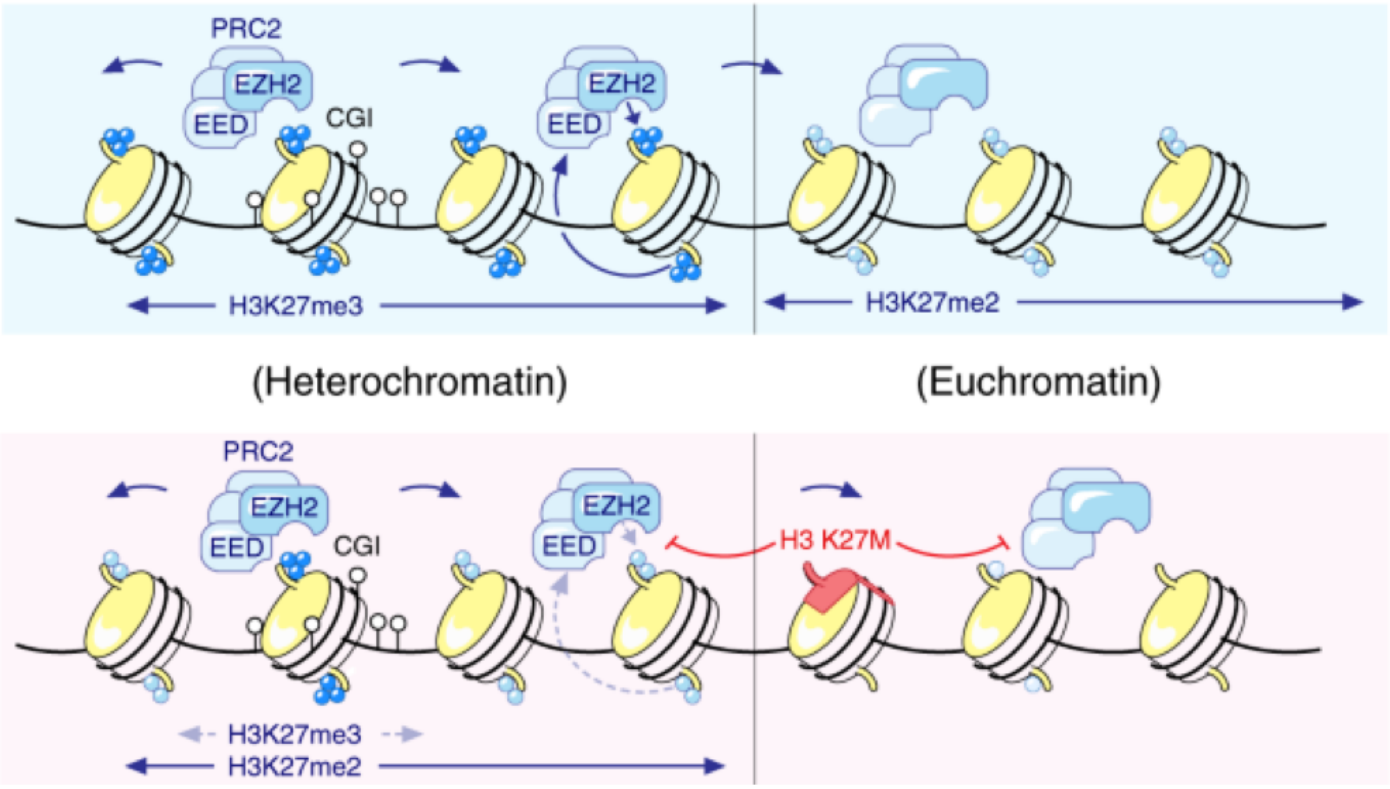

Adapted from PMID: 30890717

Figure 9 K-to-M mutations trap methyltransferases and perturb methylation genome-wide. Proposed mechanism for knockdown of H3K27 methylation on chromatin containing H3K27M.

cells expressing H3K27M, etc.) [57]. It is thought that the methionine, which mimics the mono-methylated substrate, tricks the histone methyltransferase into trying to accommodate it as a substrate and undergo catalysis. However, a methionine is chemically and structurally different from lysine and instead of catalysis, the HMT gets stuck and is prevented from methylating downstream targets. This leads to global knockdown in methylation at residues harboring the mutation and it often affects multiple methylation states (me1, me2, me3, etc.). In summary, epigenetic modifications and their mediators are essential to proper gene expression and cellular homeostasis. Perturbations in the deposition, removal or interpretation of histone PTMs has been linked to diseases such as cancer and neurodegeneration [30], [58], [59] and highlights the need to fully characterize how each individual histone PTM affects chromatin structure.

Chapter 2: The writing and reading of H3K18 and H3K23 methylation on mammalian chromatin

i. Background

Posttranslational modifications (PTMs) on lysines of histone proteins have long been implicated in regulating gene expression, DNA replication, DNA damage repair, transposon silencing and other template-dependent processes [5], [11], [18], [31], [36], [60], [61]. Histone lysine methylation is added by histone methyltransferases (HMTs) that catalyze the addition of one (mono-), two (di-) or three (tri-) methyl groups ($-CH_3$) onto a single lysine [11], [17], [31], [62]. These different modification states can often facilitate differential binding of effector proteins, which *read* the various modification states and help direct additional chromatin modifying complexes to specific genomic regions and help drive locus-specific chromatin remodeling events [33], [34], [37], [49],

[63], [64]. The HMTs responsible for the addition of methyl groups to histones are sometimes capable of writing more than one modification state, but often must work in concert with other proteins and HMTs to generate all three modification states genome-wide [59], [60], [65]-[69].

Histone H3, one of the four core histones, contains several well-characterized lysine targets for modification by methyltransferases within its N-terminal tail, including H3K4, H3K9, H3K27, and H3K36. In eukaryotes where methylation is detected at these positions, some methylation events are linked to gene repression and facilitating a closed chromatin conformation (H3K9me and H3K27me), while methylation at other H3 lysines is connected to active gene transcription and facilitating an open chromatin conformation (H3K4me and H3K36me) [30], [47], [59], [60], [63], [65], [70], [71]. Another conserved site of histone H3 methylation in organisms ranging from ciliates to mammals is H3K23. Although the biological roles for methylation on this residue are poorly characterized, they have been associated with gene repression and maintaining genome integrity [48], [72], [73]. While methyltransferases catalyzing H3K23 methylation have been identified in protists, nematodes, and plants, mammalian writers of these methylation marks have not been reported.

In this chapter, we report that H3K23 represents a new target of the enzymes euchromatic histone methyltransferase 1 (EHMT1/GLP) and euchromatic histone methyltransferase 2 (EHMT2/G9a). More specifically, we report that while both EHMT1/GLP and EHMT2/G9a enzymes can catalyze the addition of mono- and di-methylation on H3K23, only EHMT1/GLP can catalyze the addition of tri-methylation on H3K23 *in vitro*. Additionally, we show that perturbations in EHMT1/GLP and/or

EHMT2/G9a at either the protein or gene level decreased methylation on H3K23 *in vivo*. Interestingly, our *in vitro* and *in vivo* studies also revealed H3K18 as a new target for mono-, di- and tri-methylation by both EHMT1/GLP and EHMT2/G9a. Additionally in this chapter, we explore readers of H3K18me and H3K23me and show that while they may share writers, they likely have non-overlapping readers. Lastly, we identify combinatorial modification states involving H3K18 methylation and H3K23 acetylation, which may shed light on the functional role of these combinatorial states. Taken together, this work establishes histone H3 lysines 18 and 23 as new methylation targets for EHMT1/GLP and EHMT2/G9a, identifies their differential activity on H3K23 and explores the reading and combinatorial modification states as it relates to histone H3 lysines 18 and 23.

ii. Methods

Cell Culture Methods 50B11 cells were grown and propagated in culture as described previously [59]. Briefly, growth media consisted of NeuroPlex Serum-free Neuronal Medium (Gemini Bioscience, #600-300) and supplemented with Fetal Bovine Serum (10% final, Gemini Biosciences, Cat. 100-106), 100 mM L-Glutamate (275 uM final, Gibco, Cat. 25030-081), 20% glucose (0.2% v/v final), and 10X Gem21 NeuroPlex supplement (1X final, Gemini Biosciences, Cat. 400-160). 50B11 cells were grown in an incubator at 37C, 5% CO_2 and were passaged no more than 5 times. HEK293 and MC38 cells were grown in 1X DMEM media (Gibco, Cat. 11995-065) containing 10% v/v FBS (Gemini Biosciences, Cat. 100-106) and 1X Penn/Strep (Gibco, Cat. 10378-016) and were passaged no more than 5 times. Mouse ESCs were grown on TC treated plates coated with 0.1% w/v gelatin (Millipore-Sigma, Cat. ES-006-B) with 1X DMEM media (Gibco, Cat. 11995-065) containing 15% v/v knock-out serum replacement

(ThermoFisher, Cat. 10828010), 2-mercaptoethanol (100 uM, Gibco, Cat. 31350-010), non-essential amino acids (1X, Sigma, Cat. M7145-100mL), glutamine (2 mM, Gibco, Cat. 25030-081), 1X Penn/Strep as previously described. Mouse ESCs were passaged every 1-2 days to remove differentiated cells and media was changed daily. All cell types were harvested by washing cells 3X in 1X DPBS (Gibco, Cat. 14190-136), trypsinization, and spinning down at 500 rpm at 4C to pellet cells. All mammalian cell lines were STR profiled and mycoplasma tested for interspecies contamination and mycoplasma bacteria, respectively.

Generation of transgenic 50B11 cells expressing mutant histones Plasmids encoding mammalian histone H3.1 with various lysine to methionine mutants were constructed using iterative rounds of mutagenic PCR. Once sanger-sequence validated, the resulting H3.1 mutant DNA sequence was subcloned into a lentiviral vector (pLVX-IRES-mCherry). To prepare lentivirus containing the construct encoding the mutant histone, HEK293 cells were plated and grown in 1X DMEM (containing 10% FBS and 1X Penn/Strep) to approximately 70% confluency. To transfect HEK293 cells, Fugene transfection reagent was mixed with 400 uL complete DMEM media and incubated at room temperature for 5 minutes at a ratio of 3:1 of Fugene to total DNA. To the Fugene/DMEM mixture, 5 ug of the vector encoding mutant H3.1, 3.75 ug of Δ8.9 packaging plasmid and 2.5 ug of VSV-G envelope plasmid was added and allowed to incubate at room temperature for 15 minutes. The resulting mixture was added to HEK293 cells and incubated at 37C for 3 hours. 90 uL of 1M sodium butyrate was added (final concentration 110 mg/mL). The following day, the media was discarded

and replaced with Opti-MEM, without 1X Penn/Strep, and allowed to incubate for 12-18 hours. The virus-enriched supernatant was collected and stored at 4C. This process was repeated 3 times, each time pooling the viral supernatant. Pooled viral supernatant was filtered through a 0.45 uM filter to remove any HEK293 cells carried over. 0.5 mL of viral supernatant was used to transduce 50B11 cells for 24 hours. Following transduction, the media was removed and cells allowed to incubate for 2 days. At this point, a small portion of the heterogeneously transduced cells were collected for analysis (Supplementary Figure 3B). The remaining cells were FACS sorted for high vs low mCherry expression into wells in a 384 well plate (1 cell per well). Colonies were expanded, harvested, lysed, and western blotting was performed to evaluate FLAG expression as well as for various tri-methyl lysine histone modifications.

Generation of mouse ESCs

Wild-type and transgenic mouse ESCs (G9a -/-, GLP -/-, G9a/GLP -/-) were graciously provided by the lab of Dr. Yoichi Shinkai from the Cellular Memory Laboratory at the RIKEN Advanced Science Institute in Japan and generated as previously described [35]. KO cells were validated via western blotting.

In vitro histone methyltransferase assay *In vitro* histone methyltransferase reactions were prepared in buffer containing 20 mM Tris, pH 8.0, 50 mM NaCl, 1 mM EDTA, 3 mM $MgCl_2$, 0.1 mg/mL BSA, 1 mM DTT, 20 uM S-adenosyl methonine (Promega, Cat. V7601), 1 ug human recombinant H3.1 (New England Biolabs, Cat. M2503S) and 10 ng of either EHMT1/GLP (Active Motif, Cat. 31920) or EHMT2/G9a (Active Motif, Cat.

31410) and allowed to incubate for 18-24 hours at 25C. Reactions were quenched with TFA (0.012% v/v final concentration). Following quenching, samples were submitted for EthD mass spectrometry or used for western blotting analysis. To prepare samples for western blotting, 1X SDS sample buffer and 1 uL of BME was added to the reactions and the samples were incubated at 98C for 5 min, cooled, run on a 16% acrylamide gel, transferred to a PVDF membrane, and blotted for various histone H3 methyl-lysine marks (blotting conditions below).

In vitro histone methyltransferase inhibition assay *In vitro* histone methyltransferase reactions were prepared in buffer containing 20 mM Tris, pH 8.0, 50 mM NaCl, 1mM EDTA, 3 mM $MgCl_2$, 0.1 mg/mL BSA, 1mM DTT, and 10 uM UNC0642 (or the corresponding amount of DMSO as a control), 20 uM S-adenosyl methonine, 1 ug human recombinant H3.1 and 10 ng of either EHMT1/GLP or EHMT2/G9a. These reactions were allowed to incubate for 18-24 hours at 25C. Reactions were quenched with TFA (0.012% v/v final concentration). 1X SDS sample buffer and 1 uL of BME was added to the reactions and the samples were subjected to SDS-PAGE separation (run on a 16% acrylamide gel) followed by western blotting against the histone modifications of interest (see blotting conditions below). To assess enzymatic turnover of SAM to SAH by the HMTs, the MTase-Glo kit (Promega, V7601) was used.

In vivo GLP/G9a inhibition with UNC0642 The corresponding mammalian cell line was cultured in the appropriate media containing 10 uM UNC0642 inhibitor (Sigma Aldrich

HY-13980) or the corresponding volume of DMSO as a control for 5 days (media changed daily). All mammalian cell lines were grown at 37C, 5% CO_2.

Mass Spectrometry Sample Preparation:

Each 5 ug of recombinant histone was first resuspended in 50 ul of 20 mM Ammonium Bicarbonate pH 8.5. Samples were then reduced by adding 5 uL of 7.5 mg/ml (DTT) and put on a heat block at 60C for 1 hr. After cooling to room temperature samples were then alkylated with 5 uL of 18.5 mg/mL iodoacetamide for 15 min at room temperature in the dark before adding 0.5 ug of Lysyl Endopeptidase MS Grade (Wako/Fuji Osaka, Japan) to make a protein/protease ratio of 10:1. Samples were digested overnight at 37C before adding 10 ul of 10% v/v TFA and evaporated to dryness in a speed vac and stored at -80C. Prior to analysis, samples were resuspended in 100 ul of 10 mM TEAB and subjected to SPE cleanup using stage tips constructed with styrenedivinylbenzene disks (Empore SDB-XC, 3M Corp.) under basic conditions. This was found to be necessary for retention due to the extremely hydrophilic nature of the modified peptides. Stage tips were wetted with 20 ul 100% acetonitrile followed by preparation with two 20ul aliquots of 10mM TEAB followed by loading of 20ul of the resuspended solution or 1ug of LysC digested protein. This was then eluted with a solution of 10mM TEAB in 75% v/v acetonitrile and evaporated to dryness.

Mass Spectrometry Analysis:

Due to significant loss of these early eluting peptides, a direct on column approach was taken for the stage tipped samples. The entire 1 ug aliquot was resuspended in 5 ul of 2% v/v acetonitrile, 0.1% formic acid and loaded onto the nanoLC column (75um x 20cm in house packed with ReproSil-Pur C18-AQ, 3um Dr. Maisch, Ammerbuch, Germany) at 500 nl/minute using an EasyLC chromatography system (Thermo Scientific). Once the entire volume was loaded onto the column a shallow gradient was started at 300 nl/minute into an Orbitrap Fusion Lumos mass spectrometer (Thermo Scientific) equipped with Electron Transfer Dissociation (ETD) capability. The samples were run in HCD mode at first but none of the methylated peptides were positive hits when searched. Upon switching to EThcD, several of the isoforms of methylated peptides were found to exist in the +4, +5, and +6 charge states eluting early in the run before the bulk of the unmodified peptides. Since the methylation of the lysines creates a missed cleavage by the LysC enzyme, the peptides were found to be methylated at K18, K23, and K27 of the same peptide in a variety of permutations. Tri-methylation on K27 and K18 were easily detected, but the H3K23 tri-methyl lysine was not found in the first few runs. At that point, a permutation mass to charge list was created in Skyline (University of Washington) consisting of all peptides that contain a H3K23 tri-methylation in the +4, +5, or +6 and the list was imported as an inclusion list into the instrument acquisition parameters giving the expected peptides priority over any other m/z. The final method of acquisition ran with a 60-minute gradient using a resolution of 120,000 for precursors and 60,000 for fragment ions. The instrument was run using ETD mode with a supplemental collision energy of 20 (EThcD). Since duty cycle was

not an issue with the targeted run, the AGC target and maximum injection time were each set to 1000 giving maximum sensitivity for the inclusion masses.

Mass Spectrometry Data Analysis:

Mass spec data were searched against the UniProt version 5640 Homo sapiens database using Mascot search engine version 2.8.0 through Proteome Discoverer version 2.5. The search parameters were set to include up to 5 missed cleavages with LysC as the enzyme and EThcD as the instrument type. Mass tolerances were set to 5 ppm for precursors and 20 ppm for fragments, although this was later filtered to 2 ppm for all conclusive spectra. Dynamic modifications were set as methyl K, di-methyl K, and tri-methyl K, in addition to oxidation on methionine and deamidation on asparagine and glutamine. Carbamidomethylation was set as a static modification. Database hits were filtered at the 1% FDR level using target-decoy validation.

In vitro peptide pulldowns To prepare beads for the peptide pulldown, 25 uL of M280 Streptavidin-conjugated Dynabeads (Invitrogen, Cat. # 11205D) were washed three times with 1X PBS-T (0.1% Triton-X 100) and resuspended in 500 uL of 1X PBS-T. 1 ug of biotinylated peptide was added and allowed to incubate for 1 hour at room temperature. Following peptide conjugation, the peptide-conjugated beads were washed with 1X PBS-T three times to displace any unconjugated peptide. Following the washes, 2 ug of the recombinantly expressed EHMT2/G9a (Active Motif 31410) or 5 ug of recombinantly expressed EHMT1/GLP (Active Motif 31920) was incubated with the peptide-conjugated dynabeads overnight at 4C with mild agitation. Following incubation,

the beads were washed with buffer containing 300 mM KCl, 0.2% v/v Triton-X 100, 1 mM PMSF. Tubes containing the beads were changed on the fifth wash to eliminate any contaminating protein remaining on the sides of the tube. Following the tube-change, a sixth wash was performed. Following the last wash, the beads were resuspended in 1X SDS loading buffer, boiled and subjected to SDS-PAGE for analysis. Flag-tagged EHMT2/G9a was blotted using 1:10,000 anti-Flag antibody (Sigma F1804) followed by a 1:10,000 anti-mouse secondary incubation (GE Healthcare, NA9310). GST-tagged EHMT1/GLP was blotted using anti-GST antibody 1:10,000 (GE Healthcare, 27457701) followed by a rabbit anti-goat HRP secondary incubation (Invitrogen, A27014). The biotinylated peptides were blotted using streptavidin-HRP conjugate (Sigma, #RABHRP3, 1:10,000, 1 hr room temperature). All western blots were imaged using an Acura Biosystems Imager.

In cellulo peptide pulldown from nuclear extracts To prepare beads for the peptide pulldown, 25 uL of M280 Streptavidin-conjugated Dynabeads were washed three times with 1X PBST (0.1% Triton-X 100) and resuspended in 500 uL of 1X PBST. 1 ug of biotinylated peptide was added and allowed to incubate for 1 hour at room temperature. Following peptide conjugation, the peptide-conjugated beads were washed with 1X PBS-T three times to displace any unconjugated peptide. To prepare the nuclear protein extract for pulldown, 50B11 nuclei were harvested by resuspending cells in lysis buffer (250 mM Sucrose, 1 mM phenylmethylsulfonly fluoride (PMSF) protease inhibitor, 1 mM sodium butyrate, 0.1% Triton-X 100, 5mM $MgCl_2$, 50 mM Tris, pH 7.4, 5 mM KCl) followed by dounce homogenization (60-100 dounces per sample). The lysate was spun

down at 500 rpm for 5 minutes at 4C to pellet intact nuclei. Intact nuclei were transferred to a 1.5 mL Eppendorf tube and total packed cell volume was estimated visually. Nuclei were then resuspended in a high salt extraction buffer (20 mM Hepes, pH 7.9, 25% glycerol, 500 mM KCl, 1.5 mM $MgCl_2$, 0.2 mM EDTA, 1mM DTT and 1mM PMSF) and allowed to extract at 4C for at least four hours. The extract was spun down at 16,000 rpm at 4C for 10 minutes to pellet the insoluble nuclear debris. The supernatant was transferred to a different 1.5 mM Eppendorf tube and was diluted with buffer containing 20 mM Hepes, pH 7.9, 25% glycerol, 1.5 mM $MgCl_2$, 0.2 mM EDTA, 1 mM DTT and 1 mM PMSF such that the final KCl concentration is 150 mM. The resulting diluted extract was quantitated using a BCA assay. The quantitated nuclear protein extract was added to the peptide-conjugated beads at a concentration of 1 mg of total protein per peptide pulldown. The pulldown proceeded overnight at 4C. The following day, the protein extract is removed and the beads are washed six times with buffer containing 300 mM KCl, 0.2% Triton-X 100, 1mM PMSF followed by a final wash containing 4 mM LiCl, 10 mM Hepes, pH 7.9. The peptides/pulled-down proteins were eluted by resuspending the beads in 1X SDS sample buffer and boiling for 5 minutes. The resulting eluate is collected and subjected to SDS-PAGE followed by western blotting to detect the proteins of interest.

ELISA antibody validation: Histone methyl-lysine peptides were serially diluted in high-bind, hydrophobic 96-well plates (Sigma, #M9410) and allowed to incubate 37C, 100 rpm, overnight. The following day, plates were washed with 1X PBS twice, and blocked with 1X PBS containing 4% BSA for 2 hours, 37C. Following blocking, plates were

washed twice with 1X PBS containing 0.15% Tween-20. All antibodies were diluted 1:10,000 in 1X PBS (containing 4% BSA and 0.15% v/v Tween-20), added to plates and allowed to incubate at 37C for 2 hours. Peptide competition reactions were pre-incubated 2 hours at room temperature with the respective antibody prior to addition to the ELISA plates. Following incubation with primary antibody, the plates were washed 3X with 1X PBS containing 0.15% v/v Tween-20 and incubated with secondary antibody (1:10,000) for 2 hours at 37C. Following incubation in secondary antibody, the plates were washed 3X with 1X PBS containing 0.15% v/v Tween-20. The plates were then incubated with buffer containing dibasic sodium phosphate (20 mM), citric acid (10 mM) and fresh hydrogen peroxide (final concentration: 0.0012%), and incubated for 30 minutes at room temperature in the dark. The reaction was quenched with 1M H_2SO_4 and imaged on a spectrometer at 492 nm. All data is represented in supplemental figure 5.

Western blotting conditions for *in vitro* HMT and *in vivo* inhibition assays:

anti-H3K9me1; abcam 8896; 1:5,000

anti-H3K9me2; active motif 39753; 1:5,000

anti-H3K9me3; abcam 8898; 1:5,000

anti-H3K18me1; diagenode C15410290; 1:500

anti-H3K18me2; diagenode C15410291; 1:500

anti-H3K18me3; diagenode C15410292; 1:500

anti-H3K23me1; active motif 39387; 1:10,000 (1:500 for *in vivo*)

anti-H3K23me2; abcam 214654; 1:2000

anti-H3K23me3; active motif 61499; 1:500

anti-H3K27me1; active motif 61015; 1:500

anti-H3K27me2; active motif 61435; 1:1000

anti-H3K27me3; Millipore sigma 07-449; 1:5,000

anti-EHMT1/GLP; abcam ab41969; 1:500

anti-EHMT2/GLP; abcam ab185050; 1:500

anti-Actin; Thermo Fisher MA1-91399; 1:2,000

anti-H3; abcam ab1791; 1:5,000

anti-GST; GE Healthcare, 27457701; 1:10,000

anti-Flag; sigma Aldrich F1804; 1:10,000

iii. Results

EHMT1/GLP and EHMT/G9a can *de novo* methylate histone H3K18 and H3K23 *in vitro*

While H3K23 methylation has been observed in mammalian chromatin, mammalian HMTs that catalyze H3K23 methylation have not been reported. However, in other species such as *A. thaliana*, *C. elegans* and *T. thermophila*, histone methyltransferases that modify or are similar to those that modify H3K9 and H3K27 have been shown to also target H3K23 [48], [72]-[74]. To screen which mammalian HMTs act on histone H3K23, we employed an *in vitro* histone methyltransferase assay. We chose to screen potential H3K23 methyltransferase activity of six known mammalian H3K9 methyltransferases, Suv39h1, Suv39h2, SetDB1, SetDB2, EHMT1/GLP, and EHMT2/G9a. As previously reported [11], [17], [31], [60], recombinant Suv39h1, Suv39h2, SetDB1, SetDB2, EHMT1/GLP, and EHMT2/G9a, were all able to *de novo*

methylate H3K9 to different extents (data not shown). Of the HMTs screened, only EHMT1/GLP and EHMT2/G9a showed activity on H3K23. More specifically, our data shows that while both EHMT1/GLP and EHMT2/G9a can mono- and di-methylate H3K23, only EHMT1/GLP can tri-methylate H3K23 as evaluated both by western blotting using histone modification specific antibodies for H3K9 and H3K23 (Figure 10A) and Electron Transfer Dissociation (EthD) mass spectrometry (Figure 10C). To validate that EHMT1/GLP and EHMT2/G9a were not indiscriminately targeting lysines on H3, we tested for two additional well described histone H3 tri-methyl marks by western blotting: H3K4me3 and H3K36me3. Our data shows that neither H3K4me3 nor H3K36me3 are generated in our *in vitro* HMT system by EHMT1/GLP or EHMT2/G9a, suggesting that these enzymes are indeed discriminating between targets and methylation states (Supplemental Figure 1B). In our western blotting and mass spectrometry analysis, we also observed EHMT1/2-dependent H3K27 and H3K18 methylation to various extents (Figure 10A and C and Supplemental Figure 1B). While the ability of EHMT1/GLP and EHMT2/G9a to catalyze methylation at H3K27 has been previously reported [75], we could not find examples in the literature of either of these two enzymes targeting H3K18. Finally, to ensure that the differential production of certain methylation states at specific targets was not due to differential enzyme activity or enzyme abundance, we measured turnover of SAM in each reaction at two different, non-saturating, substrate conditions (0.5 ug and 1 ug of rH3.1) while keeping the enzyme concentration constant (Figure 10B). Our data shows that enzyme activity is comparable even at different concentrations of substrate, suggesting that the rate of turnover of SAM is comparable between both enzymes. A summary of methylation sites targeted by EHMT1/GLP and

A.

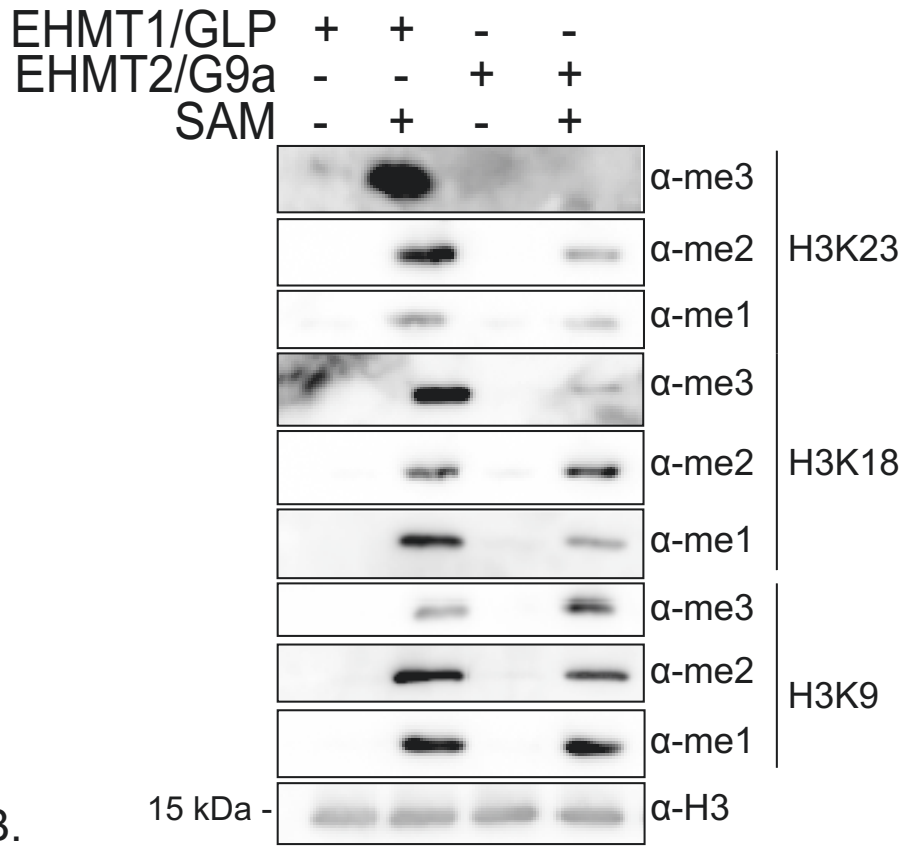
EHMT1/GLP + + - -
EHMT2/G9a - - + +
SAM - + - +
α-me3
α-me2
α-me1
H3K23
α-me3
α-me2
α-me1
H3K18
α-me3
α-me2
α-me1
H3K9
15 kDa -
α-H3

B.

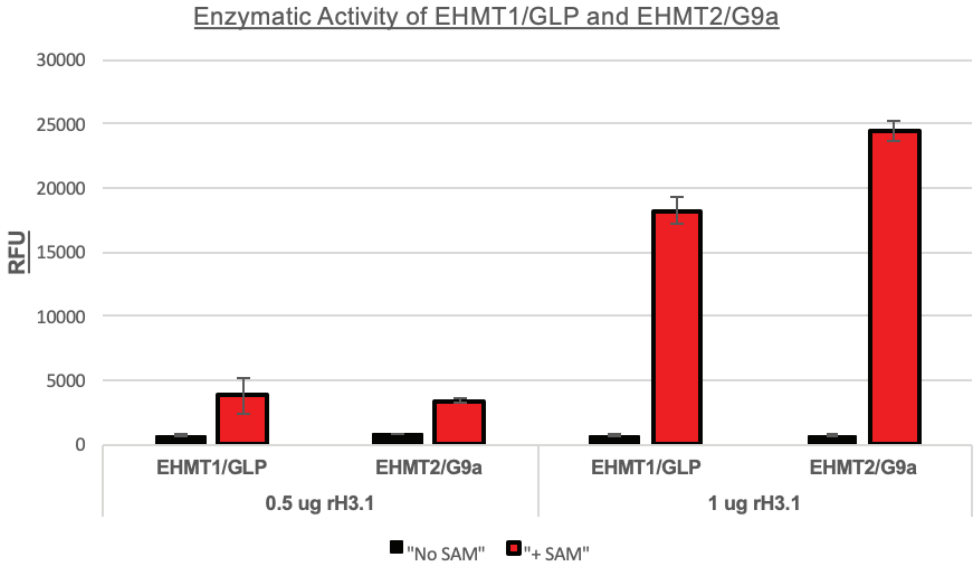
Enzymatic Activity of EHMT1/GLP and EHMT2/G9a
30000
25000
20000
15000
10000
5000
0
RFU
EHMT1/GLP
EHMT2/G9a
EHMT1/GLP
EHMT2/G9a
0.5 ug rH3.1
1 ug rH3.1
"No SAM"
"+ SAM"

C.

H3K23me1 (EHMT1/GLP) Annotated Spectrum

APRK$_{18}$QLATK$_{23}$AARK$_{27}$SAPATGGVK$_{36}$

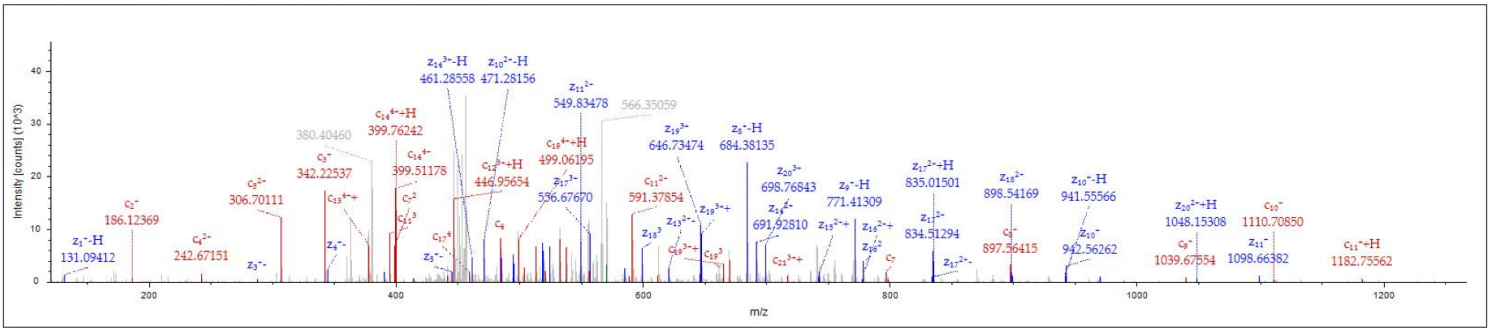

H3K23me2 (EHMT1/GLP) Annotated Spectrum

APRK$_{18}$QLATK$_{23}$AARK$_{27}$SAPATGGVK$_{36}$

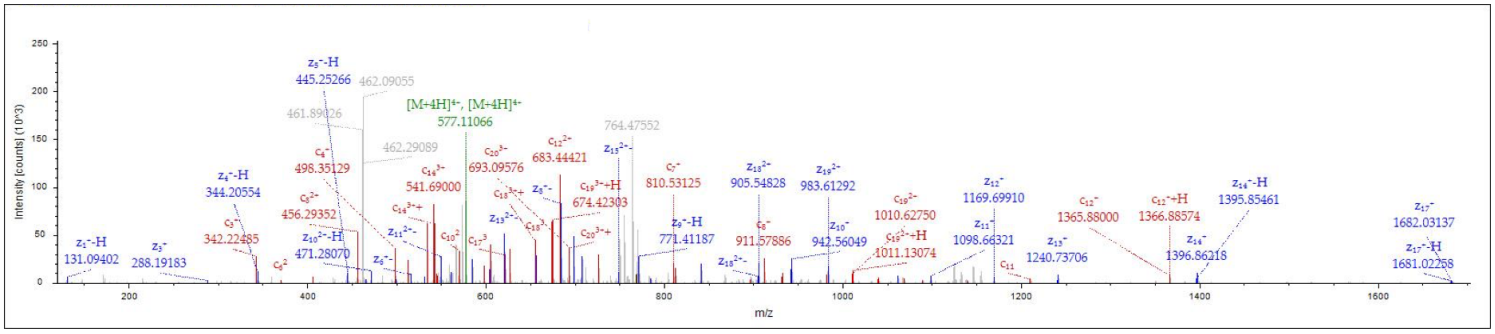

H3K23me3 (EHMT1/GLP) Annotated Spectrum

APRK$_{18}$QLATK$_{23}$AARK$_{27}$SAPATGGVK$_{36}$

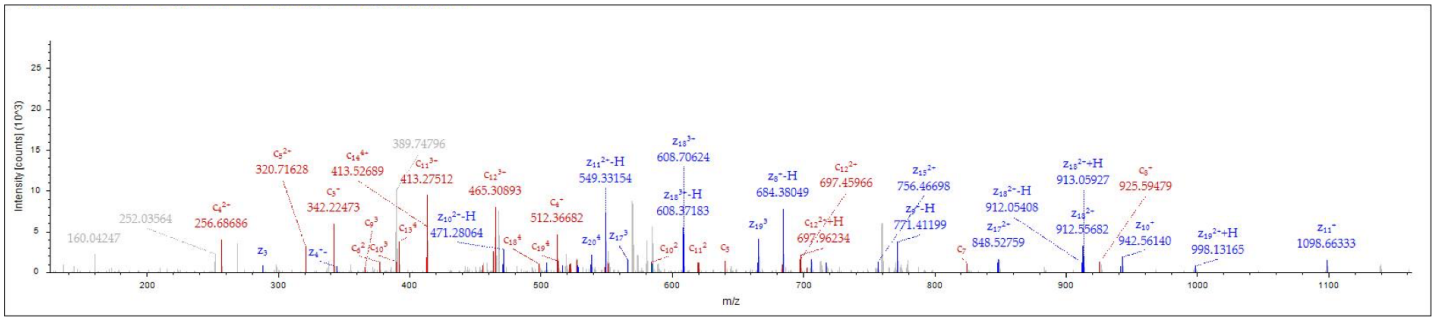

D.

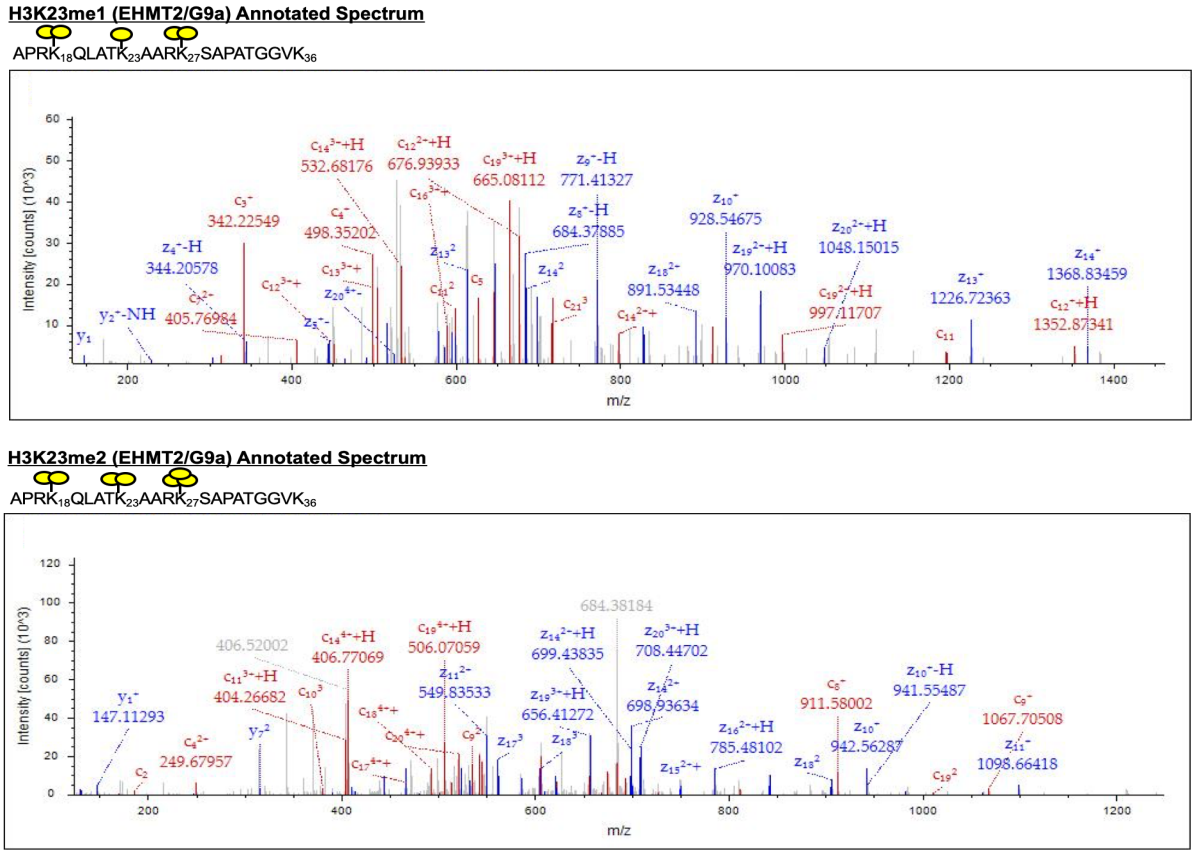

E.

Table 1: Summary of Histone H3 methylation produced by EHMT1/GLP

	Mono-methyl	Di-methyl	Tri-methyl
Lysine 4	x	x	x
Lysine 9	✓	✓	✓
Lysine 14	x	x	x
Lysine 18	✓	✓	✓
Lysine 23	✓	✓	✓
Lysine 27	✓	✓	✓
Lysine 36	x	x	x

Table 2: Summary of Histone H3 methylation produced by EHMT2/G9a

	Mono-methyl	Di-methyl	Tri-methyl
Lysine 4	x	x	x
Lysine 9	✓	✓	✓
Lysine 14	x	x	x
Lysine 18	✓	✓	✓
Lysine 23	✓	✓	x
Lysine 27	✓	✓	✓
Lysine 36	x	x	x

Figure 10 GLP and G9a *de novo* methylate H3K9, H3K18 and H3K23 *in vitro* (A) Western blot panel of H3K9, H3K18 and H3K23 methylation states produced by EHMT1/GLP or EHMT2/G9a via the *in vitro* HMT reactions **(B)** EHMT1/GLP and EHMT2/G9a enzyme activity at two concentrations of rH3.1 substrate, measured by the MTase-Glo assay **(C)** Annotated mass spectra of H3K18/K23/K27 methylation states produced by EHMT1/GLP HMT reactions **(D)** Annotated mass spectra of H3K18/K23/K27 methylation states produced by EHMT2/G9a HMT reactions **(E)** Tables summarizing targets and methylation states detected in the EHMT1/GLP and EHMT2/G9a HMT reactions.

EHMT2/G9a as detected by our combined western blotting and mass spectrometry data and can be found in Table 1. Taken together, this data identifies H3K18 and H3K23 as new targets of EHMT1/GLP and EHMT2/G9a.

Pharmacologic inhibition of EHMT1/GLP and EHMT2/G9a by reduces H3K18 and H3K23 methylation levels *in vitro*

To further corroborate the enzymatic activity of EHMT1/GLP and EHMT2/G9a on H3K18 and H3K23, we assessed whether an inhibitor of these enzymes, UNC0642 [76], [77] reduce levels of H3K18 and H3K23 methylation states in our biochemical assay system. UNC0642 is a competitive inhibitor which binds the active site of the SET methyltransferase domain, and prevents the enzyme from accommodating a peptide substrate, like recombinant histone H3 [76]. To compare selectivity of the UNC0642 inhibitor among EHMT1/GLP, EHMT2/G9a, and other SET-domain containing H3K9 HMTs, we performed a UNC0642 dose titration against EHMT1/GLP, EHMT2/G9a, SetDB1, and Suv39h2, using the MTase-Glo activity assay. Of the four enzymes tested, only EHMT1/GLP and EHMT2/G9a showed a significant dose dependent decline in enzyme activity compared to a DMSO control (Figure 11A and Supplemental Figure 2A). This inhibition is consistent with prior studies showing specificity of UNC0642 to EHMT1/GLP and EHMT2/G9a as compared to other HMTs (PRMT3, SETD7, SETDB1, and SETD8) [29]. Using western blot analysis to evaluate the products of our *in vitro* methyltransferase reaction, we observed that incubation of recombinant EHMT1/GLP or EHMT2/G9a with UNC0642 causes a decrease in H3K9, H3K18 H3K23 methylation (Figure 11B). Additionally, we observed that UNC0642-treated EHMT1/GLP or EHMT2/G9a reactions decreased production of H3K27 methylation (Supplemental

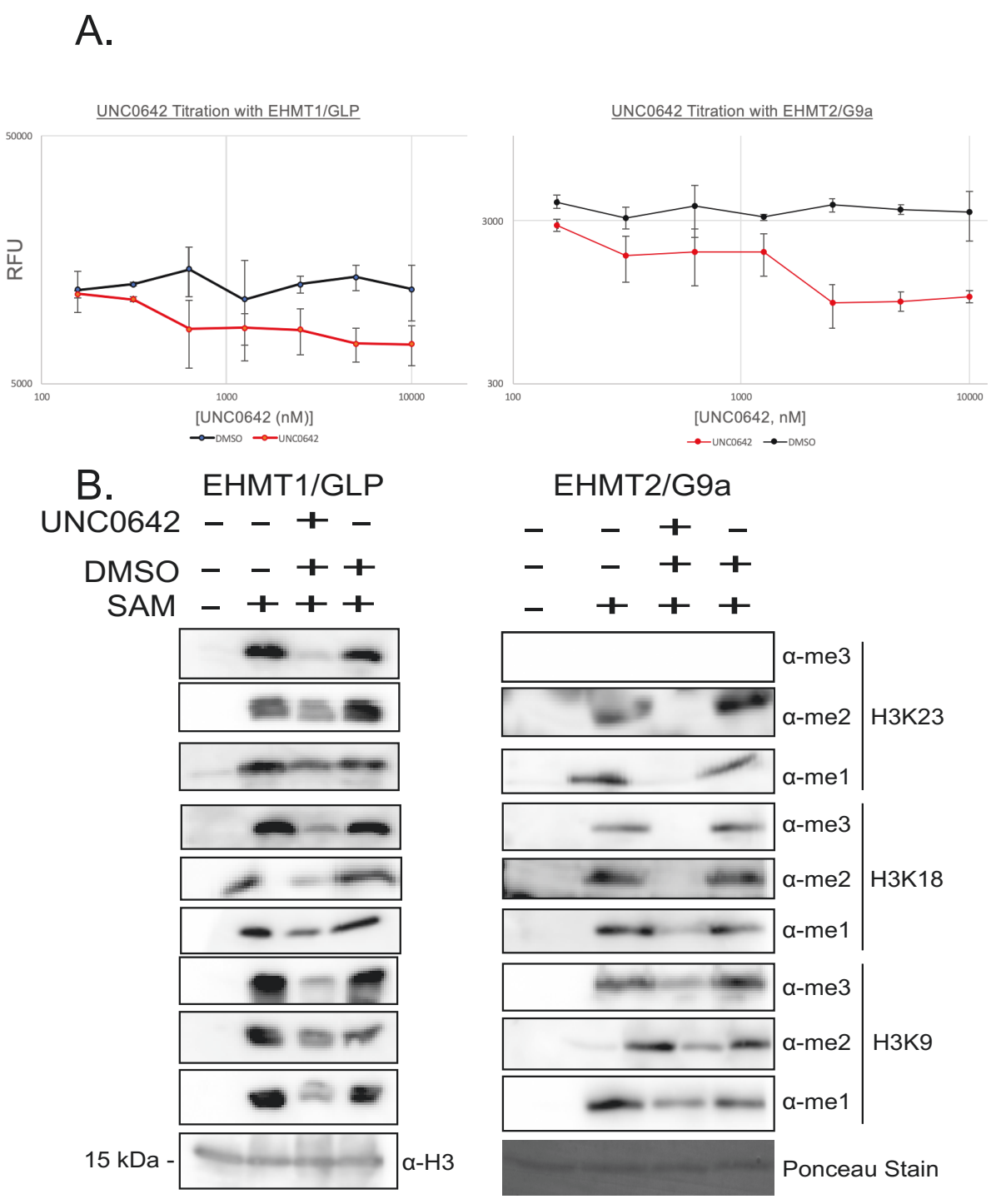

Figure 11 Pharmacologic inhibition of GLP and G9a reduces H3K9, H3K18 and H3K23 methylation levels in vitro. **(A)** UNC0642 dose titration (vs DMSO control) with EHMT1/GLP and EHMT2/G9a **(B)** Western blot panel of H3K9, H3K18 and H3K23 methylation states detected in the inhibited HMT reactions with EHMT1/GLP and EHMT2/G9a.

Figure 2C). This data suggests that specific enzyme activity of EHMT1/GLP and EHMT2/G9a is responsible for methylation at histone H3K9, H3K18, H3K23, and H3K27 *in vitro*.

Inhibition of EHMT1/GLP and EHMT2/G9a, by UNC0642, reduces H3K18 and H3K23 methylation levels in mammalian cells.

UNC062 has also been shown to inhibit EHMT1/GLP and EHMT2/G9a methyltransferase activity *in vivo* [76]-[78]. We treated various mammalian cell lines with 10 uM UNC0642 for five days, after which the cells were harvested, lysed, and blotted for various methylation states of histone H3K9, H3K18, and H3K23. Consistent with our *in vitro* studies, our data shows that treatment of 50B11 (rat), HEK293 (human), and MC38 (mouse) cell lines with UNC0642 decreased at least one of the methylation states of H3K9, H3K18, and H3K23, and to a lesser extent H3K27, *in vivo* when compared to a DMSO treated control (Figure 12). More specifically, mono- and di-methylation were greatly reduced, and tri-methylation was more subtly reduced, if at all, at H3K9, H3K18, H3K23, and H3K27. Taken together with the known selectivity of the UNC0642 inhibitor, this data implicates the enzymatic activity of EHMT1/GLP and EHMT2/G9a in the catalysis of H3K9, H3K18, H3K23, and H3K27 methylation *in vivo*.

Lysine-to-Methionine (K-to-M) mutations differentially bind EHMT1/GLP and EHMT2/G9a, and decrease H3K9, H3K18 and H3K23 methylation levels *in vivo*

It has been reported that certain lysine-to-methionine (K-to-M) mutations in histone proteins perturb methylation at residues harboring the mutation [55], [79], [80]. While the mechanism of methylation inhibition in K-to-M mutants is not well understood, structural

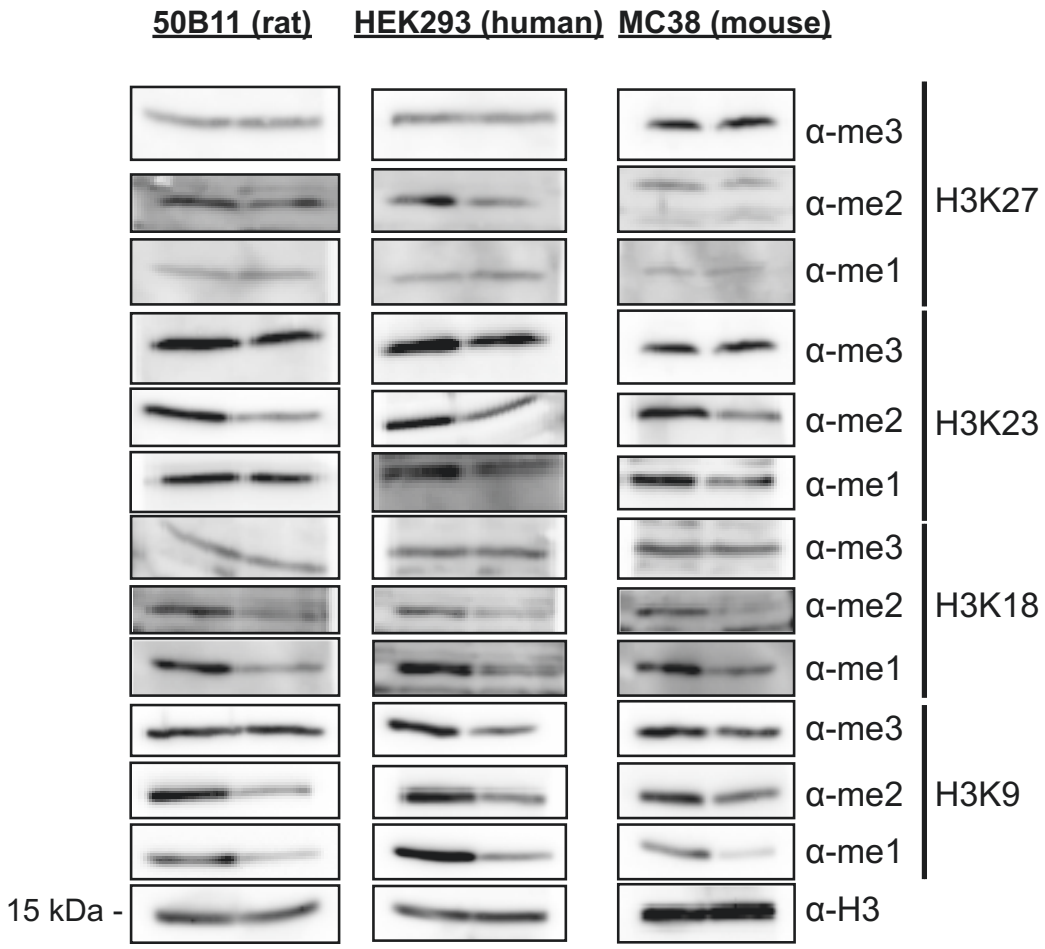

Figure 12 Pharmacologic inhibition of GLP and G9a decreases of H3K9, H3K18, H3K23 and H3K27 methylation states *in vivo*. Western blot panel of H3K9, H3K18, H3K23 and H3K27 methylation states in 50B11, HEK293 and MC38 mammalian cell lines treated with either DMSO or UNC0642.

and biochemical work suggests that the methionine mimics a mono-methylated lysine and sequesters the cognate histone methyltransferase (HMT) at the mutated residue, preventing it from methylating lysines on native histone tails [55], [79], [80]. We employed this K-to-M approach in an attempt to inhibit H3K23 methylation *in vivo*, and assessed the ability of these K-to-M mutant histones to bind EHMT1/GLP and EHMT2/G9a *in vitro*. Accordingly, we employed an *in vitro* peptide pulldown assay where we separately incubated recombinant EHMT1/GLP or EHMT2/G9a with biotinylated histone peptides representing unmodified H3K9, unmodified H3K23, and the corresponding biotinylated K-to-M mutant peptide. Interestingly, our data shows that while both enzymes interact with H3K9M peptide as expected [55], [79], [80], only recombinant EHMT2/G9a, not EHMT1/GLP, interacts with H3K23M peptide *in vitro* (Figure 13A). We next wondered if the H3K9M and H3K23M transgenes decrease H3K23 methylation *in vivo*, and generated transgenic 50B11 cells expressing wild type H3.1, H3K9M, or H3K23M mutant histones. Whole cell extracts from these lines were evaluated by western blotting for mono-, di-, and tri-methylation at H3K9 and H3K23. Interestingly, our data shows that mono- and di-, but not tri-methylation at H3K23 is perturbed in cells expressing H3K23M. Strikingly, our data also shows that only the di- and tri-, but not the mono-methylation states are perturbed in cells expressing H3K9M mutant histones (Figure 13B). To ensure that the effects of the H3K9M and H3K23M were not cell type specific, we engineered a similar set of K-to-M mutants in MC38 cells, and observed a similar ability of H3K9M, but not H3K23M, transgene to perturb H3K23me3 (Supplemental Figure 3A). We did not observe perturbation of H3K23 methylation in K-to-M mutations other than H3K9M or H3K23M (Supplemental Figure 4B). While our data also shows perturbations in H3K18 methylation

by H3K9M and H3K23M transgenes, we did not engineer an H3K18M cell line or peptide due to time constraints, but would be interested in evaluating if it reciprocally perturbs H3K9 and H3K23 methylation. Taken together, our data suggests that EHMT2/G9a, a writer of mono- and di-methylation at H3K18 and H3K23, can bind and be sequestered *in vivo* by H3K23M, which leads to global perturbations in mono- and di-methylation; whereas EHMT1/GLP, a di- and tri- methyltransferase for lysines 18 and 23, is sequestered by H3K9M, leading to global decreases in di- and tri-methylation at H3K18 and H3K23. This data also suggests that, *in vivo*, EHMT2/G9a may function as the principal mono- and di- methyltransferase for H3K18 and H3K23, while EHMT1/GLP could be the principal tri-methylase for H3K18 and H3K23.

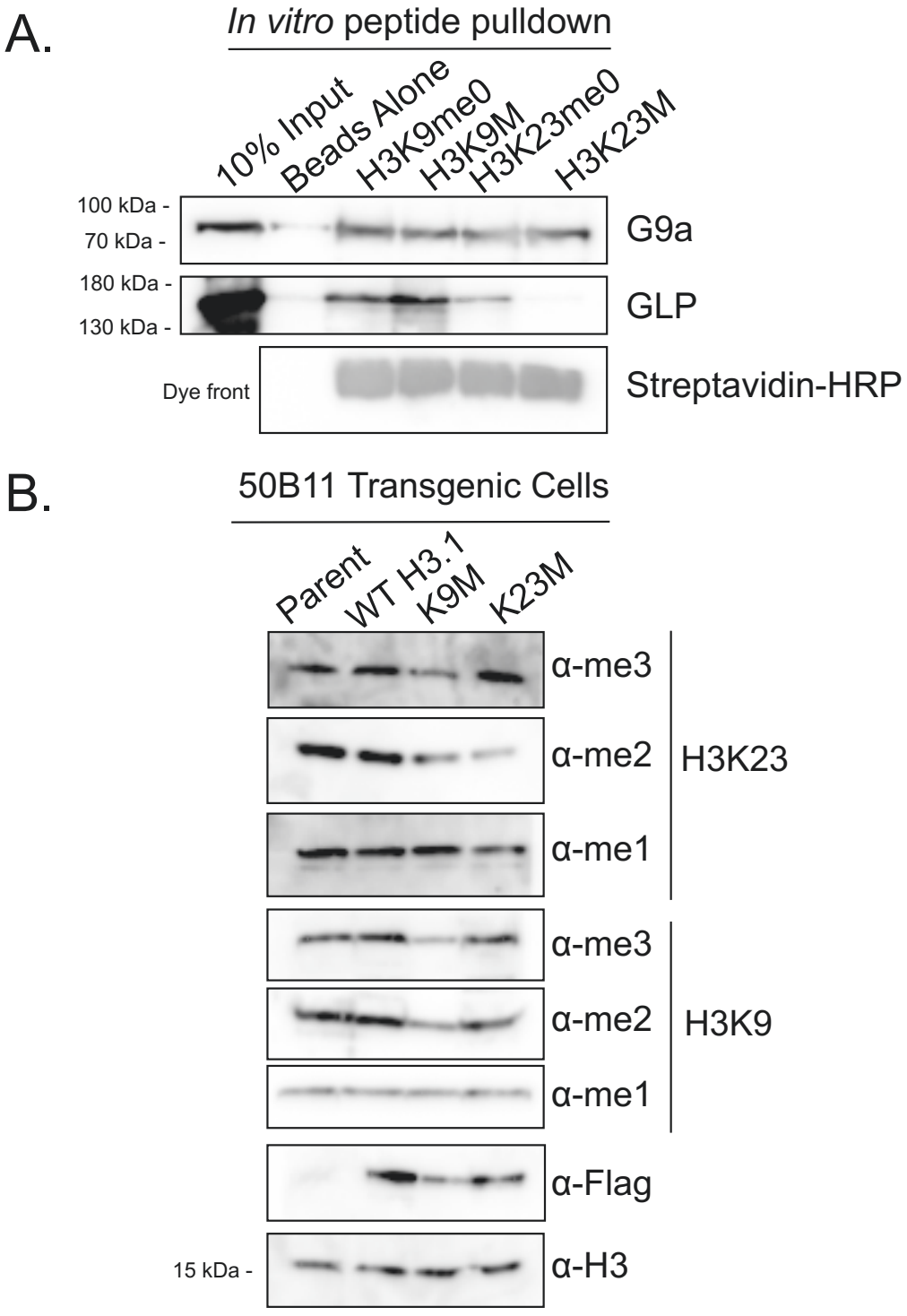

Figure 13 H3K23M perturbs H3K23me1 and H3K23me2 but not H3K23me3 and differentially interacts with GLP and G9a (A) *in vitro* peptide pulldown using H3K9me0, H3K9M, H3K23me0 and H3K23M peptides with recombinant EHMT1/GLP and EHMT2/G9a **(B)** Western blot panel of H3K9 and H3K23 methylation states in transgenic 50B11 clones expressing WT H3.1, H3K9M or H3K23M transgenes.

Deletion of either EHMT1/GLP, EHMT2/G9a, or both genes perturbs H3K18 and H3K23 methylation in mouse embryonic cells

To further validate that EHMT1/GLP and/or EHMT2/G9a contribute to H3K18 and H3K23 methylation levels *in vivo*, we tested mouse embryonic stem cells in which the genes for either EHMT1/GLP, EHMT2/G9a, or both enzymes were deleted, using western blotting analysis of various methylation states of histone H3K9, H3K18 and H3K23. Consistent with our inhibition studies, we observe that deletion of either EHMT1/GLP and/or EHMT2/G9A decreases levels of all methylation states of H3K9 and H3K23 (Figure 14). Interestingly, previous reports [75], [81] have shown that deletion of either EHMT1/GLP and/or EHMT2/G9a perturbs H3K27 methylation levels *in vivo*, which we were also able to observe (Supplemental Figure 4). Additionally, we observed that deletion of EHMT1/GLP, but not so much EHMT2/G9a, decreased H3K18 methylation levels *in vivo* (Figure 14). Taken together, this data suggests that EHMT1/GLP and/or EHMT2/G9a may indeed contribute to H3K18 and H3K23 methylation levels in mammalian cells, in addition to their well-established roles catalyzing H3K9 methylation, *in vivo*.

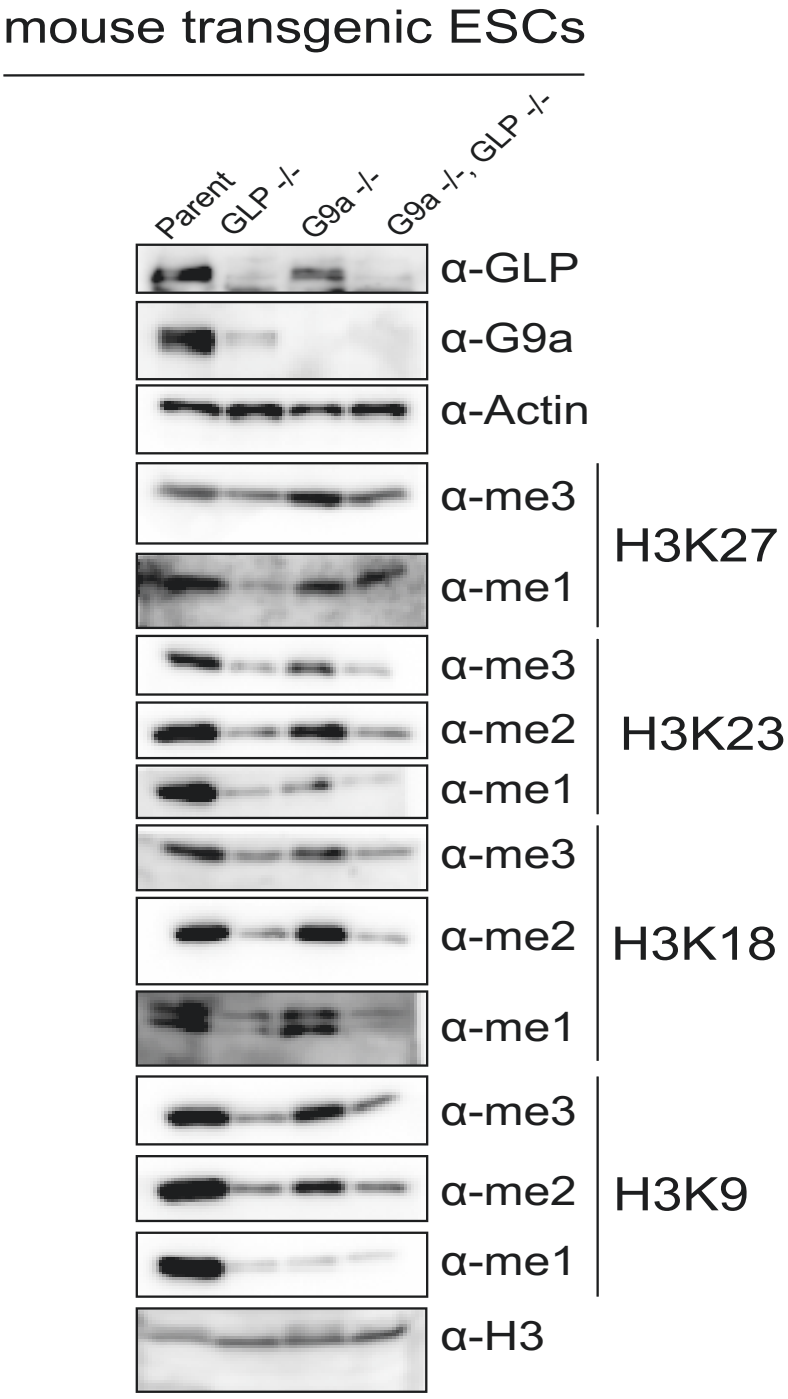

Figure 14 Deletion of GLP, G9a or both perturbs H3K9, H3K18, H3K23 and H3K27 methylation states *in vivo*. Western blot panel of H3K9, H3K18, H3K23 and H3K27 methylation states in mouse ESCs knocked down for GLP, G9a or both genes.

Peptide pulldown reveals potential readers of H3K18 and H3K23 methylation

With the identification of EHMT1/GLP and EHMT2/G9a as a shared writer for H3K9, H3K18, and H3K23 methylation, we next postulated that perhaps H3K18 and H3K23 also share a subset of H3K9 reader proteins. To accomplish this, we again used the *in vitro* peptide pulldown assay utilizing histone peptides with various methylation states installed at position 18 or 23 (and positions 4 and 9 as negative controls and positive controls, respectively). We incubated these peptides with known recombinant H3K9 reader proteins including HP1 alpha, HP1 beta, HP1 gamma, and the chromo-domain of MPP8. Interestingly, our data shows that while H3K9 and H3K23 methylation states interact with members of the HP1 family and the chromodomain of MPP8, no interactions were observed with any of the methylation states of H3K18 (Figure 15).

We next introduced a series of reader proteins that have been shown to promote an open chromatin state and interact with H3K4me3: Yng1 and ING5. Yng1 is a member of the NuA3 HAT complex, while ING5 is a human homolog of Yng1 and associates in the MOZ/MORF HAT complex. Both Yng1 and ING5 have been shown to interact with H3K4me3 (*in vitro* or *in vivo*, respectively),promote H3 acetylation and promote open chromatin confirmations [49], [82]. Intriguingly, our *in vitro* pulldown data shows that while no interactions of H3K9 or H3K23 were observed between Yng1 or ING5, certain methylation states of H3K18 did show an interaction with both Yng1 and ING5 *in vitro* (Figure 15).

To validate that the interaction between ING5 and H3K18 methylation is relevant *in vivo* (in mammals, rather than yeast), we performed an *in cellulo* peptide pulldown using methylated H3K18 peptides and whole-cell extract from 50B11. Consistent with

the *in vitro* pulldown, the *in vivo* pulldown shows a strong interaction between ING5 and H3K4me3 (the positive control) and a slightly weaker, but positive signal for H3K18me1, but not H3K23me1. This suggests that perhaps H3K18 methylation possesses readers of the ING-family of proteins, rather than heterochromatin proteins, and that these interactions are likely relevant *in vivo*.

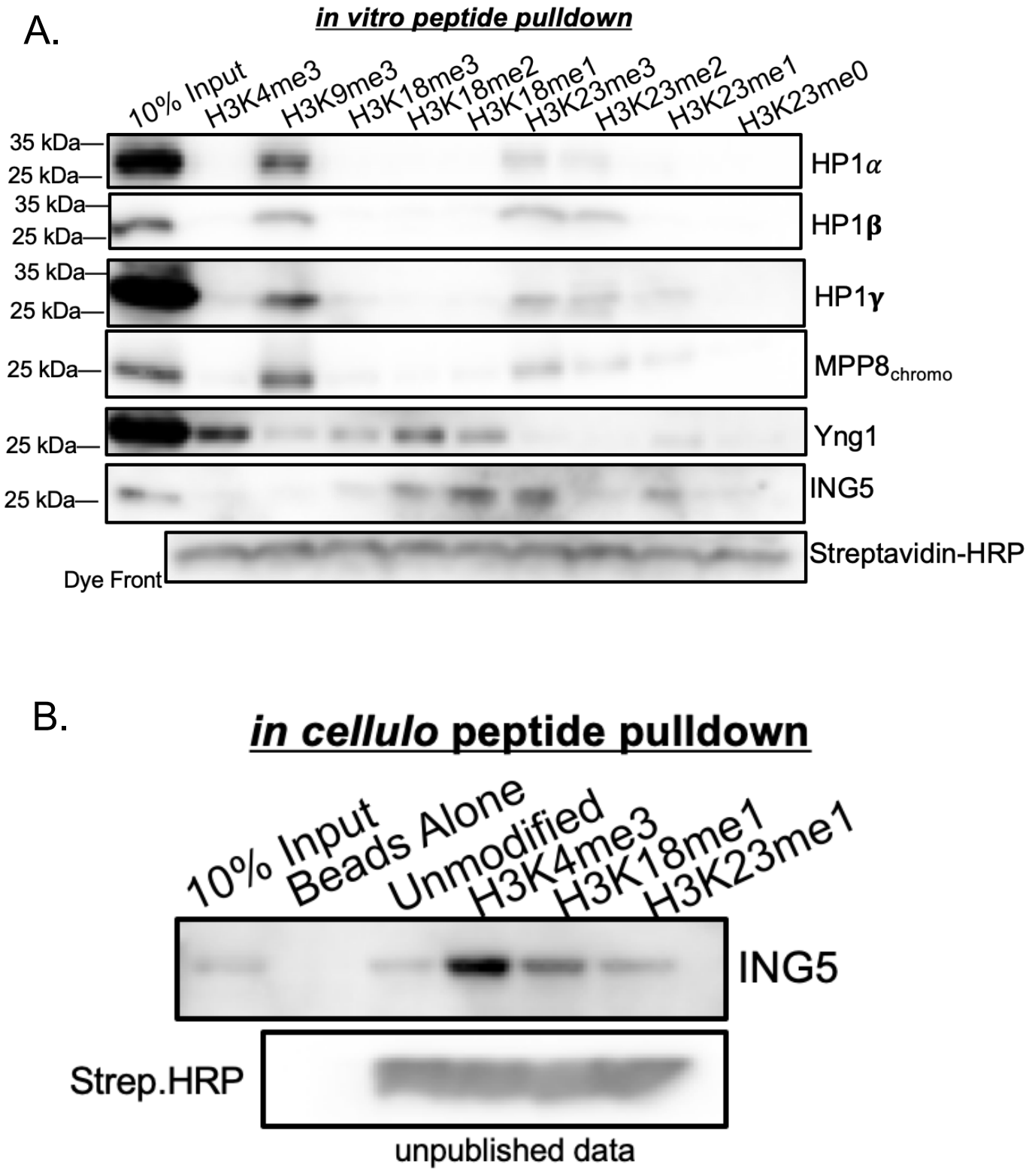

Figure 15 ***In vitro*** **peptide pulldown reveals readers of H3K18 and H3K23 methylation (A)** In vitro peptide pulldown with H3K4, H3K9, H3K18, H3K23 methylated peptides with common H3K9 and H3K4 reader proteins **(B)** Western blot panel of ING5 *in cellulo* peptide pulldown with H3K4me3, H3K18me1 and H3K23me1 peptides from 50B11 whole cell lysate.

In cellulo mono-nucleosome pulldown reveals combinatorial H3K18 methylation states

To expand on the data suggesting that H3K18 methylation and ING-family proteins interact *in vivo*, we sought to investigate if we could detect certain combinatorial modification states involving H3K18 methylation and H3 acetylation as was suggested through prior studies involving Yng1 and ING5 interactions with H3K4me3 [49], [82]. As previously mentioned, ING5 is a member of the MOZ/MORF HAT complex that has been shown to target H3K23 for acetylation [83]. To interrogate H3K18me1 combinatorial states *in vivo*, we employed a mono-nucleosome pulldown assay whereby chromatin was isolated from native sources (50B11 nuclei) and subsequently digested with micrococcal nuclease into mono-nucleosomes and validated by gel electrophoresis (Figure 16A). We then pulled down nucleosomes containing H3K18me1 or H3K23Ac (and the corresponding IgG control) using native ChIP (nChIP). Following the pulldown, the immunoprecipitated nucleosomes were resuspended in SDS sample buffer, run on a 16% gel and blotted for various H3 methyl and acetyl marks. Interestingly, H3K23Ac can be detected on nucleosomes containing H3K18me1 and vice versa (Figure 16B). Taken together, this data suggests that H3K18 methylation might exist in combination with H3K23Ac on mammalian chromatin.

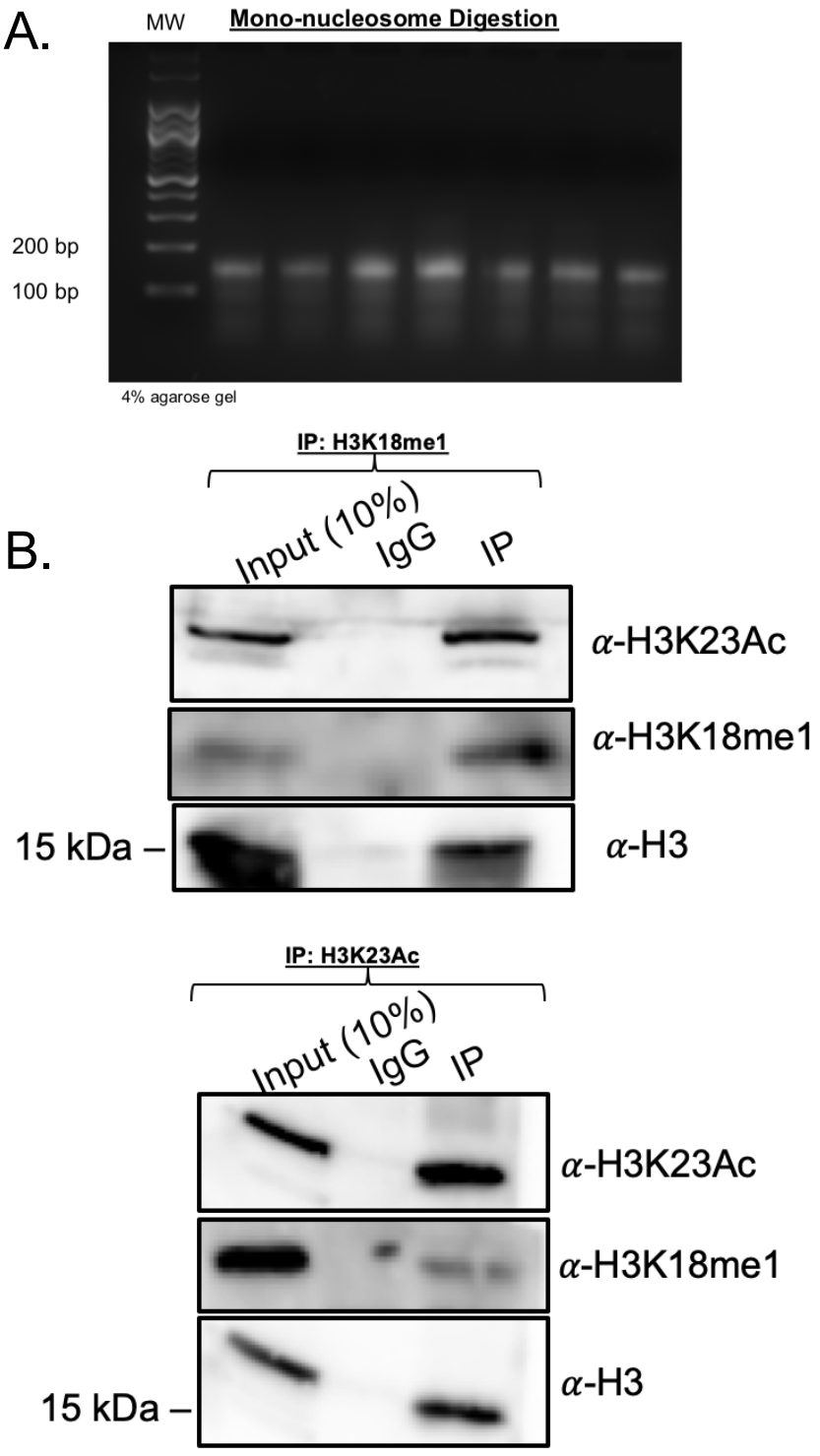

Figure 16 Combinatorial H3K18me1-H3K23Ac states detected in 50B11 (A) Digestion of 50B11 chromatin into mono-nucleosomes which were run on a 4% agarose gel **(B)** Western blot panel of H3K23Ac, H3K18me1 and H3 in which mono-nucleosomes containing either H3K18me1 or H3K23Ac marks were immunoprecipitated and subsequently blotted for the corresponding mark to evaluate combinatorial status.

iv. Discussion

Methylation of specific lysine residues on the N-terminal tail of histone H3 helps confer specific chromatin states that regulate access of the underlying DNA sequence to the nuclear environment [11], [17], [31], [59], [60], [63], [65], [70], [84]. While many histone lysine methylation sites have been identified, the full complement of enzymes that generate mono-, di-, and tri-methylation at specific residues is not fully known. Here, we identify histone H3K18 and H3K23 as two new targets for the methyltransferases EHMT1/GLP and EHMT2/G9a. We show that while both enzymes can mono-, di-, and tri-methylate H3K18, they display differential activity on H3K23. While both enzymes catalyzed the addition of mono- and di-methylation to H3K23, only EHMT1/GLP catalyzed the tri-methylation of lysine 23 *in vitro*. We also demonstrate that pharmacological and genetic disruption of EHMT1/GLP and EHMT2/G9a decreased H3K18 and H3K23 methylation *in vivo*.

More broadly, this work elucidates an expanded repertoire of histone methylation modifications catalyzed by EHMT1/GLP and EHMT2/G9a. While these enzymes were already known to be promiscuous on both non-histone and histone targets [66], [85], this work draws attention to the phenomenon that multiple, biologically distinct, histone methylation marks can be catalyzed by the same HMTs *in vivo* [28], [86]. This work could also shed light on combinatorial post-translational modification states involving these newly identified targets *in vivo*, as well as provide new insights into mechanisms of PTM cross-talk and how oncohistones can impart changes in the epigenome [87], [88]. More interestingly, *in vivo* perturbations in EHMT1/GLP and EHMT2/G9a have been implicated in many cellular processes including autophagy [81], DNA methylation

[81], [89], hypoxia [90], tumor suppression [13], [91]-[93], chromatin remodeling [69], and synaptic plasticity [94] to name a few, and homozygous loss of EHMT1/GLP results in embryonic lethality in mice [95]. Additionally, both enzymes have been the focus of cancer therapies in recent years [13], [54], [89], [92], [96], [97]. While this work does not address the functional role of H3K18 and H3K23 methylation, it is possible that methylation at these targets could contribute to these cellular processes and pathologies. More extensive studies need to be done to determine the full complement of H3K18 and H3K23 methylation writers, readers, and erasers, and to understand the biological contexts in which such methylation modifications operate.

The EHMT1/GLP and EHMT2/G9a methyltransferases are being pursued as targets for drug development, particularly as potential anti-cancer therapeutics [13], [54], [89], [92], [96], [97] including the inhibitor used in this study, UNC0642, as well as multiple additional agents, including a recently described dual inhibitor of EHMT2/G9a and the DNA methyltransferase DNMT1 [89]. These enzymes have been targeted largely due to their well-characterized role in mediating H3K9 methylation, an important heterochromatic mark that is often used by cancer cells to repress large chromatin blocks and repress expression of key tumor suppressor genes and pathways [28], [68], [80], [88]. However, based on the current work, it will be important to assess the impact of such EHMT1/GLP and EHMT2/G9a inhibitors on methylation at other histone lysine methylation modifications including at H3K18, H3K23, and H3K27, since these would represent on-target modifications that, upon EHMT1/GLP or EHMT2/G9a inhibition, may have unanticipated consequences apart from inhibiting H3K9 methylation alone.

Additionally, the *in vitro* and *in vivo* peptide pulldowns, revealing interactions between the ING-family proteins and H3K18 methylation, coupled to the H3K18me1 and H3K23Ac mono-nucleosome pulldowns, suggests that perhaps epigenetic cross-talk is at play. As previously mentioned, both Yng1 and ING5 are members of HAT complexes who have been shown to interact with histone methylation and subsequently stimulate histone acetylation of nearby residues. This cross talk has already been demonstrated in yeast with Yng1 in Taverna et. al., 2007 and with ING5 in human cells [98]. In both cases, these proteins interacted with H3K4me3, as we recapitulated both *in vitro* or *in vivo*. ING5 is a member of the MOZ/MORF complex and has been implicated in acetylating H3K23 [83]. Our detection of H3K18me1-H3K23Ac dual modified nucleosomes, coupled to our *in vitro* and *in vivo* detection of interactions between H3K18me1 and ING5 suggests that perhaps the MOZ/MORF complex interacts with H3K18 methylation, *in vivo*, and that those interactions may lead to H3K23ac on H3K18me1 occupied nucleosomes. However, more work needs to be done to connect H3K18me1-ING5 interactions with the MOZ/MORF complex and H3K23Ac before such conclusions can be drawn. However, if true, this could shed light on a potential role for H3K18 methylation in promoting H3 acetylation via its potential association with HATs *in vivo*.

Chapter 3: Genome-wide characterization, combinatorial signatures, bivalent readers and potential cross-talk of H3K23me3 on mammalian chromatin

i. Background

It is well understood that chromatin modifications, which can occur on the DNA itself or the histone proteins in which DNA wraps around, can affect gene expression through recruitment of various transcriptional activators or repressors that further propagate closed or open chromatin states [10], [19], [58], [99]. These modifications can be differentially positioned along gene bodies and recruit unique effector proteins that play distinct roles in directing template dependent chromatin remodeling events [19]. Posttranslational modifications in histone proteins have been shown to play an important role in facilitating proper gene expression [100], mitotic partition of chromosomes [101], transposon silencing [61], [67], DNA repair [5]-[7] and many other essential pathways [88], [100], [102], [103].

Methylation of histones is one of the most abundant posttranslational modifications genome-wide and is universally conserved from plants to mammals [11], [47], [48], [58], [68], [73]. Methylation of histone proteins has been implicated in driving both repressive and permissive chromatin states and although many histone PTMs are studied singularly, many of the modifications exist in combinations with other histone modifications, and work in concert to drive locus-specific molecular events [10], [18], [43], [104]. One such combinatorial modification state that has been investigated are *bivalent* histone marks. These dual modifications comprise two histone modifications in which one mark carries a canonical repressive function (e.g. bind heterochromatin proteins, recruit repressors, etc.) while the other mark carries a canonical permissive

function (e.g. recruiting co-activators, histone acetyltransferases, etc.) all while occupying the same nucleosome [12], [50], [51].

In this chapter, we characterize the poorly understood histone H3K23me3 modification and found its dominate epigenetic state to be bivalent with H3K4me3 at gene promoters on mammalian chromatin. We also show that both H3K23me3 and H3K4me3 likely associate with reader KDM4A, a lysine demethylase capable of reading H3K4me3 and H3K23me3 and demethylating H3K9me3 and H3K36me3, *in vivo*. Additionally, our studies show that in differentiating 50B11, the bivalent H3K4me3-H3K23me3 promoters epigenetically reprogram such that bivalent H3K4me3 increases while bivalent H3K23me3 decreases. A corresponding RNA-Seq analysis shows that gene expression increases after differentiation at the epigenetically reprogrammed monovalent H3K4me3 and bivalent H3K4me3-H3K23me3 marked promoters, but not monovalent H3K23me3 marked genes. Furthermore, our studies show that monovalent H3K23me3 occupies the TSS, unlike bivalent H3K23me3 which occupies promoters, suggesting that H3K23me3 silences gene expression by occluding the TSS. Lastly, our data suggests that knockdown of H3K4 methylation cause specific global aberrations in H3K9, H3K23 and H3K36 methylation; however knockdown of H3K9 and H3K23 does not reciprocally perturb H3K4 or H3K36 methylation, suggesting unique one-directional cross-talk between these epigenetic marks *in vivo*. Taken together, this chapter characterizes genome-wide localization of H3K23 methylation states, introduces a new bivalent chromatin signature: H3K23me3-H3K4me3, elucidates potential repressive function of H3K23me3, and sheds light on potential cross-talk between H3K23me3 and H3K4me3.

ii. Methods

Cell Culture Methods 50B11 cells were grown in NeuroPlex Serum-free Neuronal Medium (Gemini Bioscience 600-300) and supplemented with Fetal Bovine Serum (10% final), 100 mM L-Glutamate (275 uM final), 20% glucose (0.2% final), 10X Gem21 NeuroPlex supplement (1X final). Cells were grown in an incubator at 37C, 5% CO_2 and were passaged no more than 5 passages.

Generation of transgenic 50B11 cells expressing mutant histones Plasmids encoding mammalian histone H3.1 with various lysine to methionine mutants were constructed using mutagenic PCR. Once sanger sequence validated, the resulting H3.1 mutant DNA sequence was cloned into a lentiviral vector (pLVX-IRES-mCherry). To prepare lentivirus containing the construct encoding the mutant histone, HEK293 cells plated and grown in DMEM (containing 10% FBS and 1X Penn/Strep) to approximately 70% confluency. To transfect HEK293 cells, Fugene transfection reagent was mixed with 400 uL DMEM and incubated at room temperature for 5 minutes at a ratio of 3:1 of Fugene to total DNA. To the Fugene/DMEM mixture 5 ug of the vector encoding mutant H3.1, 3.75 ug of Δ8.9 packaging plasmid and 2.5 ug of VSV-G envelop plasmid is added and allowed to incubate at room temperature for 15 minutes. The resulting mixture was added to HEK293 cells and incubated at 37^{o}C for 3 hours. 90 uL of 1M sodium butyrate is added (final concentration 110 mg/mL) to open up the chromatin. The following day, the media is discarded and replaced with Opti-MEM and allowed to incubate for 12-18 hours. The virus-enriched supernatant is collected and stored at 4^{o}C. This process was repeated 3 times, each time pool the viral supernatant. Pooled viral supernatant is

filtered through a 0.45 uM filter to remove any cells carried over. 0.5 mL of viral supernant was used to transduce 50B11 cells for 24 hours. Following transduction, the media is removed and cells allowed to incubate for 2 days. Following the two-day incubation, cells were FACS sorted for high vs low mCherry expression into cell per well in a 384 well plate. Colonies were expanded, harvested, lysed and western blotting was performed to evaluate Flag expression as well as for various histone modifications. Western blotting conditions were as follows: H3K4me3 (ab8580, 1:5,000, 2^o: 1:10,000), H3K9me3 (ab8898; 1:5000, 2^o: 1:10,000), H3K23me3 (active motif 61499, 1:500, 2^o: 1:1000), H3K27me3 (Millipore 07-449, 1:2500, 2^o: 1:5000), H3K36me3 (ab9050, 1:5000, 2^o: 1:10,000).

Native Chromatin Immunoprecipitation and library preparation 50B11 cells were grown to 80-90% confluency and subsequently harvested. Cells were resuspended in a lysis buffer containing 250 mM Sucrose, 1mM phenylmethylsulfonly fluoride (PMSF) protease inhibitor, 1mM sodium butyrate, 0.1% Triton-X 100, 5mM $MgCl_2$, 50 mM Tris, pH 7.4, 5 mM KCl. Cells were lysed using a dounce homogenizer (60 -100 dounces per sample). Lysate was spun down at 500 rpm, 5 minutes at 4^oC to pellet the intact nuclei. Harvested nuclei were resuspended in MNase reaction buffer (50 mM Tris, pH 7.4, 5 mM $CaCl_2$) and counted using a hemocytometer with DAPI staining. To fragment the DNA, Nuclei were incubated with 1 unit miccrococcal nuclease per 3 million nuclei for 90 minutes at 37C. To quench the reaction, EDTA is supplemented to a final concentration of 10 mM and placed on ice for 5 minutes. To prepare antibody conjugated dynabeads for immunoprecipitation, 15 uL of Protein A conjugated

dynabeads were washed with incubation buffer (50 mM Tris, pH 7.4, 150 mM NaCl, 0.1% Triton-X 100, 10 mM EDTA, 1mM PMSF). Following the washes, 1ug of IgG antibody of interest is added and incubated for 10 minutes at room temperature, with mild agitation, to conjugate the antibody to the beads. Next, the antibody-conjugated dynabeads are washed with incubation buffer to clear any unconjugated antibody. Next, the antibody-conjugated beads are resuspended in 500 uL of incubation buffer and the digested chromatin input is added and allowed to immunoprecipitate overnight at 4C with mild agitation. Following immunoprecipitation, the beads are washed five times with low salt buffer (150 mM NaCl, 50 mM Tris, pH 7.4, 0.1% SDS, 1% Triton-X 100, 1 mM PMSF, 10 mM EDTA), five times with high salt wash buffer (500 mM NaCl, 50 mM Tris, pH 7.4, 0.1% SDS, 1% Triton-X 100, 1 mM PMSF, 10 mM EDTA), and one time with buffer containing 250 mM LiCl and 10 mM Tris, pH 7.4. To elute the immunoprecipitated material, the beads are resuspended in 33 uL of elution buffer (1% SDS, 100 mM Sodium Bicarbonate, pH 8) and incubated 65C for 15 minutes with aggressive agitation. The eluate is collected and the elution steps is repeated two more times (pooling the elutions). Following elution, 1 uL of RNAse A is added and incubated at 37C for 30 minutes to digest any residual RNA. Following RNA digestion, 1 uL of Proteinase K is added and incubated at 37C for 30 minutes to digest the protein. Following protein digestion, the immunoprecipitated DNA was harvested using a Zymo ChIP DNA Cleaner and Concentrator. The recovered DNA is quantitated using Qubit. To prepare DNA libraries for next generation sequencing, the NEBNext Ultra II DNA Library prep kit (NEB E7645L) and dual barcoded. Quality control was performed using a bio analyzer

chip and quantitated using qPCR using the NEBNext Library Quantitation kit (NEB E7630S).

Cross-linked chromatin immunoprecipitation: Approximately 5 million cells per IP were used. Cell pellets were resuspended in 500 uL of a 1% formaldehyde solution, vortexed, and rocked gently for 10 minutes at room temperature. Cross linking was quenched with 25 uL of 125 mM glycine solution and rocked gently for 5 minutes. Cross-linked cells were pelleted and supernatant was decanted. Cross-linked cells were resuspended in 1 mL of cell lysis buffer (5 mM Hepes pH 7.4, 85 mM KCl, 1% IGEPAL, 1X protease inhibitor tablet) for 10 minutes and room temperature. Cells were then washed with 1X PBS to remove residual cell lysis buffer. Cells were then resuspended in 300 uL of nuclear lysis buffer (5 mM Tris-HCl, 10 mM EDTA, 1% SDS, 1X protease inhibitor tablet), transferred to a PCR tube, and incubated for 10 minutes. Cells were then sonicated for 30 cycles, 75% power, 30 seconds on 30 seconds off (15 minutes total). The cells were then spun down to pellet insoluble cellular/nuclear debris. The supernatant was decanted and used an input for IP. To prepare antibody conjugated dynabeads for immunoprecipitation, 15 uL of Protein A conjugated dynabeads were washed with incubation buffer (50 mM Tris, pH 7.4, 150 mM NaCl, 0.1% Triton-X 100, 10 mM EDTA, 1mM PMSF). Following the washes, 1ug of IgG antibody of interest is added and incubated for 10 minutes at room temperature, with mild agitation, to conjugate the antibody to the beads. Next, the antibody-conjugated dynabeads are washed with incubation buffer to clear any unconjugated antibody. Next, the antibody-conjugated beads are resuspended in 500 uL of incubation buffer and the digested

chromatin input is added and allowed to immunoprecipitate overnight at 4 ^{o}C with mild agitation. Following immunoprecipitation, the beads are washed five times with low salt buffer (150 mM NaCl, 50 mM Tris, pH 7.4, 0.1% SDS, 1% Triton-X 100, 1 mM PMSF, 10 mM EDTA), five times with high salt wash buffer (500 mM NaCl, 50 mM Tris, pH 7.4, 0.1% SDS, 1% Triton-X 100, 1 mM PMSF, 10 mM EDTA), and one time with buffer containing 250 mM LiCl and 10 mM Tris, pH 7.4. To elute the immunoprecipitated material, the beads are resuspended in 33 uL of elution buffer (1% SDS, 100 mM Sodium Bicarbonate, pH 8) and incubated 65^{o}C for 15 minutes with aggressive agitation. The eluate is collected and the elution steps is repeated two more times (pooling the elutions). To reverse cross-link, 5M NaCl was added to the pooled elutions and allowed to incubate overnight 65C. Following reverse cross-linking, the temperature was reduced to 37C and 1 uL of RNAse A is added and incubated at 37C for 30 minutes to digest any residual RNA. Following RNA digestion, 1 uL of Proteinase K is added and incubated at 37C for 30 minutes to digest the protein. Following protein digestion, the immunoprecipitated DNA was harvested using a Zymo ChIP DNA Cleaner and Concentrator.

RNA isolation and library preparation 50B11 cells were harvested (~3 million cells per replicate) and total RNA was isolated using Qiagen RNAeasy Mini Prep kit (Qiagen 74104). RIN score was assessed using Agilent RNA 6000 nanochips (5067-1511). RNA libraries were prepared using NEBNext Ultra II RNA Library prep kit (NEB #E6310). RNA-seq libraries were sequenced on a Nova-Seq.

Next generation sequencing and data processing DNA and cDNA libraries were deep sequenced on a Nova-Seq. Following sequencing, adaptor sequences were removed, computationally, using the package trim galore. Following trimming, the adaptor trimmed sequences were aligned to the rn7 genome using bowtie2. Following generation of the corresponding SAM files, samtools was used to convert the aligned SAM files into BAM files. The resulting BAM files were indexed and removed of all PCR duplicates. MACS2 was used to call peaks. Consensus peak files for all modifications were generated using the R package consensusSeekeR. Feature distribution maps and peak annotations were performed using ChIP-Seeker. Statistical overlap analyses were done using GenometriCorr. Genome-wide overlap between bed files of various modifications was done using bedtools intersect. Signal averaging and heat maps were generated using deeptools compute matrix and plot heat map functions.

In cellulo peptide pulldown from nuclear extracts To prepare beads for the peptide pulldown, 25 uL of M280 Streptavidin-conjugated Dynabeads were washed three times with 1X PBST (0.1% Triton-X 100) and resuspended in 500 uL of 1X PBST. 1 ug of biotinylated peptide was added and allowed to incubate for 1 hour at room temperature. Following peptide conjugation, the peptide-conjugated beads were washed with 1X PBST three times to displace any unconjugated peptide. To prepare the nuclear protein extract for pulldown, 50B11 nuclei were harvested by resuspending cells in lysis buffer (250 mM Sucrose, 1mM phenylmethylsulfonly fluoride (PMSF) protease inhibitor, 1mM sodium butyrate, 0.1% Triton-X 100, 5mM $MgCl_2$, 50 mM Tris, pH 7.4, 5 mM KCl) followed by dounce homogenization (60-100 dounces per sample). The lysate was spun

down at 500 rpm for 5 minutes at 4C to pellet intact nuclei. Intact nuclei were transferred to a 1.5 mL Eppendorf tube and total packed cell volume was estimated visually. Nuclei were then resuspended in a high salt extraction buffer (20 mM Hepes, pH 7.9, 25% glycerol, 500 mM KCl, 1.5 mM $MgCl_2$, 0.2 mM EDTA, 1mM DTT and 1mM PMSF) and allowed to extract at 4C for at least four hours. The extract was spun down at 16,000 rpm at 4C for 10 minutes to pellet the insoluble nuclear debris. The supernatant was transferred to a different 1.5 mM Eppendorf tube and was diluted with buffer containing 20 mM Hepes, pH 7.9, 25% glycerol, 1.5 mM $MgCl_2$, 0.2 mM EDTA, 1mM DTT and 1mM PMSF such that the final KCl concentration is 150 mM. The resulting diluted extract was quantitated using a BCA assay. The quantitated nuclear protein extract was added to the peptide-conjugated beads at a concentration of 1 mg of total protein per peptide pulldown. The pulldown was allowed to proceed overnight at 4C. The following day, the protein extract is removed and the beads are washed six times with buffer containing 300 mM KCl, 0.2% Triton-X 100, 1mM PMSF followed by a final wash containing 4 mM LiCl, 10 mM Hepes, pH 7.9. The peptides/pulled down proteins were eluted by resuspending the beads in 1X SDS sample buffer and boiling for 5 minutes. The resulting eluate is collected and subjected to SDS-PAGE followed by western blotting to detect the proteins of interest.

In vivo mono-nucleosome pulldowns 50B11 nuclei are harvested and digested as previously described in chapter 2. To prepare antibody conjugated dynabeads for immunoprecipitation, 15 uL of Protein A conjugated dynabeads were washed with incubation buffer (50 mM Tris, pH 7.4, 150 mM NaCl, 0.1% Triton-X 100, 10 mM EDTA,

1mM PMSF). Following the washes, 1ug of IgG antibody of interest is added and incubated for 10 minutes at room temperature, with mild agitation, to conjugate the antibody to the beads. Next, the antibody-conjugated dynabeads are washed with incubation buffer to clear any unconjugated antibody. Next, the antibody-conjugated beads are resuspended in 500 uL of incubation buffer and the digested chromatin input is added and allowed to immunoprecipitate overnight at 4C with mild agitation. Following immunoprecipitation, the beads are washed five times with low salt buffer (150 mM NaCl, 50 mM Tris, pH 7.4, 0.1% SDS, 1% Triton-X 100, 1 mM PMSF, 10 mM EDTA), five times with high salt wash buffer (500 mM NaCl, 50 mM Tris, pH 7.4, 0.1% SDS, 1% Triton-X 100, 1 mM PMSF, 10 mM EDTA), and one time with buffer containing 250 mM LiCl and 10 mM Tris, pH 7.4. Following the washes, the beads are suspended in 1X SDS sample buffer and subjected to SDS-PAGE followed by western blotting against the histone modification of interest.

Quantitative PCR Following isolation of nChIP (or XChIP) DNA and quantitation via Qubit, qPCR analysis was performed by mixing together nChIP DNA as input with sso advanced universal SYBR green supermix with the desired primers of interest (final concentration: 200 nM). The resulting qPCR mixtures were loaded into a 384-well white plate and run on a Bio-Rad CFX qPCR instrument.

iii. Results

H3K23 methylation states tracks with promoter enrichment

While histone H3K23 methylation has been studied in *T. thermophila*, [72] and A*. thaliana* [48], there is little characterization on mammalian chromatin. To first assess where all methylation states of histone H3K23 (me1, me2, and me3) localize genome-wide, we employed native chromatin immunoprecipitation followed by deep sequencing (nChIP-Seq) in a renewable, clonal cell line enriched for H3K23 methylation (50B11). To annotate our nChIP-Seq data, we used an R packaged called ChIP-SeekeR to generate genome-wide feature distribution profiles for H3K23me1, H3K23me2, H3K23me3 in 50B11. Our data shows that H3K23 methylation displays strong enrichment at gene bodies and regulatory elements (Figure 17A). Interestingly, our data shows that H3K23 methylation becomes enriched at promoters as a function of the methylation state. More specifically, over 50% of H3K23me3 peaks are promoter localized, while only >25% and <10% H3K23me2 and H3K23me1 peaks, respectively, are promoter localized. This is further supported through signal averaging and heat map profiles of H3K23me1, H3K23me2 and H3K23me3 about TSSs (Figure 17B). The profiles reveal distinct partitioning of each H3K23 methylation state about TSSs. Our data shows that the H3K23me1 signal is quite weak flanking TSSs, while H3K23me2 and H3K23me3 both give strong signals flanking TSSs. However, H3K23me2 signal appears more evenly distributed flanking TSSs, while H3K23me3 is asymmetrically distributed about TSSs and is more heavily enriched towards the gene body (Figure 17B).

To evaluate statistical enrichment of H3K23me1, H3K23me2, and H3K23me3 in various genome compartments, we used the R package GenometriCorr. GenometriCorr

uses a series of tests to compare the similarity between two (or more) genomic datasets and determine how overlap (e.g. the jaccard index) between the genomic datasets compares to the overlap observed in a random distribution. The genome compartments of interests are CpG Islands (heavily enriched at 70% of mammalian promoters), Exons, Introns, 5' UTRs, 3' UTRs and the 1000 bp surrounding TSSs. Consistent the feature distribution profiles, all three methylation states of H3K23 showed statistical enrichment (p-value << 0.001) at regions surrounding or associated with the TSSs (e.g. TSS bed and CpG Islands) and gene bodies (introns and exons) to a lesser extent (Figure 17C-E and Table 3).

Taken together, this data shows enrichment of H3K23 methylation at gene bodies with a distinct partitioning of higher H3K23 methylation states (me2 and me3) at promoters. This suggests that while H3K23 methylation states are encoded by the same enzymes, they have distinct localizations genome-wide, which may hint at unique functions for each H3K23 methylation state in regulating gene expression. i

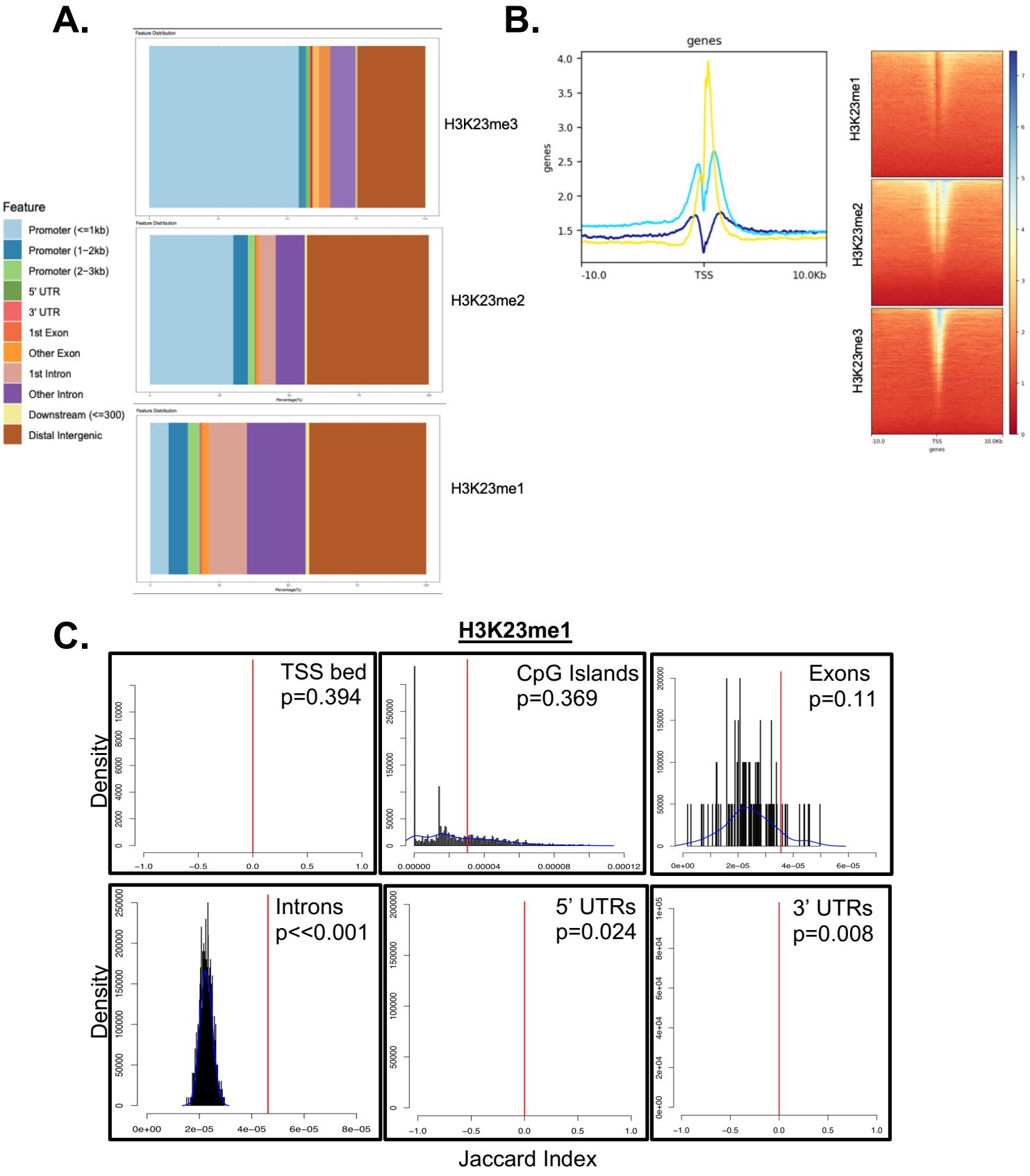
A.
Feature
Promoter (<=1kb)
Promoter (1-2kb)
Promoter (2-3kb)
5' UTR
3' UTR
1st Exon
Other Exon
1st Intron
Other Intron
Downstream (<=300)
Distal Intergenic
H3K23me3
H3K23me2
H3K23me1
B.
genes
genes
4.0
3.5
3.0
2.5
2.0
1.5
-10.0
TSS
10.0Kb
H3K23me1
H3K23me2
H3K23me3
C.
H3K23me1
TSS bed
p=0.394
CpG Islands
p=0.369
Exons
p=0.11
Introns
p<<0.001
5' UTRs
p=0.024
3' UTRs
p=0.008
Density
Density
Jaccard Index

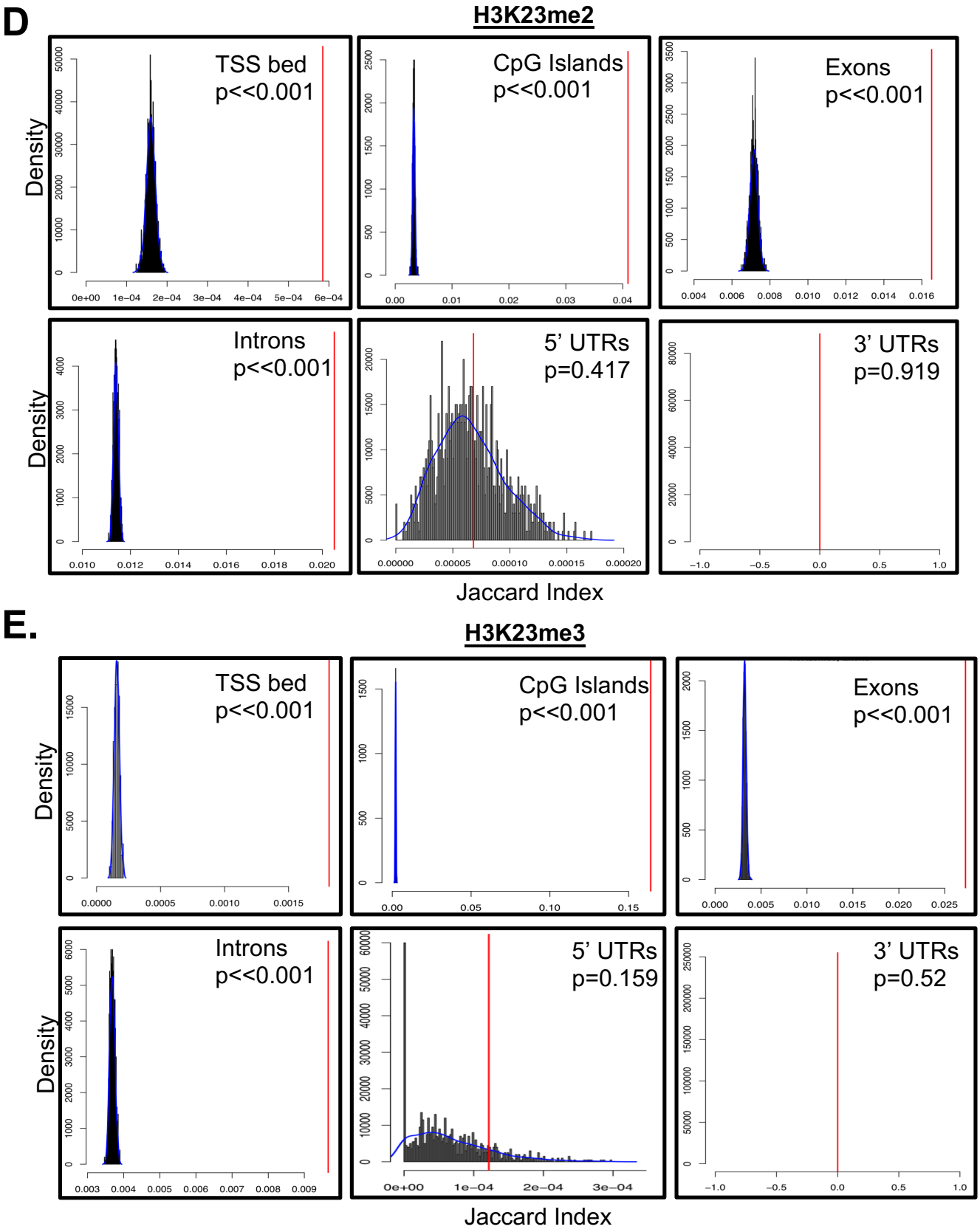
D
H3K23me2
TSS bed
p<<0.001
CpG Islands
p<<0.001
Exons
p<<0.001
Introns
p<<0.001
5' UTRs
p=0.417
3' UTRs
p=0.919
Density
Jaccard Index
E.
H3K23me3
TSS bed
p<<0.001
CpG Islands
p<<0.001
Exons
p<<0.001
Introns
p<<0.001
5' UTRs
p=0.159
3' UTRs
p=0.52
Density
Jaccard Index

Table 3: Statistical enrichment of H3K23 methylation states in various genome compartments

	Compartment	Jaccard Index	P-value
H3K23me1	CpG Islands	3.035322e-05	0.369
	TSS bed	0	0.394
	Exons	3.554307e-05	0.11
	Introns	4.619769e-05	<< 0.001
	3' UTR	0	0.008
	5' UTR	0	0.024
H3K23me2	CpG Islands	0.04092206	<< 0.001
	TSS bed	0.000584678	<< 0.001
	Exons	0.01651704	<< 0.001
	Introns	0.02049831	<< 0.001
	3' UTR	0	0.417
	5' UTR	6.808238e-05	0.919
H3K23me3	CpG Islands	0.1636	<0.001
	TSS bed	0.001816	<0.001
	Exons	0.02725	<0.001
	Introns	0.009659	<0.001
	3' UTR	0	0.52
	5' UTR	0	0.159

Figure 17 H3K23 methylation localizes, primarily, at gene bodies **(A)** Feature distribution maps showing percentage of H3K23me1/2/3 peaks localizing to various genome compartments. **(B)** Signal averaging and heat maps of H3K23me1/2/3 about transcription start sites (TSSs). **(C)** GenometriCorr distribution plots showing statistical enrichment of H3K23me1 **(C)**, H3K23me2 **(D)** and H3K23me3 **(E)** in various genome compartments. **Table 3** summarizes GenometriCorr statistics regarding H3K23me1/2/3 enrichment in gene compartments.

H3K23me3 is overwhelmingly bivalent with H3K4me3 at promoters in 50B11

Of the methylation states surveyed, our nChIP-Seq data revealed H3K23me3 as a clear promoter mark, so we became interested in another well-characterized histone methyl-lysine promoter mark, H3K4me3 [30], [70], and wondered if there might be a potential relationship between H3K23me3 and H3K4me3 genome-wide at promoters. To investigate H3K4me3 genome-wide, we performed nChIP-Seq on H3K4me3 in 50B11. Again, using ChIP-SeekeR to annotate the H3K4me3 nChIP peaks, we created a genome-wide feature distribution profile (Figure 18A). Consistent with previous studies [44], [100] and similar to the profile of H3K23me3, H3K4me3 peaks mostly localize at promoters (> 30%) and gene bodies (Figure 18A). To check statistically significant overlap of H3K4me3 in various genome compartments, we again used GenometriCorr to evaluate H3K4me3 enrichment in various genome compartments. Similar to H3K23me3, our H3K4me3 data show the highest statistical enrichment in regions surrounding the TSS over other genome compartments (Figure 18B). To evaluate H3K4me3 signal over TSSs and H3K23me3 regions, we generated heat maps and signal averaging plots for H3K4me3 signal about genome-wide TSSs and H3K23me3 peak centers and performed H3K23me3 signal averaging over H3K4me3 peak centers and TSSs. Similar to H3K23me3, H3K4me3 exhibits an asymmetric distribution about TSSs with higher build-up of H3K4me3 signal facing the gene body (Figure 18C). Additionally, there is a strong correlation in H3K4me3 signal about

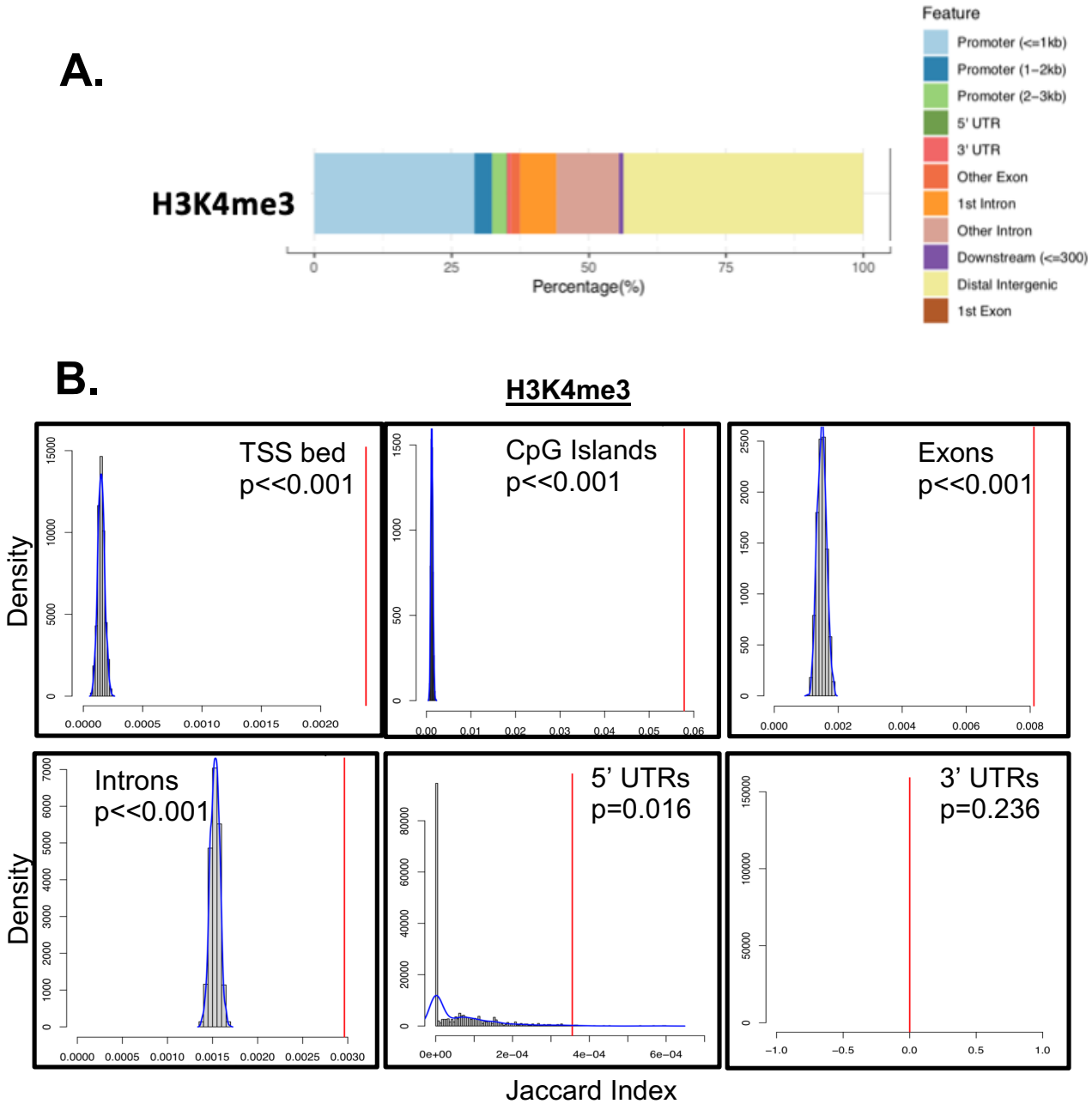

Table 4: Statistical enrichment of H3K4me3 statistical enrichment in various genome compartments

Compartment	Jaccard Index	P-value
CpG Islands	0.0578	<< 0.001
TSS Bed -/+ 1000 bp	0.00238	<< 0.001
Exons	0.00811	<< 0.001
Introns	0.00296	<< 0.001
3' UTR	0.0967	0.236
5' UTR	0.000355	0.016

C.

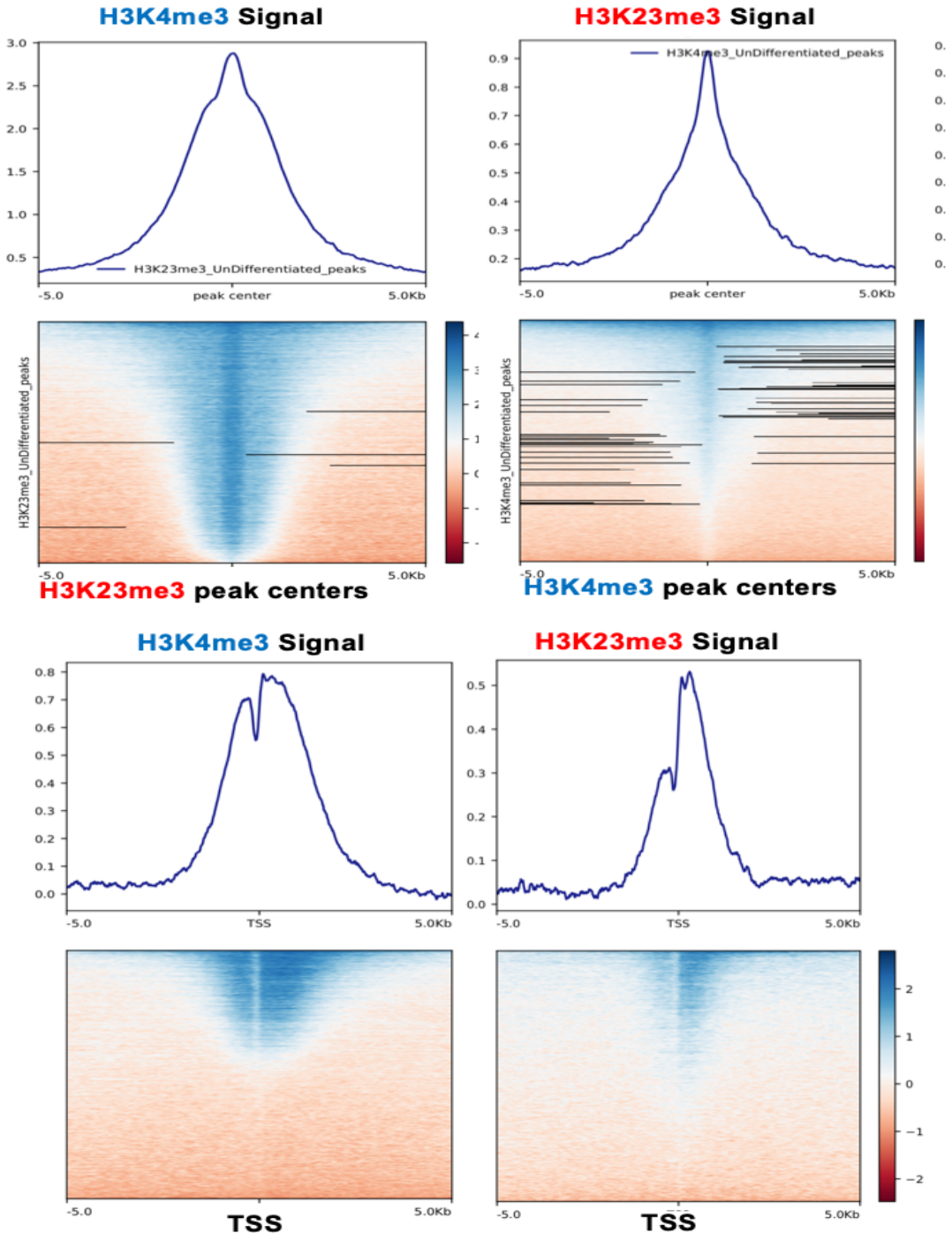
H3K4me3 Signal
H3K23me3 Signal
H3K23me3_UnDifferentiated_peaks
peak center
-5.0
5.0Kb
H3K4me3_UnDifferentiated_peaks
H3K23me3 peak centers
H3K4me3 peak centers
TSS

D.

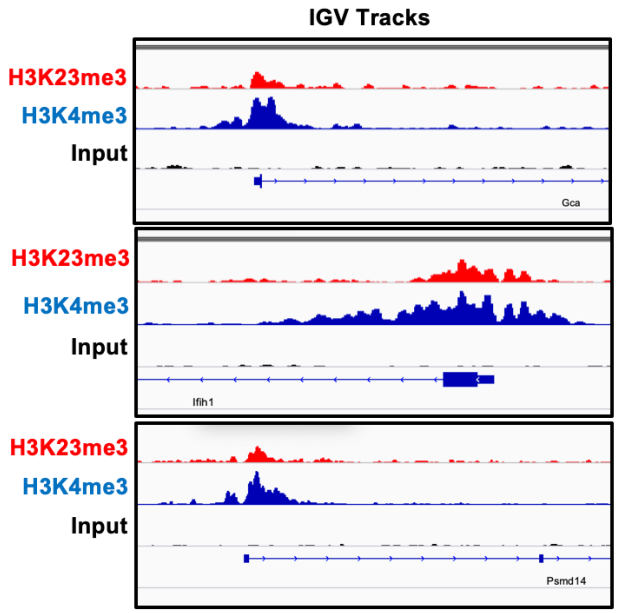
IGV Tracks
H3K23me3
H3K4me3
Input
Gca
H3K23me3
H3K4me3
Input
Ifih1
H3K23me3
H3K4me3
Input
Psmd14

E.

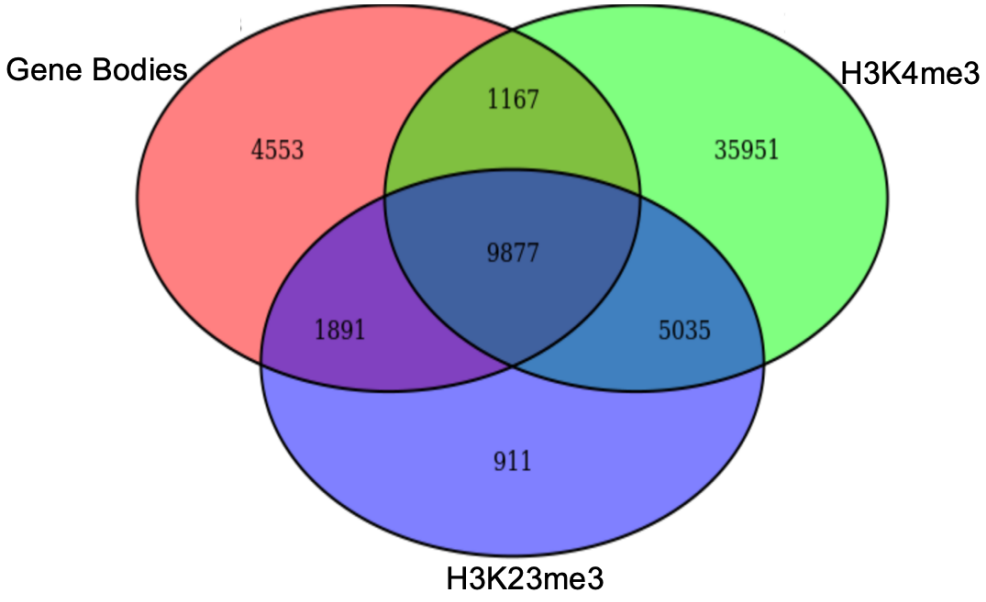
Gene Bodies
H3K4me3
H3K23me3
4553
1167
35951
9877
1891
5035
911

F.

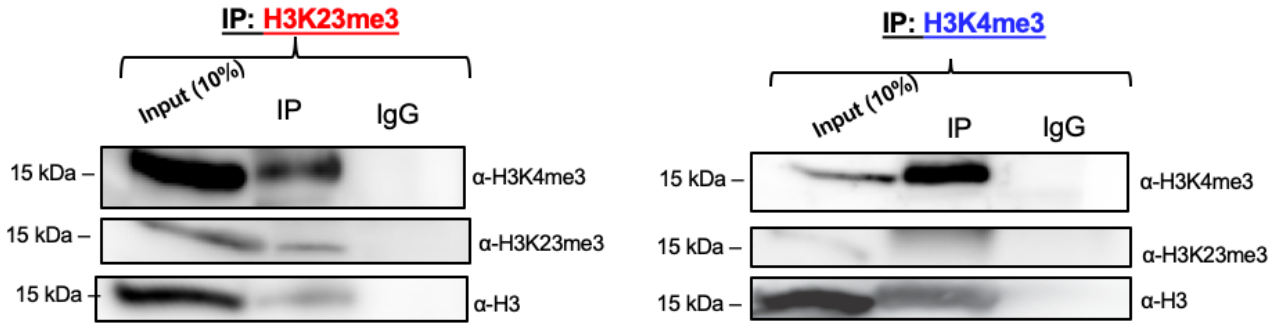
IP: H3K23me3
Input (10%)
IP
IgG
15 kDa –
α-H3K4me3
15 kDa –
α-H3K23me3
15 kDa –
α-H3
IP: H3K4me3
Input (10%)
IP
IgG
15 kDa –
α-H3K4me3
15 kDa –
α-H3K23me3
15 kDa –
α-H3

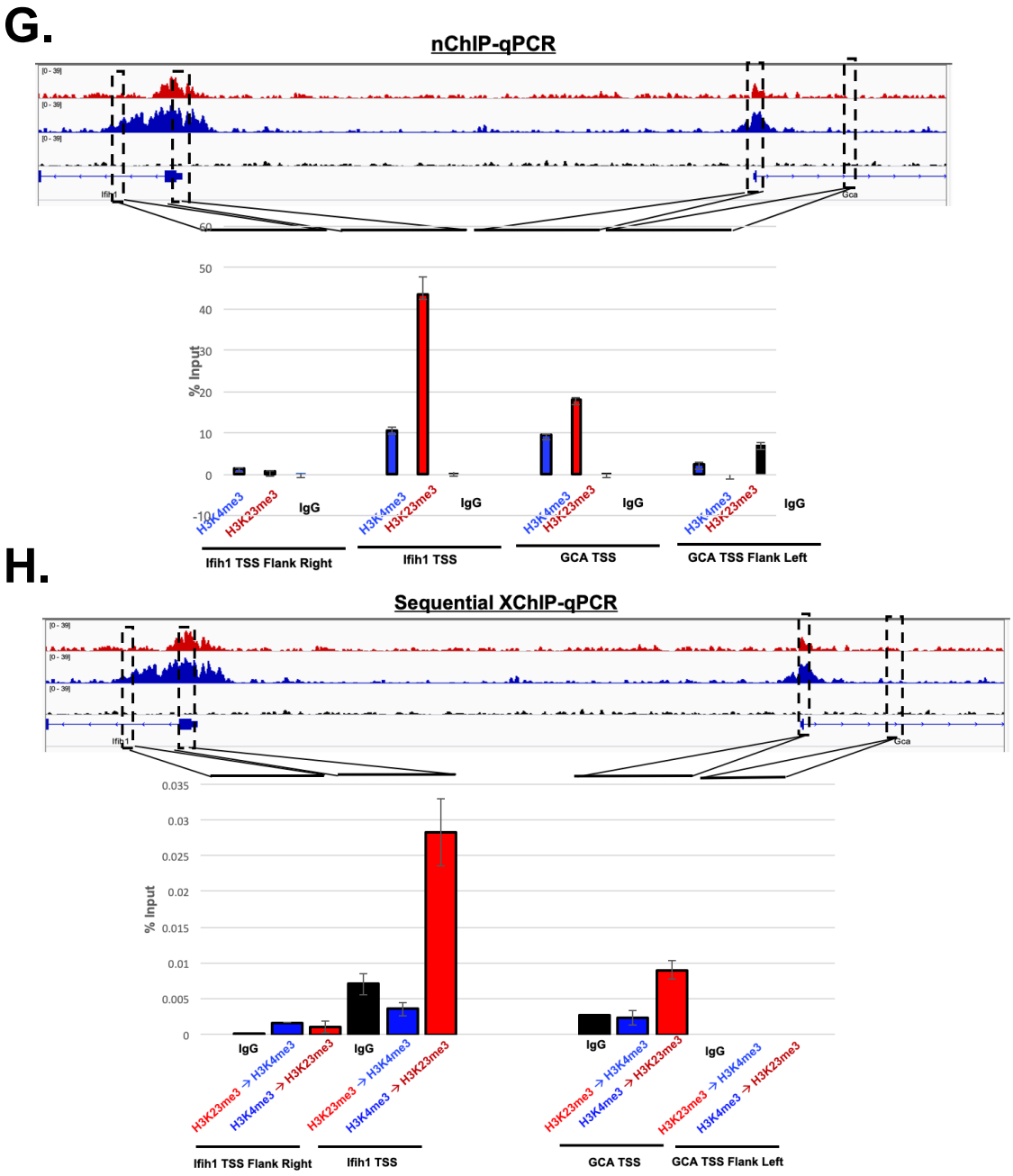

Figure 18 H3K23me3 is bivalent with H3K4me3 at promoters (A) Feature distribution map showing percentage of H3K4me3 peaks in various genome compartments **(B)** GenometriCorr plots evaluating statistical enrichment of H3K4me3 in various genome compartments. **Table 4** summarizes GenometriCorr statistics regarding H3K4me3 enrichment in gene compartments **(C)**, Signal averaging and heat maps of H3K4me3 and H3K23me3 signal about all TSSs and about each other's peak centers **(D)** IGV tracks showing colocation of H3K4me3 and H3K23me3. **(E)** Venn diagram showing overlap between H3K4me3, H3K23me3 with gene bodies. **(F)** Mono-nucleosome pulldowns of H3K4me3 and H3K23me3 from undifferentiated 50B11 cells. **(G)** nChIP-qPCR of H3K4me3 and H3K23me3 at GCA and Ifih1 promoters and the flanking regions. **(H)** Sequential XChIP-qPCR of H3K4me3 followed by H3K23me3 (or vice versa) at GCA TSS, Ifih1 TSS or a corresponding flanking region.

H3K23me3 peak centers and vice versa, suggesting that these modifications might indeed overlap genome wide with each other.

To interrogate the apparent co-localization of H3K4me3 and H3K23me3 at individual gene promoters, we loaded input-normalized bigwig files for H3K4me3 and H3K23me3 into an IGV browser. In addition to observing the association of H3K4me3 and H3K23me3 at gene promoters, our data shows that H3K4me3 peaks are encompassing H3K23me3 peaks rather than being of equal width (Figure 18D). To examine the percentage of H3K4me3-colocating H3K23me3 peaks and vice versa, we used bedtools to evaluate strict overlap (100% cutoff) between H3K4me3 and H3K23me3 peaks at gene bodies (rat genome assembly: rn7). Interestingly, over 60% of the H3K23me3 peaks have complete overlap with H3K4me3 peaks; however, because there are so many more H3K4me3 peaks relative to H3K23me3 peaks (approximately 10-fold), the overlap only comprises a small percentage (< 20%) of the total H3K4me3 peaks (Figure 18E).

The sequencing data suggests strict overlap of H3K23me3 with H3K4me3 at the DNA level, so we hypothesized that these modifications might share the same histone tail, but minimally the same nucleosome. To interrogate if H3K4me3 could be detected on H3K23me3 nucleosomes and vice versa, we employed a mono-nucleosome pulldown assay which entails digesting the native chromatin into mono-nucleosomes and pulling down nucleosomes containing one histone mark of interest (H3K23me3) and western blotting for a second query histone mark of interest (H3K4me3) and vice versa. We digested 50B11 chromatin with micrococcal nuclease to ensure digestion into mono-nucleosomes and pulled down either H3K4me3 or H3K23me3 nucleosomes and

blotted for the corresponding histone mark. Consistent with the sequencing data, our mono-nucleosome pulldown data shows that H3K4me3 can be detected on H3K23me3 nucleosomes; however, we cannot detect H3K23me3 on H3K4me3 nucleosomes (Figure 18F). This is most likely because the amount of H3K23me3-positive H3K4me3 nucleosomes is so small that the amount pulled down is likely below the detection threshold for a western blot. This is consistent with the idea that H3K23me3 is only present on a small percentage of H3K4me3 nucleosomes whereas H3K4me3 is present on the majority of H3K23me3 nucleosomes.

To further validate the association of H3K23me3 and H3K4me3 with the same piece of DNA *in vivo* and to validate our sequencing data, we performed nChIP-qPCR and XChIP-reChIP at various gene promoters identified from the initial H3K23me3 and H3K4me3 sequencing data. Our nChIP-qPCR data, consistent with the nChIP-Seq data, shows enrichment of H3K4me3 and H3K23me3 at Ifih1 and GCA gene promoters (arbitrarily selected), but not on the DNA immediately flanking those same promoters (Figure 18G). To further validate the sequencing data, we performed XChIP-reChIP in which we immunoprecipitated either H3K4me3 or H3K23me3 associated nucleosomes and performed a sequential immunoprecipitation in which the other mark was targeted for immunoprecipitation. Our data shows that immunoprecipitation of H3K23me3 followed by an H3K4me3 IP showed enrichment of Ifih1 and GCA promoters; however, immunoprecipitation of H3K4me3 followed by an H3K23me3 IP failed to show enrichment above an IgG control (Figure 18G). Again, we hypothesize that this discrepancy is because many H3K23me3 nucleosomes carry H3K4me3, leading to detectable DNA from a X-ChIP-reChIP; however, our data shows that most H3K4me3

nucleosomes do not carry H3K23me3. For the same reason that the H3K4me3 mono-nucleosome pulldowns failed to detect H3K23me3 signal, the XChIP of H3K4me3 nucleosomes followed by reChIP of H3K23me3 nucleosomes failed to detect DNA likely because the amount of H3K23me3 in the nucleosomal population became so dilute after enriching for H3K4me3 in the first IP that there simply wasn't enough to be detected in the second IP. Taken together, this data suggest that H3K23me3 might be present on a subset of H3K4me3 and that this bivalent chromatin signature might comprise one of the dominant epigenetic states as it relates to H3K23me3.

Reader KDM4A interacts with H3K4me3 and H3K23me3, *in vitro* and *in vivo*, and H3K36me3, a target of KDM4A, is compartmentalized away from H3K4me3 and H3K23me3.

Our biochemical data suggests that rather than being two independent promoter marks, H3K23me3 might have a strong association with H3K4me3. We next investigated to see if there were any known epigenetic reader proteins that are shared between H3K4me3 and H3K23me3. In 2016, Su and colleagues [41] identified members of the lysine demethylase family 4 (KDM4) family that contain DTD domains that can specifically *read* H3K4me3 and H3K23me3 *in vitro* and, to a lesser extent, H4K20me3, but with much lower affinity: KDM4A (Figure 19A). KDM4A has been extensively characterized in the literature and is known to target H3K9 and H3K36 for demethylation [47], [60], [69], [70]. We found it interesting that KDM4A can *read* both H3K4me3 and H3K23me3, and demethylate H3K36 methylation, and wanted to

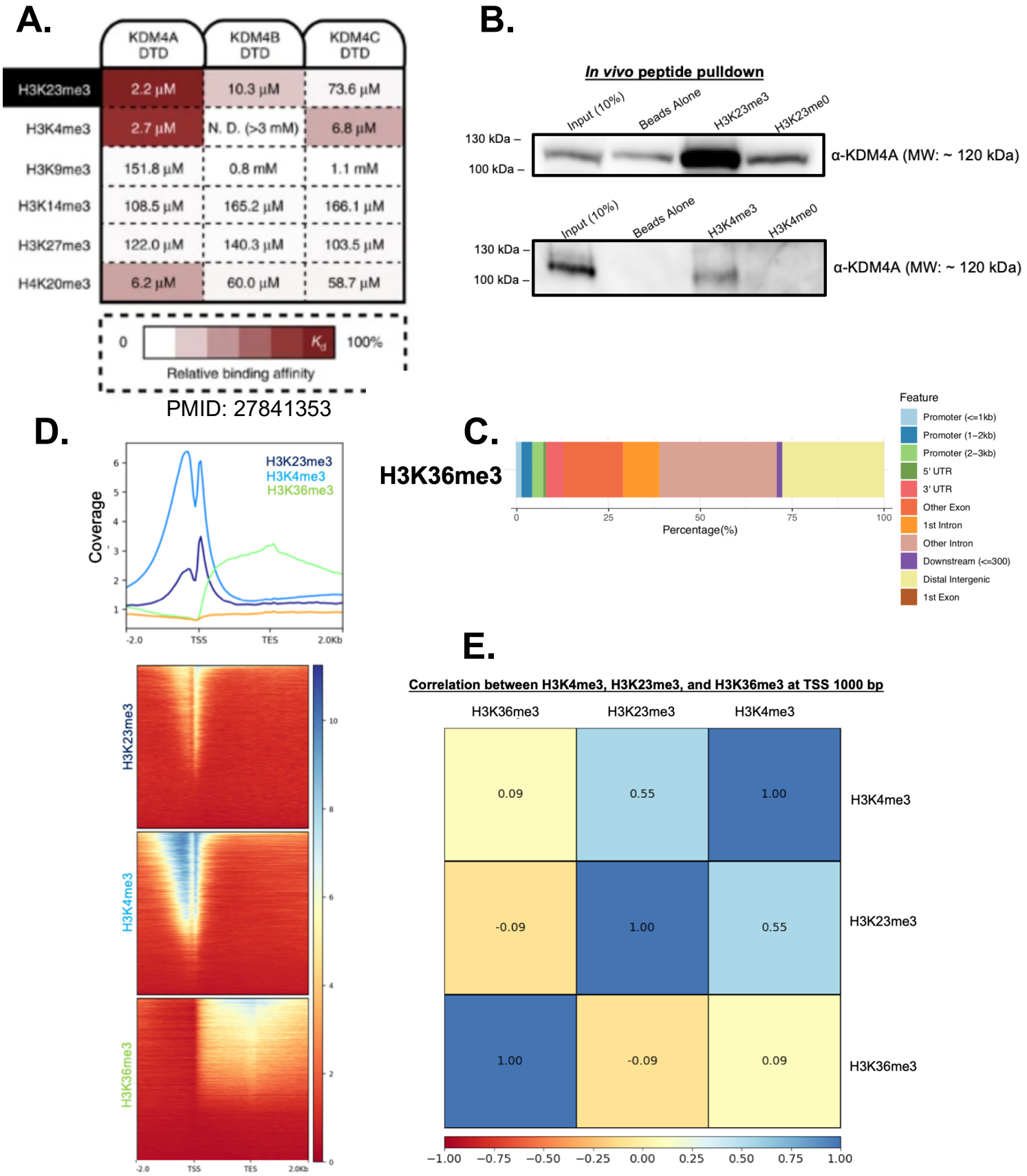
A.
KDM4A DTD
KDM4B DTD
KDM4C DTD
H3K23me3
2.2 µM
10.3 µM
73.6 µM
H3K4me3
2.7 µM
N. D. (>3 mM)
6.8 µM
H3K9me3
151.8 µM
0.8 mM
1.1 mM
H3K14me3
108.5 µM
165.2 µM
166.1 µM
H3K27me3
122.0 µM
140.3 µM
103.5 µM
H4K20me3
6.2 µM
60.0 µM
58.7 µM
0
100%
Relative binding affinity
PMID: 27841353
B.
In vivo peptide pulldown
Input (10%)
Beads Alone
H3K23me3
H3K23me0
130 kDa –
100 kDa –
α-KDM4A (MW: ~ 120 kDa)
Input (10%)
Beads Alone
H3K4me3
H3K4me0
130 kDa –
100 kDa –
α-KDM4A (MW: ~ 120 kDa)
C.
H3K36me3
Feature
Promoter (<=1kb)
Promoter (1–2kb)
Promoter (2–3kb)
5' UTR
3' UTR
Other Exon
1st Intron
Other Intron
Downstream (<=300)
Distal Intergenic
1st Exon
0
25
50
75
100
Percentage(%)
D.
Coverage
H3K23me3
H3K4me3
H3K36me3
-2.0
TSS
TES
2.0Kb
E.
Correlation between H3K4me3, H3K23me3, and H3K36me3 at TSS 1000 bp
H3K36me3
H3K23me3
H3K4me3
0.09
0.55
1.00
H3K4me3
-0.09
1.00
0.55
H3K23me3
1.00
-0.09
0.09
H3K36me3
−1.00
−0.75
−0.50
−0.25
0.00
0.25
0.50
0.75
1.00

F.

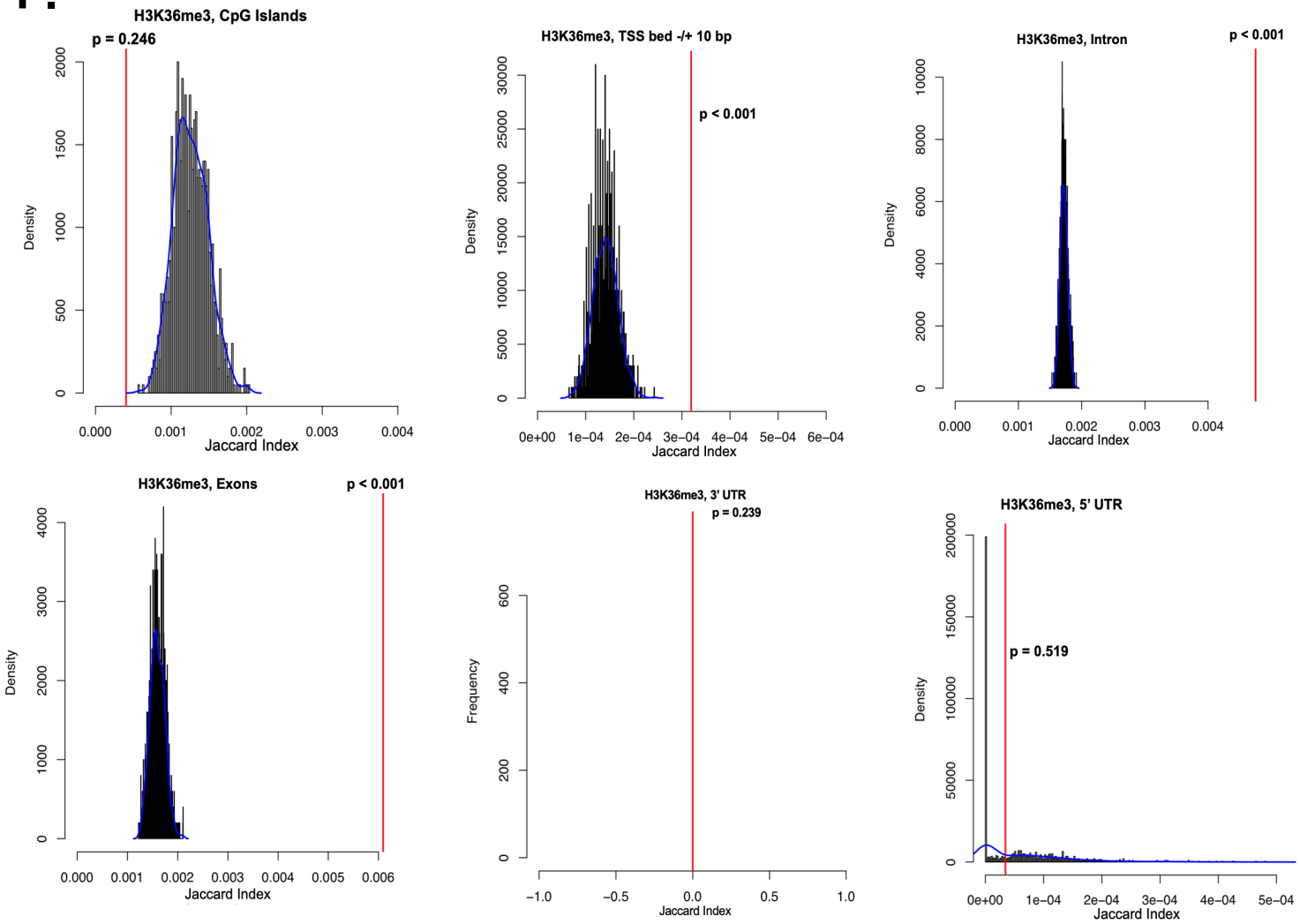

Table 5: Statistical enrichment of H3K36me3 statistical enrichment in various genome compartments

Compartment	Jaccard Index	P-value
CpG Islands	0.2416	1
TSS Bed -/+ 1000 bp	0.000319	<< 0.001
Exons	0.00609	<< 0.001
Introns	0.00475	<< 0.001
3' UTR	0.1299	0.239
5' UTR	0.2562	0.519

Figure 19 KDM4A is a dual reader of H3K4me3 and H3K23me3 and H3K36me3 is compartmentalized away from H3K4me3 and H3K23me3 (A) KDM4A DTD binds, most tightly, to H3K23me3 and H3K4me3 *in vitro* (from PMID:27841353) **(B)** KDM4A interacts with H3K4me3 and H3K23me3 *in vivo* **(C)** Feature distribution map of H3K36me3 ChIP-Seq data **(D)** Signal averaging and heat maps of H3K4me3, H3K23me3 and H3K36me3 at gene bodies **(E)** Correlation heat map of H3K4me3, H3K23me3 and H3K36me3 about all TSSs (1000 bp window) **(F)** GenometriCorr plots analyzing H3K36me3 statistical enrichment in various genome compartments**. Table 5** summarizes GenometriCorr statistics regarding H3K36me3 enrichment in gene compartments.

examine if there was a relationship between these three marks and the KDM4A enzyme *in vivo*.

To evaluate if the interaction between KDM4A with H3K4me3 and H3K23me3 is relevant *in vivo*, we performed an *in vivo* peptide pulldown in which we generated a nuclear lysate from 50B11 cells and incubated with either H3K4me3 peptide, H3K23me3 peptide, beads alone, or the corresponding unmodified peptide overnight at 4C, un-crosslinked. We found that H3K4me3 and H3K23me3 peptides, over their unmodified counterparts, do indeed enrich for KDM4A out of a nuclear lysate (Figure 19B).

To evaluate genome-wide distribution of one of the demethylation targets of KDM4A, H3K36me3, we performed nChIP-Seq of H3K36me3 in 50B11. Annotating H3K36me3 peaks using ChIP-SeekeR, we created a genome-wide feature distribution plot for H3K36me3. Consistent with previous reports, [7], [47], [105], [106] only a very small percentage (<~5%) of H3K36me3 peaks localize to promoters, with a large percentage localizing to gene bodies (Figure 19C).

To evaluate H3K36me3 signal intensity at gene bodies in comparison to H3K4me3 and H3K23me3 signal, we generated input-normalized bigwig files for H3K36me3 and generated heat maps and signal averaging profiles for the three marks at gene bodies. Consistent with the literature [7], [47], [105], [106], H3K36me3 signal is largely enriched along the gene body and depleted at the TSS and promoter regions (Figure 19D). To expand on this, we next evaluated the correlation between H3K4me3, H3K23me3 and H3K36me3 at all TSSs (adding in a 1000 bp window). Consistent with

Figure 19C and D, H3K36me3 shows a low correlation with both H3K4me3 and H3K23me3 at TSSs (1000 bp window).

To evaluate statistically significant overlap of H3K36me3 in various genome compartments, we again used GenometriCorr. Consistent with the feature distribution profiles showing very few promoter peaks and the heat maps/signal averaging profiles showing low signal flanking TSSs, our data shows that H3K36me3 is not statistically enriched at regions surrounding the TSS, but rather in other genome compartments such as exons and introns (Figure 19F and G).

Holistically, this data shows that H3K36me3 is largely compartmentalized away from H3K4me3 and H3K23me3 at promoters and that KDM4A, a dual reader of H3K4me3 and H3K23me3 an eraser of H3K36me3, associates with both H3K4me3 and H3K23me3 *in vivo.*

Differentiation of 50B11 causes genome-wide epigenetic reprogramming of H3K4me3 and H3K23me3

In 2007, Bernstein and colleagues showed that H3K4me3-H3K27me3 bivalent promoters reprogrammed after differentiation from mouse ESCs into neuronal progenitors [12] . Specifically, they noted these H3K4me3-H3K27me3 bivalent domains reprogrammed such that H3K4me3 increased and H3K27me3 decreased, if not disappeared entirely at a subset of key developmental genes including Sox2 and Pax5. They dubbed this reprogramming event a *resolution* into monovalent H3K4me3 (or H3K27me3 in some cases) and attributed the change in enrichment to a change in cellular state (e.g. differentiation). In a separate study, Price and colleagues [51] showed that a H3K9me3-H3K14ac bivalent signature, over time, reprogrammed as a

A.

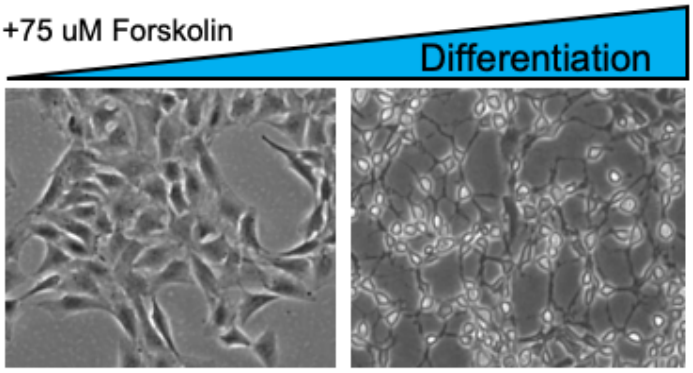

B.

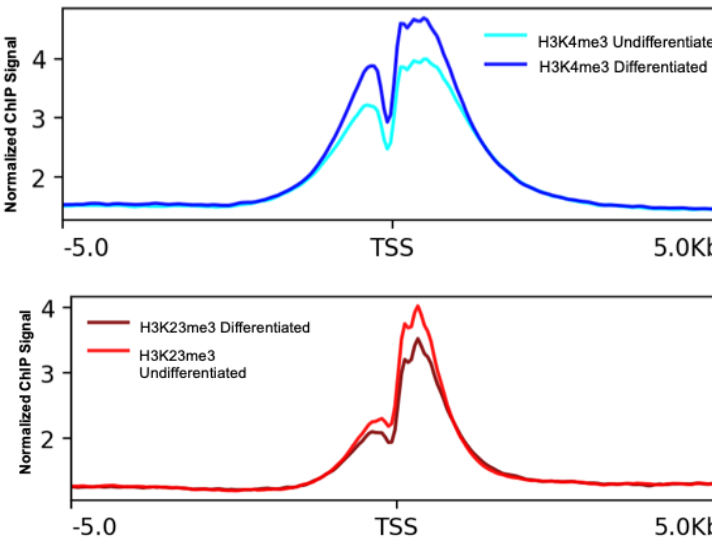

C.

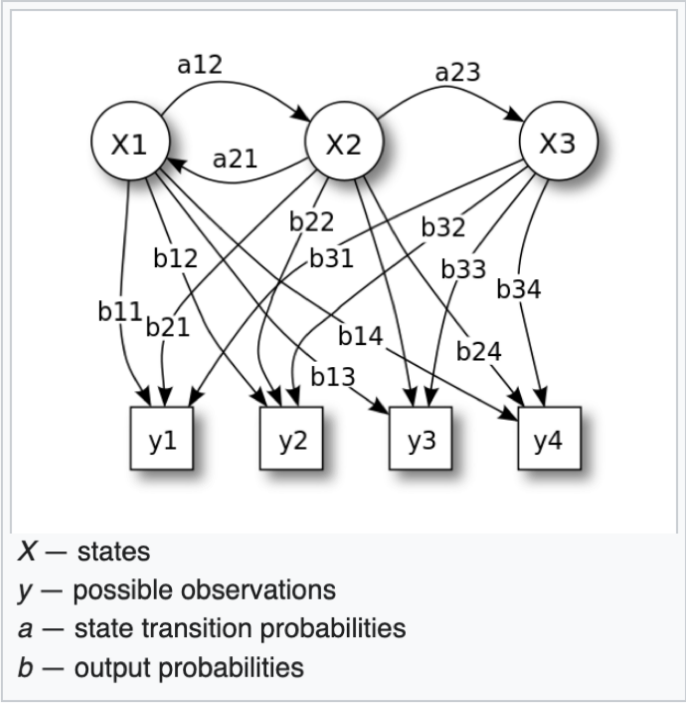

X — states
y — possible observations
a — state transition probabilities
b — output probabilities

Adapted from wikipedia

D.

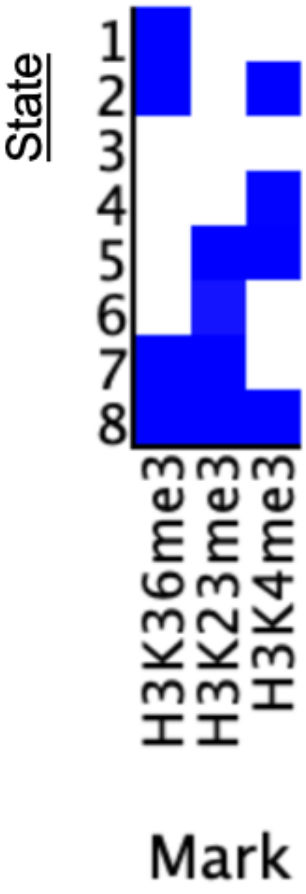

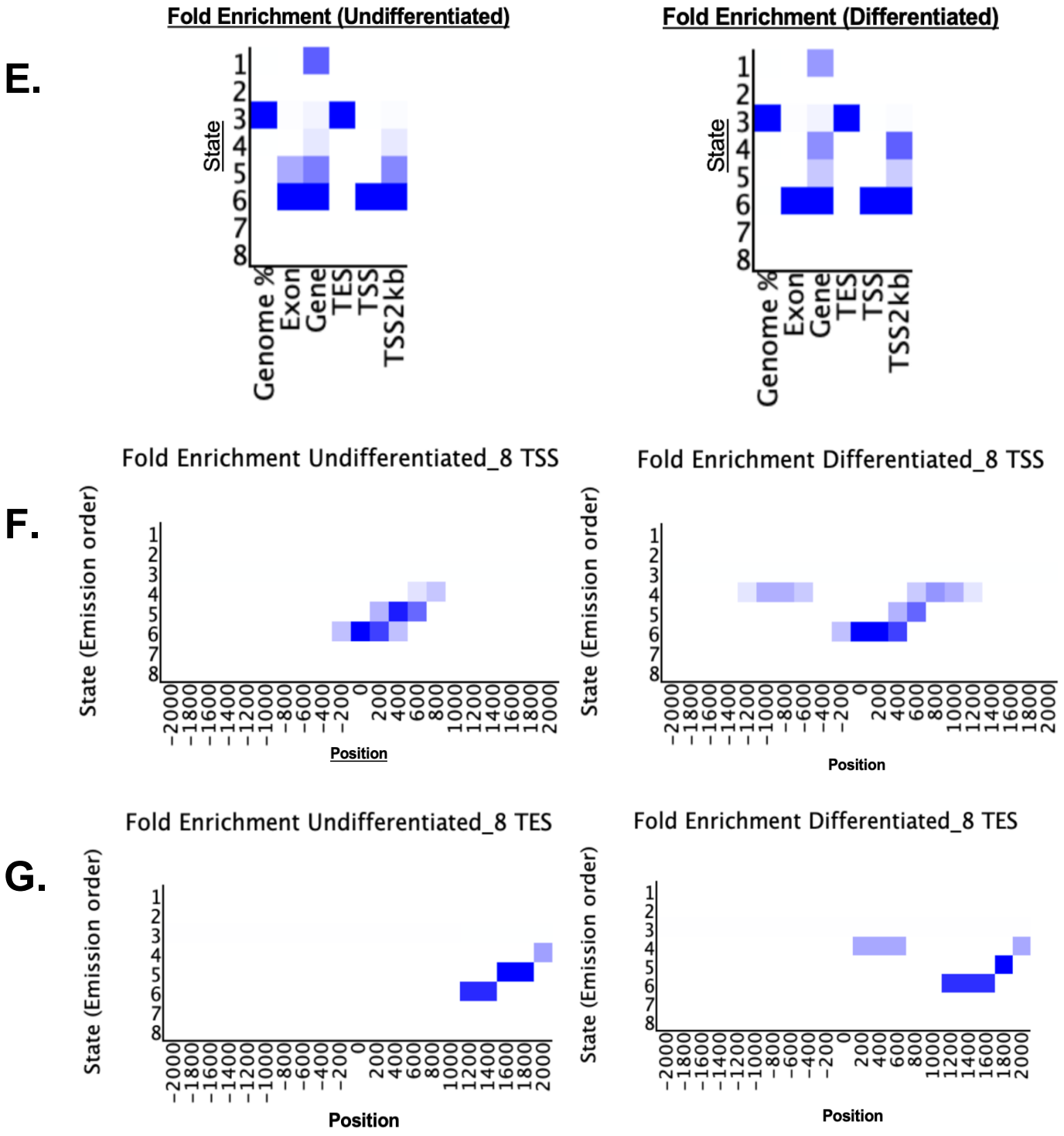

Figure 20 Differentiation-induced epigenetic reprogramming of H3K4me3 and H3K23me3 **(A)** Model for differentiation of 50B11 progenitors into nociceptors **(B)** Signal averaging/heat map of H3K4me3 and H3K23me3 about all TSSs in the undifferentiated and differentiated states. **(C)** Schematic of Hidden Markov Modeling of ChromHMM data **(D)** 8-state modeling of monovalent and combinatorial states of H3K4me3, H3K23me3 and H3K36me3 from ChIP-Seq data **(E)** Changes in chromatin states detected at various genome compartments in the undifferentiated and differentiated cells. Neighborhood enrichment profiles for the 8-state model about the TSS **(F)** or TES **(G)**.

function of age in mouse liver [51]. These bivalent regions showed that H3K9me3-H3K14ac reprogrammed into monovalent H3K9me3 or H3K14ac as mouse livers aged. Given the trends in changes in bivalent chromatin modifications, we wanted to test if H3K4me3-H3K23me3 bivalent promoters reprogrammed as a function of differentiation in 50B11. To accomplish this, we differentiated 50B11 cells from neuronal progenitors into nociceptors by stimulating with 75 uM forskolin for 8 hours. Undifferentiated and differentiated 50B11 cells were harvested and subjected to nChiP-Seq for H3K4me3, H3K23me3 and H3K36me3. Screening H3K4me3-H3K23me3 bivalent promoters, in the undifferentiated and differentiated state, in IGV showed a clear increase in H3K4me3 and decrease in H3K23me3 after differentiation (data not shown). This observation was also captured in signal averaging/heat maps of H3K4me3 and H3K23me3 in the undifferentiated and differentiated states (Figure 20B). To evaluate changes in individual chromatin states in the undifferentiated vs differentiated 50B11 cells, we used a java program called ChromHMM. This package uses Hidden Markov Modeling on binarized ChIP-Seq data and evaluates relationships between monovalent and combinatorial chromatin states in various genome compartments and compares changes in chromatin states as a function of changes in cellular states such as differentiation (Figure 20C, adapted from wikipedia). Using ChromHMM [107], we created an 8-state model encompassing individual and combinatorial modification states involving H3K4me3, H3K23me3 and H3K36me3 (Figure 20D). Consistent with our previous data, there are no H3K36me3 combinatorial states detected with either H3K4me3 or H3K23me3 in any genome compartment in the undifferentiated or differentiated state. In contrast, the H3K4me3-H3K23me3 bivalent signature is

detectable in both the undifferentiated and differentiated states. Interestingly, our ChromHMM data shows changes with monovalent and combinatorial modification states in various genome compartments as a function of differentiation. More specifically, monovalent H3K36me3 becomes less enriched at genes after differentiation and remains distinct from H3K4me3 and H3K23me3. Monovalent H3K4me3 becomes more enriched at genes and promoters (TSS 2kb) while bivalent H3K4me3-H3K23me3 becomes less enriched at genes and promoters after differentiation. Monovalent H3K23me3 largely remains unchanged before and after differentiation. Interestingly, our data also revealed that monovalent H3K23me3, unlike bivalent H3K23me3 which occupies promoters, instead occupies TSSs, in addition to flanking regions. This suggests that the TSS is occluded by a nucleosome modified with monovalent H3K23me3, physically blocking it from transcriptional activation, which is not the case for bivalent H3K23me3. (Figure 20 E).

We next used ChromHMM to evaluate changes in enrichment of specific chromatin states as a function of differentiation about TSSs and TESs (2kb on each side). Consistent with Figure 20E, our data shows enrichment of monovalent H3K4me3 within the a 2kb window of TSSs and TESs after differentiation while the bivalent H3K4me3-H3K23me3 state decreases at TSSs and TESs (Figure 20F and G). Although monovalent H3K23me3 does not change in location relative to the TSS or TES, our data shows that it does change in intensity, becoming slightly more enriched after differentiation, in contrast to bivalent H3K23me3, which becomes less enriched after differentiation (Figure 20F and G). Collectively, this data reveals changes in the monovalent and combinatorial bivalent H3K4me3 and H3K23me3 combinatorial states

as a function of differentiation in 50B11, and elucidates potential antagonistic cross-talk between H3K4me3 and H3K23me3 at bivalent promoters.

Transcriptional effect of H3K23me3 on mammalian gene expression

To investigate the transcriptional consequences of the global changes in H3K4me3 and H3K23me3 methylation after differentiation, we performed RNA-seq of 50B11 in the undifferentiated and differentiated state. To integrate the nChIP-Seq data with the RNA-Seq data, we employed BETA, a python package developed by Shirley Liu's lab [108], that takes binding-sites (ChIP-Seq data) and expression data (RNA-Seq data) and identifies if changes in gene expression correlated with the query regions (*binding sites*) of interest. Using BETA on the monovalent H3K4me3, bivalent H3K4me3-H3K23me3, and monovalent H3K23me3 regions with our RNA-Seq data in the undifferentiated and differentiated state, we identified a subset of genes that are marked with either monovalent H3K4me3 or bivalently marked with H3K4me3-H3K23me3 that were upregulated after differentiation. BETA was not able to identify genes that were up- or downregulated that were marked by monovalent H3K23me3 (Figure 21A-C). It is worth noting that there was a subset of monovalent H3K4me3 marked genes that were downregulated after differentiation, but the p-value associated with that measurement was less statistically significant than the genes that were upregulated after differentiation.

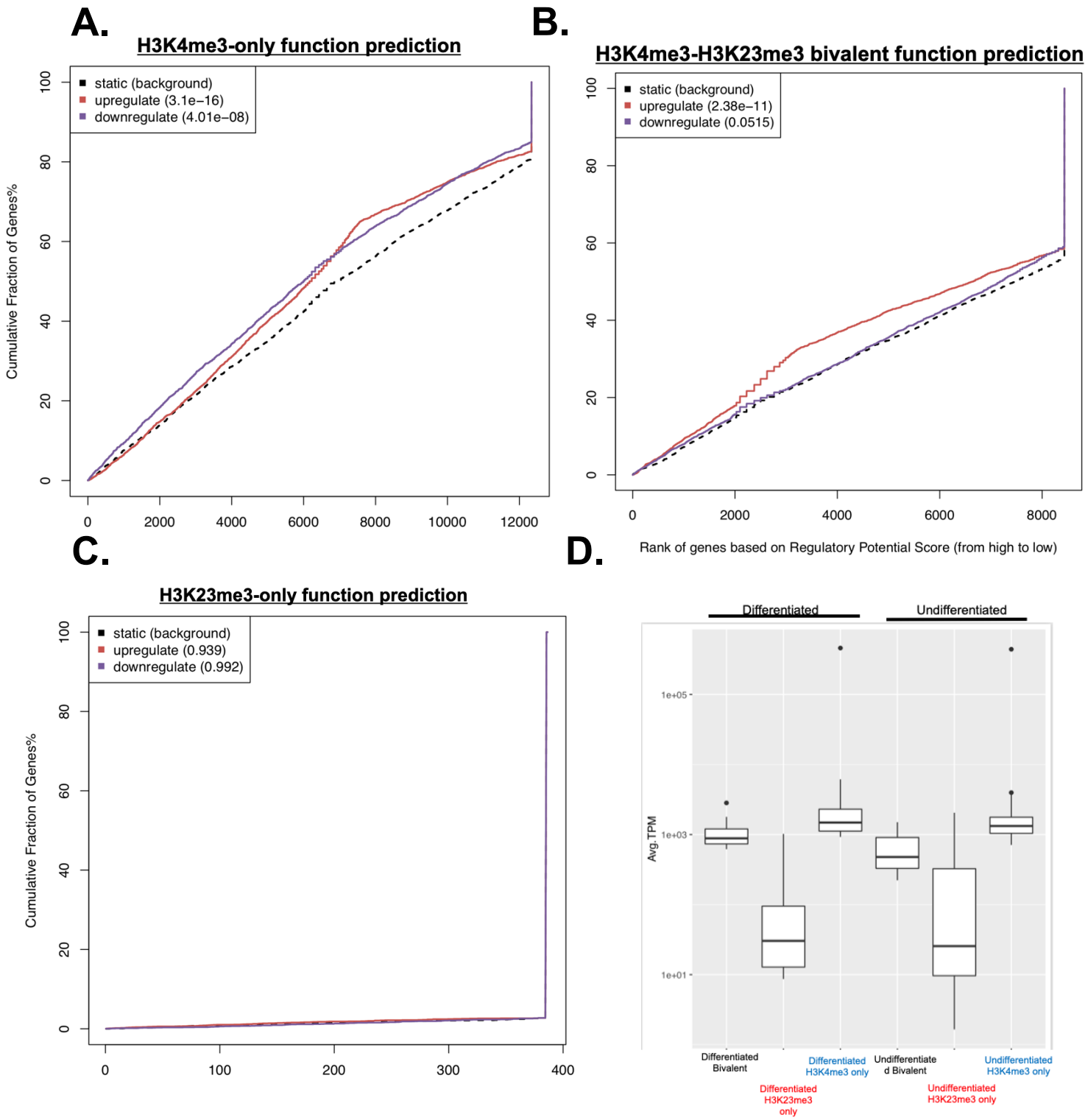
A.
H3K4me3-only function prediction
static (background)
upregulate (3.1e−16)
downregulate (4.01e−08)
Cumulative Fraction of Genes%
B.
H3K4me3-H3K23me3 bivalent function prediction
static (background)
upregulate (2.38e−11)
downregulate (0.0515)
Rank of genes based on Regulatory Potential Score (from high to low)
C.
H3K23me3-only function prediction
static (background)
upregulate (0.939)
downregulate (0.992)
Cumulative Fraction of Genes%
D.
Differentiated
Undifferentiated
Avg. TPM
Differentiated Bivalent
Differentiated H3K23me3 only
Differentiated H3K4me3 only
Undifferentiated Bivalent
Undifferentiated H3K23me3 only
Undifferentiated H3K4me3 only

Figure 21 Differential gene expression by epigenetic state Activation/Repressive function prediction for H3K4me3-only (A) , bivalent H3K4me3-H3K23me3 (B) or H3K23me3-only (C) genes during 50B11 differentiation**. (D)** Box and whisker plots displaying average transcripts produced for monovalent H3K4me3, H3K23me3 and bivalent H3K4me3-H3K23me3 **(E)** Pathway ontologies for H3K4me3-only, H3K23me3-only or bivalent H3K4me3-H3K23me3 marked genes.

To more directly evaluate the effect H3K23me3 has on gene expression, we plotted the average transcripts per million reads (TPM) for the top 50 highest expression genes for monovalent H3K4me3, bivalent H3K4me3-H3K23me3, or monovalent H3K23me3 marked genes in the undifferentiated and differentiated state. Strikingly, our data shows that the top 50 highest expressing monovalent H3K23me3 marked genes express far fewer transcripts, on average, compared to their monovalent H3K4me3 or bivalent H3K4me3-H3K23me3 marked counterparts (Figure 21D). A pathways ontology revealed that monovalent H3K4me3 and bivalent H3K4me3-H3K23me3 marked genes are related to pathways involving sensory perception and detection of stimuli while monovalent H3K23me3 marked genes related to multi-cellular developmental pathways (Figure 21E). Collectively, this data suggests that there are differential transcriptional changes associated with monovalent and bivalent H3K4me3 and H3K23me3 and suggests that H3K23me3 might dampen transcription relative to H3K4me3.

Epigenetic cross talk between methyl-lysines *in vivo*

The *in vivo* nChIP-Seq data for H3K4me3, H3K23me3 and H3K36me3 suggested that certain methyl-lysine marks might be influencing others. To investigate further, we used transgenic 50B11 cells expressing mutant histones containing various lysine to methionine mutations (Figure 22A). Our prior studies with K-to-M mutations yielded H3K4M and H3K9M clones that we expanded and used to perturb H3K4 and H3K9 (and H3K23) methylation respectively (See Supplemental Figure 3B). Using these mutants, we wanted to ask if perturbations in H3K4 methylation caused perturbations in H3K23 methylation and vice versa. Interestingly, when perturbing H3K4 methylation using H3K4M, we observe changes in H3K9, H3K23, and H3K36 methylation.

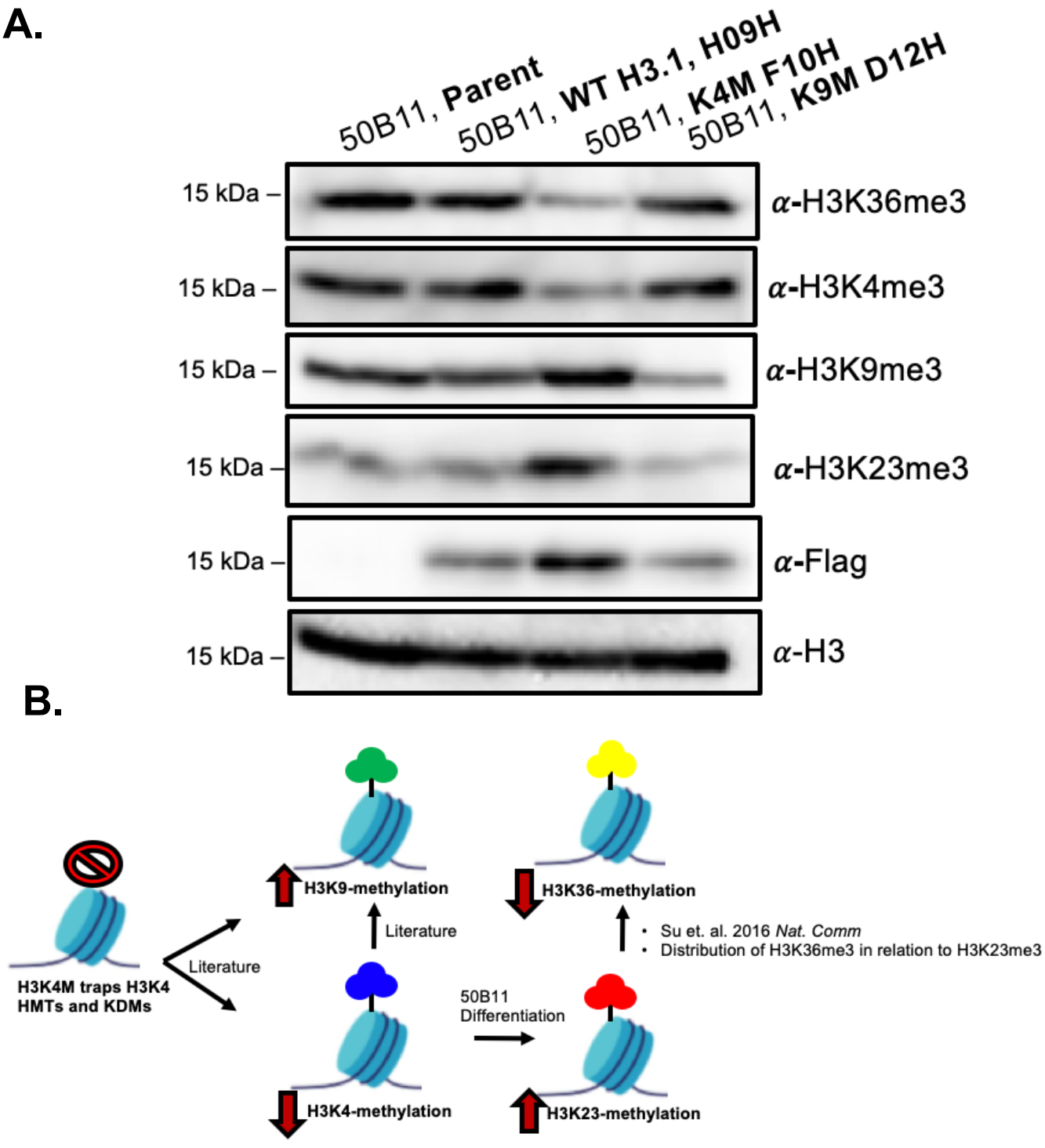

Figure 22 Methyl-lysine epigenetic cross-talk in 50B11 (A) Western blot panel of transgenic 50B11 K-to-M clones blotted for H3K4me3, H3K9me3, H3K23me3 and H3K36me3 **(B)** Proposed model of epigenetic cross talk with common histone H3 methyl-lysine marks.

More specifically, when H3K4me3 decrease, H3K9me3 and H3K23me3 increase while H3K36me3 decreases. However, when perturbing H3K9 and H3K23 methylation using H3K9M, we do not observe changes in either H3K4me3 or H3K36me3, suggesting that whatever cross-talk caused the perturbations in tri-methyl H3K9, H3K23, and H3K36 in H3K4M cells does not reciprocate in H3K9M cells. To integrate the observations regarding H3K4me3 and H3K23me3 interplay, Figure 22B shows a proposed schematic for the apparent cross-talk involving methylation at lysines 4, 9, 23, and 36, much of which is already published [105], [109], [110]. H3K4 methylation has been shown antagonize H3K9 methylation via KDM4A/B, but not vice versa. Similarly, H3K23 methylation has been shown to antagonize H3K36 methylation via KDM4B, but only *in vitro* and not vice versa [41]. In this chapter, we show evidence that H3K4me3 influences H3K23me3 positioning at promoters and its enrichment, suggesting potential antagonistic cross-talk by H3K4me3 onto H3K23me3.

Taken together, this evidence points to clear cross-talk between H3K4me3 and H3K23me3 and adds to the expanding repertoire of bivalent chromatin signatures.

iv. Discussion.

Post-translational modifications on histone proteins can modulate the interaction of the histones with the DNA to form open, transcriptionally permissive states or repressive, transcriptionally silent states [4], [81], [84]. Methylation of histone proteins has long been implicated in forming both repressive (e.g. H3K9-methyl, H3K27-methyl, H4K20-methyl, etc.) and permissive (e.g. H3K4-methyl, H3K36-methyl) chromatin states each with unique roles in regulating chromatin accessibility through interaction

with specific effector proteins (e.g. readers) that help drive the specificity of chromatin remodeling events [7], [44], [46], [60], [69], [95]. Regulation by these methyl-lysine chromatin signatures has proven essential for transcription, replication, repair and other template dependent processes [6], [72], [84]. Here, we report information on the poorly characterized H3K23me3 histone PTM in the neuronal progenitor cell line 50B11. Our studies uncovered that H3K23me3 is a promoter-enriched PTM that strongly associates with a subset of H3K4me3 nucleosomes. We also showed that KDM4A, a specific reader of H3K4me3 and H3K23me3, associates with both modifications *in vivo*, suggesting that the mechanisms characterized in the literature regarding H3K4me3-KDM4A and H3K23me3-KDM4A interactions might be relevant in this system. Additionally, our studies show that, upon differentiation, H3K4me3 and H3K23me3 epigenetically reprogram at bivalent promoters, whereby H3K4me3 increases and H3K23me3 decreases, and also results in a net increase in gene expression. Lastly, our data points to necessary cross-talk between H3K4me3 and H3K23me3 as monovalent H3K23me3 localizes at TSSs while bivalent H3K4me3-H3K23me3 localizes at promoters, along with monovalent H3K4me3. We suspect that H3K4me3 itself, or the associated machinery, is working to direct H3K23 methylation at promoters whereas in the absence of H3K4me3, H3K23me3 is directed to TSSs to silence gene expression. Additionally, our K-to-M studies showed that perturbations in H3K4me3 causes changes in H3K23me3 but not vice versa, suggesting, again, that the cross-talk between H3K4me3 and H3K23me3 is one directional. This is quite conceivable as H3K4me3 has been shown to antagonize H3K9 methylation, encoded by the same methyltransferases

as H3K23, whereby demethylation of H3K4 allows for expansion of H3K9 methylation [109], [110].

This work also raises interesting questions regarding cross-talk with other histone H3 methyl-lysines such as H3K9 and H3K36. As previously mentioned, Su and colleagues [41] showed that, *in vitro*, the presence of H3K23me3 stimulated demethylation of H3K36 by KDM4B, and while there is turnover of H3K36 methylation independent of H3K23me3 occupied regions, there are only a handful of enzymes that target H3K36 for demethylation, so it begs the question of whether or not the KDM4A-H3K23me3 axis is partially contributing to global regulation of H3K36 methylation at gene promoters. Our data, and others, have found, in multiple species, the anti-correlation between multiple methylation states of H3K23 and H3K36 [73]. H3K36 methylation has been well characterized as being enriched at exons to help facilitate transcriptional elongation and differential splicing, but it has rarely been characterized as a being a promoter mark [7]. Many have pointed to this phenomenon to explain how PTMs are differentially positioned throughout gene bodies and regulatory regions, but this work helps shed light on a potential regulatory mechanism whereby H3K36 methylation may be partially excluded from some promoters through activity of KDM4A and H3K23me3; however, more work needs to be done to determine the extent of cross-talk between H3K23me3 and H3K36me3 and if such cross-talk is mediated by KDM4A *in vivo*.

Changes to bivalent promoters as a function of gene expression has been studied in the context of H3K4me3-H3K27me3 bivalency. In 2007, Bernstein and colleagues [12] showed that mESC differentiated into neuronal progenitors showed an

increase in H3K4me3 and a decrease in H3K27me3 at a subset of key developmental genes. They purported that the resolution of H3K4me3-H3K27me3 was linked to the change the cellular state and that the bivalent chromatin signature was a way to *poise* gene expression for rapid activation or repression by having both a repressive and permissive chromatin mark already written at target loci. Here, our data similarly shows upregulation of the permissive mark (H3K4me3) and downregulation of the repressive mark (H3K23me3) as a function of differentiation in 50B11. However, our data shows that the H3K4me3-H3K23me3 bivalent state remains bivalent, albeit less so given the corresponding changes in both histone marks and the net increase in gene expression. Collectively, this suggests that bivalent histone modifications belong to a more general mechanism of transcriptional regulators rather than one that is developmentally linked. This is further supported by the detection of bivalent H3K9me3-H3K14ac dual modification found in terminally differentiated mouse liver [51]. In that study, Price and colleagues showed that the H3K9me3-H3K14ac bivalency changed as a function of age, with bivalent regions resolving into either H3K9me3 or H3K14ac or losing both marks entirely. Another study by Matsumura and colleagues showed that H3K4me3-H3K9me3 bivalency played a role in adipocyte differentiation [111]. These works further highlight the diversity of bivalent histone modifications and their attenuation based on cellular cues (differentiation, aging, etc.) as well as the need to develop new tools for unbiased detection of combinatorial modification states. Collectively, this study unveils a new bivalent chromatin signature, H3K4me3-H3K23me3, and explores cross-talk with other histone H3 methyl-lysines in regulating gene expression. More work needs to be done to elucidate how these bivalent chromatin domains are established and regulated.

Additionally, the full repertoire of combinatorial modification states should be a focus in future studies as the cross-talk between epigenetic marks can influence the behavior of other epigenetic marks in unanticipated ways.

Appendix

Supplementary Figure 1

A.

H3K23me1 (EHMT2/G9a) Fragmentation Mass Error (ppm) EThcD

#1	c^+	$c+H^+$	$c+H^{2+}$	$c+H^{3+}$	Seq.	z^+	z^{2+}	z^{3+}	$z-H^{2+}$	#2
1					A					22
2					P					21
3	-1.97				R			-1.88		20
4	-1.89				K-Dimethyl			-0.84		19
5	-1.38				Q		-1.17	-1.78	-0.30	18
6					L		-1.78			17
7					A		-0.53			16
8	-1.38	-0.63			T					15
9					K-Methyl	-1.78	+0.95			14
10					A	-1.70	+1.04			13
11	-0.17	+1.89			A		+1.53			12
12		-0.83	+0.67	+1.43	R					11
13				+0.88	K-Dimethyl	-0.58			0.00	10
14			-0.07	-0.09	S					9
15					A					8
16				-0.93	P					7
17					A					6
18				+1.17	T					5
19			-0.08	-1.05	G					4
20				-1.00	G					3
21				+0.38	V					2
22					K					1

H3K23me1 (EHMT2/G9a) Fragmentation EThcD

#1	c^+	$c+H^+$	$c+H^{2+}$	$c+H^{3+}$	Seq.	z^+	z^{2+}	z^{3+}	$z-H^{2+}$	#2
1	89.07094	90.07876	45.54302	30.69777	A					22
2	186.12370	187.13153	94.06940	63.04869	P	2191.33973	1096.17350	731.11809	1095.66959	21
3	342.22481	343.23264	172.11996	115.08240	R	2094.28697	1047.64712	698.76717	1047.14321	20
4	498.35108	499.35890	250.18309	167.12449	K-Dimethyl	1938.18586	969.59657	646.73347	969.09265	19
5	626.40965	627.41748	314.21238	209.81068	Q	1782.05959	891.53343	594.69138	891.02952	18
6	739.49372	740.50154	370.75441	247.50537	L	1654.00102	827.50415	552.00519	827.00023	17
7	810.53083	811.53866	406.27297	271.18440	A	1540.91695	770.96211	514.31050	770.45820	16
8	911.57851	912.58634	456.79681	304.86696	T	1469.87984	735.44356	490.63146	734.93964	15
9	1053.68912	1054.69695	527.85211	352.23717	K-Methyl	1368.83216	684.91972	456.94890	684.41581	14
10	1124.72624	1125.73406	563.37067	375.91621	A	1226.72155	613.86441	409.57870	613.36050	13
11	1195.76335	1196.77118	598.88923	399.59524	A	1155.68443	578.34585	385.89966	577.84194	12
12	1351.86446	1352.87229	676.93978	451.62895	R	1084.64732	542.82730	362.22062	542.32339	11
13	1507.99073	1508.99855	755.00291	503.67103	K-Dimethyl	928.54621	464.77674	310.18692	464.27283	10
14	1595.02275	1596.03058	798.51893	532.68171	S	772.41994	386.71361	258.14483	386.20970	9
15	1666.05987	1667.06769	834.03748	556.36075	A	685.38792	343.19760	229.13416	342.69368	8
16	1763.11263	1764.12046	882.56387	588.71167	P	614.35080	307.67904	205.45512	307.17513	7
17	1834.14974	1835.15757	918.08242	612.39071	A	517.29804	259.15266	173.10420	258.64875	6
18	1935.19742	1936.20525	968.60626	646.07327	T	446.26092	223.63410	149.42516	223.13019	5
19	1992.21889	1993.22671	997.11699	665.08042	G	345.21325	173.11026	115.74260	172.60635	4
20	2049.24035	2050.24818	1025.62773	684.08758	G	288.19178	144.59953	96.73545	144.09562	3
21	2148.30876	2149.31659	1075.16193	717.11038	V	231.17032	116.08880	77.72829	115.58489	2
22					K	132.10191	66.55459	44.70549	66.05068	1

H3K23me2 (EHMT2/G9a) Fragmentation EThcD

#1	c+H²⁺	c+H³⁺	c+H⁴⁺	c²⁺	Seq.	z⁺	z+H²⁺	z+H³⁺	z²⁺	#2
1	45.54302	30.69777	23.27515	45.03911	A					22
2	94.06940	63.04869	47.53834	93.56549	P	2219.37103	1110.69307	740.79780	1110.18915	21
3	172.11996	115.08240	86.56362	171.61605	R	2122.31827	1062.16668	708.44688	1061.66277	20
4	250.18309	167.12449	125.59518	249.67918	K-Dimethyl	1966.21716	984.11613	656.41318	983.61222	19
5	314.21238	209.81068	157.60983	313.70847	Q	1810.09089	906.05300	604.37109	905.54908	18
6	370.75441	247.50537	185.88084	370.25050	L	1682.03232	842.02371	561.68490	841.51980	17
7	406.27297	271.18440	203.64012	405.76905	A	1568.94825	785.48168	523.99021	784.97776	16
8	456.79681	304.86696	228.90204	456.29289	T	1497.91114	749.96312	500.31117	749.45921	15
9	534.85994	356.90905	267.93361	534.35603	K-Dimethyl	1396.86346	699.43928	466.62861	698.93537	14
10	570.37849	380.58809	285.69289	569.87458	A	1240.73720	621.37615	414.58652	620.87224	13
11	605.89705	404.26713	303.45216	605.39314	A	1169.70008	585.85759	390.90749	585.35368	12
12	683.94761	456.30083	342.47744	683.44369	R	1098.66297	550.33904	367.22845	549.83512	11
13	769.01856	513.01480	385.01292	768.51465	K-Trimethyl	942.56186	472.28848	315.19475	471.78457	10
14	812.53458	542.02548	406.77093	812.03067	S	772.41994	387.21752	258.48077	386.71361	9
15	848.05313	565.70452	424.53021	847.54922	A	685.38792	343.70151	229.47010	343.19760	8
16	896.57952	598.05544	448.79340	896.07560	P	614.35080	308.18295	205.79106	307.67904	7
17	932.09807	621.73447	466.55267	931.59416	A	517.29804	259.65657	173.44014	259.15266	6
18	982.62191	655.41703	491.81459	982.11800	T	446.26092	224.13801	149.76110	223.63410	5
19	1011.13264	674.42419	506.06996	1010.62873	G	345.21325	173.61417	116.07854	173.11026	4
20	1039.64338	693.43134	520.32533	1039.13946	G	288.19178	145.10344	97.07139	144.59953	3
21	1089.17758	726.45415	545.09243	1088.67367	V	231.17032	116.59271	78.06423	116.08880	2
22					K	132.10191	67.05850	45.04143	66.55459	1

H3K23me2 (EHMT2/G9a) Fragmentation Mass Error (ppm) EThcD

#1	c+H²⁺	c+H³⁺	c+H⁴⁺	c²⁺	Seq.	z⁺	z+H²⁺	z+H³⁺	z²⁺	#2
1					A					22
2					P					21
3					R		-1.10	-0.20		20
4				-1.57	K-Dimethyl			+0.70		19
5					Q		+0.49		+0.28	18
6					L		+1.04	+1.67		17
7					A		+0.84			16
8					T		+0.23			15
9	+1.51			+0.23	K-Dimethyl	+0.65	+1.33		-1.39	14
10		-0.11			A		-0.61		-0.42	13
11	+0.53	+0.76			A				-0.04	12
12	+0.86				R	-1.10			-0.38	11
13		-0.29			K-Trimethyl	-1.07				10
14		-0.74	+0.58		S					9
15					A					8
16					P					7
17		+0.55	+1.77		A					6
18		-1.25	-1.21		T					5
19		-0.64	-1.24	+1.28	G					4
20		-1.14	+0.01		G					3
21			-0.29		V					2
22					K					1

H3K23me1 (EHMT1/GLP)Fragmentation Mass Error (ppm) EThcD

#1	c^{+}	$c+H^{3+}$	$c+H^{4+}$	c^{2+}	c^{3+}	Seq.	z^{+}	z^{2+}	$z-H^{2+}$	$z-H^{3+}$	#2
1						A					22
2	+0.07					P					21
3	-1.62					R					20
4	-1.93			-0.65		K-Methyl					19
5				-1.53		Q		-0.48	-0.83		18
6						L		-1.16	-0.58		17
7	-1.16			-1.53		A		-1.84	-1.54	-1.96	16
8	-1.44					T			-1.78	-1.36	15
9	-1.99					K-Methyl	+0.55	-0.81	-1.79	-1.59	14
10	+1.88				-0.75	A		+0.65	-1.41	-1.33	13
11				-1.78	-1.50	A		+0.60	-1.92	-1.55	12
12		+1.17				R	-0.78	+0.62		-1.46	11
13		+1.00	+1.04		-1.44	K-Trimethyl	-0.81		-1.92		10
14		+0.83	+1.71	-1.99		S					9
15		-1.48				A					8
16		+0.53	+1.29			P					7
17					-1.58	A					6
18		+0.89	+0.58		+0.04	T					5
19		-0.31	+0.37	+0.04	-1.88	G					4
20		-0.46	+0.59			G					3
21		-1.32	+0.36		-1.24	V					2
22						K					1

H3K23me1 (EHMT1/GLP)Fragmentation EThcD

#1	c^{+}	$c+H^{3+}$	c^{2+}	c^{3+}	Seq.	z^{+}	z^{2+}	$z-H^{2+}$	$z-H^{3+}$	#2
1	89.07094	30.69777	45.03911	30.36183	A					22
2	186.12370	63.04869	93.56549	62.71275	P	2191.33973	1096.17350	1095.66959	730.78215	21
3	342.22481	115.08240	171.61605	114.74646	R	2094.28697	1047.64712	1047.14321	698.43123	20
4	484.33543	162.45260	242.67135	162.11666	K-Methyl	1938.18586	969.59657	969.09265	646.39753	19
5	612.39400	205.13879	306.70064	204.80285	Q	1796.07524	898.54126	898.03735	599.02732	18
6	725.47807	242.83348	363.24267	242.49754	L	1668.01667	834.51197	834.00806	556.34113	17
7	796.51518	266.51252	398.76123	266.17658	A	1554.93260	777.96994	777.46603	518.64644	16
8	897.56286	300.19508	449.28507	299.85914	T	1483.89549	742.45138	741.94747	494.96741	15
9	1039.67347	347.56528	520.34038	347.22934	K-Methyl	1382.84781	691.92754	691.42363	461.28485	14
10	1110.71059	371.24432	555.85893	370.90838	A	1240.73720	620.87224	620.36832	413.91464	13
11	1181.74770	394.92336	591.37749	394.58742	A	1169.70008	585.35368	584.84977	390.23560	12
12	1337.84881	446.95706	669.42804	446.62112	R	1098.66297	549.83512	549.33121	366.55657	11
13	1507.99073	503.67103	754.49900	503.33509	K-Trimethyl	942.56186	471.78457	471.28065	314.52286	10
14	1595.02275	532.68171	798.01502	532.34577	S	772.41994	386.71361	386.20970	257.80889	9
15	1666.05987	556.36075	833.53357	556.02481	A	685.38792	343.19760	342.69368	228.79821	8
16	1763.11263	588.71167	882.05995	588.37573	P	614.35080	307.67904	307.17513	205.11918	7
17	1834.14974	612.39071	917.57851	612.05477	A	517.29804	259.15266	258.64875	172.76826	6
18	1935.19742	646.07327	968.10235	645.73733	T	446.26092	223.63410	223.13019	149.08922	5
19	1992.21889	665.08042	996.61308	664.74448	G	345.21325	173.11026	172.60635	115.40666	4
20	2049.24035	684.08758	1025.12381	683.75163	G	288.19178	144.59953	144.09562	96.39950	3
21	2148.30876	717.11038	1074.65802	716.77444	V	231.17032	116.08880	115.58489	77.39235	2
22					K	132.10191	66.55459	66.05068	44.36954	1

H3K23me2 (EHMT1/GLP) Fragmentation EThcD

#1	c^{+}	$c+H^{+}$	c^{2+}	c^{3+}	Seq.	z^{+}	z^{2+}	z^{3+}	$z-H^{+}$	$z-H^{2+}$	$z-H^{3+}$	#2
1	89.07094	90.07876	45.03911	30.36183	A							22
2	186.12370	187.13153	93.56549	62.71275	P	2219.37103	1110.18915	740.46186	2218.36321	1109.68524	740.12592	21
3	342.22481	343.23264	171.61605	114.74646	R	2122.31827	1061.66277	708.11094	2121.31044	1061.15886	707.77500	20
4	498.35108	499.35890	249.67918	166.78854	K-Dimethyl	1966.21716	983.61222	656.07724	1965.20933	983.10830	655.74129	19
5	626.40965	627.41748	313.70847	209.47474	Q	1810.09089	905.54908	604.03515	1809.08307	905.04517	603.69921	18
6	739.49372	740.50154	370.25050	247.16942	L	1682.03232	841.51980	561.34896	1681.02449	841.01588	561.01301	17
7	810.53083	811.53866	405.76905	270.84846	A	1568.94825	784.97776	523.65427	1567.94043	784.47385	523.31833	16
8	911.57851	912.58634	456.29289	304.53102	T	1497.91114	749.45921	499.97523	1496.90331	748.95529	499.63929	15
9	1067.70477	1068.71260	534.35603	356.57311	K-Dimethyl	1396.86346	698.93537	466.29267	1395.85563	698.43146	465.95673	14
10	1138.74189	1139.74971	569.87458	380.25215	A	1240.73720	620.87224	414.25058	1239.72937	620.36832	413.91464	13
11	1209.77900	1210.78683	605.39314	403.93118	A	1169.70008	585.35368	390.57155	1168.69226	584.84977	390.23560	12
12	1365.88011	1366.88794	683.44369	455.96489	R	1098.66297	549.83512	366.89251	1097.65514	549.33121	366.55657	11
13	1536.02203	1537.02985	768.51465	512.67886	K-Trimethyl	942.56186	471.78457	314.85880	941.55403	471.28065	314.52286	10
14	1623.05405	1624.06188	812.03067	541.68954	S	772.41994	386.71361	258.14483	771.41212	386.20970	257.80889	9
15	1694.09117	1695.09899	847.54922	565.36857	A	685.38792	343.19760	229.13416	684.38009	342.69368	228.79821	8
16	1791.14393	1792.15176	896.07560	597.71949	P	614.35080	307.67904	205.45512	613.34298	307.17513	205.11918	7
17	1862.18104	1863.18887	931.59416	621.39853	A	517.29804	259.15266	173.10420	516.29021	258.64875	172.76826	6
18	1963.22872	1964.23655	982.11800	655.08109	T	446.26092	223.63410	149.42516	445.25310	223.13019	149.08922	5
19	2020.25019	2021.25801	1010.62873	674.08825	G	345.21325	173.11026	115.74260	344.20542	172.60635	115.40666	4
20	2077.27165	2078.27948	1039.13946	693.09540	G	288.19178	144.59953	96.73545	287.18396	144.09562	96.39950	3
21	2176.34006	2177.34789	1088.67367	726.11821	V	231.17032	116.08880	77.72829	230.16249	115.58489	77.39235	2
22					K	132.10191	66.55459	44.70549	131.09408	66.05068	44.36954	1

H3K23me2 (EHMT1/GLP) Fragmentation Mass Error (ppm) EThcD

#1	c^{+}	$c+H^{+}$	c^{2+}	c^{3+}	Seq.	z^{+}	z^{2+}	$z-H^{+}$	$z-H^{2+}$	$z-H^{3+}$	#2
1					A						22
2	+0.50				P						21
3	-0.10				R		-0.30			-0.89	20
4	-0.43				K-Dimethyl		-0.72				19
5	-0.81		-1.64		Q		+0.89		-1.41	-1.13	18
6			-0.06		L	+0.56	+0.83	+1.14	-0.06	-0.95	17
7	-0.52		-0.95		A	-1.24	+1.92		-0.34		16
8	-0.38		-1.37		T			+0.73	-0.77	+1.00	15
9		+0.76	-1.13		K-Dimethyl	+0.92	+1.93	+0.73	-0.61	+0.21	14
10		-0.58	-1.05		A	+0.11		+1.28	-0.62		13
11	+0.66		-0.99		A	+0.84			-0.36		12
12	+0.08	+1.61	-0.75	-0.64	R	-0.22		+1.21	-0.95		11
13			-0.16	-0.55	K-Trimethyl	+1.45		-0.18	-0.10		10
14			+0.18	-0.86	S			+0.32			9
15					A			-0.50			8
16			+0.18	-0.90	P						7
17			-0.68	-0.83	A			-0.38			6
18			+1.76	-1.16	T			+0.99			5
19			+1.22	-0.64	G			-0.34			4
20			-0.53	-0.52	G	-0.16					3
21				-1.04	V						2
22					K			+0.46			1

H3K23me3 (EHMT1/GLP) Fragmentation EThcD

#1	c^{2+}	c^{3+}	c^{4+}	Seq.	z^{2+}	z^{3+}	$z\text{-}H^{2+}$	$z\text{-}H^{3+}$	#2
1	45.03911	30.36183	23.02319	A					22
2	93.56549	62.71275	47.28638	P	1124.20480	749.80563	1123.70089	749.46969	21
3	171.61605	114.74646	86.31166	R	1075.67842	717.45471	1075.17451	717.11876	20
4	256.68700	171.46043	128.84714	K-Trimethyl	997.62787	665.42100	997.12395	665.08506	19
5	320.71629	214.14662	160.86178	Q	912.55691	608.70703	912.05300	608.37109	18
6	377.25832	251.84131	189.13280	L	848.52762	566.02084	848.02371	565.68490	17
7	412.77688	275.52035	206.89208	A	791.98559	528.32615	791.48168	527.99021	16
8	463.30072	309.20290	232.15400	T	756.46703	504.64711	755.96312	504.31117	15
9	548.37168	365.91688	274.68948	K-Trimethyl	705.94319	470.96455	705.43928	470.62861	14
10	583.89023	389.59591	292.44875	A	620.87224	414.25058	620.36832	413.91464	13
11	619.40879	413.27495	310.20803	A	585.35368	390.57155	584.84977	390.23560	12
12	697.45934	465.30866	349.23331	R	549.83512	366.89251	549.33121	366.55657	11
13	782.53030	522.02263	391.76879	K-Trimethyl	471.78457	314.85880	471.28065	314.52286	10
14	826.04632	551.03330	413.52680	S	386.71361	258.14483	386.20970	257.80889	9
15	861.56487	574.71234	431.28607	A	343.19760	229.13416	342.69368	228.79821	8
16	910.09125	607.06326	455.54927	P	307.67904	205.45512	307.17513	205.11918	7
17	945.60981	630.74230	473.30854	A	259.15266	173.10420	258.64875	172.76826	6
18	996.13365	664.42486	498.57046	T	223.63410	149.42516	223.13019	149.08922	5
19	1024.64438	683.43201	512.82583	G	173.11026	115.74260	172.60635	115.40666	4
20	1053.15511	702.43917	527.08120	G	144.59953	96.73545	144.09562	96.39950	3
21	1102.68932	735.46197	551.84830	V	116.08880	77.72829	115.58489	77.39235	2
22				K	66.55459	44.70549	66.05068	44.36954	1

H3K23me3 (EHMT1/GLP) Fragmentation Mass Error (ppm) EThcD

#1	c^{2+}	c^{3+}	c^{4+}	Seq.	z^{2+}	z^{3+}	$z\text{-}H^{2+}$	$z\text{-}H^{3+}$	#2
1				A					22
2				P					21
3				R		+0.93			20
4	+0.55			K-Trimethyl	-1.35	-0.67	-1.48	-1.86	19
5	+0.03			Q	+0.10	+1.30	-1.19	-1.22	18
6	-0.26			L	+0.04	+1.66	-1.33	-0.82	17
7	-0.03			A	+0.76	+1.80	-0.17	+0.08	16
8	-0.59			T	+0.07	+1.26	+0.87	-0.15	15
9	+0.17	-0.15		K-Trimethyl	-0.32		-1.37	-0.36	14
10	-0.36	-1.09		A					13
11	-0.83	-0.41		A			+1.62		12
12	-0.45	-0.59		R			-0.60		11
13		-0.74	+0.61	K-Trimethyl			+0.03		10
14		-0.92	-0.23	S					9
15				A					8
16		+0.55	-1.26	P					7
17		-0.70		A					6
18		-1.66	-0.25	T					5
19		-0.80	+0.99	G					4
20		+1.93	-0.09	G					3
21			-0.38	V					2
22				K					1

B.

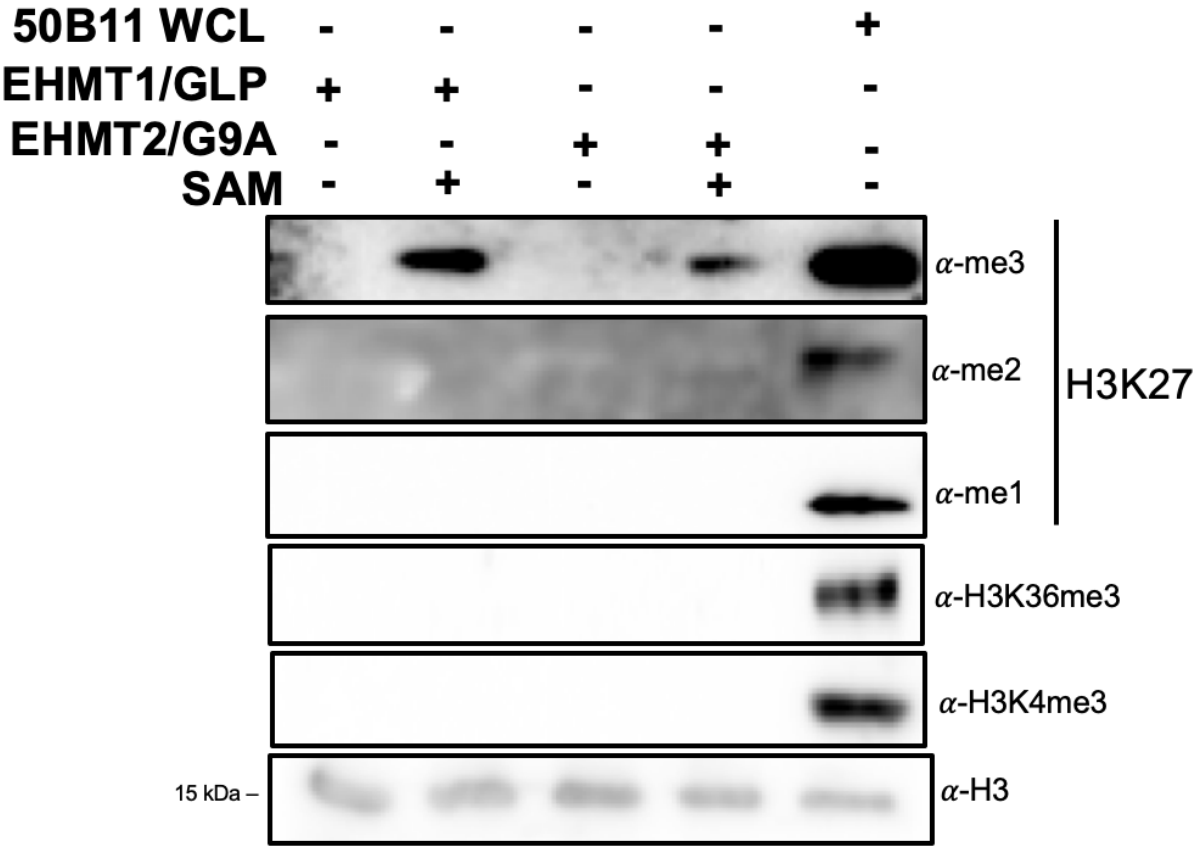

<u>Supplemental Figure 1. EHMT1/GLP and EHMT2/G9a can *de novo* methylate H3K27, but not H3K4 or H3K36, *in vitro*</u>

(A) Ions counts and mass error tables for the corresponding spectra in Figure 10C **(B)** Panel of western blots of various H3K27 methylation states, H3K4me3 and H3K36me3 (as negative controls) for the *in vitro* HMT reaction with EHMT1/GLP or EHMT2/G9a with recombinant histone H3.1. H3K27me1 and H3K27me2 were undetectable in these reactions.

Supplementary Figure 2

A.

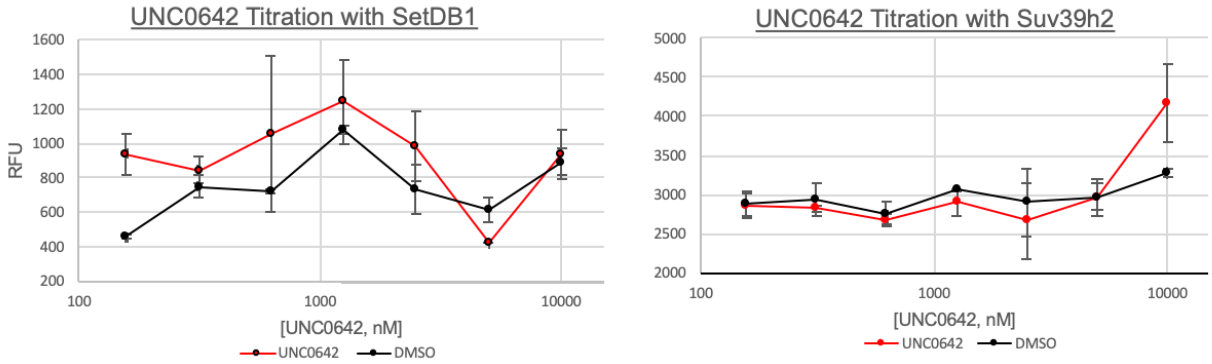

B.

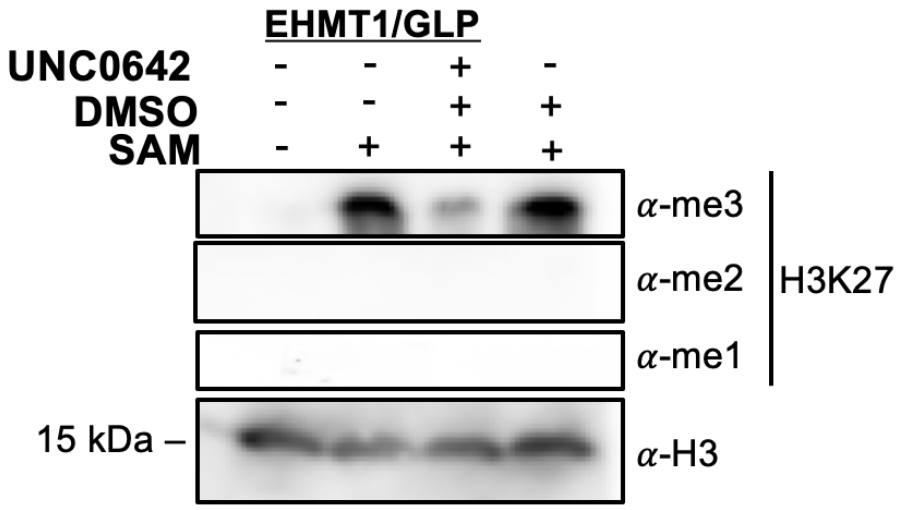

C.

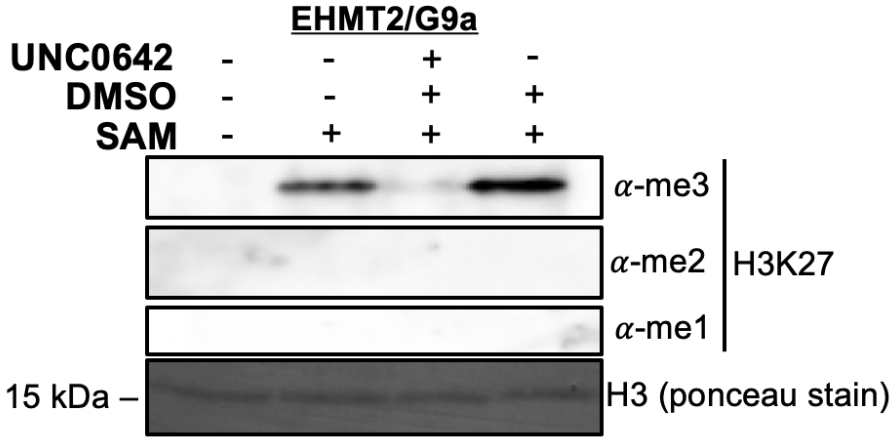

Supplementary Figure 2 Inhibition of G9a/EHMT2 by UNC0642 perturbs *de novo* methylation of H3K27 *in vitro*.

(A) UNC0642 dose titration with recombinant SETDB1 and Suv39h2, as measured via MTase-Glo Assay. **(B)** Western blot panel showing production and inhibition of H3K27 methylation states by EHMT1/GLP. H3K27me1 and H3K27me2 were undetectable in these *in vitro* reactions. **(C)** Western blot panel showing production and inhibition of H3K27 methylation states by EHMT2/G9a. H3K27me1 and H3K27me2 were undetectable in these *in vitro* reactions.

Supplementary Figure 3

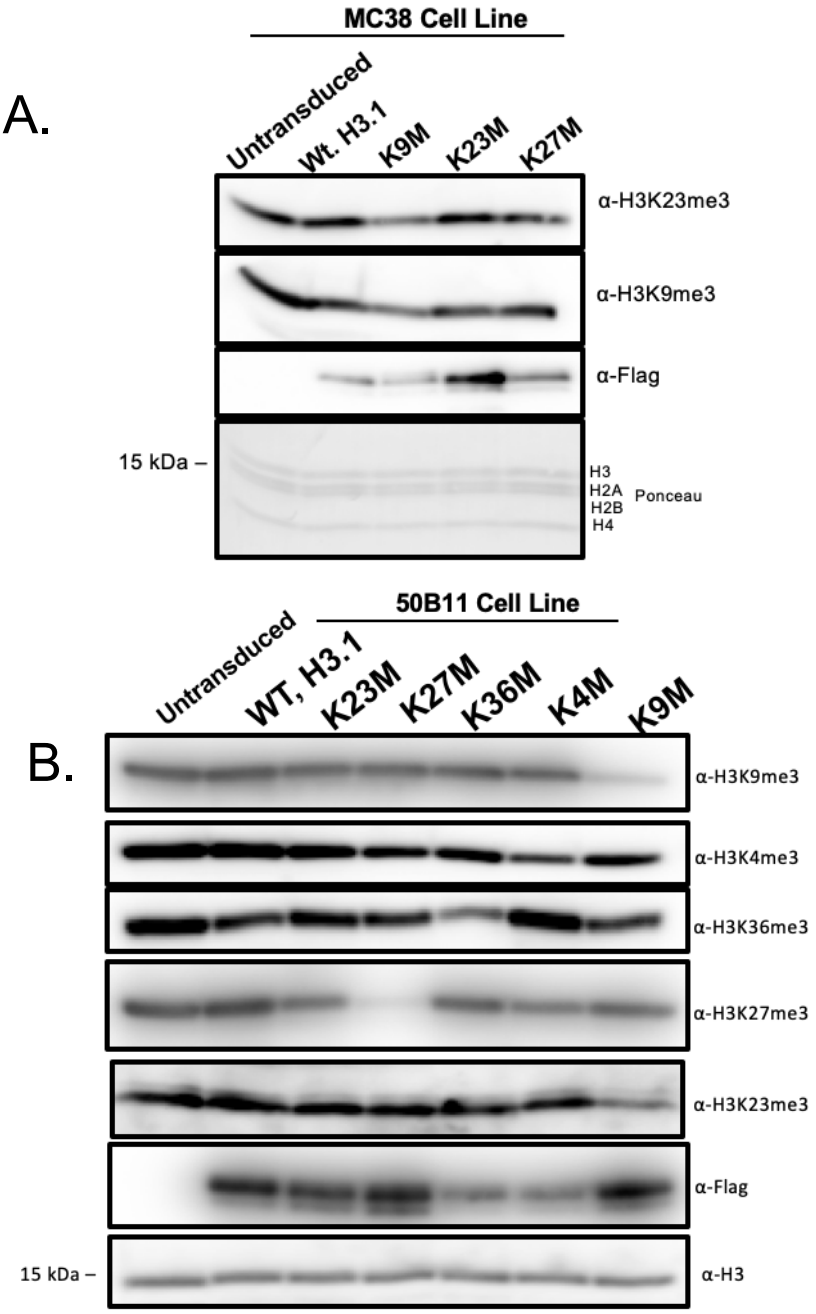

Supplementary Figure 3. H3K9M, but not H3K23M, perturbs H3K9me3 and H3K23me3 in mammalian cell lines expressing H3 K-to-M mutants

MC38 **(A)** and 50B11 **(B)** parent cell lines was transduced with lentivirus carrying a lentiviral plasmid encoding various K-to-M mutants (e.g. 9, 23 and 27). Once stable, confluent populations were established, the cells were harvested, lysates were prepared for SDS-PAGE and blotted for various histone H3 tri-methyl marks. The flag blot gauges transgene expression as the transgenic histone H3 is FLAG-HA tagged.

Supplementary Figure 4

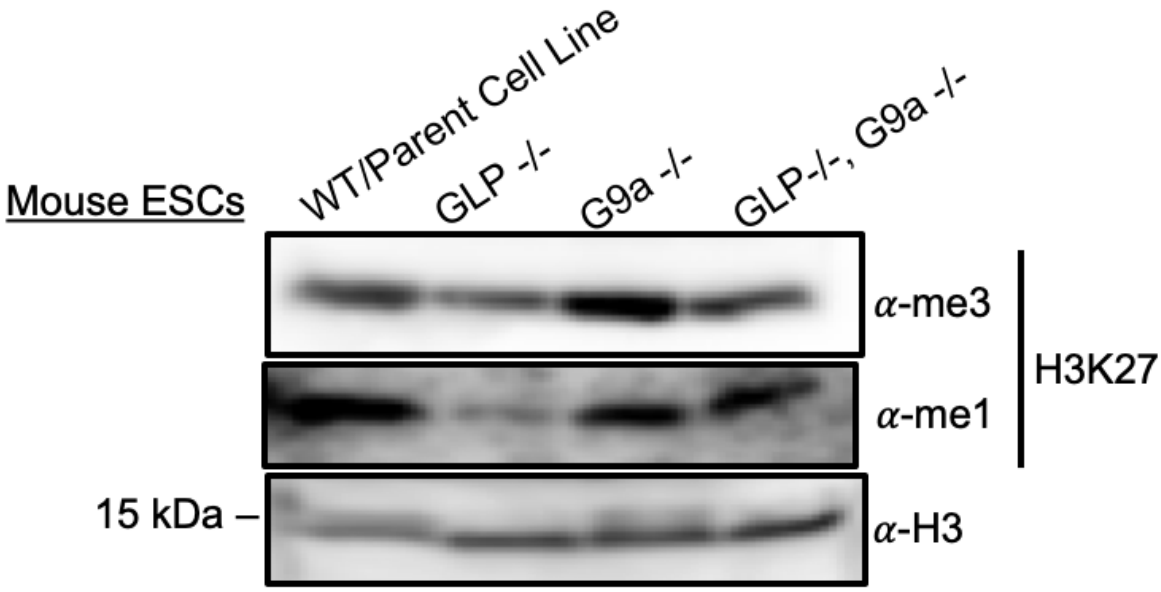

Supplementary Figure 4. Deletion of EHMT1/GLP and/or EHMT2/G9a perturbs H3K27 methylation levels *in vivo*.
Western blot panel of H3K27 methylation states in mouse ESCs knocking out either EHMT1/GLP, EHMT2/G9a or both.

Supplementary Figure 5

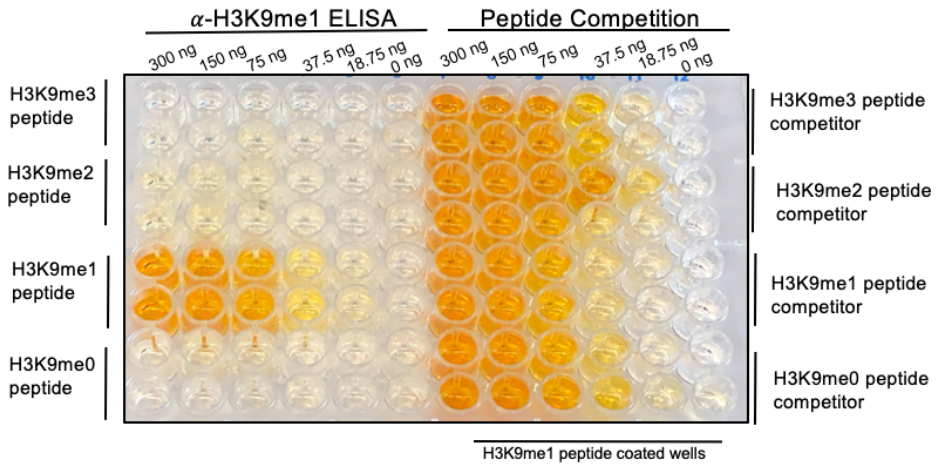

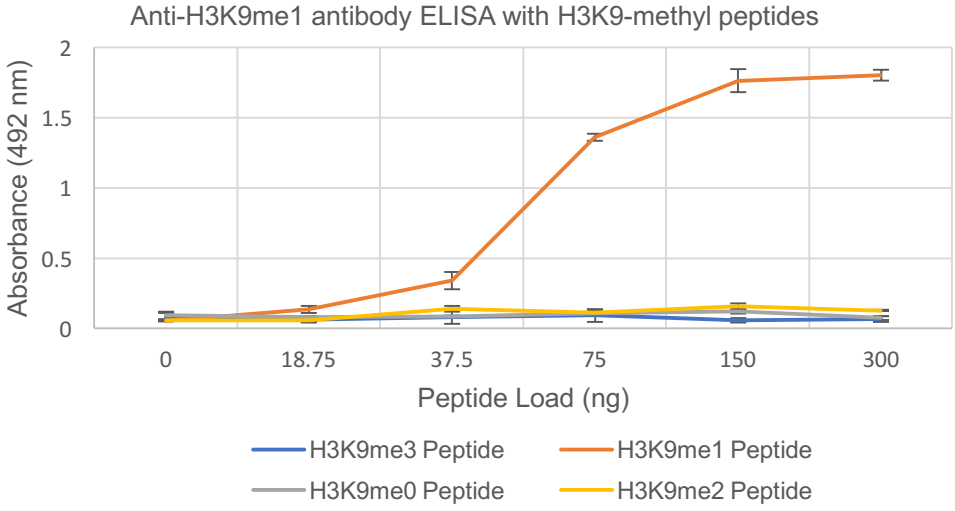

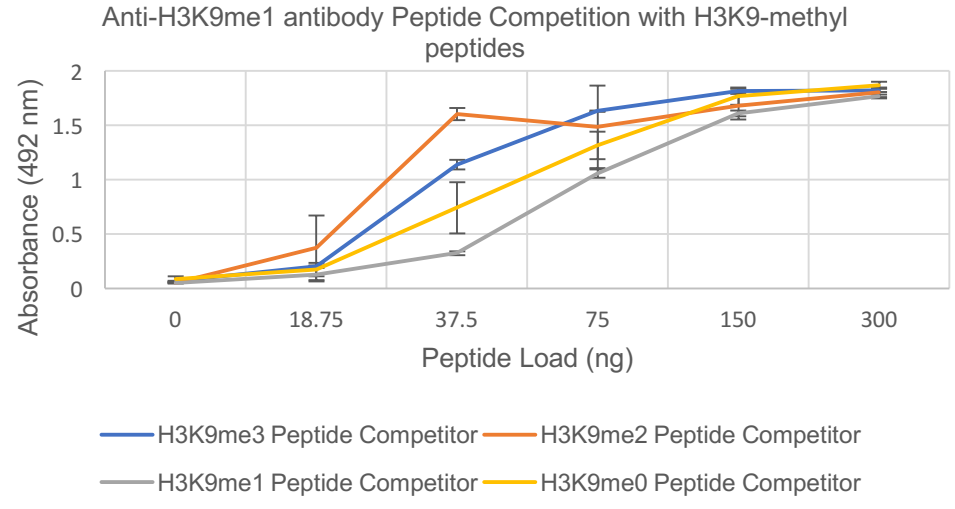

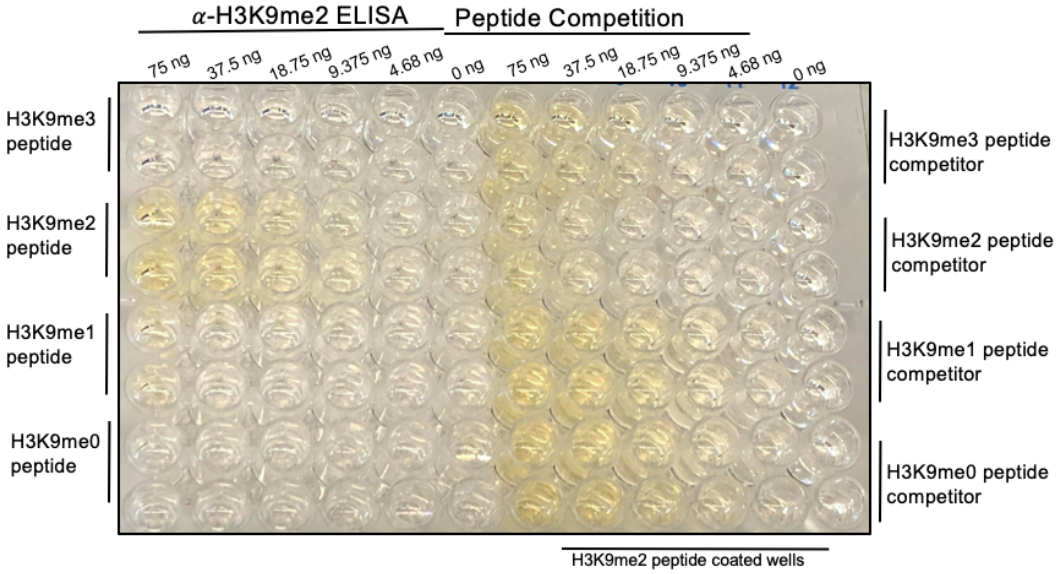
α-H3K9me2 ELISA
Peptide Competition
75 ng
37.5 ng
18.75 ng
9.375 ng
4.68 ng
0 ng
H3K9me3 peptide
H3K9me2 peptide
H3K9me1 peptide
H3K9me0 peptide
H3K9me3 peptide competitor
H3K9me2 peptide competitor
H3K9me1 peptide competitor
H3K9me0 peptide competitor
H3K9me2 peptide coated wells

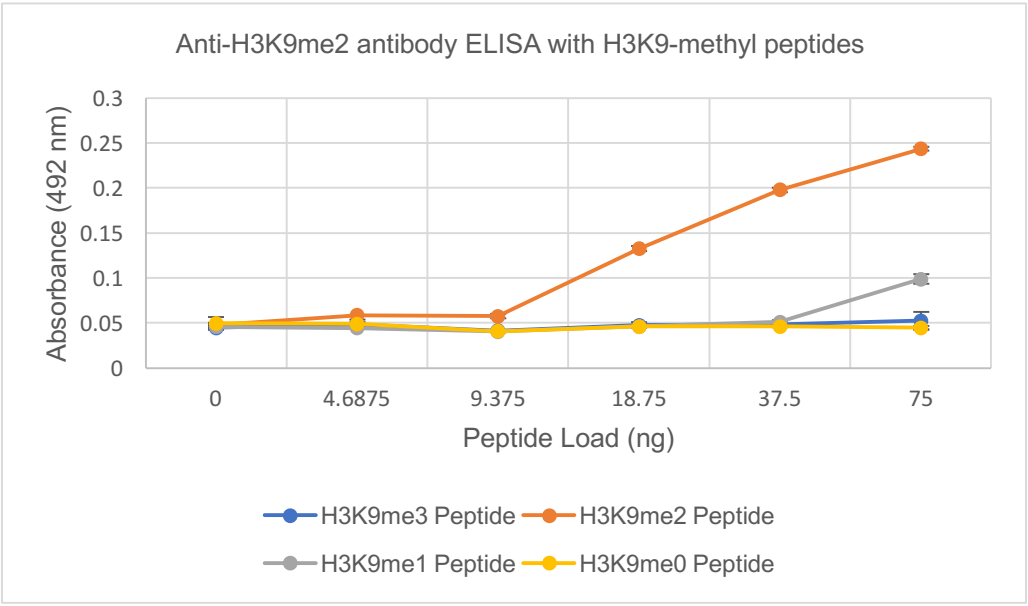
Anti-H3K9me2 antibody ELISA with H3K9-methyl peptides
Absorbance (492 nm)
0.3
0.25
0.2
0.15
0.1
0.05
0
0
4.6875
9.375
18.75
37.5
75
Peptide Load (ng)
H3K9me3 Peptide
H3K9me2 Peptide
H3K9me1 Peptide
H3K9me0 Peptide

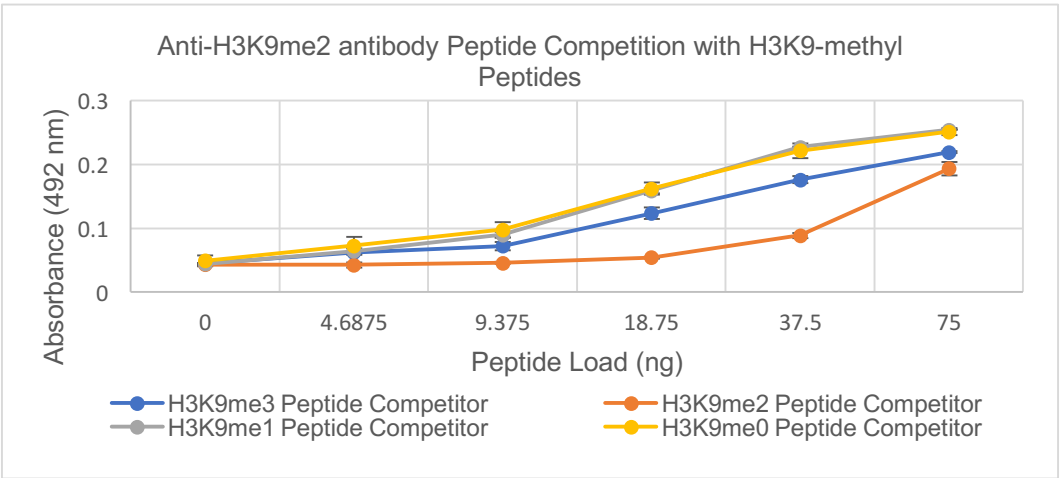
Anti-H3K9me2 antibody Peptide Competition with H3K9-methyl Peptides
Absorbance (492 nm)
0.3
0.2
0.1
0
0
4.6875
9.375
18.75
37.5
75
Peptide Load (ng)
H3K9me3 Peptide Competitor
H3K9me2 Peptide Competitor
H3K9me1 Peptide Competitor
H3K9me0 Peptide Competitor

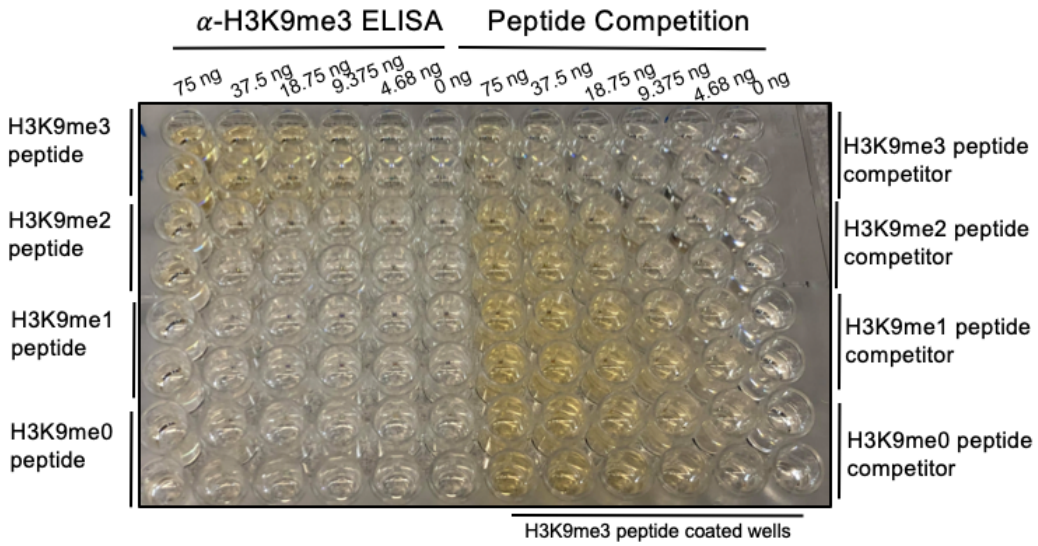
α-H3K9me3 ELISA
Peptide Competition
75 ng
37.5 ng
18.75 ng
9.375 ng
4.68 ng
0 ng
75 ng
37.5 ng
18.75 ng
9.375 ng
4.68 ng
0 ng
H3K9me3 peptide
H3K9me2 peptide
H3K9me1 peptide
H3K9me0 peptide
H3K9me3 peptide competitor
H3K9me2 peptide competitor
H3K9me1 peptide competitor
H3K9me0 peptide competitor
H3K9me3 peptide coated wells

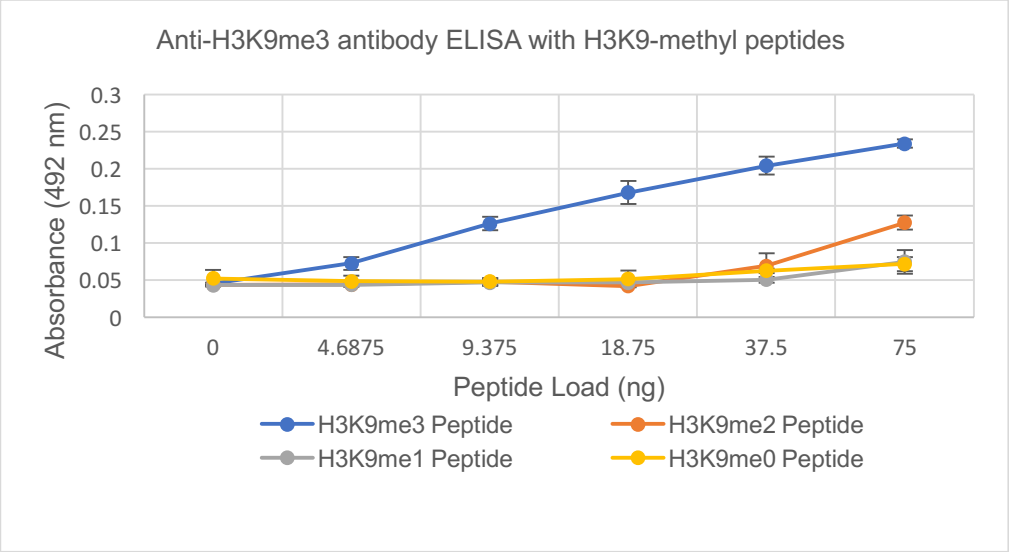
Anti-H3K9me3 antibody ELISA with H3K9-methyl peptides
Absorbance (492 nm)
0.3
0.25
0.2
0.15
0.1
0.05
0
0
4.6875
9.375
18.75
37.5
75
Peptide Load (ng)
H3K9me3 Peptide
H3K9me2 Peptide
H3K9me1 Peptide
H3K9me0 Peptide

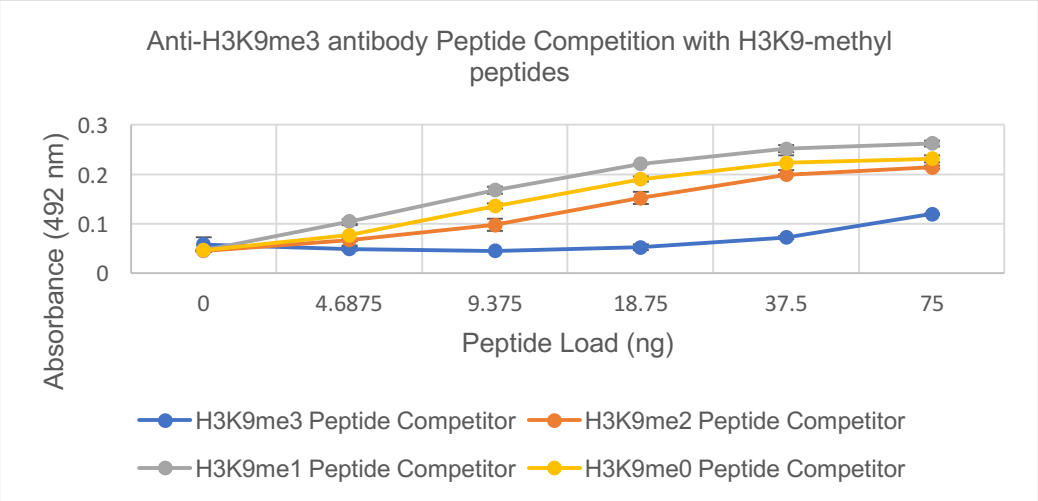
Anti-H3K9me3 antibody Peptide Competition with H3K9-methyl peptides
Absorbance (492 nm)
0.3
0.2
0.1
0
0
4.6875
9.375
18.75
37.5
75
Peptide Load (ng)
H3K9me3 Peptide Competitor
H3K9me2 Peptide Competitor
H3K9me1 Peptide Competitor
H3K9me0 Peptide Competitor

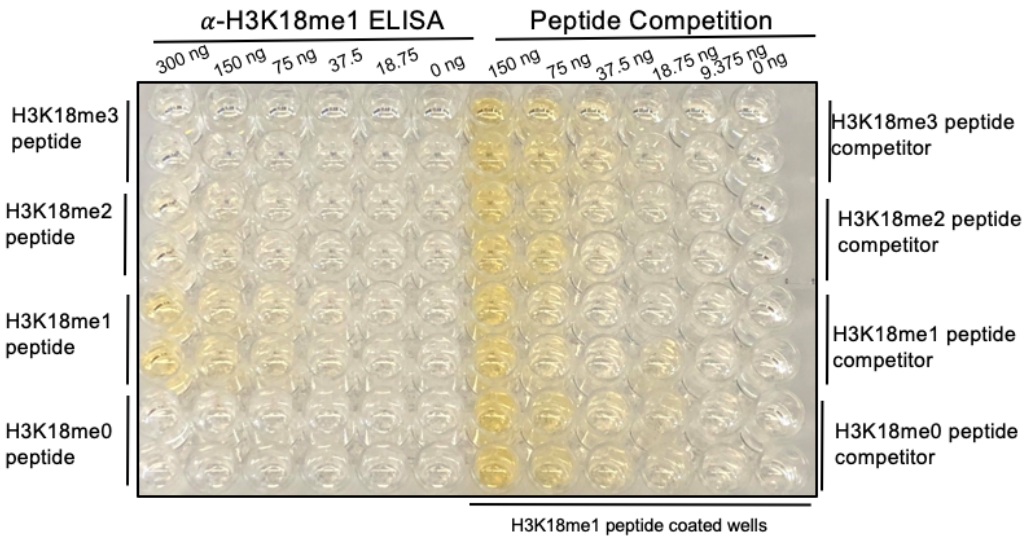
α-H3K18me1 ELISA
Peptide Competition
300 ng
150 ng
75 ng
37.5
18.75
0 ng
150 ng
75 ng
37.5 ng
18.75 ng
9.375 ng
0 ng
H3K18me3 peptide
H3K18me2 peptide
H3K18me1 peptide
H3K18me0 peptide
H3K18me3 peptide competitor
H3K18me2 peptide competitor
H3K18me1 peptide competitor
H3K18me0 peptide competitor
H3K18me1 peptide coated wells

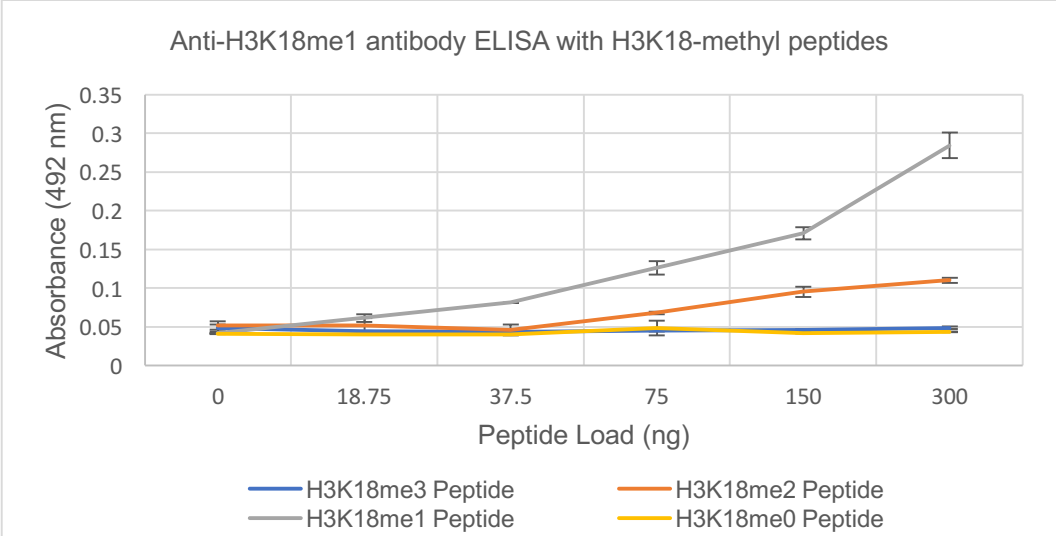
Anti-H3K18me1 antibody ELISA with H3K18-methyl peptides
Absorbance (492 nm)
0.35
0.3
0.25
0.2
0.15
0.1
0.05
0
0
18.75
37.5
75
150
300
Peptide Load (ng)
H3K18me3 Peptide
H3K18me2 Peptide
H3K18me1 Peptide
H3K18me0 Peptide

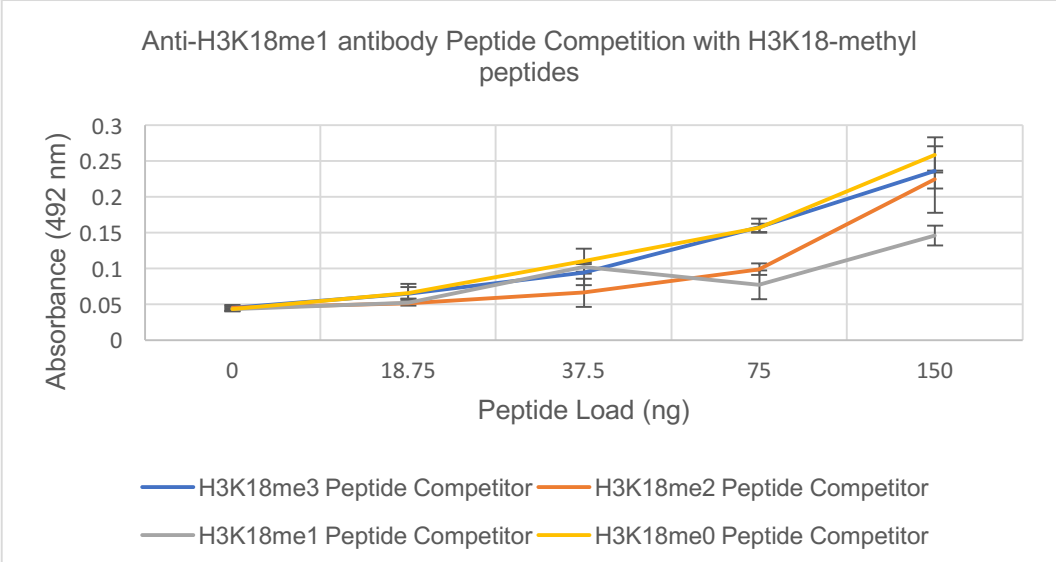
Anti-H3K18me1 antibody Peptide Competition with H3K18-methyl peptides
Absorbance (492 nm)
0.3
0.25
0.2
0.15
0.1
0.05
0
0
18.75
37.5
75
150
Peptide Load (ng)
H3K18me3 Peptide Competitor
H3K18me2 Peptide Competitor
H3K18me1 Peptide Competitor
H3K18me0 Peptide Competitor

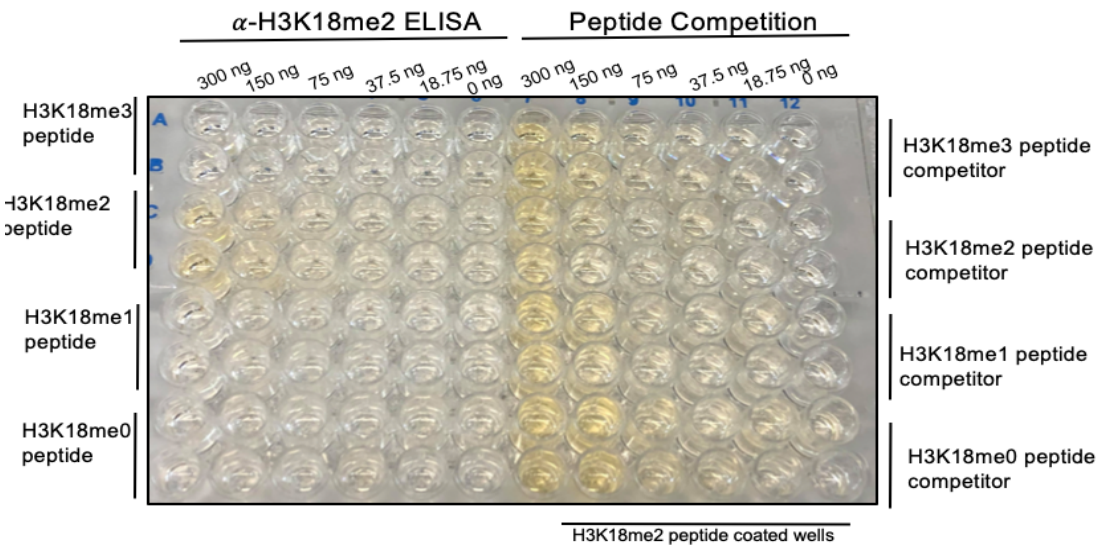
α-H3K18me2 ELISA
Peptide Competition
300 ng
150 ng
75 ng
37.5 ng
18.75 ng
0 ng
H3K18me3 peptide
H3K18me2 peptide
H3K18me1 peptide
H3K18me0 peptide
H3K18me3 peptide competitor
H3K18me2 peptide competitor
H3K18me1 peptide competitor
H3K18me0 peptide competitor
H3K18me2 peptide coated wells

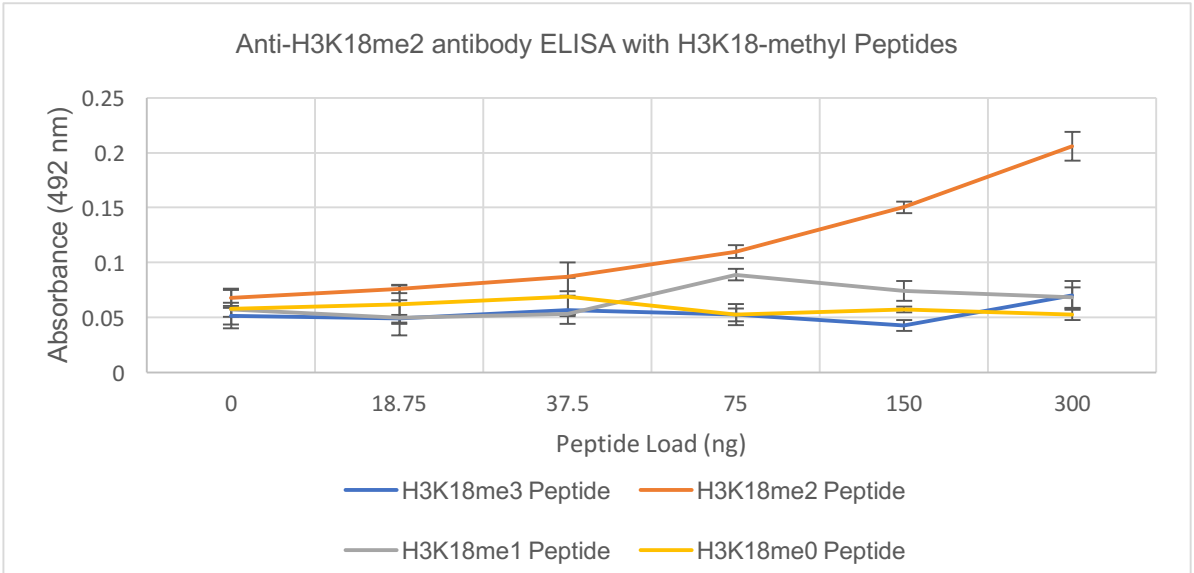
Anti-H3K18me2 antibody ELISA with H3K18-methyl Peptides
Absorbance (492 nm)
0.25
0.2
0.15
0.1
0.05
0
0
18.75
37.5
75
150
300
Peptide Load (ng)
H3K18me3 Peptide
H3K18me2 Peptide
H3K18me1 Peptide
H3K18me0 Peptide

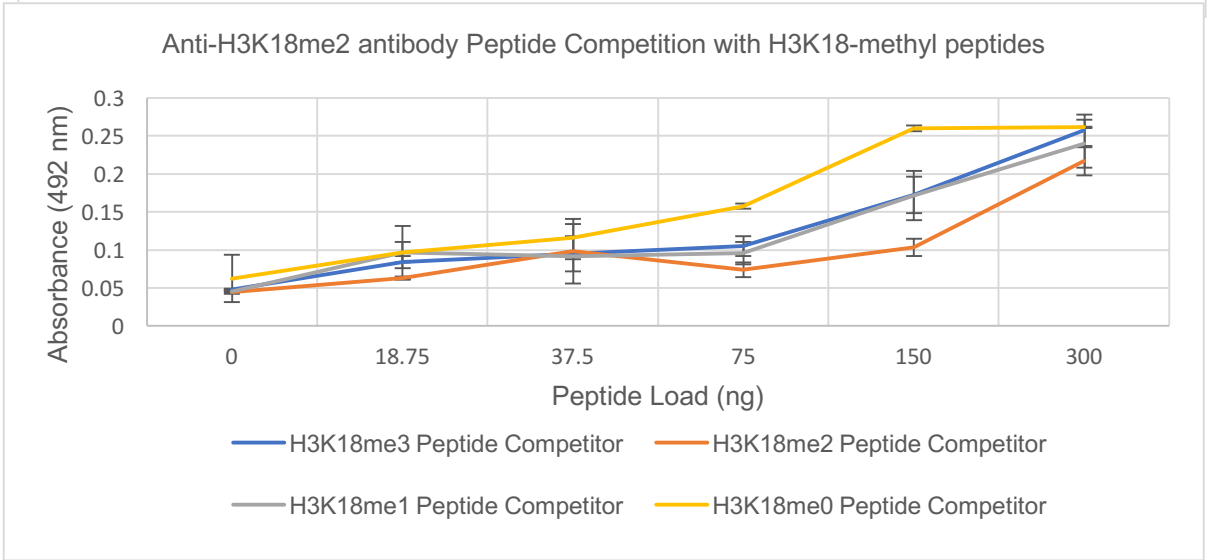
Anti-H3K18me2 antibody Peptide Competition with H3K18-methyl peptides
Absorbance (492 nm)
0.3
0.25
0.2
0.15
0.1
0.05
0
0
18.75
37.5
75
150
300
Peptide Load (ng)
H3K18me3 Peptide Competitor
H3K18me2 Peptide Competitor
H3K18me1 Peptide Competitor
H3K18me0 Peptide Competitor

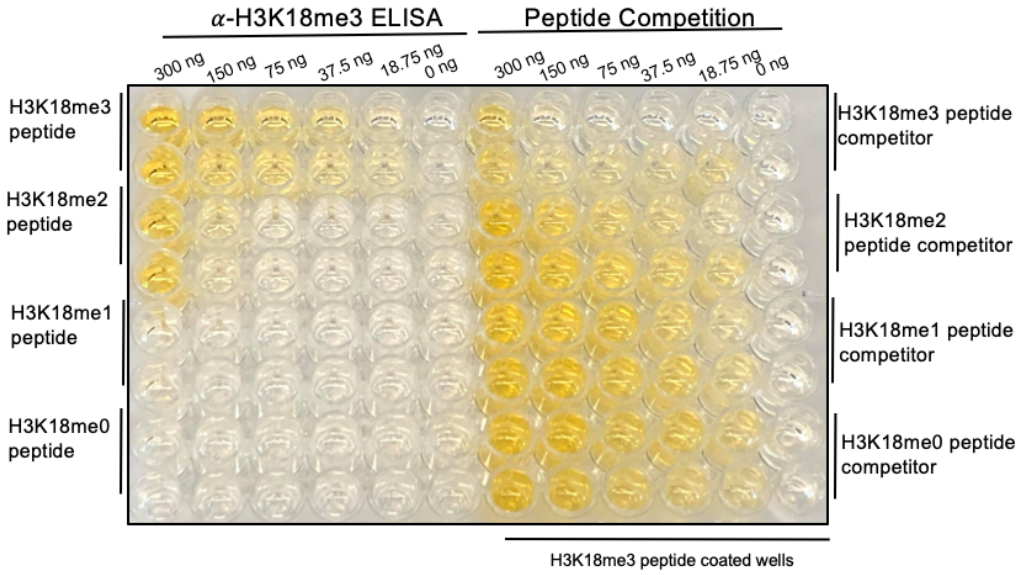
α-H3K18me3 ELISA
Peptide Competition
300 ng
150 ng
75 ng
37.5 ng
18.75 ng
0 ng
H3K18me3 peptide
H3K18me2 peptide
H3K18me1 peptide
H3K18me0 peptide
H3K18me3 peptide competitor
H3K18me2 peptide competitor
H3K18me1 peptide competitor
H3K18me0 peptide competitor
H3K18me3 peptide coated wells

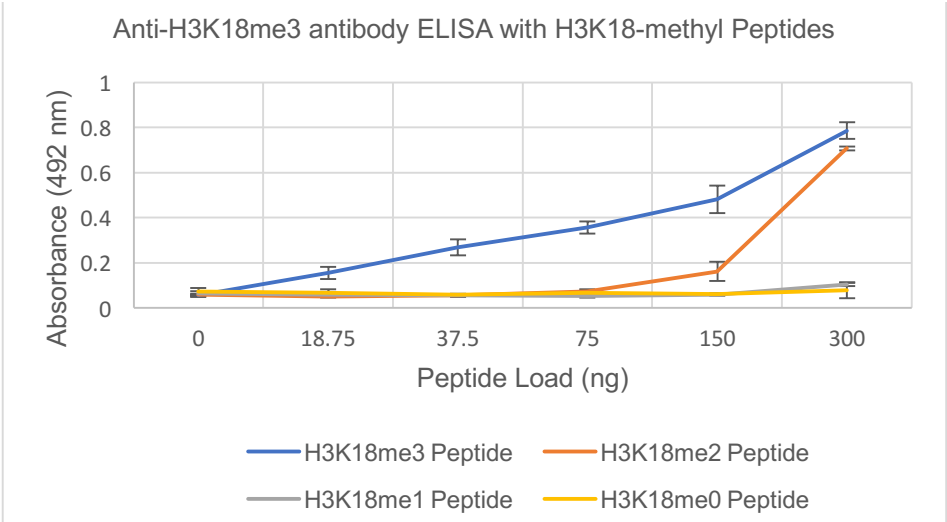
Anti-H3K18me3 antibody ELISA with H3K18-methyl Peptides
Absorbance (492 nm)
1
0.8
0.6
0.4
0.2
0
0
18.75
37.5
75
150
300
Peptide Load (ng)
H3K18me3 Peptide
H3K18me2 Peptide
H3K18me1 Peptide
H3K18me0 Peptide

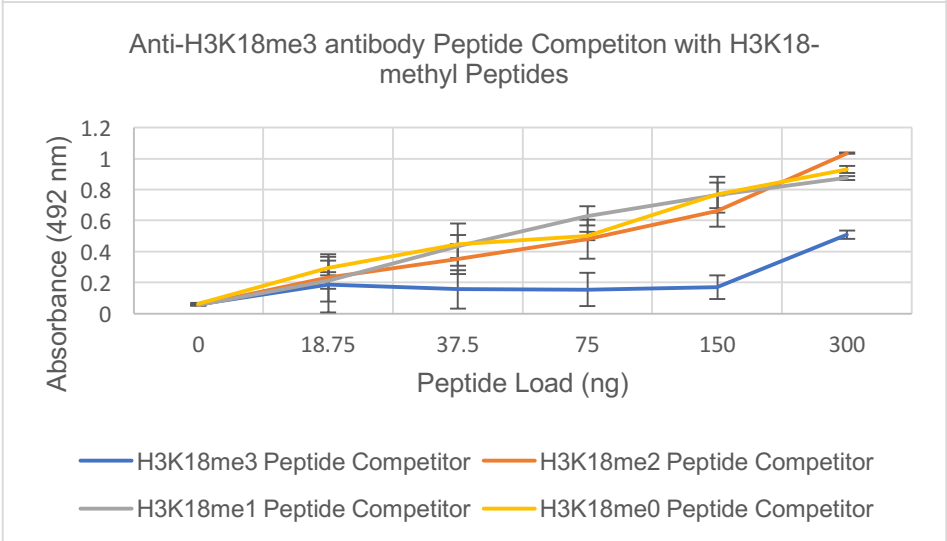
Anti-H3K18me3 antibody Peptide Competiton with H3K18-methyl Peptides
Absorbance (492 nm)
1.2
1
0.8
0.6
0.4
0.2
0
0
18.75
37.5
75
150
300
Peptide Load (ng)
H3K18me3 Peptide Competitor
H3K18me2 Peptide Competitor
H3K18me1 Peptide Competitor
H3K18me0 Peptide Competitor

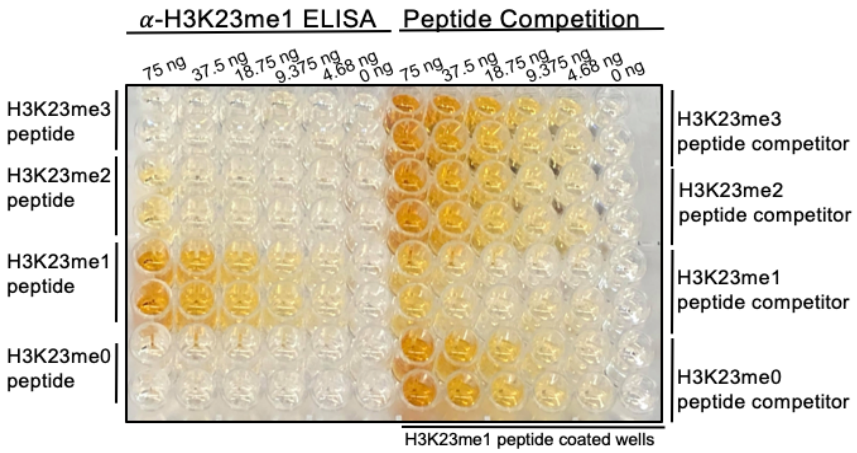
α-H3K23me1 ELISA
Peptide Competition
75 ng
37.5 ng
18.75 ng
9.375 ng
4.68 ng
0 ng
H3K23me3 peptide
H3K23me2 peptide
H3K23me1 peptide
H3K23me0 peptide
H3K23me3 peptide competitor
H3K23me2 peptide competitor
H3K23me1 peptide competitor
H3K23me0 peptide competitor
H3K23me1 peptide coated wells

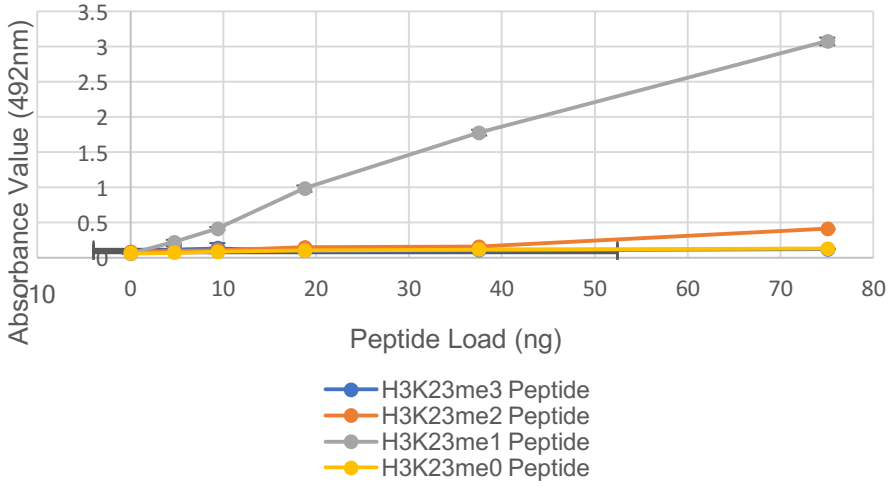
Anti-H3K23me1 antibody ELISA on H3K23-methyl peptides
Absorbance Value (492nm)
Peptide Load (ng)
H3K23me3 Peptide
H3K23me2 Peptide
H3K23me1 Peptide
H3K23me0 Peptide

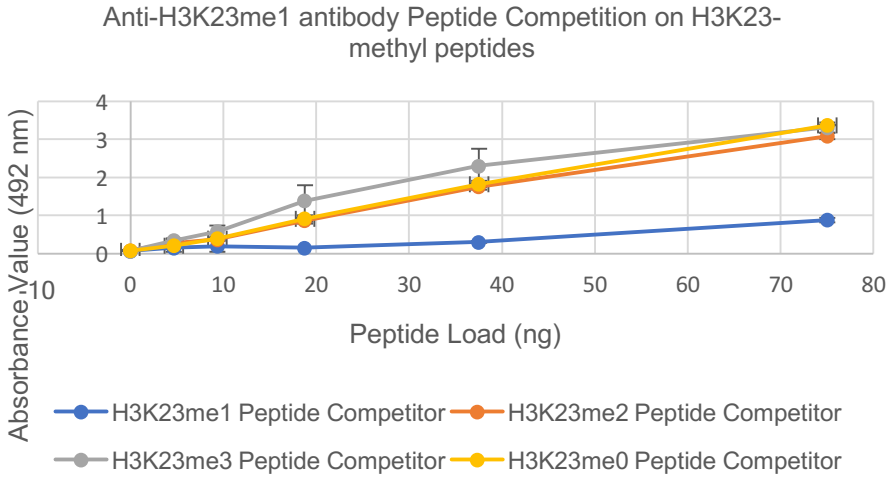
Anti-H3K23me1 antibody Peptide Competition on H3K23-methyl peptides
Absorbance Value (492 nm)
Peptide Load (ng)
H3K23me1 Peptide Competitor
H3K23me2 Peptide Competitor
H3K23me3 Peptide Competitor
H3K23me0 Peptide Competitor

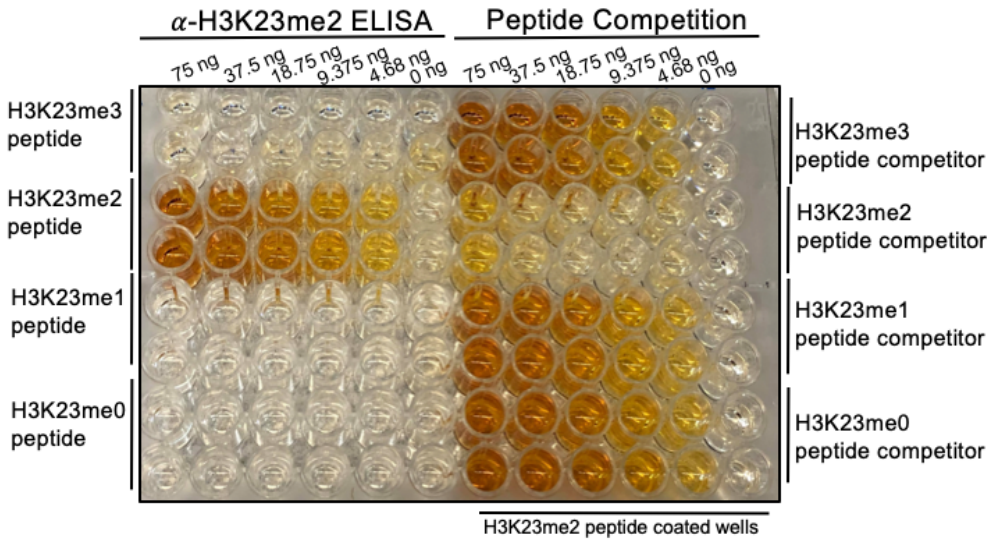
α-H3K23me2 ELISA
Peptide Competition
75 ng
37.5 ng
18.75 ng
9.375 ng
4.68 ng
0 ng
H3K23me3 peptide
H3K23me2 peptide
H3K23me1 peptide
H3K23me0 peptide
H3K23me3 peptide competitor
H3K23me2 peptide competitor
H3K23me1 peptide competitor
H3K23me0 peptide competitor
H3K23me2 peptide coated wells

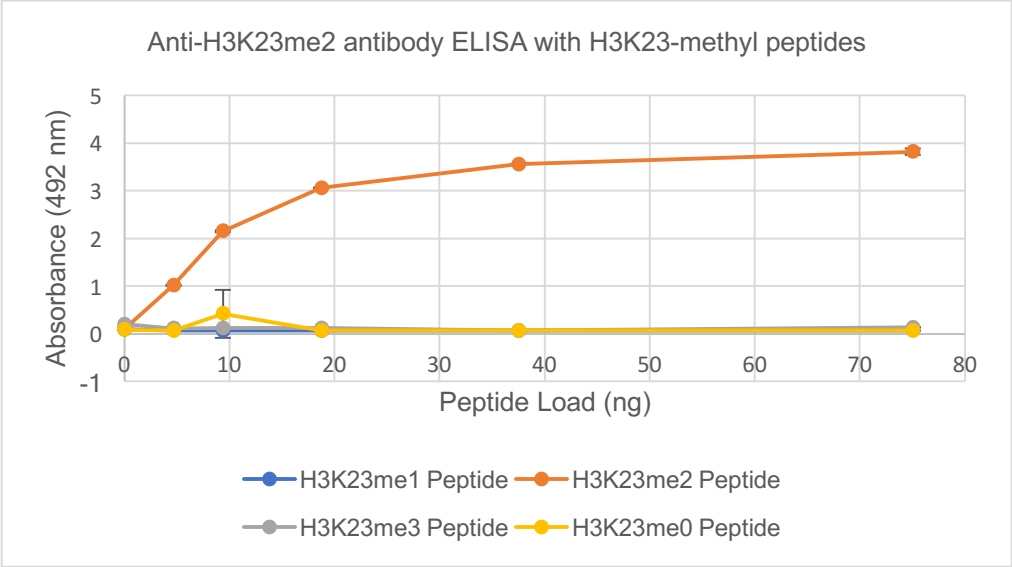
Anti-H3K23me2 antibody ELISA with H3K23-methyl peptides
Absorbance (492 nm)
Peptide Load (ng)
H3K23me1 Peptide
H3K23me2 Peptide
H3K23me3 Peptide
H3K23me0 Peptide

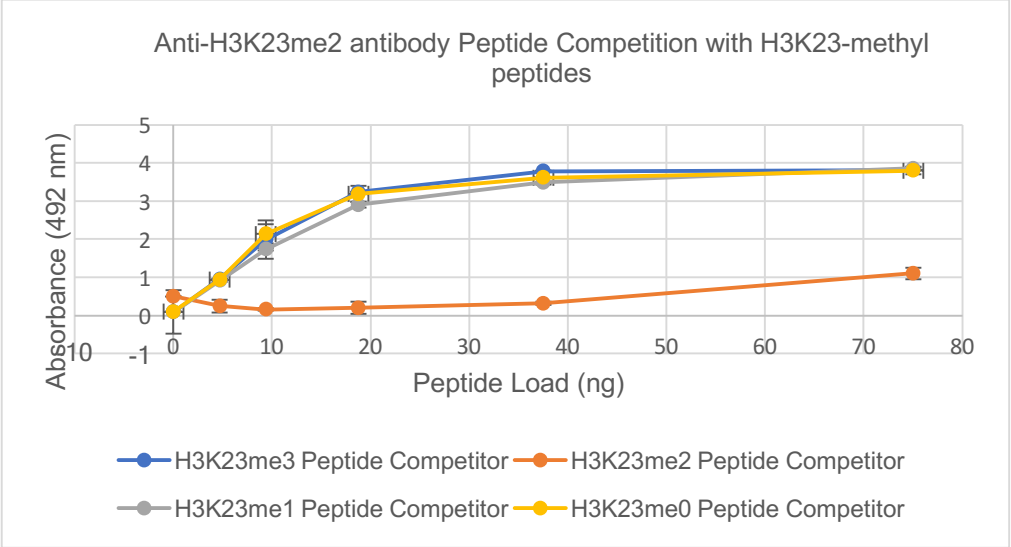
Anti-H3K23me2 antibody Peptide Competition with H3K23-methyl peptides
Absorbance (492 nm)
Peptide Load (ng)
H3K23me3 Peptide Competitor
H3K23me2 Peptide Competitor
H3K23me1 Peptide Competitor
H3K23me0 Peptide Competitor

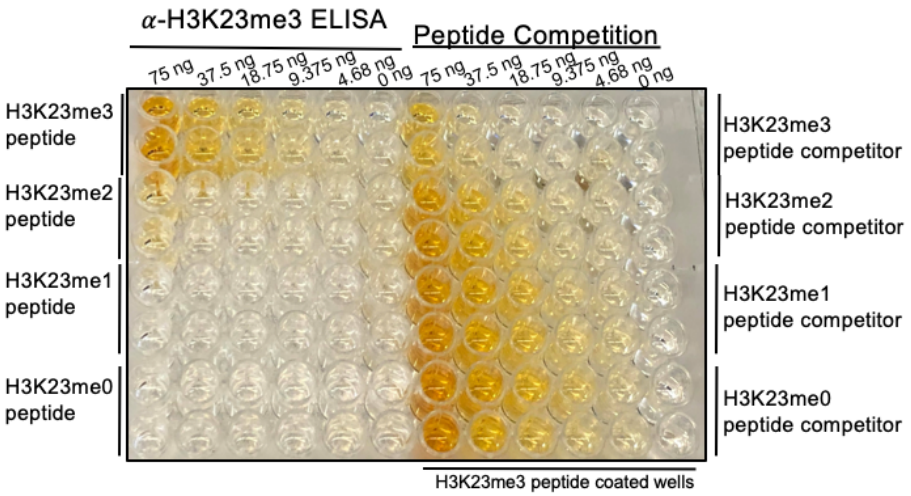
α-H3K23me3 ELISA
Peptide Competition
75 ng
37.5 ng
18.75 ng
9.375 ng
4.68 ng
0 ng
H3K23me3 peptide
H3K23me2 peptide
H3K23me1 peptide
H3K23me0 peptide
H3K23me3 peptide competitor
H3K23me2 peptide competitor
H3K23me1 peptide competitor
H3K23me0 peptide competitor
H3K23me3 peptide coated wells

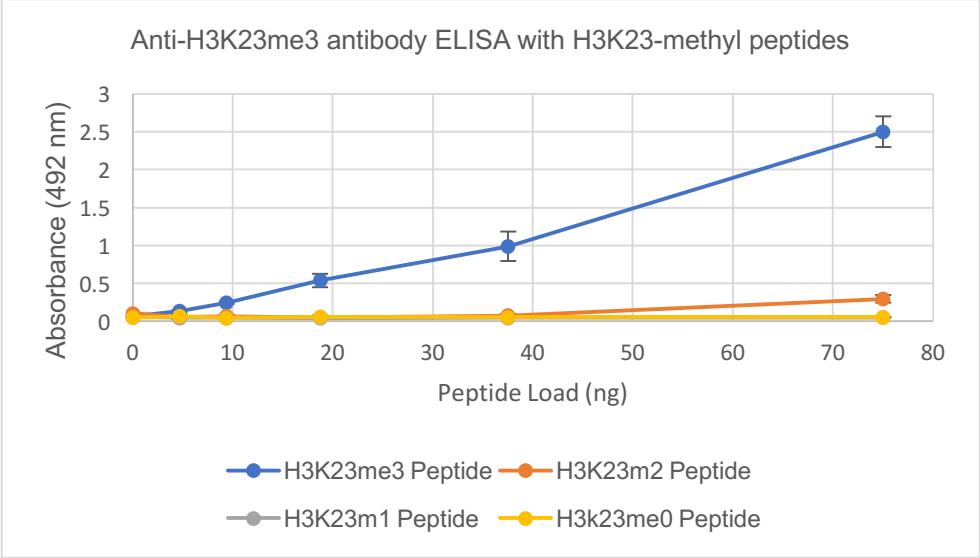
Anti-H3K23me3 antibody ELISA with H3K23-methyl peptides
Absorbance (492 nm)
Peptide Load (ng)
H3K23me3 Peptide
H3K23m2 Peptide
H3K23m1 Peptide
H3k23me0 Peptide

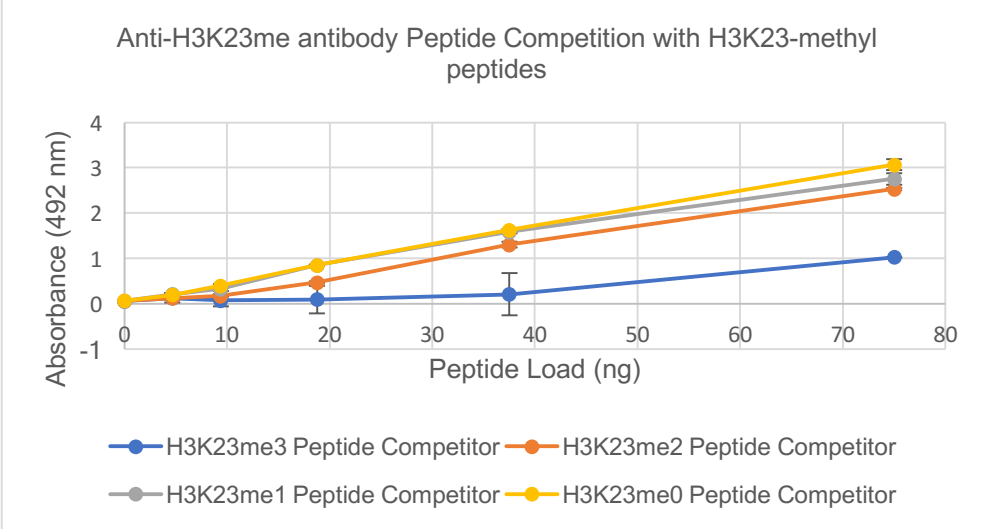
Anti-H3K23me antibody Peptide Competition with H3K23-methyl peptides
Absorbance (492 nm)
Peptide Load (ng)
H3K23me3 Peptide Competitor
H3K23me2 Peptide Competitor
H3K23me1 Peptide Competitor
H3K23me0 Peptide Competitor

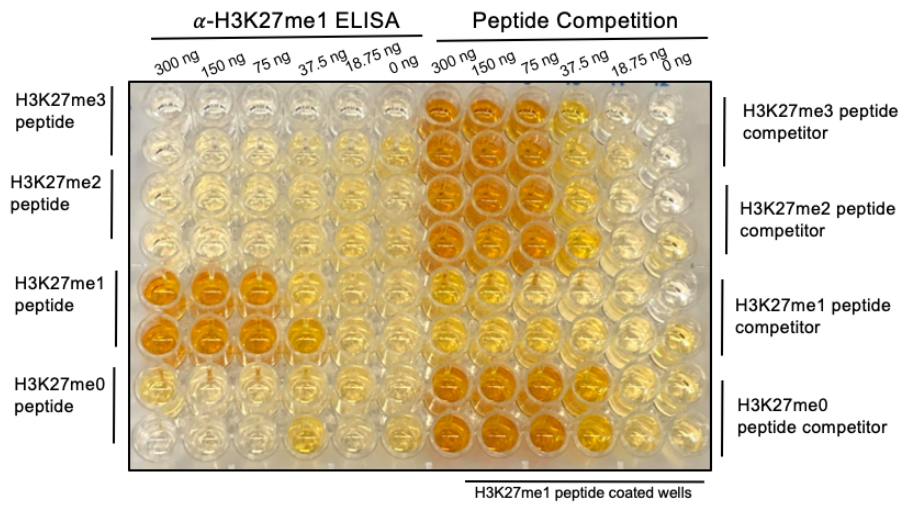
α-H3K27me1 ELISA
Peptide Competition
300 ng
150 ng
75 ng
37.5 ng
18.75 ng
0 ng
H3K27me3 peptide
H3K27me2 peptide
H3K27me1 peptide
H3K27me0 peptide
H3K27me3 peptide competitor
H3K27me2 peptide competitor
H3K27me1 peptide competitor
H3K27me0 peptide competitor
H3K27me1 peptide coated wells

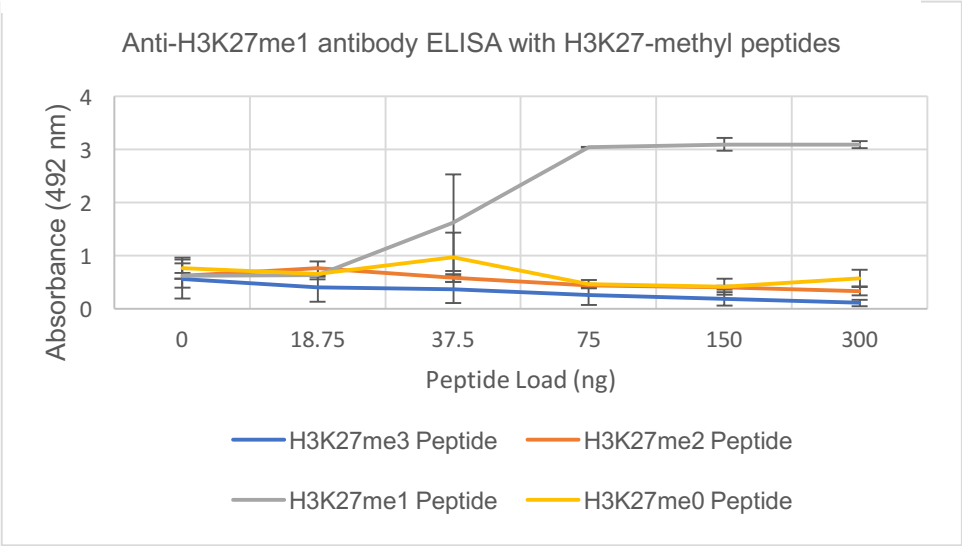
Anti-H3K27me1 antibody ELISA with H3K27-methyl peptides
Absorbance (492 nm)
0
1
2
3
4
0
18.75
37.5
75
150
300
Peptide Load (ng)
H3K27me3 Peptide
H3K27me2 Peptide
H3K27me1 Peptide
H3K27me0 Peptide

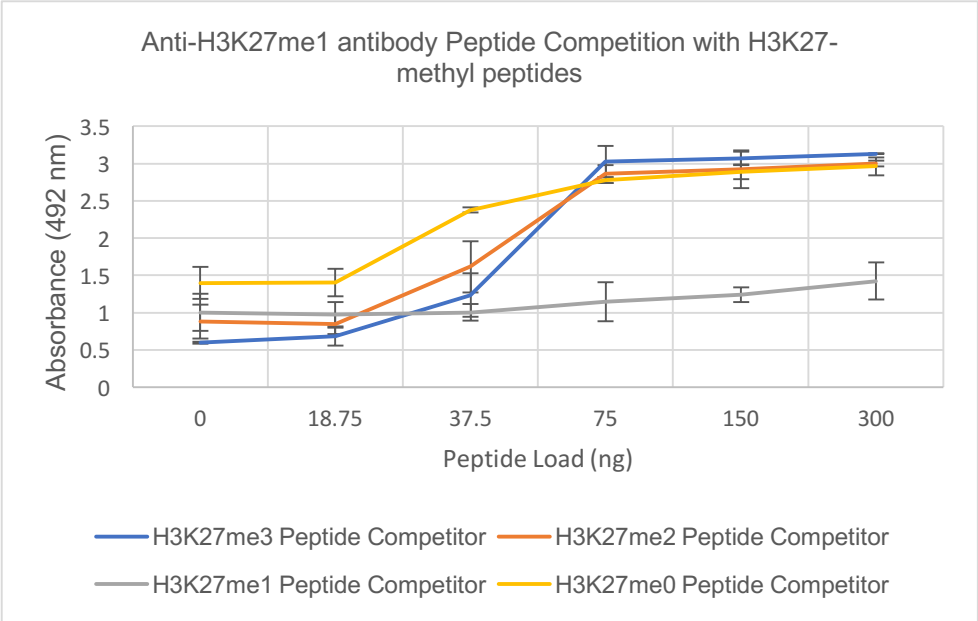
Anti-H3K27me1 antibody Peptide Competition with H3K27-methyl peptides
Absorbance (492 nm)
0
0.5
1
1.5
2
2.5
3
3.5
0
18.75
37.5
75
150
300
Peptide Load (ng)
H3K27me3 Peptide Competitor
H3K27me2 Peptide Competitor
H3K27me1 Peptide Competitor
H3K27me0 Peptide Competitor

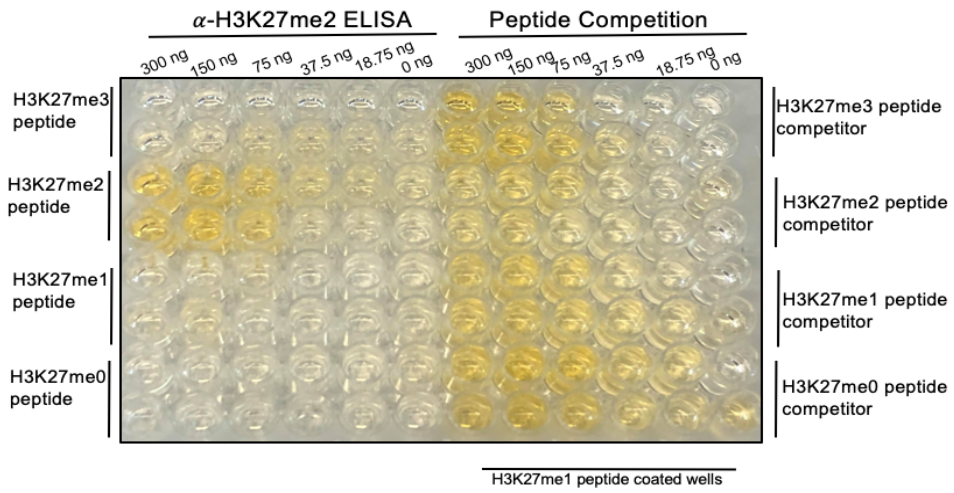
α-H3K27me2 ELISA
Peptide Competition
300 ng
150 ng
75 ng
37.5 ng
18.75 ng
0 ng
H3K27me3 peptide
H3K27me2 peptide
H3K27me1 peptide
H3K27me0 peptide
H3K27me3 peptide competitor
H3K27me2 peptide competitor
H3K27me1 peptide competitor
H3K27me0 peptide competitor
H3K27me1 peptide coated wells

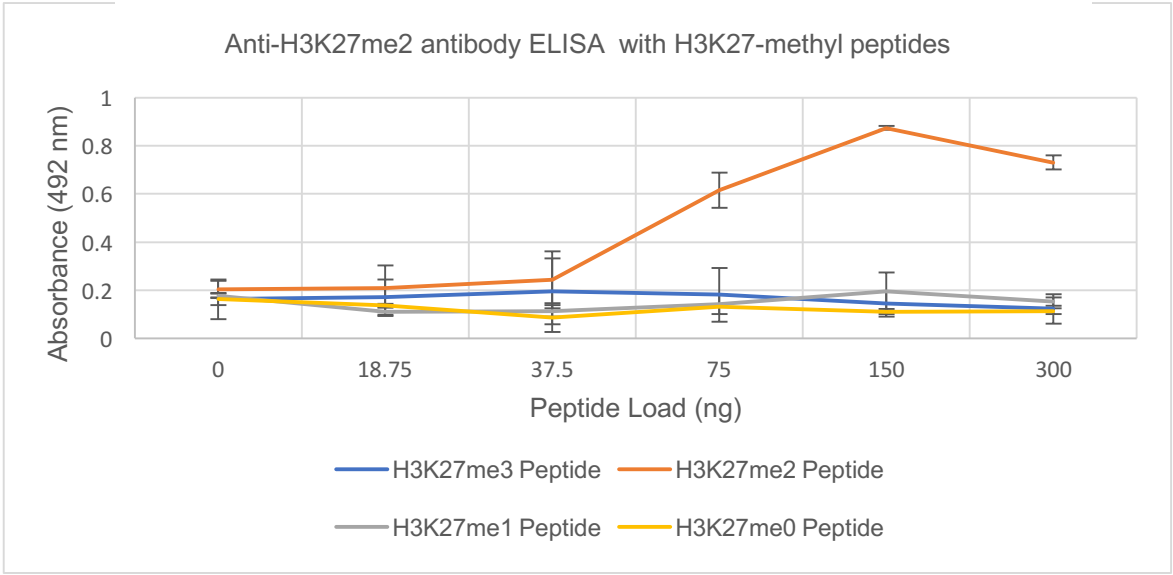
Anti-H3K27me2 antibody ELISA with H3K27-methyl peptides
Absorbance (492 nm)
1
0.8
0.6
0.4
0.2
0
0
18.75
37.5
75
150
300
Peptide Load (ng)
H3K27me3 Peptide
H3K27me2 Peptide
H3K27me1 Peptide
H3K27me0 Peptide

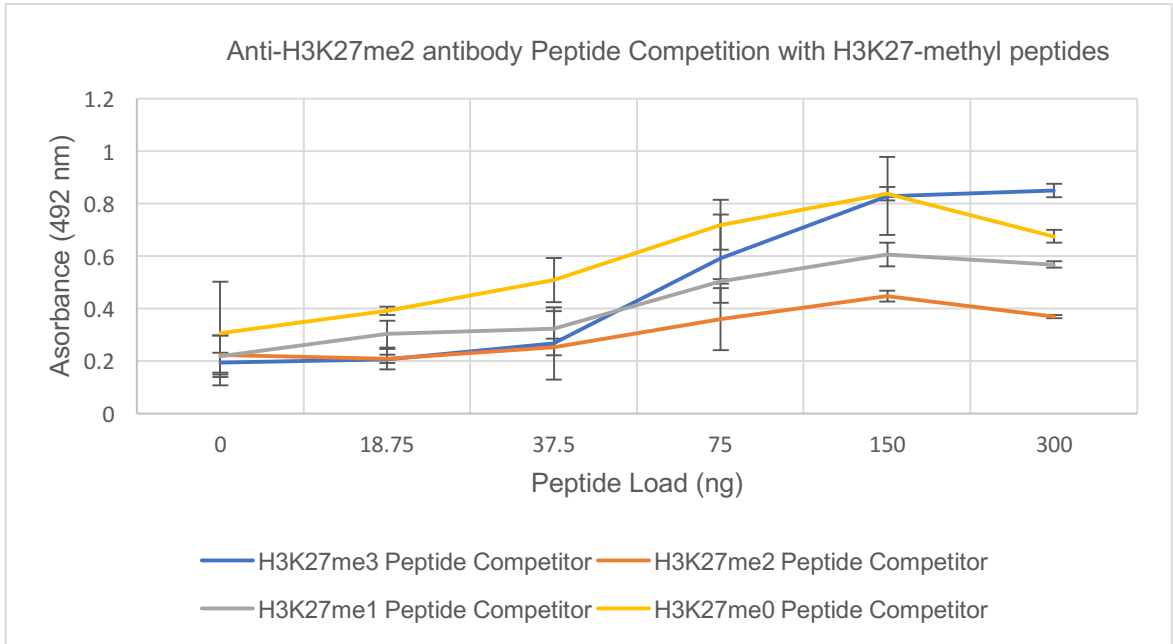
Anti-H3K27me2 antibody Peptide Competition with H3K27-methyl peptides
Asorbance (492 nm)
1.2
1
0.8
0.6
0.4
0.2
0
0
18.75
37.5
75
150
300
Peptide Load (ng)
H3K27me3 Peptide Competitor
H3K27me2 Peptide Competitor
H3K27me1 Peptide Competitor
H3K27me0 Peptide Competitor

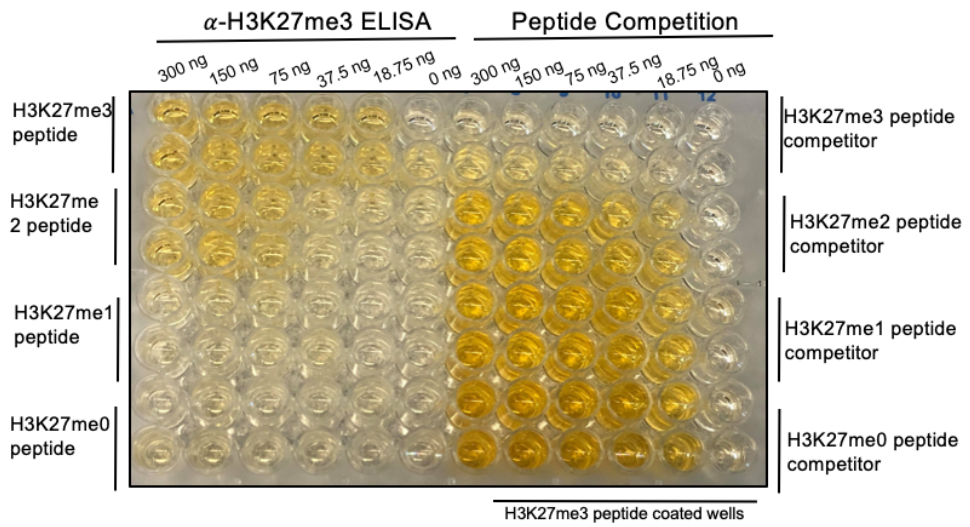
α-H3K27me3 ELISA
Peptide Competition
300 ng
150 ng
75 ng
37.5 ng
18.75 ng
0 ng
H3K27me3 peptide
H3K27me 2 peptide
H3K27me1 peptide
H3K27me0 peptide
H3K27me3 peptide competitor
H3K27me2 peptide competitor
H3K27me1 peptide competitor
H3K27me0 peptide competitor
H3K27me3 peptide coated wells

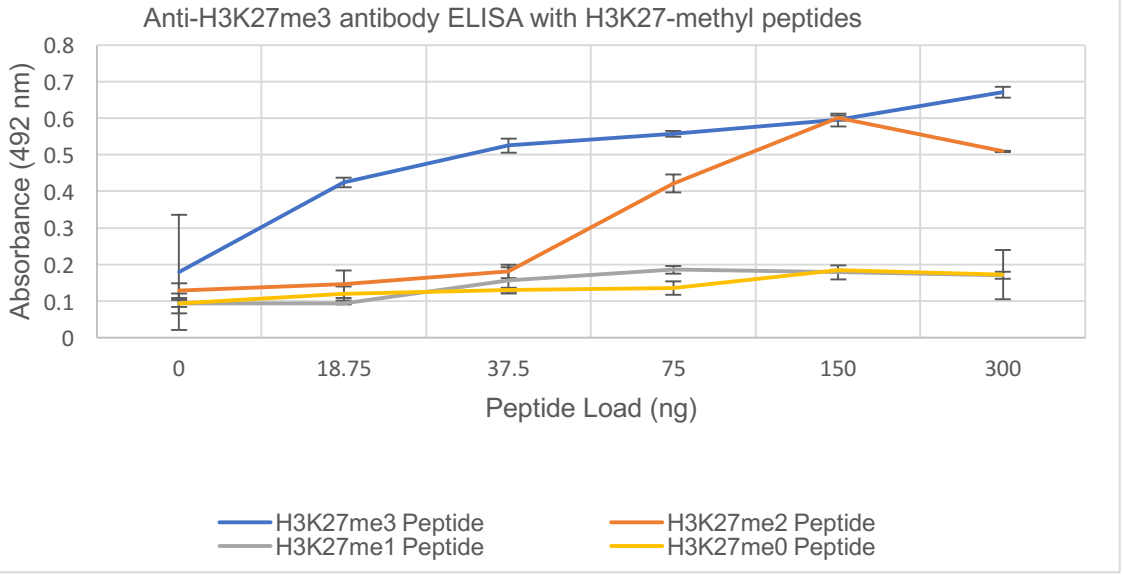
Anti-H3K27me3 antibody ELISA with H3K27-methyl peptides
Absorbance (492 nm)
0.8
0.7
0.6
0.5
0.4
0.3
0.2
0.1
0
0
18.75
37.5
75
150
300
Peptide Load (ng)
H3K27me3 Peptide
H3K27me2 Peptide
H3K27me1 Peptide
H3K27me0 Peptide

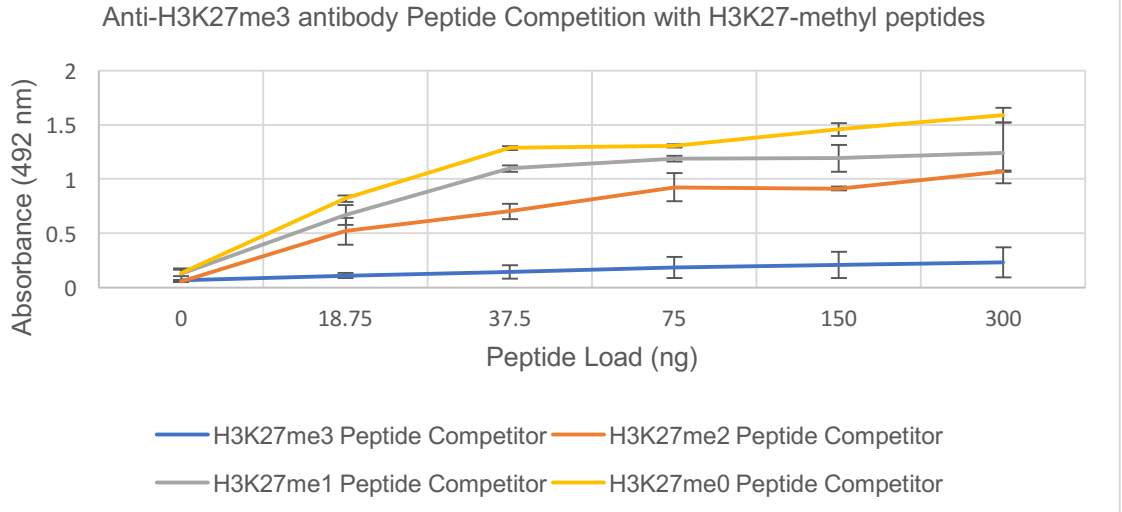
Anti-H3K27me3 antibody Peptide Competition with H3K27-methyl peptides
Absorbance (492 nm)
2
1.5
1
0.5
0
0
18.75
37.5
75
150
300
Peptide Load (ng)
H3K27me3 Peptide Competitor
H3K27me2 Peptide Competitor
H3K27me1 Peptide Competitor
H3K27me0 Peptide Competitor

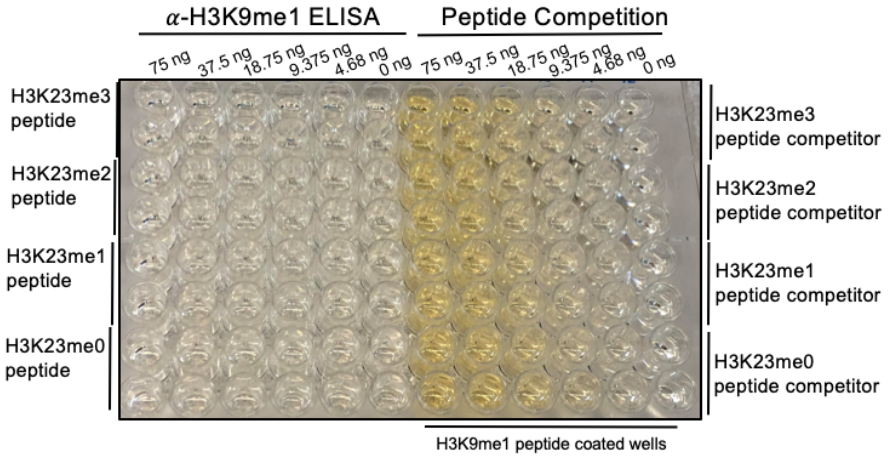
α-H3K9me1 ELISA
Peptide Competition
75 ng
37.5 ng
18.75 ng
9.375 ng
4.68 ng
0 ng
H3K23me3 peptide
H3K23me2 peptide
H3K23me1 peptide
H3K23me0 peptide
H3K23me3 peptide competitor
H3K23me2 peptide competitor
H3K23me1 peptide competitor
H3K23me0 peptide competitor
H3K9me1 peptide coated wells

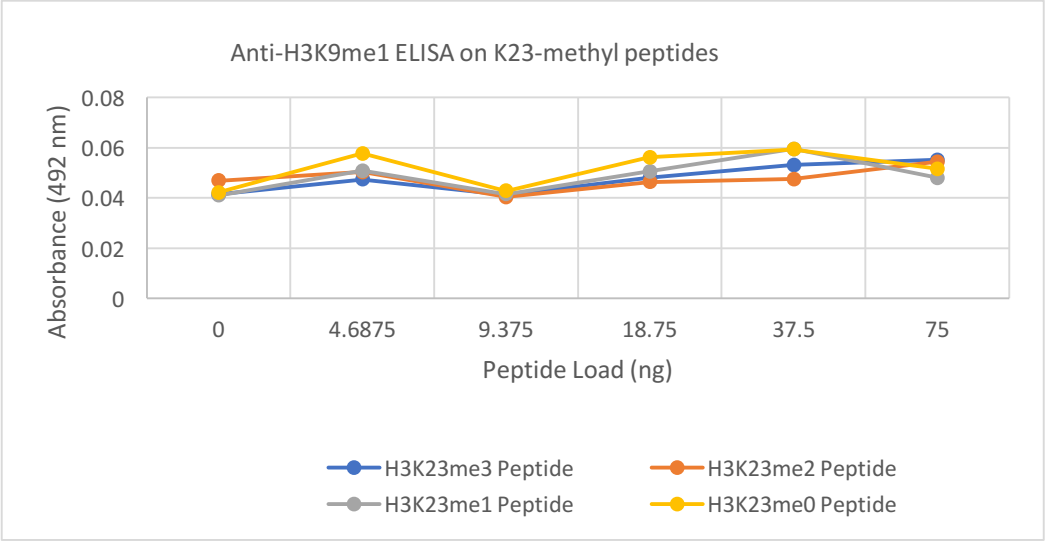
Anti-H3K9me1 ELISA on K23-methyl peptides
Absorbance (492 nm)
0.08
0.06
0.04
0.02
0
0
4.6875
9.375
18.75
37.5
75
Peptide Load (ng)
H3K23me3 Peptide
H3K23me2 Peptide
H3K23me1 Peptide
H3K23me0 Peptide

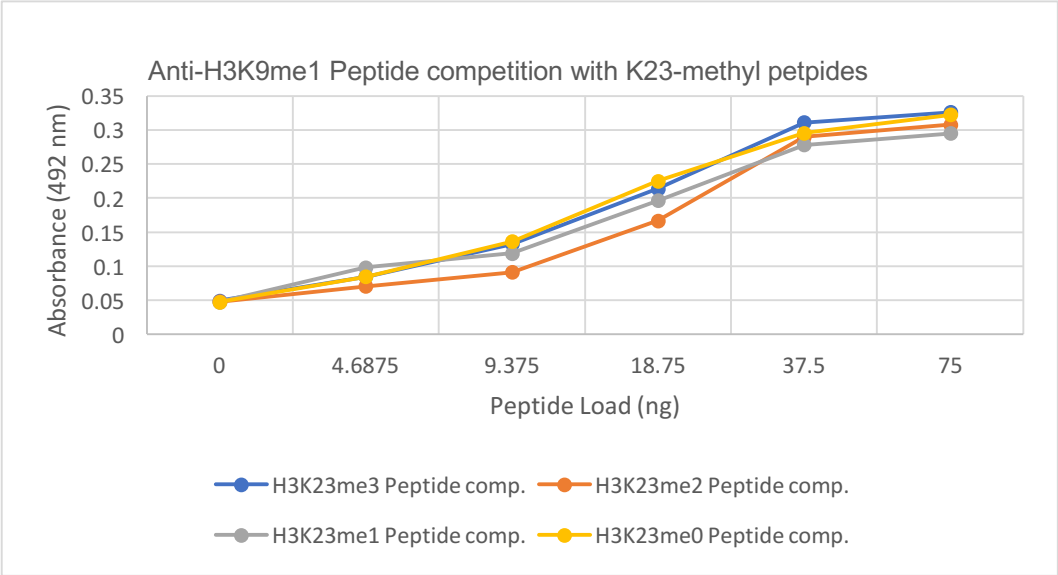
Anti-H3K9me1 Peptide competition with K23-methyl petpides
Absorbance (492 nm)
0.35
0.3
0.25
0.2
0.15
0.1
0.05
0
0
4.6875
9.375
18.75
37.5
75
Peptide Load (ng)
H3K23me3 Peptide comp.
H3K23me2 Peptide comp.
H3K23me1 Peptide comp.
H3K23me0 Peptide comp.

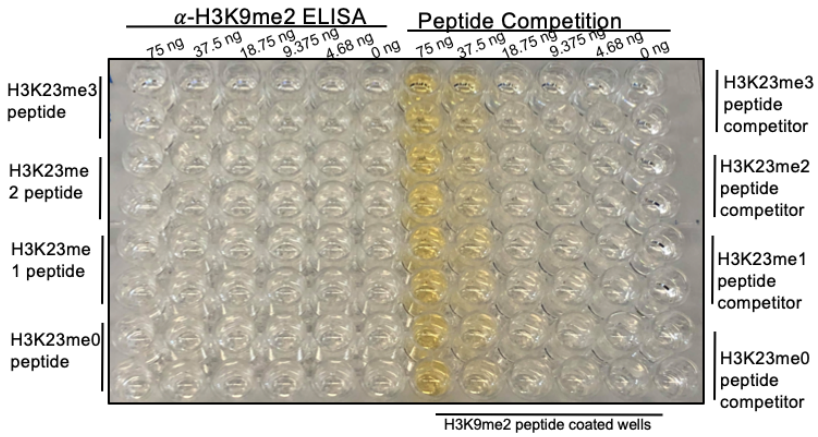
α-H3K9me2 ELISA
Peptide Competition
75 ng
37.5 ng
18.75 ng
9.375 ng
4.68 ng
0 ng
H3K23me3 peptide
H3K23me 2 peptide
H3K23me 1 peptide
H3K23me0 peptide
H3K23me3 peptide competitor
H3K23me2 peptide competitor
H3K23me1 peptide competitor
H3K23me0 peptide competitor
H3K9me2 peptide coated wells

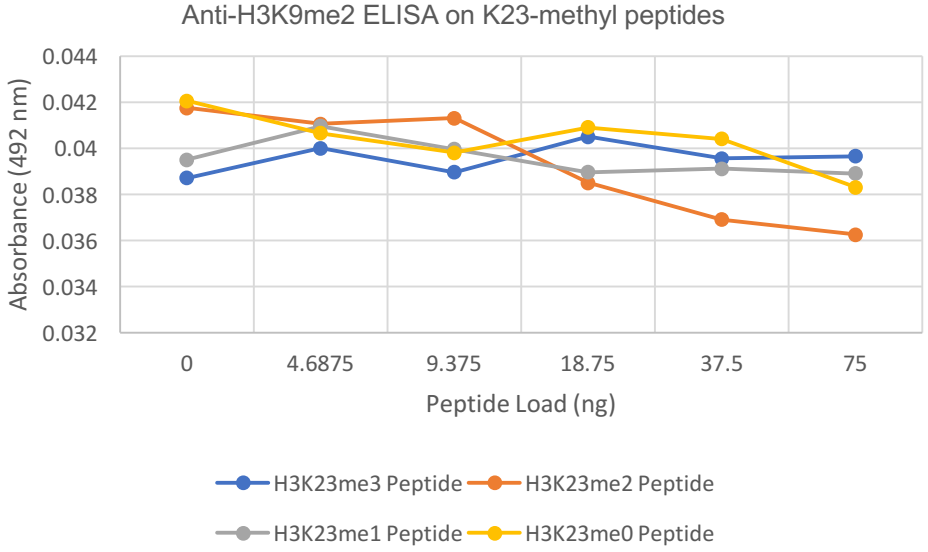
Anti-H3K9me2 ELISA on K23-methyl peptides
Absorbance (492 nm)
0.044
0.042
0.04
0.038
0.036
0.034
0.032
0
4.6875
9.375
18.75
37.5
75
Peptide Load (ng)
H3K23me3 Peptide
H3K23me2 Peptide
H3K23me1 Peptide
H3K23me0 Peptide

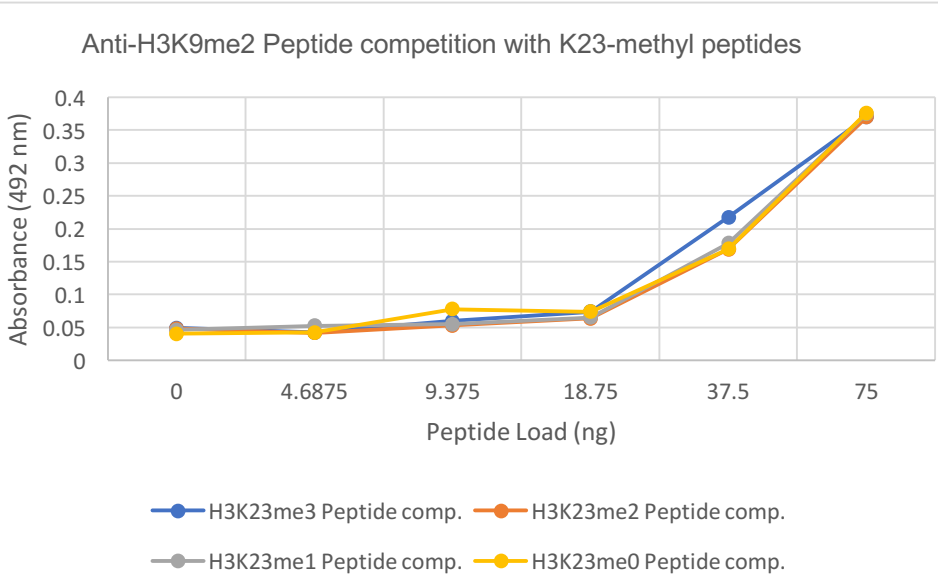
Anti-H3K9me2 Peptide competition with K23-methyl peptides
Absorbance (492 nm)
0.4
0.35
0.3
0.25
0.2
0.15
0.1
0.05
0
0
4.6875
9.375
18.75
37.5
75
Peptide Load (ng)
H3K23me3 Peptide comp.
H3K23me2 Peptide comp.
H3K23me1 Peptide comp.
H3K23me0 Peptide comp.

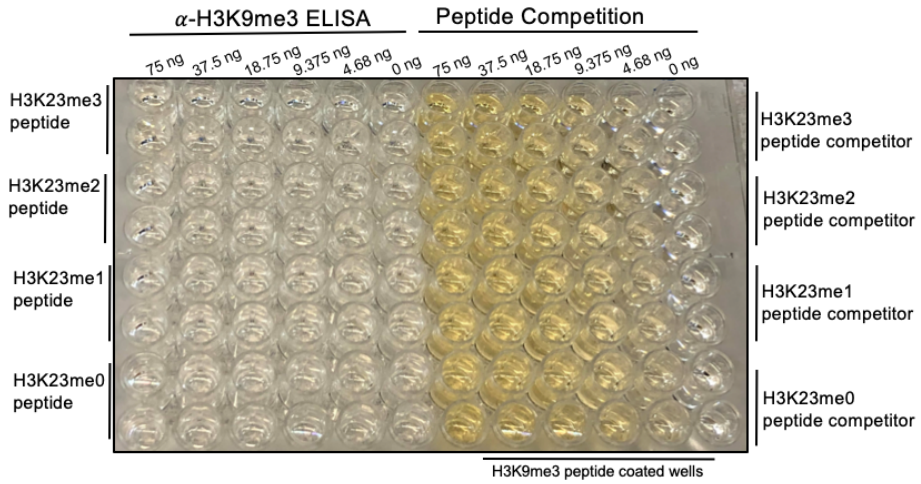
α-H3K9me3 ELISA
Peptide Competition
75 ng
37.5 ng
18.75 ng
9.375 ng
4.68 ng
0 ng
75 ng
37.5 ng
18.75 ng
9.375 ng
4.68 ng
0 ng
H3K23me3 peptide
H3K23me2 peptide
H3K23me1 peptide
H3K23me0 peptide
H3K23me3 peptide competitor
H3K23me2 peptide competitor
H3K23me1 peptide competitor
H3K23me0 peptide competitor
H3K9me3 peptide coated wells

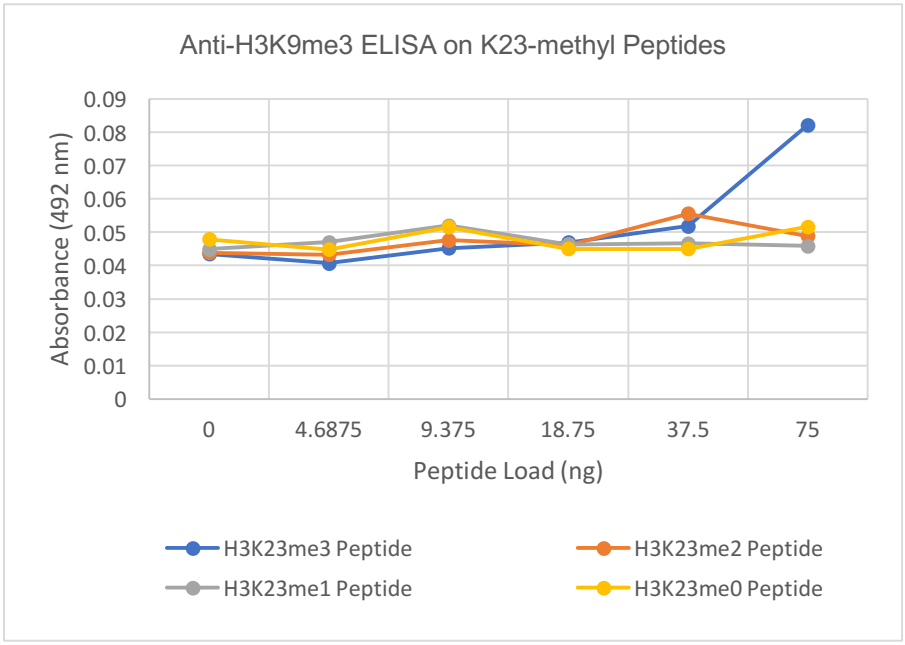
Anti-H3K9me3 ELISA on K23-methyl Peptides
Absorbance (492 nm)
0.09
0.08
0.07
0.06
0.05
0.04
0.03
0.02
0.01
0
0
4.6875
9.375
18.75
37.5
75
Peptide Load (ng)
H3K23me3 Peptide
H3K23me2 Peptide
H3K23me1 Peptide
H3K23me0 Peptide

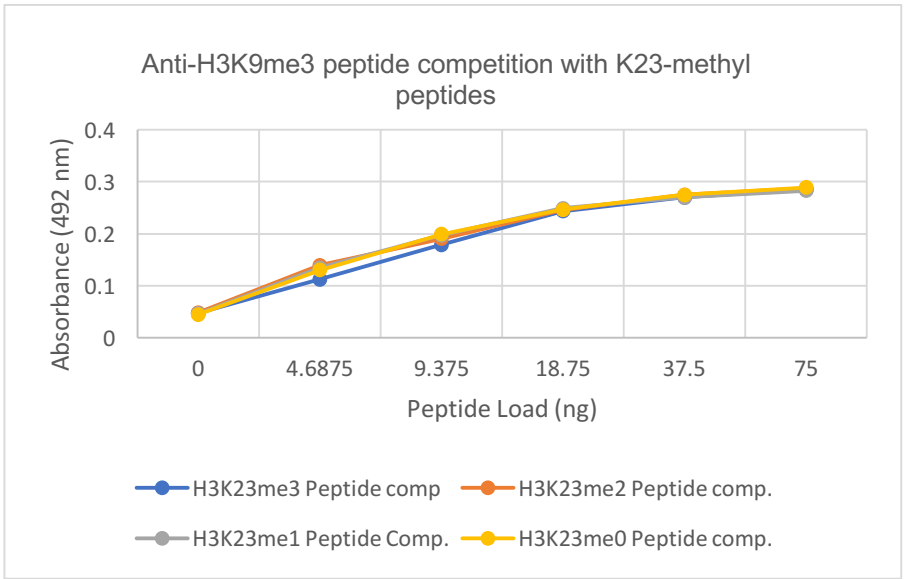
Anti-H3K9me3 peptide competition with K23-methyl peptides
Absorbance (492 nm)
0.4
0.3
0.2
0.1
0
0
4.6875
9.375
18.75
37.5
75
Peptide Load (ng)
H3K23me3 Peptide comp
H3K23me2 Peptide comp.
H3K23me1 Peptide Comp.
H3K23me0 Peptide comp.

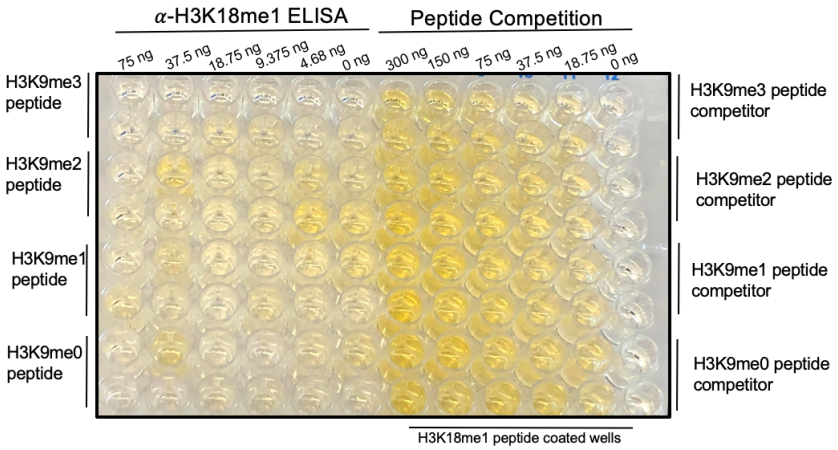
α-H3K18me1 ELISA
Peptide Competition
75 ng
37.5 ng
18.75 ng
9.375 ng
4.68 ng
0 ng
300 ng
150 ng
75 ng
37.5 ng
18.75 ng
0 ng
H3K9me3 peptide
H3K9me2 peptide
H3K9me1 peptide
H3K9me0 peptide
H3K9me3 peptide competitor
H3K9me2 peptide competitor
H3K9me1 peptide competitor
H3K9me0 peptide competitor
H3K18me1 peptide coated wells

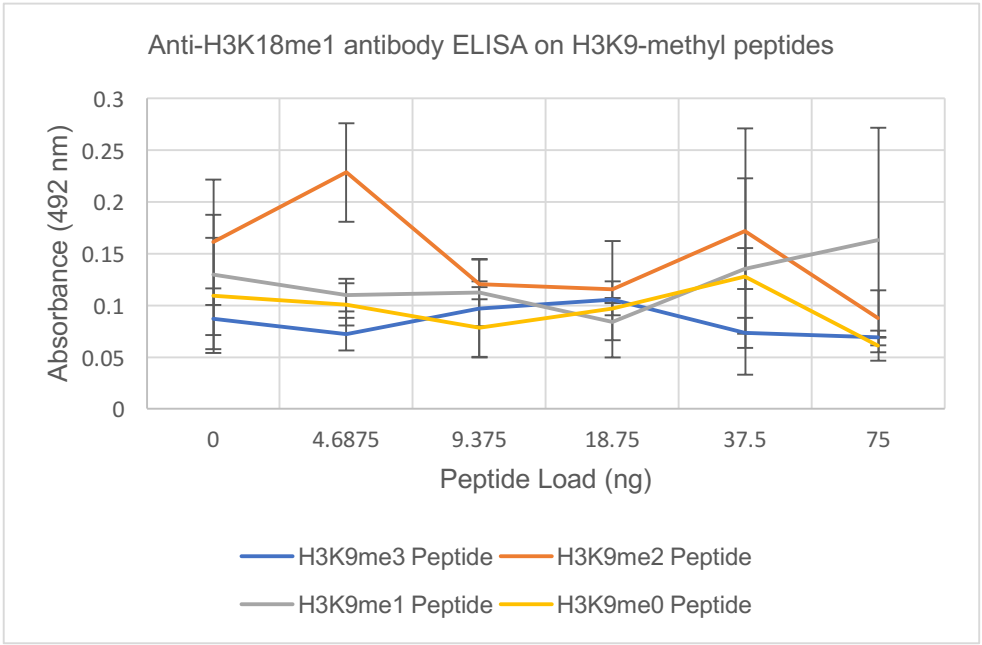
Anti-H3K18me1 antibody ELISA on H3K9-methyl peptides
Absorbance (492 nm)
0.3
0.25
0.2
0.15
0.1
0.05
0
0
4.6875
9.375
18.75
37.5
75
Peptide Load (ng)
H3K9me3 Peptide
H3K9me2 Peptide
H3K9me1 Peptide
H3K9me0 Peptide

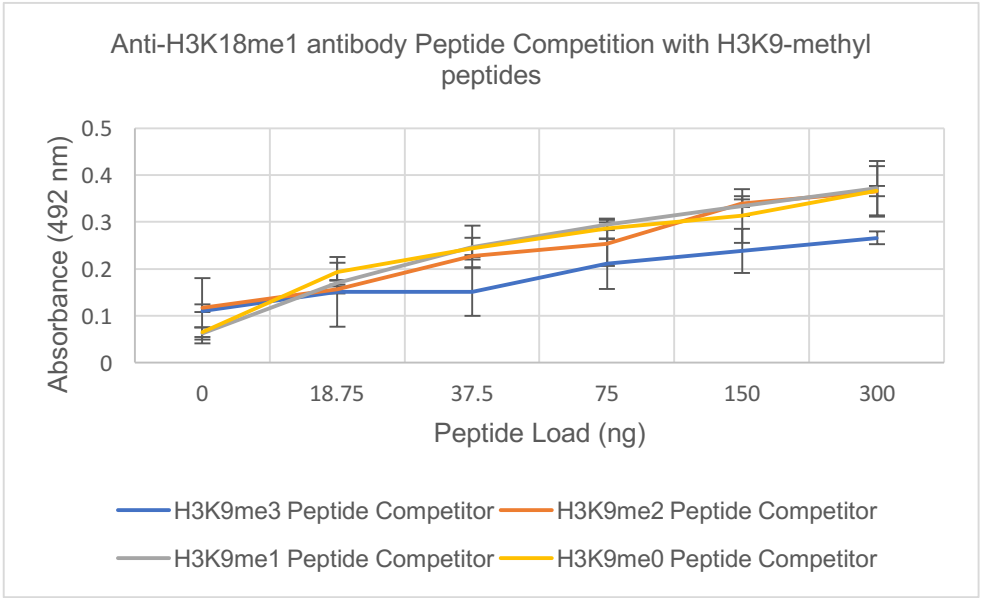
Anti-H3K18me1 antibody Peptide Competition with H3K9-methyl peptides
Absorbance (492 nm)
0.5
0.4
0.3
0.2
0.1
0
0
18.75
37.5
75
150
300
Peptide Load (ng)
H3K9me3 Peptide Competitor
H3K9me2 Peptide Competitor
H3K9me1 Peptide Competitor
H3K9me0 Peptide Competitor

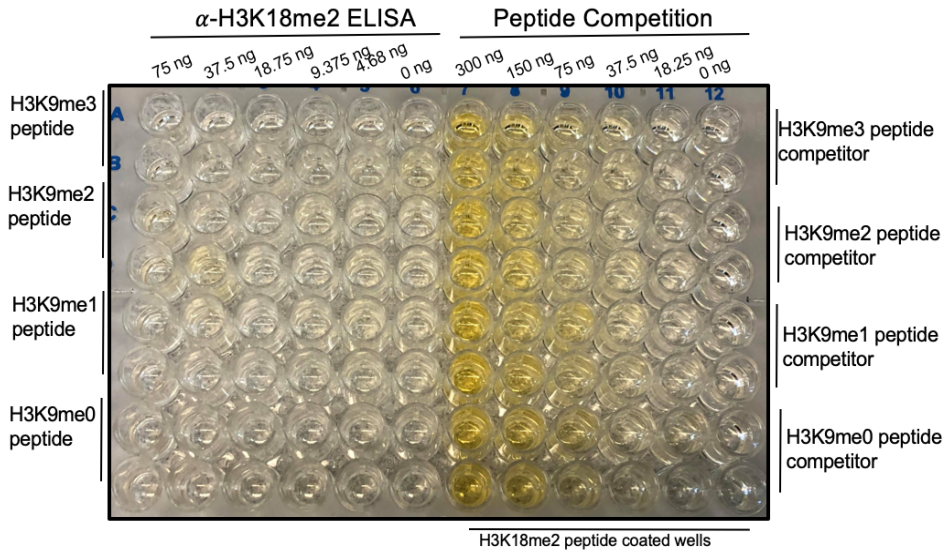
α-H3K18me2 ELISA
Peptide Competition
75 ng
37.5 ng
18.75 ng
9.375 ng
4.68 ng
0 ng
300 ng
150 ng
75 ng
37.5 ng
18.25 ng
0 ng
H3K9me3 peptide
H3K9me2 peptide
H3K9me1 peptide
H3K9me0 peptide
H3K9me3 peptide competitor
H3K9me2 peptide competitor
H3K9me1 peptide competitor
H3K9me0 peptide competitor
H3K18me2 peptide coated wells

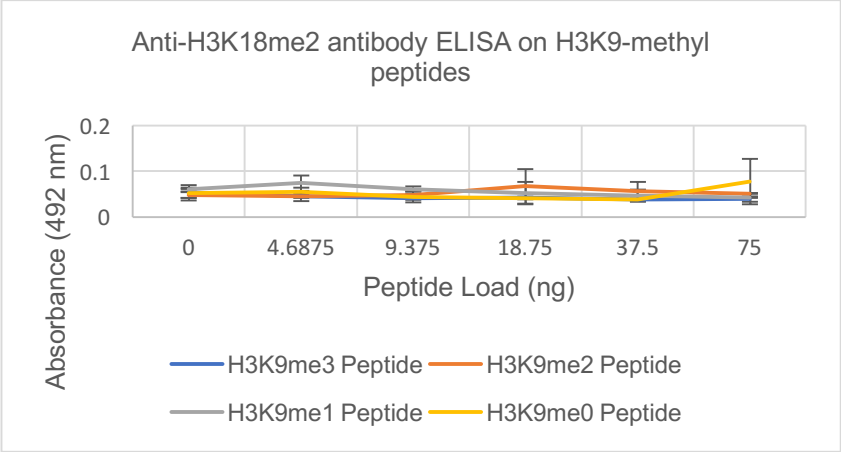
Anti-H3K18me2 antibody ELISA on H3K9-methyl peptides
Absorbance (492 nm)
0.2
0.1
0
0
4.6875
9.375
18.75
37.5
75
Peptide Load (ng)
H3K9me3 Peptide
H3K9me2 Peptide
H3K9me1 Peptide
H3K9me0 Peptide

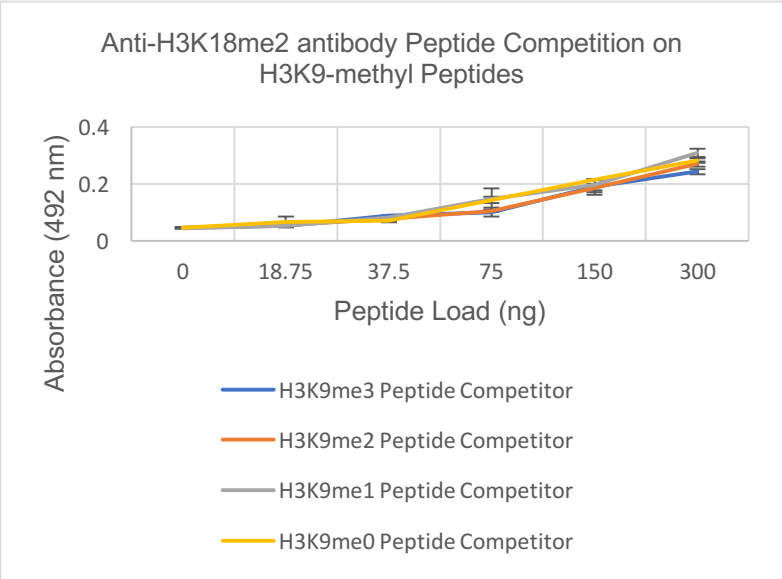
Anti-H3K18me2 antibody Peptide Competition on H3K9-methyl Peptides
Absorbance (492 nm)
0.4
0.2
0
0
18.75
37.5
75
150
300
Peptide Load (ng)
H3K9me3 Peptide Competitor
H3K9me2 Peptide Competitor
H3K9me1 Peptide Competitor
H3K9me0 Peptide Competitor

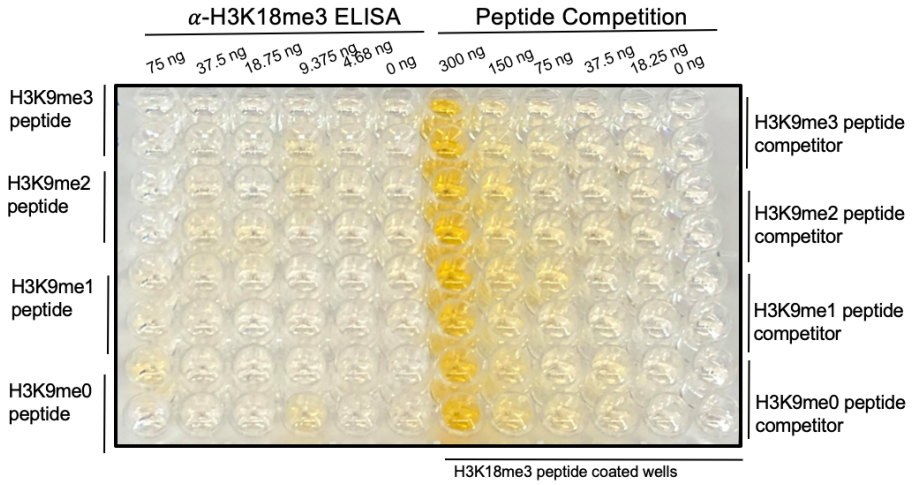
α-H3K18me3 ELISA
Peptide Competition
75 ng
37.5 ng
18.75 ng
9.375 ng
4.68 ng
0 ng
300 ng
150 ng
75 ng
37.5 ng
18.25 ng
0 ng
H3K9me3 peptide
H3K9me2 peptide
H3K9me1 peptide
H3K9me0 peptide
H3K9me3 peptide competitor
H3K9me2 peptide competitor
H3K9me1 peptide competitor
H3K9me0 peptide competitor
H3K18me3 peptide coated wells

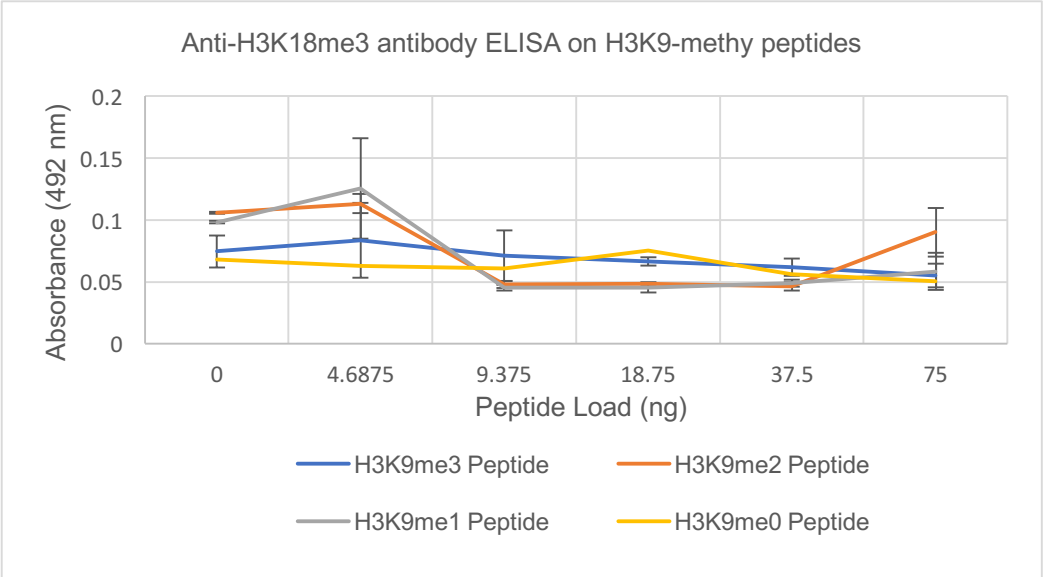
Anti-H3K18me3 antibody ELISA on H3K9-methy peptides
Absorbance (492 nm)
0.2
0.15
0.1
0.05
0
0
4.6875
9.375
18.75
37.5
75
Peptide Load (ng)
H3K9me3 Peptide
H3K9me2 Peptide
H3K9me1 Peptide
H3K9me0 Peptide

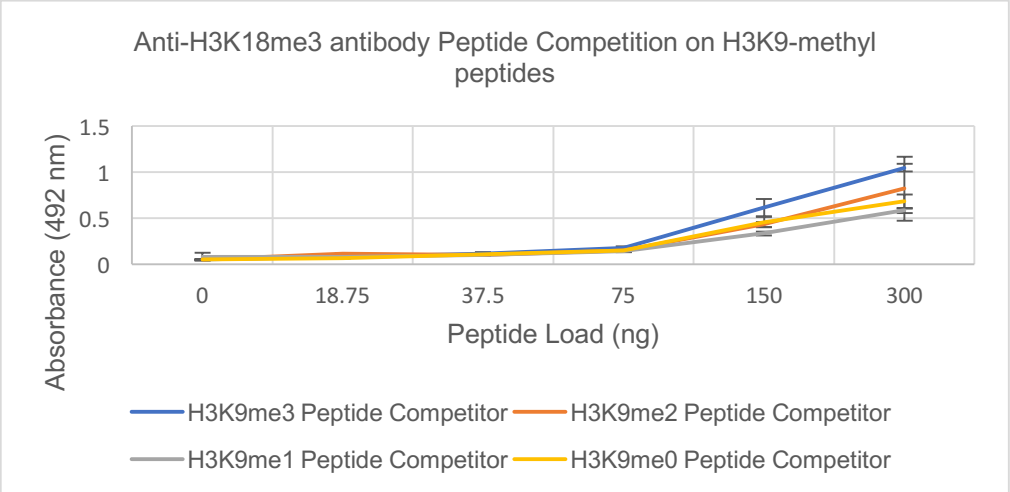
Anti-H3K18me3 antibody Peptide Competition on H3K9-methyl peptides
Absorbance (492 nm)
1.5
1
0.5
0
0
18.75
37.5
75
150
300
Peptide Load (ng)
H3K9me3 Peptide Competitor
H3K9me2 Peptide Competitor
H3K9me1 Peptide Competitor
H3K9me0 Peptide Competitor

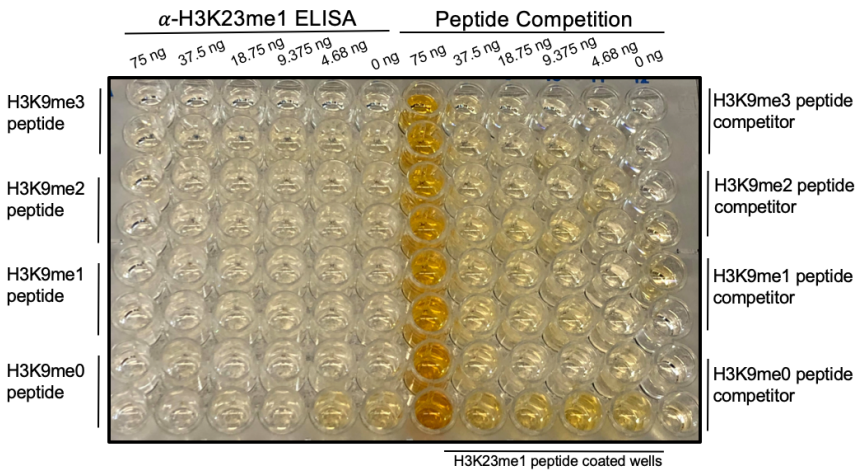
α-H3K23me1 ELISA
Peptide Competition
75 ng
37.5 ng
18.75 ng
9.375 ng
4.68 ng
0 ng
H3K9me3 peptide
H3K9me2 peptide
H3K9me1 peptide
H3K9me0 peptide
H3K9me3 peptide competitor
H3K9me2 peptide competitor
H3K9me1 peptide competitor
H3K9me0 peptide competitor
H3K23me1 peptide coated wells

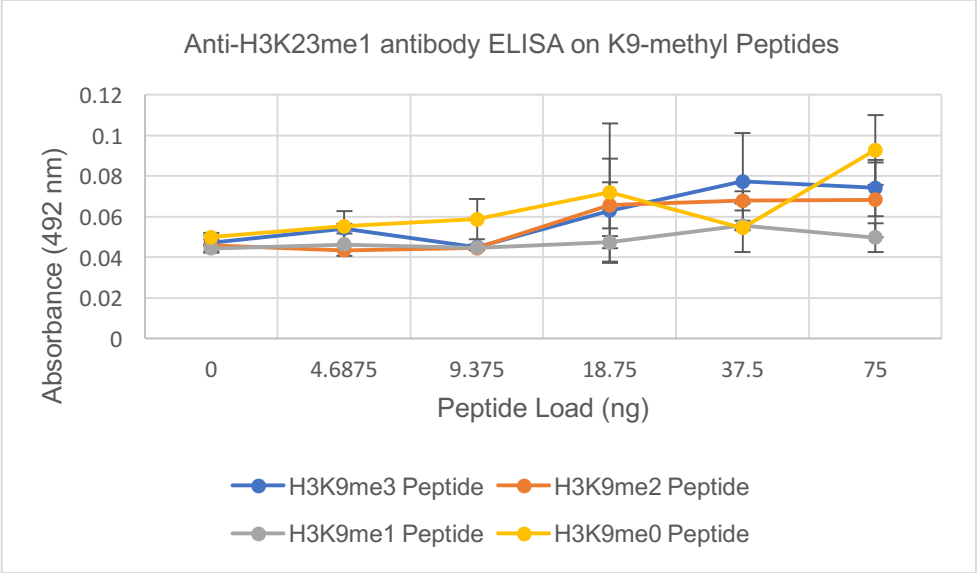
Anti-H3K23me1 antibody ELISA on K9-methyl Peptides
Absorbance (492 nm)
0.12
0.1
0.08
0.06
0.04
0.02
0
0
4.6875
9.375
18.75
37.5
75
Peptide Load (ng)
H3K9me3 Peptide
H3K9me2 Peptide
H3K9me1 Peptide
H3K9me0 Peptide

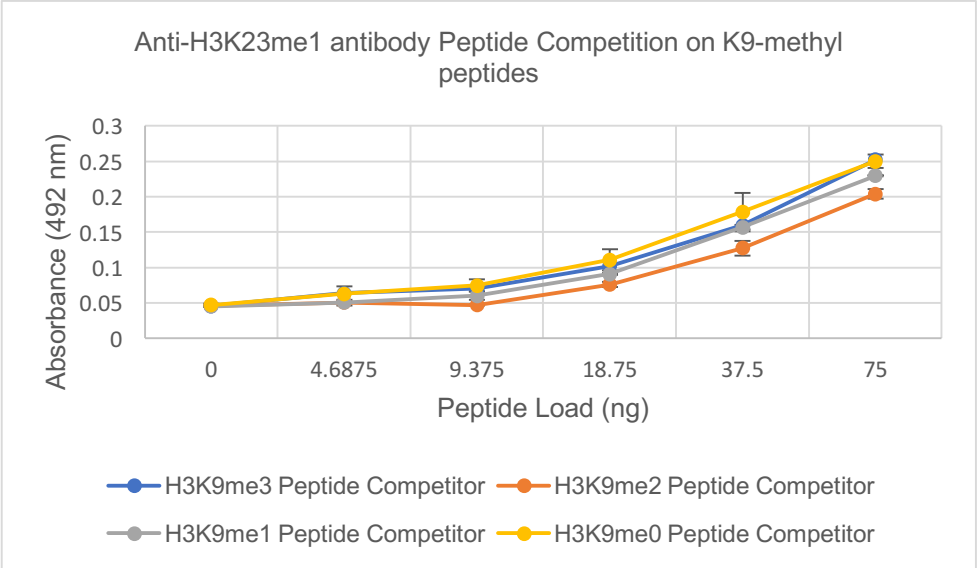
Anti-H3K23me1 antibody Peptide Competition on K9-methyl peptides
Absorbance (492 nm)
0.3
0.25
0.2
0.15
0.1
0.05
0
0
4.6875
9.375
18.75
37.5
75
Peptide Load (ng)
H3K9me3 Peptide Competitor
H3K9me2 Peptide Competitor
H3K9me1 Peptide Competitor
H3K9me0 Peptide Competitor

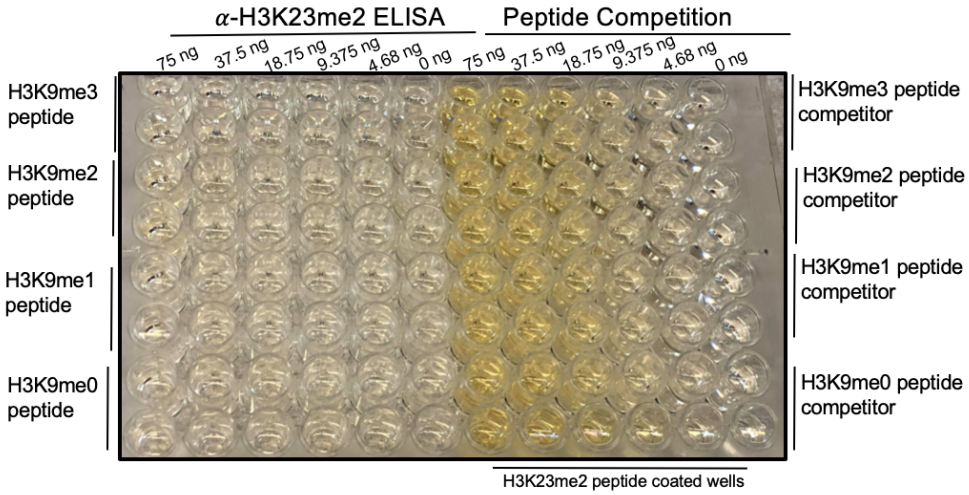
α-H3K23me2 ELISA
Peptide Competition
75 ng
37.5 ng
18.75 ng
9.375 ng
4.68 ng
0 ng
75 ng
37.5 ng
18.75 ng
9.375 ng
4.68 ng
0 ng
H3K9me3 peptide
H3K9me2 peptide
H3K9me1 peptide
H3K9me0 peptide
H3K9me3 peptide competitor
H3K9me2 peptide competitor
H3K9me1 peptide competitor
H3K9me0 peptide competitor
H3K23me2 peptide coated wells

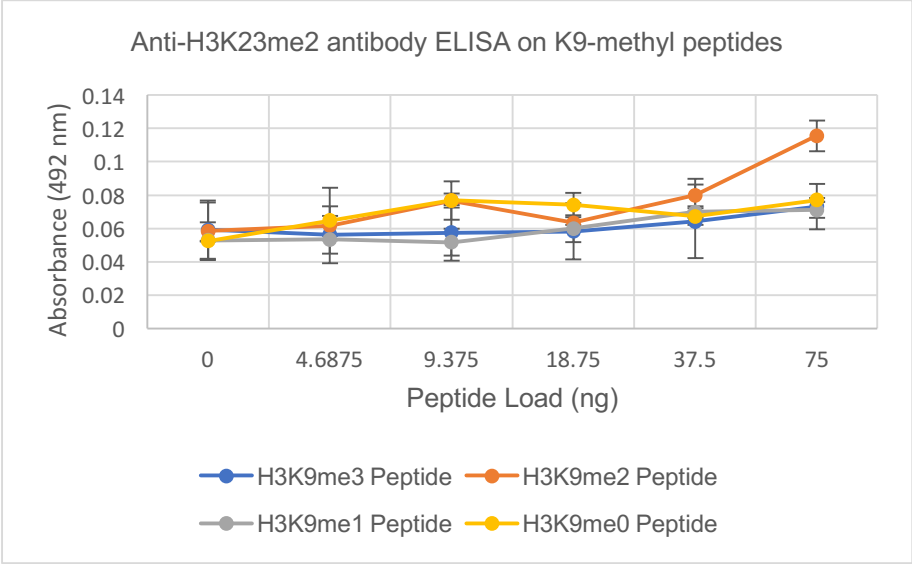
Anti-H3K23me2 antibody ELISA on K9-methyl peptides
Absorbance (492 nm)
0.14
0.12
0.1
0.08
0.06
0.04
0.02
0
0
4.6875
9.375
18.75
37.5
75
Peptide Load (ng)
H3K9me3 Peptide
H3K9me2 Peptide
H3K9me1 Peptide
H3K9me0 Peptide

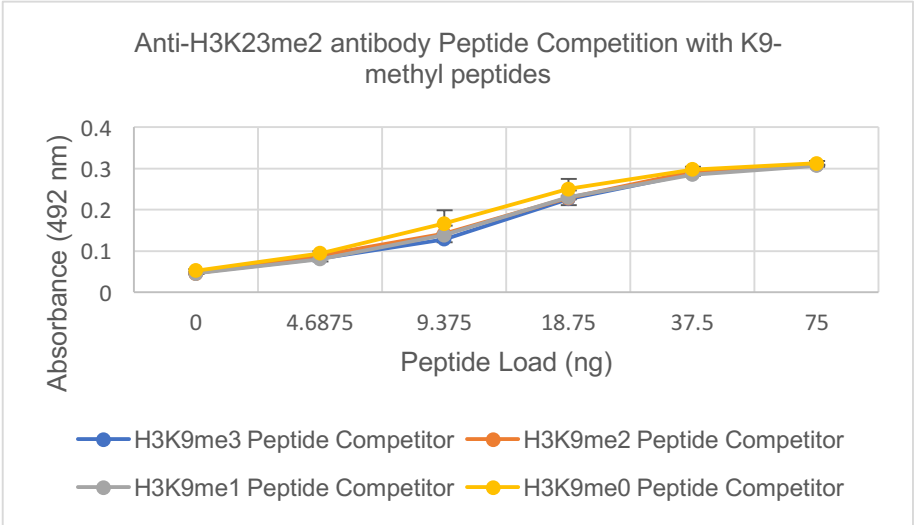
Anti-H3K23me2 antibody Peptide Competition with K9-methyl peptides
Absorbance (492 nm)
0.4
0.3
0.2
0.1
0
0
4.6875
9.375
18.75
37.5
75
Peptide Load (ng)
H3K9me3 Peptide Competitor
H3K9me2 Peptide Competitor
H3K9me1 Peptide Competitor
H3K9me0 Peptide Competitor

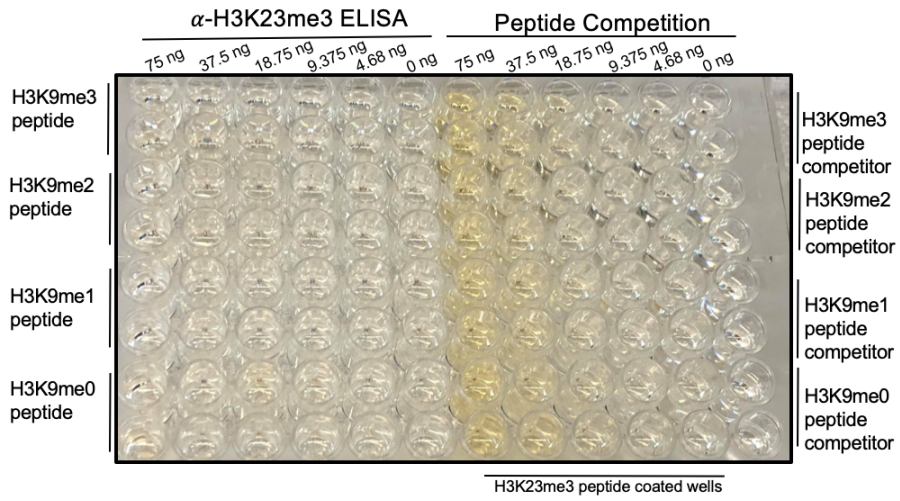
α-H3K23me3 ELISA
Peptide Competition
75 ng
37.5 ng
18.75 ng
9.375 ng
4.68 ng
0 ng
H3K9me3 peptide
H3K9me2 peptide
H3K9me1 peptide
H3K9me0 peptide
H3K9me3 peptide competitor
H3K9me2 peptide competitor
H3K9me1 peptide competitor
H3K9me0 peptide competitor
H3K23me3 peptide coated wells

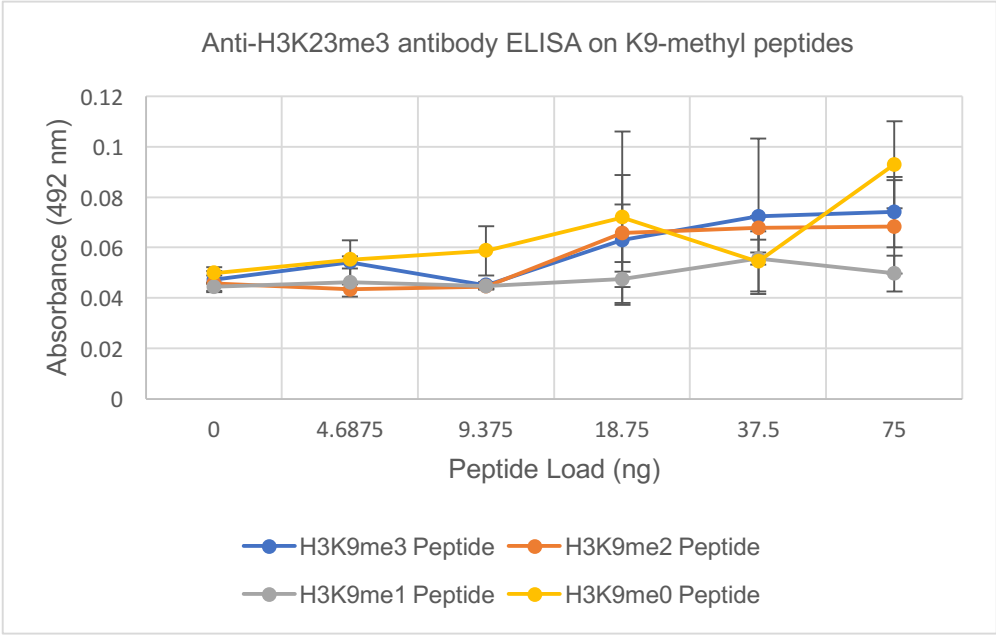
Anti-H3K23me3 antibody ELISA on K9-methyl peptides
Absorbance (492 nm)
0.12
0.1
0.08
0.06
0.04
0.02
0
0
4.6875
9.375
18.75
37.5
75
Peptide Load (ng)
H3K9me3 Peptide
H3K9me2 Peptide
H3K9me1 Peptide
H3K9me0 Peptide

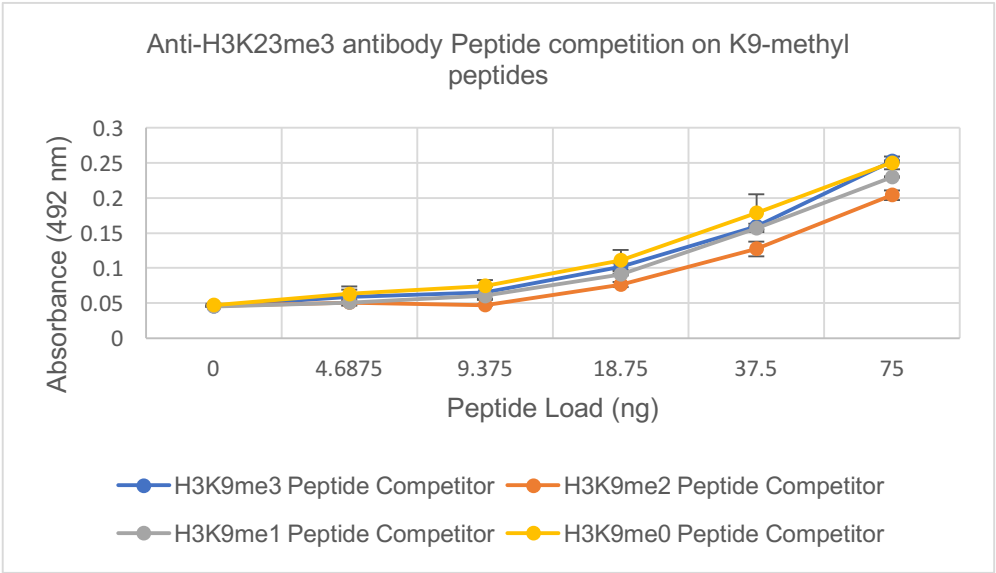
Anti-H3K23me3 antibody Peptide competition on K9-methyl peptides
Absorbance (492 nm)
0.3
0.25
0.2
0.15
0.1
0.05
0
0
4.6875
9.375
18.75
37.5
75
Peptide Load (ng)
H3K9me3 Peptide Competitor
H3K9me2 Peptide Competitor
H3K9me1 Peptide Competitor
H3K9me0 Peptide Competitor

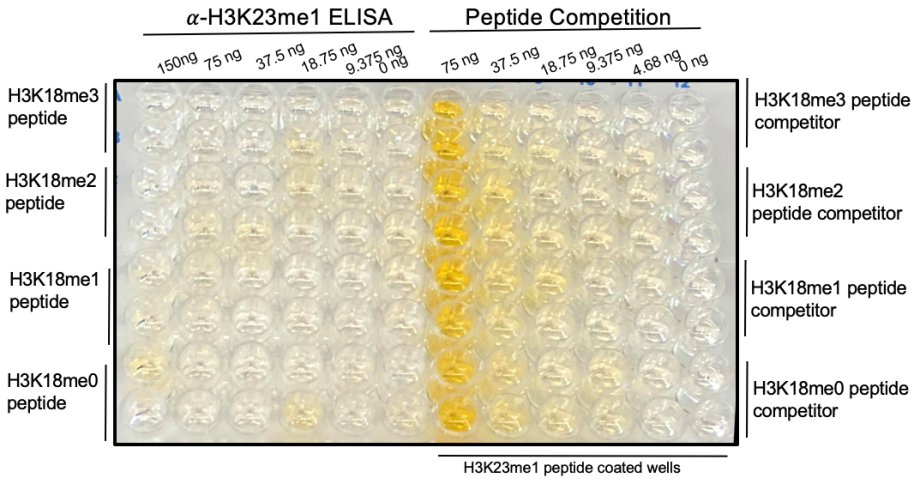
α-H3K23me1 ELISA
Peptide Competition
150ng 75 ng 37.5 ng 18.75 ng 9.375 ng 0 ng
75 ng 37.5 ng 18.75 ng 9.375 ng 4.68 ng 0 ng
H3K18me3 peptide
H3K18me2 peptide
H3K18me1 peptide
H3K18me0 peptide
H3K18me3 peptide competitor
H3K18me2 peptide competitor
H3K18me1 peptide competitor
H3K18me0 peptide competitor
H3K23me1 peptide coated wells

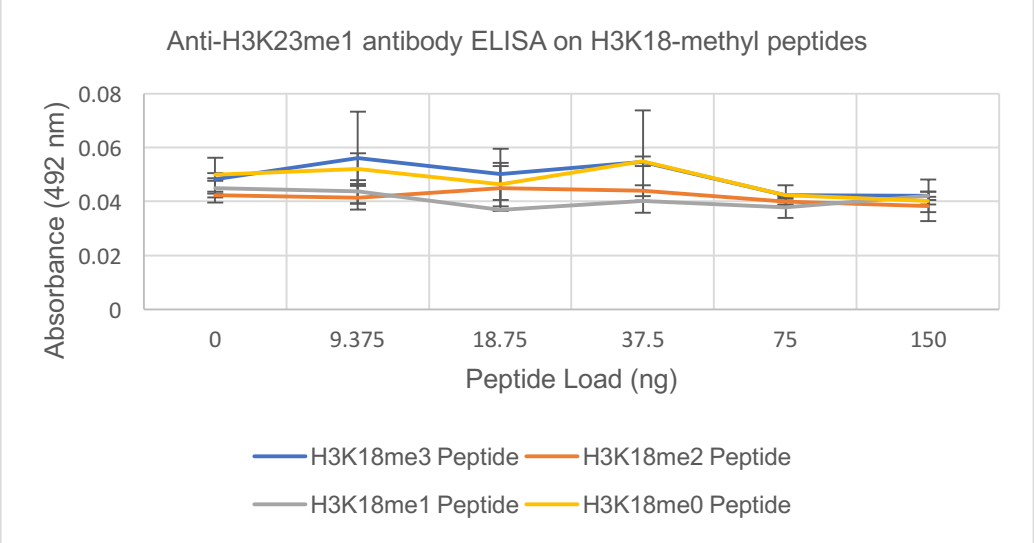
Anti-H3K23me1 antibody ELISA on H3K18-methyl peptides
Absorbance (492 nm)
0.08
0.06
0.04
0.02
0
0
9.375
18.75
37.5
75
150
Peptide Load (ng)
H3K18me3 Peptide
H3K18me2 Peptide
H3K18me1 Peptide
H3K18me0 Peptide

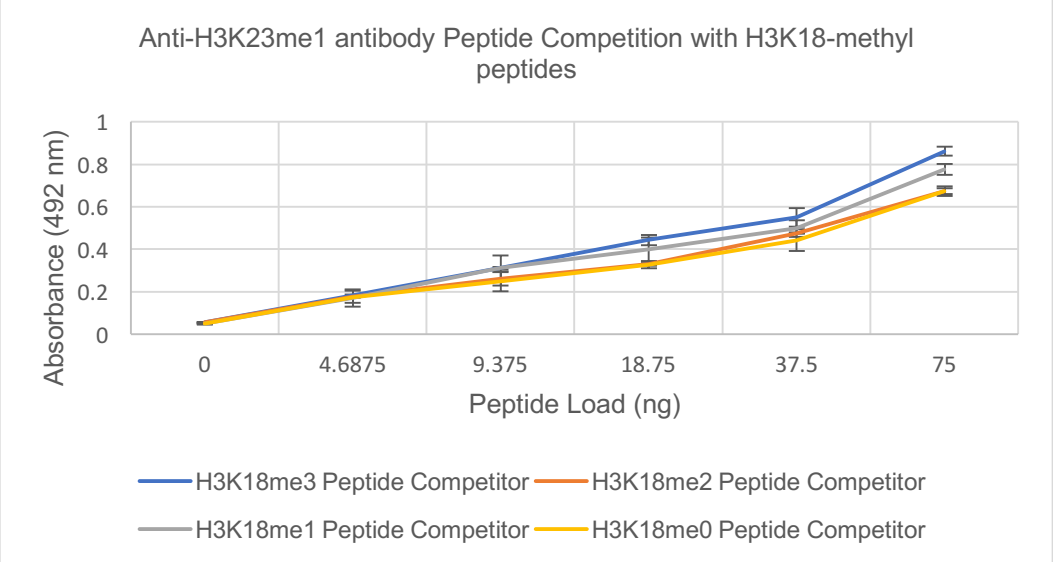
Anti-H3K23me1 antibody Peptide Competition with H3K18-methyl peptides
Absorbance (492 nm)
1
0.8
0.6
0.4
0.2
0
0
4.6875
9.375
18.75
37.5
75
Peptide Load (ng)
H3K18me3 Peptide Competitor
H3K18me2 Peptide Competitor
H3K18me1 Peptide Competitor
H3K18me0 Peptide Competitor

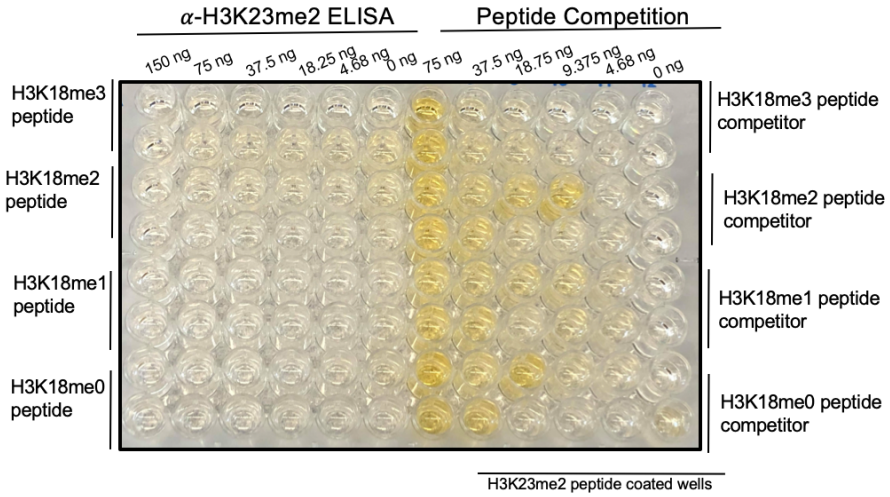
α-H3K23me2 ELISA
Peptide Competition
150 ng
75 ng
37.5 ng
18.25 ng
4.68 ng
0 ng
75 ng
37.5 ng
18.75 ng
9.375 ng
4.68 ng
0 ng
H3K18me3 peptide
H3K18me2 peptide
H3K18me1 peptide
H3K18me0 peptide
H3K18me3 peptide competitor
H3K18me2 peptide competitor
H3K18me1 peptide competitor
H3K18me0 peptide competitor
H3K23me2 peptide coated wells

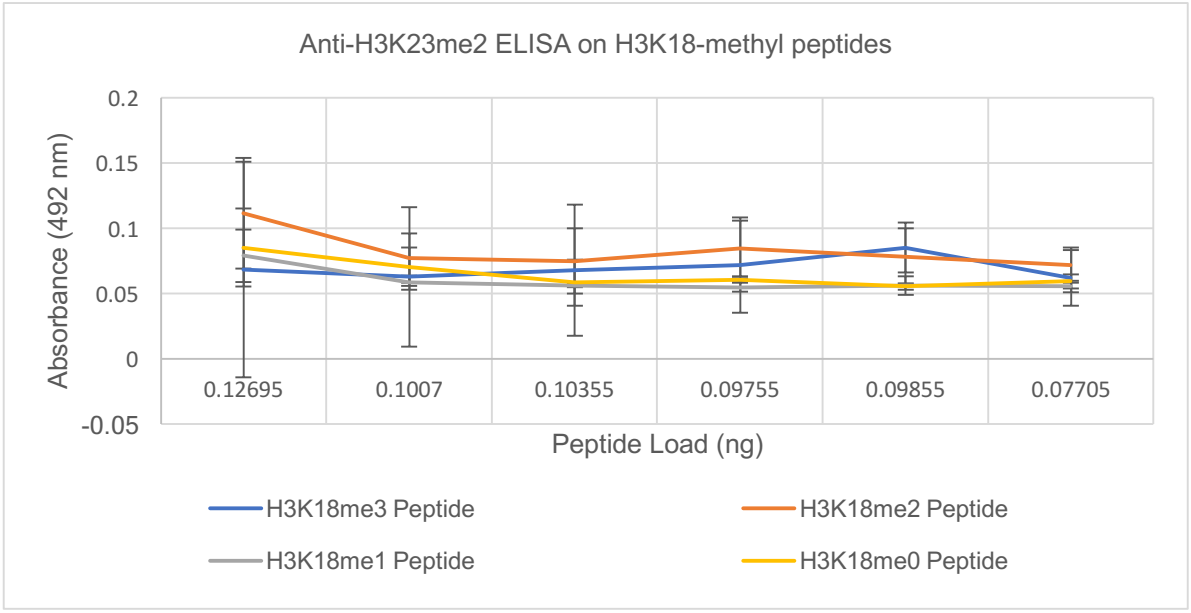
Anti-H3K23me2 ELISA on H3K18-methyl peptides
Absorbance (492 nm)
0.2
0.15
0.1
0.05
0
-0.05
0.12695
0.1007
0.10355
0.09755
0.09855
0.07705
Peptide Load (ng)
H3K18me3 Peptide
H3K18me2 Peptide
H3K18me1 Peptide
H3K18me0 Peptide

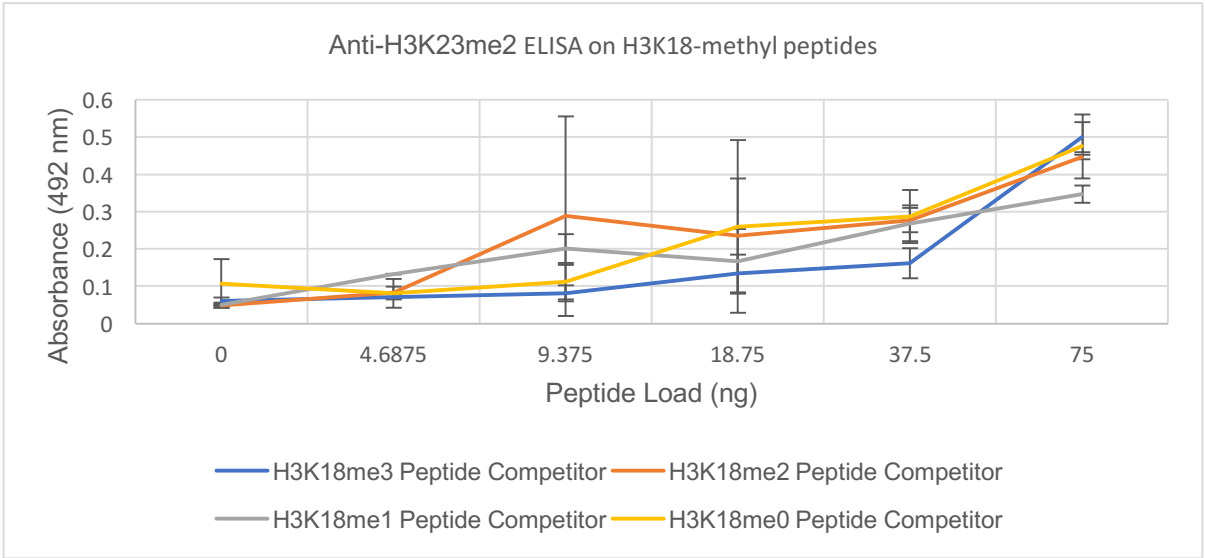
Anti-H3K23me2 ELISA on H3K18-methyl peptides
Absorbance (492 nm)
0.6
0.5
0.4
0.3
0.2
0.1
0
0
4.6875
9.375
18.75
37.5
75
Peptide Load (ng)
H3K18me3 Peptide Competitor
H3K18me2 Peptide Competitor
H3K18me1 Peptide Competitor
H3K18me0 Peptide Competitor

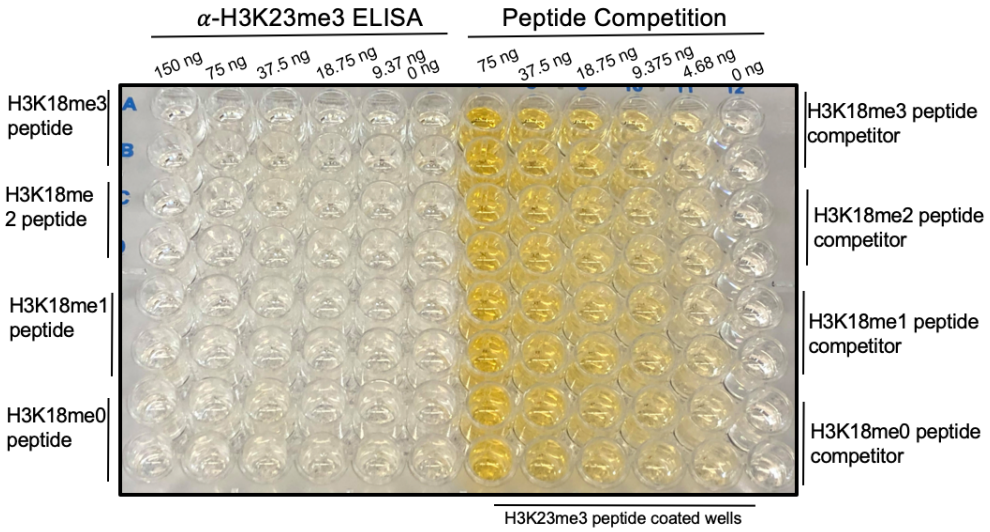
α-H3K23me3 ELISA
Peptide Competition
150 ng
75 ng
37.5 ng
18.75 ng
9.37 ng
0 ng
75 ng
37.5 ng
18.75 ng
9.375 ng
4.68 ng
0 ng
H3K18me3 peptide
H3K18me 2 peptide
H3K18me1 peptide
H3K18me0 peptide
H3K18me3 peptide competitor
H3K18me2 peptide competitor
H3K18me1 peptide competitor
H3K18me0 peptide competitor
H3K23me3 peptide coated wells

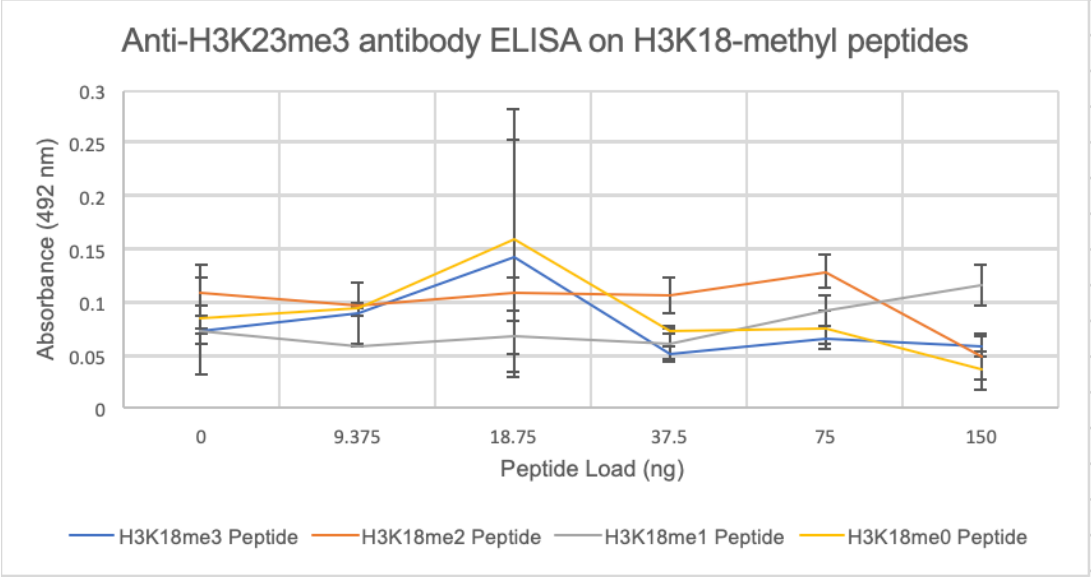
Anti-H3K23me3 antibody ELISA on H3K18-methyl peptides
Absorbance (492 nm)
0.3
0.25
0.2
0.15
0.1
0.05
0
0
9.375
18.75
37.5
75
150
Peptide Load (ng)
H3K18me3 Peptide
H3K18me2 Peptide
H3K18me1 Peptide
H3K18me0 Peptide

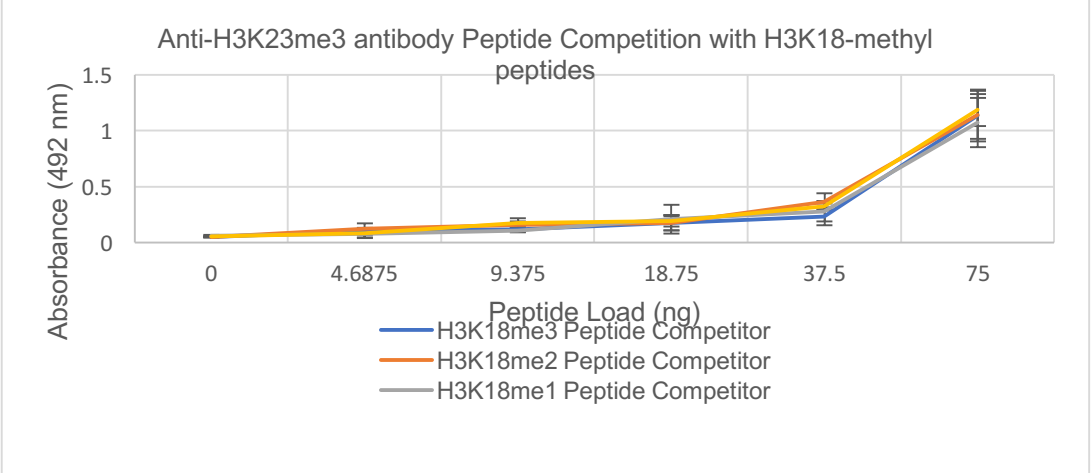
Anti-H3K23me3 antibody Peptide Competition with H3K18-methyl peptides
Absorbance (492 nm)
1.5
1
0.5
0
0
4.6875
9.375
18.75
37.5
75
Peptide Load (ng)
H3K18me3 Peptide Competitor
H3K18me2 Peptide Competitor
H3K18me1 Peptide Competitor

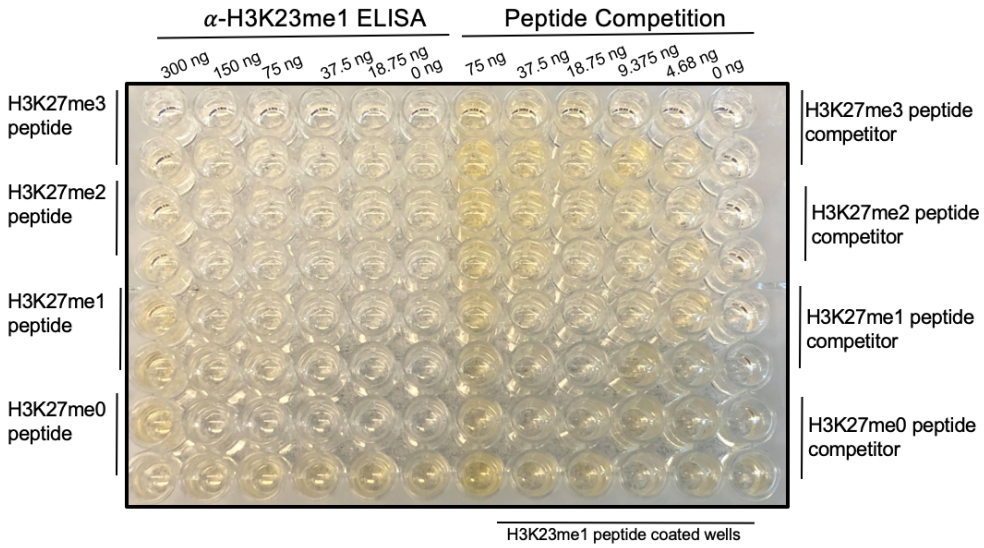
α-H3K23me1 ELISA
Peptide Competition
300 ng
150 ng
75 ng
37.5 ng
18.75 ng
0 ng
75 ng
37.5 ng
18.75 ng
9.375 ng
4.68 ng
0 ng
H3K27me3 peptide
H3K27me2 peptide
H3K27me1 peptide
H3K27me0 peptide
H3K27me3 peptide competitor
H3K27me2 peptide competitor
H3K27me1 peptide competitor
H3K27me0 peptide competitor
H3K23me1 peptide coated wells

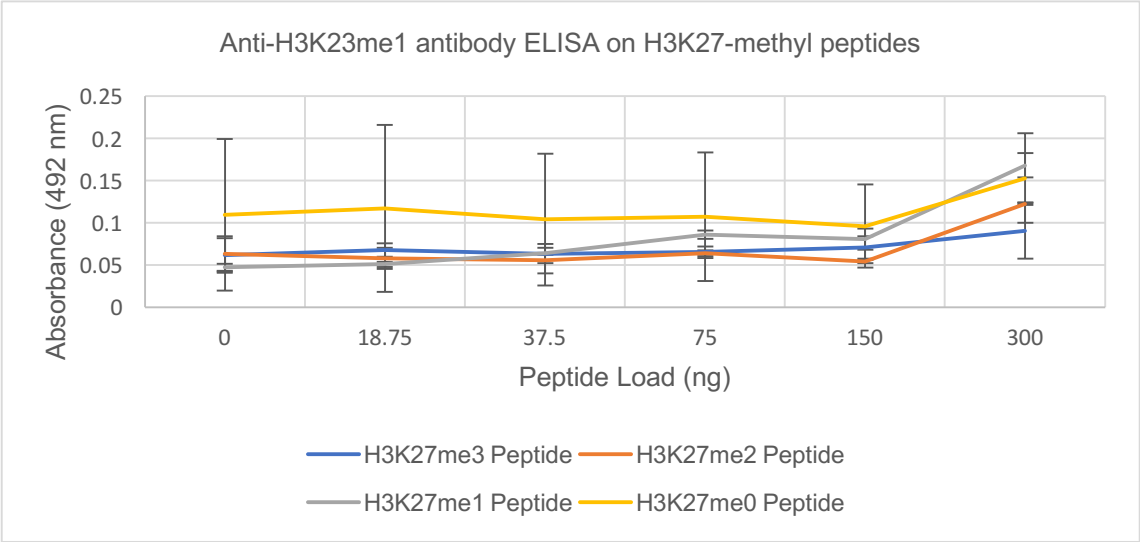
Anti-H3K23me1 antibody ELISA on H3K27-methyl peptides
Absorbance (492 nm)
0.25
0.2
0.15
0.1
0.05
0
0
18.75
37.5
75
150
300
Peptide Load (ng)
H3K27me3 Peptide
H3K27me2 Peptide
H3K27me1 Peptide
H3K27me0 Peptide

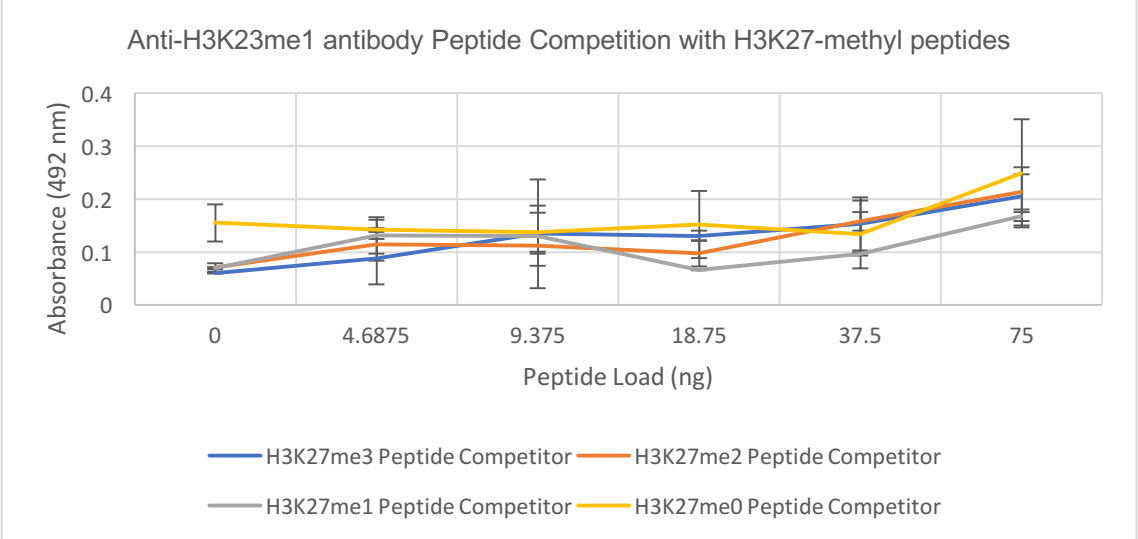
Anti-H3K23me1 antibody Peptide Competition with H3K27-methyl peptides
Absorbance (492 nm)
0.4
0.3
0.2
0.1
0
0
4.6875
9.375
18.75
37.5
75
Peptide Load (ng)
H3K27me3 Peptide Competitor
H3K27me2 Peptide Competitor
H3K27me1 Peptide Competitor
H3K27me0 Peptide Competitor

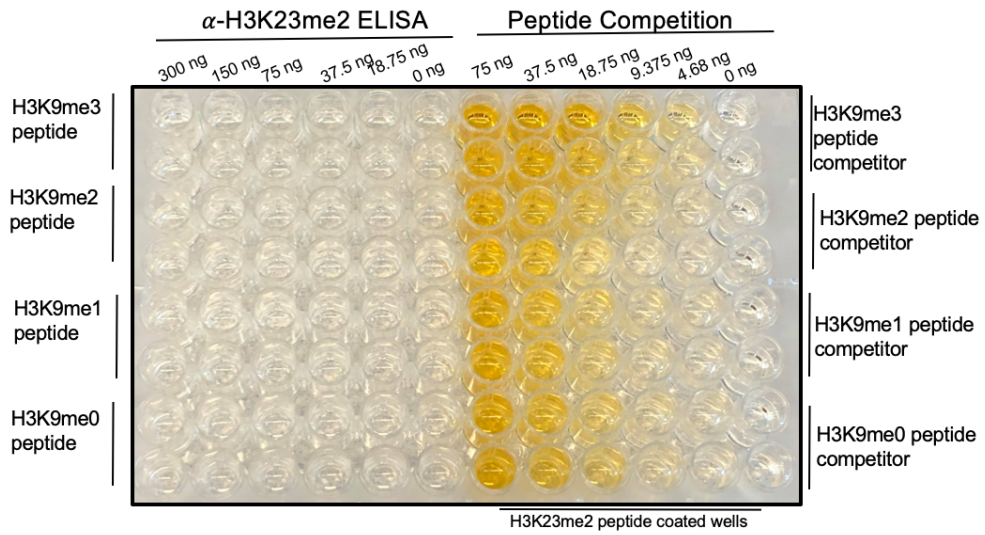
α-H3K23me2 ELISA
Peptide Competition
300 ng
150 ng
75 ng
37.5 ng
18.75 ng
0 ng
75 ng
37.5 ng
18.75 ng
9.375 ng
4.68 ng
0 ng
H3K9me3 peptide
H3K9me2 peptide
H3K9me1 peptide
H3K9me0 peptide
H3K9me3 peptide competitor
H3K9me2 peptide competitor
H3K9me1 peptide competitor
H3K9me0 peptide competitor
H3K23me2 peptide coated wells

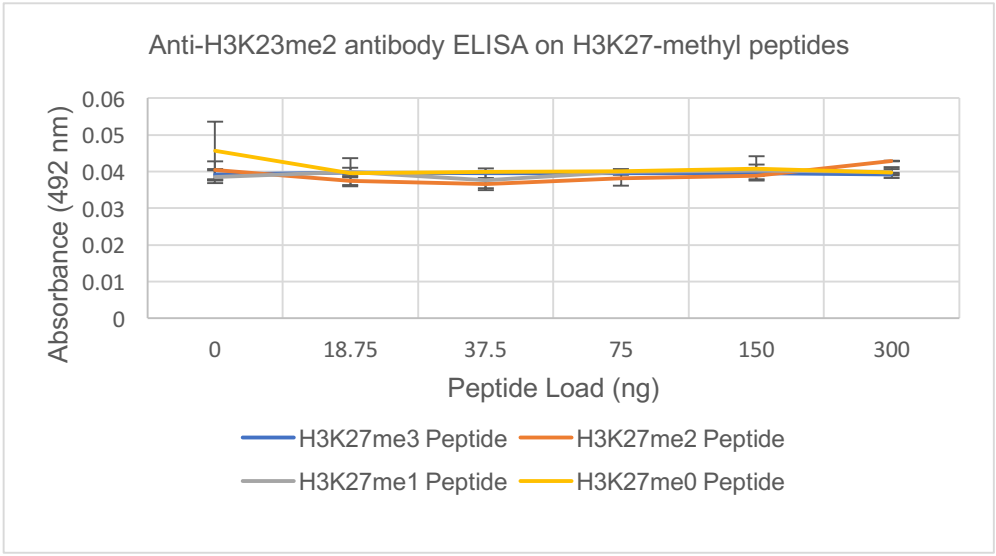
Anti-H3K23me2 antibody ELISA on H3K27-methyl peptides
Absorbance (492 nm)
0.06
0.05
0.04
0.03
0.02
0.01
0
0
18.75
37.5
75
150
300
Peptide Load (ng)
H3K27me3 Peptide
H3K27me2 Peptide
H3K27me1 Peptide
H3K27me0 Peptide

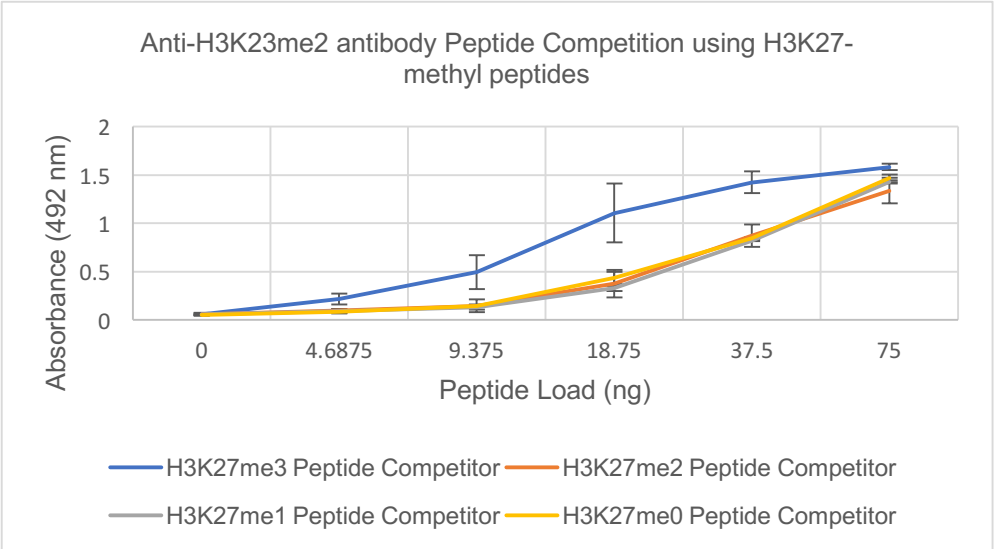
Anti-H3K23me2 antibody Peptide Competition using H3K27-methyl peptides
Absorbance (492 nm)
2
1.5
1
0.5
0
0
4.6875
9.375
18.75
37.5
75
Peptide Load (ng)
H3K27me3 Peptide Competitor
H3K27me2 Peptide Competitor
H3K27me1 Peptide Competitor
H3K27me0 Peptide Competitor

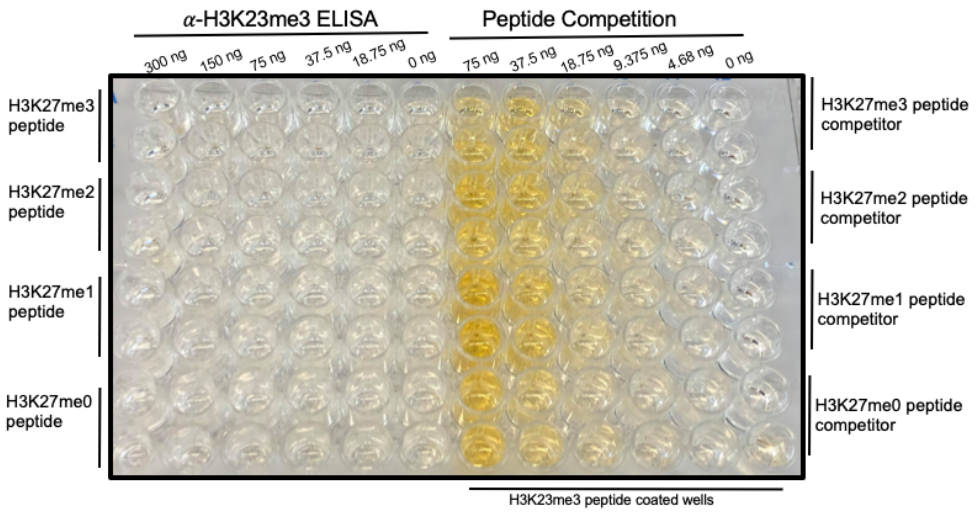
α-H3K23me3 ELISA
Peptide Competition
300 ng
150 ng
75 ng
37.5 ng
18.75 ng
0 ng
75 ng
37.5 ng
18.75 ng
9.375 ng
4.68 ng
0 ng
H3K27me3 peptide
H3K27me2 peptide
H3K27me1 peptide
H3K27me0 peptide
H3K27me3 peptide competitor
H3K27me2 peptide competitor
H3K27me1 peptide competitor
H3K27me0 peptide competitor
H3K23me3 peptide coated wells

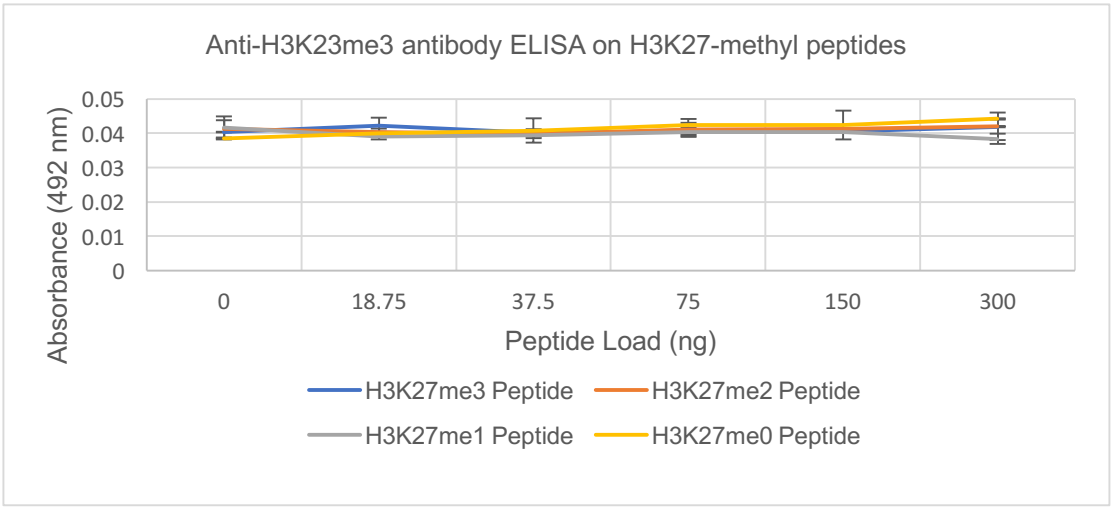
Anti-H3K23me3 antibody ELISA on H3K27-methyl peptides
Absorbance (492 nm)
0.05
0.04
0.03
0.02
0.01
0
0
18.75
37.5
75
150
300
Peptide Load (ng)
H3K27me3 Peptide
H3K27me2 Peptide
H3K27me1 Peptide
H3K27me0 Peptide

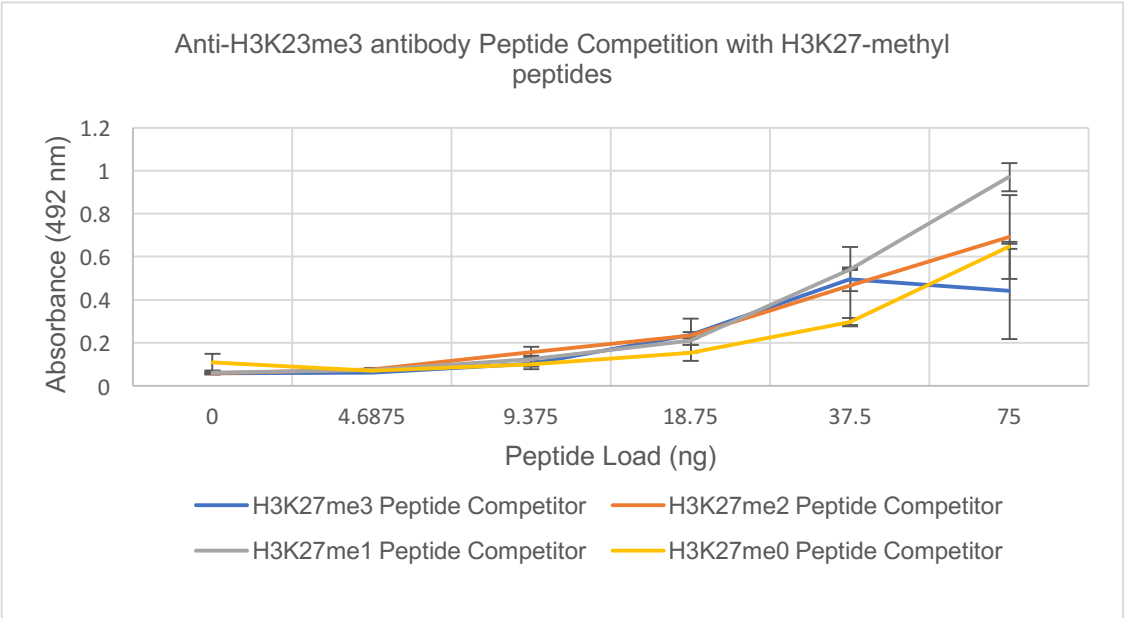
Anti-H3K23me3 antibody Peptide Competition with H3K27-methyl peptides
Absorbance (492 nm)
1.2
1
0.8
0.6
0.4
0.2
0
0
4.6875
9.375
18.75
37.5
75
Peptide Load (ng)
H3K27me3 Peptide Competitor
H3K27me2 Peptide Competitor
H3K27me1 Peptide Competitor
H3K27me0 Peptide Competitor

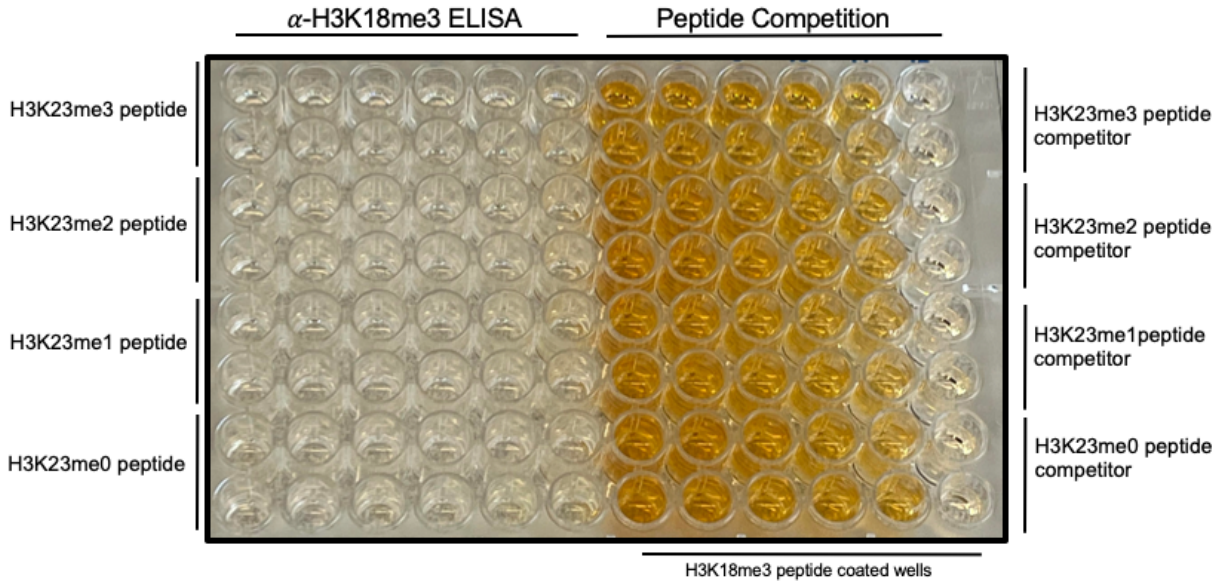
α-H3K18me3 ELISA
Peptide Competition
H3K23me3 peptide
H3K23me2 peptide
H3K23me1 peptide
H3K23me0 peptide
H3K23me3 peptide competitor
H3K23me2 peptide competitor
H3K23me1peptide competitor
H3K23me0 peptide competitor
H3K18me3 peptide coated wells

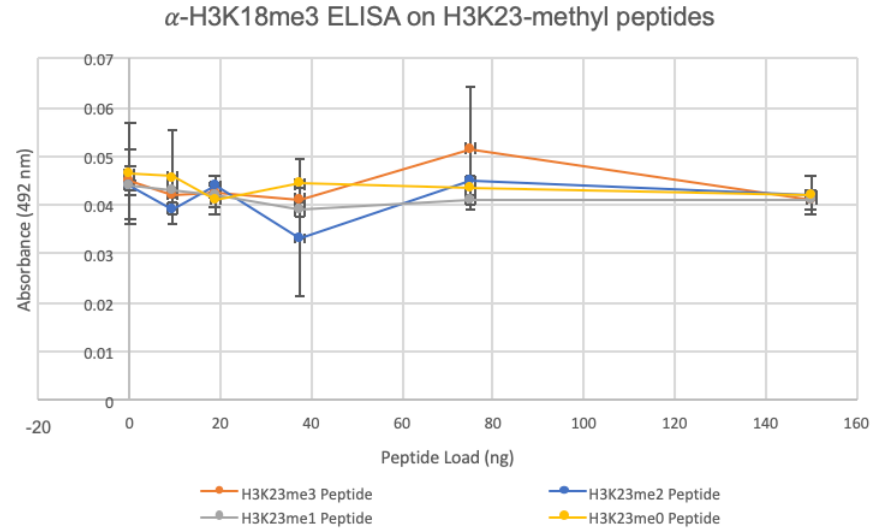
α-H3K18me3 ELISA on H3K23-methyl peptides
Absorbance (492 nm)
Peptide Load (ng)
H3K23me3 Peptide
H3K23me2 Peptide
H3K23me1 Peptide
H3K23me0 Peptide

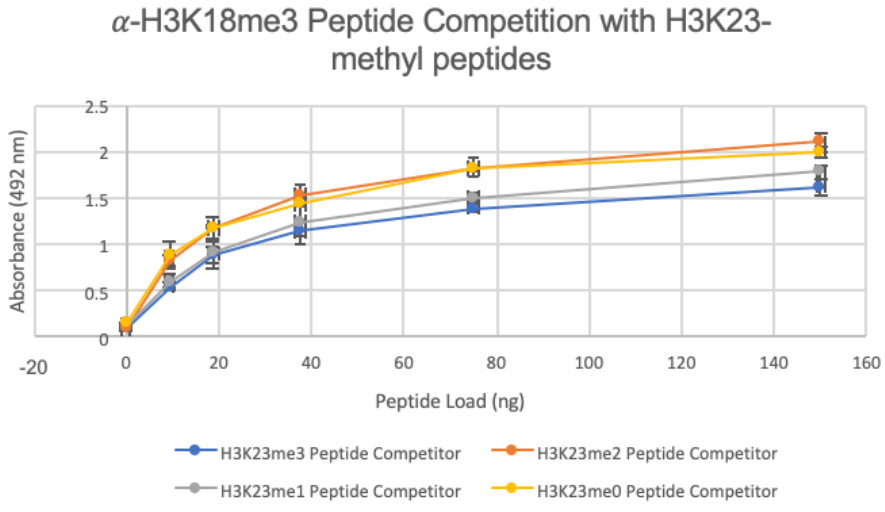
α-H3K18me3 Peptide Competition with H3K23-methyl peptides
Absorbance (492 nm)
Peptide Load (ng)
H3K23me3 Peptide Competitor
H3K23me2 Peptide Competitor
H3K23me1 Peptide Competitor
H3K23me0 Peptide Competitor

Supplementary Figure 5. Antibody validation via ELISA and peptide competition assays

Using a 96-well plate ELISA format, ELISAs and peptide competition assays were done to validate H3K9me1, H3K9me2, H3K9me3, H3K18me1, H3K18me2, H3K18me3, H3K23me1, H3K23me2, H3K23me3, H3K27me1, H3K27me2 and H3K27me3 antibodies for their target methylation state, cross-reactivity with other methylation states of the same epitope and cross-reactivity with methyl-lysines of a different epitope (e.g. H3K9 antibodies with H3K23-methyl peptides, etc.)

Supplementary Figure 6

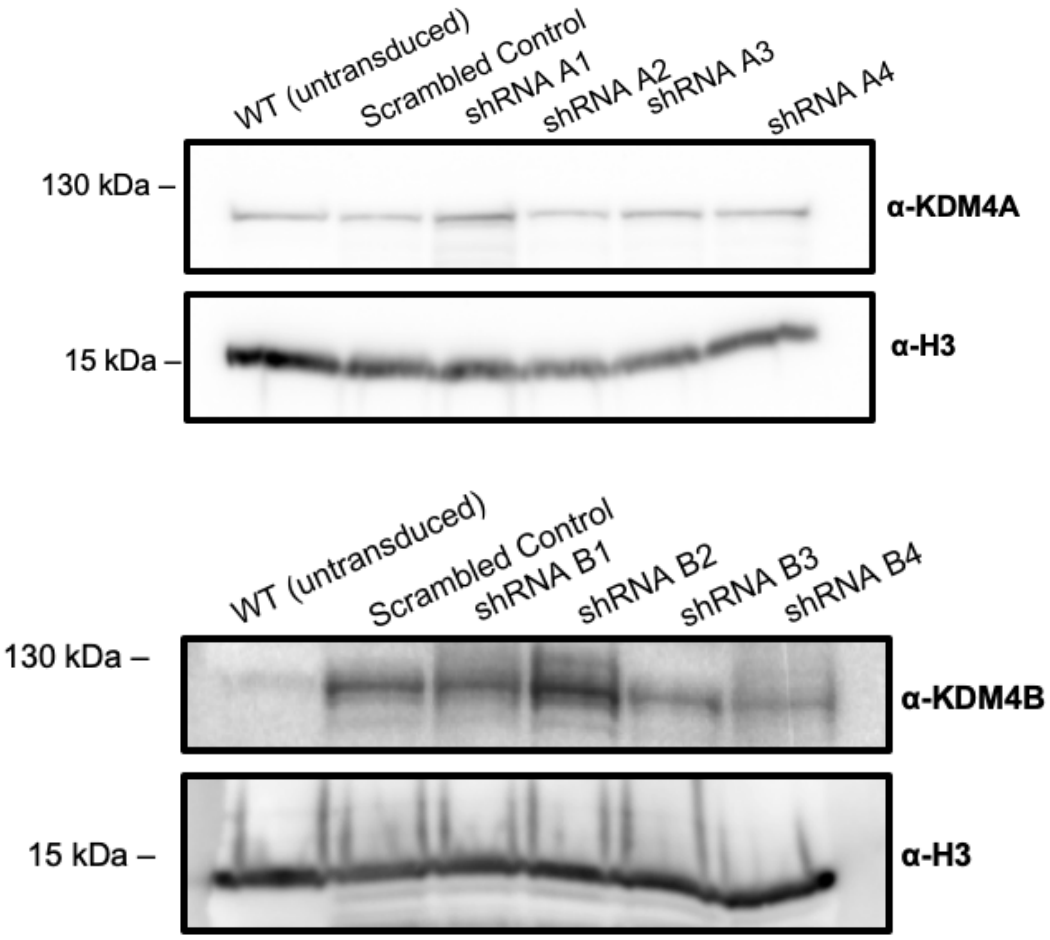

Supplementary Figure 6. Attempts to knockdown KDM4A and KDM4B via shRNA
Western blot panels showing attempts to knockdown KDM4A and KDM4B via shRNA in 50B11 cells.

References

[1] G. Bernardi, "The isochore organization of the human genome and its evolutionary history—a review," *Gene,* vol. 135, *(1-2),* pp. 57-66, 1993.

[2] A. Travers and G. Muskhelishvili, "DNA structure and function," *The FEBS Journal,* vol. 282, *(12),* pp. 2279-2295, 2015.

[3] E. I. Campos and D. Reinberg, "Histones: annotating chromatin," *Annu. Rev. Genet.,* vol. 43, pp. 559-599, 2009.

[4] A. M. Deaton and A. Bird, "CpG islands and the regulation of transcription," *Genes Dev.,* vol. 25, *(10),* pp. 1010-1022, 2011.

[5] S. Hasan and M. O. Hottiger, "Histone acetyl transferases: a role in DNA repair and DNA replication," *Journal of Molecular Medicine,* vol. 80, *(8),* pp. 463-474, 2002.

[6] J. D. Moore and J. E. Krebs, "Histone modifications and DNA double-strand break repair," *Biochemistry and Cell Biology,* vol. 82, *(4),* pp. 446-452, 2004.

[7] Z. Sun *et al*, "H3K36me3, message from chromatin to DNA damage repair," *Cell & Bioscience,* vol. 10, *(1),* pp. 1-9, 2020.

[8] M. Durand-Dubief and K. Ekwall, "Heterochromatin tells CENP-A where to go," *Bioessays,* vol. 30, *(6),* pp. 526-529, 2008.

[9] P. Han *et al*, "Epigenetic response to environmental stress: Assembly of BRG1–G9a/GLP–DNMT3 repressive chromatin complex on Myh6 promoter in pathologically stressed hearts," *Biochimica Et Biophysica Acta (BBA)-Molecular Cell Research,* vol. 1863, *(7),* pp. 1772-1781, 2016.

[10] T. Jenuwein and C. D. Allis, "Translating the histone code," *Science,* vol. 293, *(5532),* pp. 1074-1080, 2001.

[11] M. Lachner, R. J. O'Sullivan and T. Jenuwein, "An epigenetic road map for histone lysine methylation," *J. Cell. Sci.,* vol. 116, *(11),* pp. 2117-2124, 2003.

[12] B. E. Bernstein *et al*, "A bivalent chromatin structure marks key developmental genes in embryonic stem cells," *Cell,* vol. 125, *(2),* pp. 315-326, 2006.

[13] W. Chen *et al*, "G9a-an appealing antineoplastic target," *Current Cancer Drug Targets,* vol. 17, *(6),* pp. 555-568, 2017.

[14] K. Zhou, G. Gaullier and K. Luger, "Nucleosome structure and dynamics are coming of age," *Nature Structural & Molecular Biology,* vol. 26, *(1),* pp. 3-13, 2019.

[15] A. A. Kalashnikova, R. A. Rogge and J. C. Hansen, "Linker histone H1 and protein–protein interactions," *Biochimica Et Biophysica Acta (BBA)-Gene Regulatory Mechanisms,* vol. 1859, *(3),* pp. 455-461, 2016.

[16] G. Sollberger *et al*, "Linker histone H1. 2 and H1. 4 affect the neutrophil lineage determination," *Elife,* vol. 9, pp. e52563, 2020.

[17] S. Kubicek and T. Jenuwein, "A crack in histone lysine methylation," *Cell,* vol. 119, *(7),* pp. 903-906, 2004.

[18] B. D. Strahl and C. D. Allis, "The language of covalent histone modifications," *Nature,* vol. 403, *(6765),* pp. 41-45, 2000.

[19] W. Fischle, Y. Wang and C. D. Allis, "Histone and chromatin cross-talk," *Curr. Opin. Cell Biol.,* vol. 15, *(2),* pp. 172-183, 2003.

[20] P. B. Talbert and S. Henikoff, "Histone variants at a glance," *J. Cell. Sci.,* vol. 134, *(6),* pp. jcs244749, 2021.

[21] C. Redon *et al*, "Histone H2a variants H2AX and H2AZ," *Curr. Opin. Genet. Dev.,* vol. 12, *(2),* pp. 162-169, 2002.

[22] S. V. Kumar and P. A. Wigge, "H2A. Z-containing nucleosomes mediate the thermosensory response in Arabidopsis," *Cell,* vol. 140, *(1),* pp. 136-147, 2010.

[23] C. Jin and G. Felsenfeld, "Nucleosome stability mediated by histone variants H3. 3 and H2A. Z," *Genes Dev.,* vol. 21, *(12),* pp. 1519-1529, 2007.

[24] C. Jin *et al*, "H3. 3/H2A. Z double variant–containing nucleosomes mark'nucleosome-free regions' of active promoters and other regulatory regions," *Nat. Genet.,* vol. 41, *(8),* pp. 941-945, 2009.

[25] A. Piazzesi *et al*, "Replication-independent histone variant H3. 3 controls animal lifespan through the regulation of pro-longevity transcriptional programs," *Cell Reports,* vol. 17, *(4),* pp. 987-996, 2016.

[26] Q. Wu *et al*, "Protein arginine methylation: from enigmatic functions to therapeutic targeting," *Nature Reviews Drug Discovery,* vol. 20, *(7),* pp. 509-530, 2021.

[27] M. Litt, Y. Qiu and S. Huang, "Histone arginine methylations: their roles in chromatin dynamics and transcriptional regulation," *Biosci. Rep.,* vol. 29, *(2),* pp. 131-141, 2009.

[28] D. Husmann and O. Gozani, "Histone lysine methyltransferases in biology and disease," *Nature Structural & Molecular Biology,* vol. 26, *(10),* pp. 880-889, 2019.

[29] A. K. Upadhyay and X. Cheng, "Dynamics of histone lysine methylation: structures of methyl writers and erasers," *Epigenetics and Disease,* pp. 107-124, 2011.

[30] A. Shilatifard, "Molecular implementation and physiological roles for histone H3 lysine 4 (H3K4) methylation," *Curr. Opin. Cell Biol.,* vol. 20, *(3),* pp. 341-348, 2008.

[31] R. J. Sims III, K. Nishioka and D. Reinberg, "Histone lysine methylation: a signature for chromatin function," *TRENDS in Genetics,* vol. 19, *(11),* pp. 629-639, 2003.

[32] K. Hyun *et al*, "Writing, erasing and reading histone lysine methylations," *Exp. Mol. Med.,* vol. 49, *(4),* pp. e324, 2017.

[33] M. Yun *et al*, "Readers of histone modifications," *Cell Res.,* vol. 21, *(4),* pp. 564-578, 2011.

[34] S. D. Taverna *et al*, "How chromatin-binding modules interpret histone modifications: lessons from professional pocket pickers," *Nature Structural & Molecular Biology,* vol. 14, *(11),* pp. 1025-1040, 2007.

[35] X. Zhu *et al*, "HRP2–DPF3a–BAF complex coordinates histone modification and chromatin remodeling to regulate myogenic gene transcription," *Nucleic Acids Res.,* vol. 48, *(12),* pp. 6563-6582, 2020.

[36] C. Mayr *et al*, "The role of polycomb repressive complexes in biliary tract cancer," *Expert Opinion on Therapeutic Targets,* vol. 19, *(3),* pp. 363-375, 2015.

[37] E. K. Shanle *et al*, "Histone peptide microarray screen of chromo and Tudor domains defines new histone lysine methylation interactions," *Epigenetics & Chromatin,* vol. 10, *(1),* pp. 1-11, 2017.

[38] W. Zeng, A. R. Ball Jr and K. Yokomori, "HP1: heterochromatin binding proteins working the genome," *Epigenetics,* vol. 5, *(4),* pp. 287-292, 2010.

[39] E. Dimitrova, A. H. Turberfield and R. J. Klose, "Histone demethylases in chromatin biology and beyond," *EMBO Rep.,* vol. 16, *(12),* pp. 1620-1639, 2015.

[40] K. Davis *et al*, "The role of demethylases in cardiac development and disease," *J. Mol. Cell. Cardiol.,* vol. 158, pp. 89-100, 2021.

[41] Z. Su *et al*, "Reader domain specificity and lysine demethylase-4 family function," *Nature Communications,* vol. 7, *(1),* pp. 1-15, 2016.

[42] G. Da *et al*, "Structure and function of the SWIRM domain, a conserved protein module found in chromatin regulatory complexes," *Proceedings of the National Academy of Sciences,* vol. 103, *(7),* pp. 2057-2062, 2006.

[43] S. B. Rothbart and B. D. Strahl, "Interpreting the language of histone and DNA modifications," *Biochimica Et Biophysica Acta (BBA)-Gene Regulatory Mechanisms,* vol. 1839, *(8),* pp. 627-643, 2014.

[44] C. Y. Okitsu, J. C. F. Hsieh and C. Hsieh, "Transcriptional activity affects the H3K4me3 level and distribution in the coding region," *Mol. Cell. Biol.,* vol. 30, *(12),* pp. 2933-2946, 2010.

[45] D. Clyde, "Uncovering distinct roles for H3K9me3," *Nature Reviews Genetics,* vol. 22, *(2),* pp. 69, 2021.

[46] T. Iwagawa and S. Watanabe, "Molecular mechanisms of H3K27me3 and H3K4me3 in retinal development," *Neurosci. Res.,* vol. 138, pp. 43-48, 2019.

[47] J. W. Edmunds, L. C. Mahadevan and A. L. Clayton, "Dynamic histone H3 methylation during gene induction: HYPB/Setd2 mediates all H3K36 trimethylation," *Embo J.,* vol. 27, *(2),* pp. 406-420, 2008.

[48] M. S. Trejo-Arellano *et al*, "H3K23me1 is an evolutionarily conserved histone modification associated with CG DNA methylation in Arabidopsis," *The Plant Journal,* vol. 90, *(2),* pp. 293-303, 2017.

[49] S. D. Taverna *et al*, "Yng1 PHD finger binding to H3 trimethylated at K4 promotes NuA3 HAT activity at K14 of H3 and transcription at a subset of targeted ORFs," *Mol. Cell,* vol. 24, *(5),* pp. 785-796, 2006.

[50] P. Voigt, W. Tee and D. Reinberg, "A double take on bivalent promoters," *Genes Dev.,* vol. 27, *(12),* pp. 1318-1338, 2013.

[51] A. J. Price *et al*, "Hdac3, Setdb1, and Kap1 mark H3K9me3/H3K14ac bivalent regions in young and aged liver," *Aging Cell,* vol. 19, *(2),* pp. e13092, 2020.

[52] C. Poulard *et al*, "Increasing G9a automethylation sensitizes B acute lymphoblastic leukemia cells to glucocorticoid-induced death," *Cell Death & Disease,* vol. 9, *(10),* pp. 1-13, 2018.

[53] L. Monaghan *et al*, "The emerging role of H3K9me3 as a potential therapeutic target in acute myeloid leukemia," *Frontiers in Oncology,* vol. 9, pp. 705, 2019.

[54] W. N. Pappano *et al*, "The histone methyltransferase inhibitor A-366 uncovers a role for G9a/GLP in the epigenetics of leukemia," *PloS One,* vol. 10, *(7),* pp. e0131716, 2015.

[55] P. W. Lewis *et al*, "Inhibition of PRC2 activity by a gain-of-function H3 mutation found in pediatric glioblastoma," *Science,* vol. 340, *(6134),* pp. 857-861, 2013.

[56] C. Lu *et al*, "Histone H3K36M mutation and trimethylation patterns in chondroblastoma," *Histopathology,* vol. 74, *(2),* pp. 291-299, 2019.

[57] A. S. Harutyunyan *et al*, "H3K27M induces defective chromatin spread of PRC2-mediated repressive H3K27me2/me3 and is essential for glioma tumorigenesis," *Nature Communications,* vol. 10, *(1),* pp. 1-13, 2019.

[58] M. Lachner and T. Jenuwein, "The many faces of histone lysine methylation," *Curr. Opin. Cell Biol.,* vol. 14, *(3),* pp. 286-298, 2002.

[59] K. Lepikhov and J. Walter, "Differential dynamics of histone H3 methylation at positions K4 and K9 in the mouse zygote," *BMC Developmental Biology,* vol. 4, *(1),* pp. 1-5, 2004.

[60] A. W. Snowden *et al*, "Gene-specific targeting of H3K9 methylation is sufficient for initiating repression in vivo," *Current Biology,* vol. 12, *(24),* pp. 2159-2166, 2002.

[61] Z. Lippman *et al*, "Distinct mechanisms determine transposon inheritance and methylation via small interfering RNA and histone modification," *PLoS Biology,* vol. 1, *(3),* pp. e67, 2003.

[62] A. Villar-Garea and A. Imhof, "The analysis of histone modifications," *Biochimica Et Biophysica Acta (BBA)-Proteins and Proteomics,* vol. 1764, *(12),* pp. 1932-1939, 2006.

[63] C. R. Vakoc *et al*, "Histone H3 lysine 9 methylation and HP1γ are associated with transcription elongation through mammalian chromatin," *Mol. Cell,* vol. 19, *(3),* pp. 381-391, 2005.

[64] J. Li *et al*, "Structural basis for specific binding of human MPP8 chromodomain to histone H3 methylated at lysine 9," *PloS One,* vol. 6, *(10),* pp. e25104, 2011.

[65] R. Cao *et al*, "Role of histone H3 lysine 27 methylation in Polycomb-group silencing," *Science,* vol. 298, *(5595),* pp. 1039-1043, 2002.

[66] P. Rathert *et al*, "Protein lysine methyltransferase G9a acts on non-histone targets," *Nature Chemical Biology,* vol. 4, *(6),* pp. 344-346, 2008.

[67] S. V. Veiseth *et al*, "The SUVR4 histone lysine methyltransferase binds ubiquitin and converts H3K9me1 to H3K9me3 on transposon chromatin in Arabidopsis," *PLoS Genetics,* vol. 7, *(3),* pp. e1001325, 2011.

[68] J. C. Black, C. Van Rechem and J. R. Whetstine, "Histone lysine methylation dynamics: establishment, regulation, and biological impact," *Mol. Cell,* vol. 48, *(4),* pp. 491-507, 2012.

[69] M. Pan *et al*, "G9a orchestrates PCL3 and KDM7A to promote histone H3K27 methylation," *Scientific Reports,* vol. 5, *(1),* pp. 1-8, 2015.

[70] J. C. Eissenberg and A. Shilatifard, "Histone H3 lysine 4 (H3K4) methylation in development and differentiation," *Dev. Biol.,* vol. 339, *(2),* pp. 240-249, 2010.

[71] S. Fnu *et al*, "Methylation of histone H3 lysine 36 enhances DNA repair by nonhomologous end-joining," *Proceedings of the National Academy of Sciences,* vol. 108, *(2),* pp. 540-545, 2011.

[72] R. Papazyan *et al*, "Methylation of histone H3K23 blocks DNA damage in pericentric heterochromatin during meiosis," *Elife,* vol. 3, pp. e02996, 2014.

[73] J. Vandamme *et al*, "H3K23me2 is a new heterochromatic mark in Caenorhabditis elegans," *Nucleic Acids Res.,* vol. 43, *(20),* pp. 9694-9710, 2015.

[74] L. Schwartz-Orbach *et al*, "Caenorhabditis elegans nuclear RNAi factor SET-32 deposits the transgenerational histone modification, H3K23me3," *Elife,* vol. 9, pp. e54309, 2020.

[75] H. Wu *et al*, "Histone methyltransferase G9a contributes to H3K27 methylation in vivo," *Cell Res.,* vol. 21, *(2),* pp. 365-367, 2011.

[76] F. Liu *et al*, "Discovery of an in vivo chemical probe of the lysine methyltransferases G9a and GLP," *J. Med. Chem.,* vol. 56, *(21),* pp. 8931-8942, 2013.

[77] Y. Cao *et al*, "Inhibition of G9a by a small molecule inhibitor, UNC0642, induces apoptosis of human bladder cancer cells," *Acta Pharmacol. Sin.,* vol. 40, *(8),* pp. 1076-1084, 2019.

[78] C. Griñán-Ferré *et al*, "Pharmacological inhibition of G9a/GLP restores cognition and reduces oxidative stress, neuroinflammation and β-Amyloid plaques in an early-onset Alzheimer's disease mouse model," *Aging (Albany NY),* vol. 11, *(23),* pp. 11591, 2019.

[79] D. Sanders *et al*, "Histone lysine-to-methionine mutations reduce histone methylation and cause developmental pleiotropy," *Plant Physiol.,* vol. 173, *(4),* pp. 2243-2252, 2017.

[80] H. Jayaram *et al*, "S-adenosyl methionine is necessary for inhibition of the methyltransferase G9a by the lysine 9 to methionine mutation on histone H3," *Proceedings of the National Academy of Sciences,* vol. 113, *(22),* pp. 6182-6187, 2016.

[81] M. Tachibana *et al*, "G9a/GLP complexes independently mediate H3K9 and DNA methylation to silence transcription," *Embo J.,* vol. 27, *(20),* pp. 2681-2690, 2008.

[82] G. Ormaza *et al*, "The tumor suppressor ING5 is a dimeric, bivalent recognition molecule of the histone H3K4me3 mark," *J. Mol. Biol.,* vol. 431, *(12),* pp. 2298-2319, 2019.

[83] B. J. Klein *et al*, "Histone H3K23-specific acetylation by MORF is coupled to H3K14 acylation," *Nature Communications,* vol. 10, *(1),* pp. 1-13, 2019.

[84] Y. Habu *et al*, "Epigenetic regulation of transcription in intermediate heterochromatin," *EMBO Rep.,* vol. 7, *(12),* pp. 1279-1284, 2006.

[85] R. Collins and X. Cheng, "A case study in cross-talk: the histone lysine methyltransferases G9a and GLP," *Nucleic Acids Res.,* vol. 38, *(11),* pp. 3503-3511, 2010.

[86] S. Lanouette *et al*, "The functional diversity of protein lysine methylation," *Molecular Systems Biology,* vol. 10, *(4),* pp. 724, 2014.

[87] B. A. Nacev *et al*, "The expanding landscape of 'oncohistone'mutations in human cancers," *Nature,* vol. 567, *(7749),* pp. 473-478, 2019.

[88] Y. Ho and R. Huang, "Effects of Oncohistone Mutations and PTM Crosstalk on the N-Terminal Acetylation Activities of NatD," *ACS Chemical Biology,* 2021.

[89] S. José-Enériz *et al*, "Discovery of first-in-class reversible dual small molecule inhibitors against G9a and DNMTs in hematological malignancies," *Nature Communications,* vol. 8, *(1),* pp. 1-10, 2017.

[90] L. Bao *et al*, "Methylation of hypoxia-inducible factor (HIF)-1α by G9a/GLP inhibits HIF-1 transcriptional activity and cell migration," *Nucleic Acids Res.,* vol. 46, *(13),* pp. 6576-6591, 2018.

[91] J. Huang *et al*, "G9a and Glp methylate lysine 373 in the tumor suppressor p53," *J. Biol. Chem.,* vol. 285, *(13),* pp. 9636-9641, 2010.

[92] B. K. Souza *et al*, "EHMT2/G9a as an epigenetic target in pediatric and adult brain tumors," *International Journal of Molecular Sciences,* vol. 22, *(20),* pp. 11292, 2021.

[93] J. Kang *et al*, "FIH Is an Oxygen Sensor in Ovarian Cancer for G9a/GLP-Driven Epigenetic Regulation of Metastasis-Related GenesFIH Hydroxylates and Inactivates G9a and GLP," *Cancer Res.,* vol. 78, *(5),* pp. 1184-1199, 2018.

[94] K. K. L. Pang, M. Sharma and S. Sajikumar, "Epigenetics and memory: emerging role of histone lysine methyltransferase G9a/GLP complex as bidirectional regulator of synaptic plasticity," *Neurobiol. Learn. Mem.,* vol. 159, pp. 1-5, 2019.

[95] N. Liu *et al*, "Recognition of H3K9 methylation by GLP is required for efficient establishment of H3K9 methylation, rapid target gene repression, and mouse viability," *Genes Dev.,* vol. 29, *(4),* pp. 379-393, 2015.

[96] H. Cao *et al*, "Recent progress in histone methyltransferase (G9a) inhibitors as anticancer agents," *Eur. J. Med. Chem.,* vol. 179, pp. 537-546, 2019.

[97] X. Y. Zhang *et al*, "Frequent upregulation of G9a promotes RelB-dependent proliferation and survival in multiple myeloma," *Experimental Hematology & Oncology,* vol. 9, *(1),* pp. 1-17, 2020.

[98] B. J. Klein *et al*, "Crosstalk between epigenetic readers regulates the MOZ/MORF HAT complexes," *Epigenetics,* vol. 9, *(2),* pp. 186-193, 2014.

[99] S. I. Grewal and D. Moazed, "Heterochromatin and epigenetic control of gene expression," *Science,* vol. 301, *(5634),* pp. 798-802, 2003.

[100] C. Y. Okitsu and C. Hsieh, "DNA methylation dictates histone H3K4 methylation," *Mol. Cell. Biol.,* vol. 27, *(7),* pp. 2746-2757, 2007.

[101] C. Prigent and S. Dimitrov, "Phosphorylation of serine 10 in histone H3, what for?" *J. Cell. Sci.,* vol. 116, *(18),* pp. 3677-3685, 2003.

[102] S. R. Bhaumik, E. Smith and A. Shilatifard, "Covalent modifications of histones during development and disease pathogenesis," *Nature Structural & Molecular Biology,* vol. 14, *(11),* pp. 1008-1016, 2007.

[103] H. Saze and T. Kakutani, "Differentiation of epigenetic modifications between transposons and genes," *Curr. Opin. Plant Biol.,* vol. 14, *(1),* pp. 81-87, 2011.

[104] K. R. Karch *et al*, "Identification and interrogation of combinatorial histone modifications," *Frontiers in Genetics,* vol. 4, pp. 264, 2013.

[105] J. Wei *et al*, "KDM4B-mediated reduction of H3K9me3 and H3K36me3 levels improves somatic cell reprogramming into pluripotency," *Scientific Reports,* vol. 7, *(1),* pp. 1-14, 2017.

[106] C. Lin *et al*, "HP1a targets the Drosophila KDM4A demethylase to a subset of heterochromatic genes to regulate H3K36me3 levels," *PloS One,* vol. 7, *(6),* pp. e39758, 2012.

[107] J. Ernst and M. Kellis, "Chromatin-state discovery and genome annotation with ChromHMM," *Nature Protocols,* vol. 12, *(12),* pp. 2478-2492, 2017.

[108] S. Wang *et al*, "Target analysis by integration of transcriptome and ChIP-seq data with BETA," *Nature Protocols,* vol. 8, *(12),* pp. 2502-2515, 2013.

[109] G. Dobrynin *et al*, "KDM4A regulates HIF-1 levels through H3K9me3," *Scientific Reports,* vol. 7, *(1),* pp. 1-9, 2017.

[110] A. Sankar *et al*, "KDM4A regulates the maternal-to-zygotic transition by protecting broad H3K4me3 domains from H3K9me3 invasion in oocytes," *Nat. Cell Biol.,* vol. 22, *(4),* pp. 380-388, 2020.

[111] Y. Matsumura *et al*, "H3K4/H3K9me3 bivalent chromatin domains targeted by lineage-specific DNA methylation pauses adipocyte differentiation," *Mol. Cell,* vol. 60, *(4),* pp. 584-596, 2015.